

Donor-Acceptor Substituted

Triplet Emitters

Dissertation zur Erlangung des
naturwissenschaftlichen Doktorgrades
der Julius-Maximilians-Universität Würzburg

vorgelegt von

Barbara Geiß

aus Seßlach

Würzburg 2009

Eingereicht am: _____

bei der Fakultät für Chemie und Pharmazie

1. Gutachter: _____

2. Gutachter: _____

der Dissertation

1. Prüfer: _____

2. Prüfer: _____

3. Prüfer: _____

des öffentlichen Promotionskolloquiums

Tag des öffentlichen Promotionskolloquiums: _____

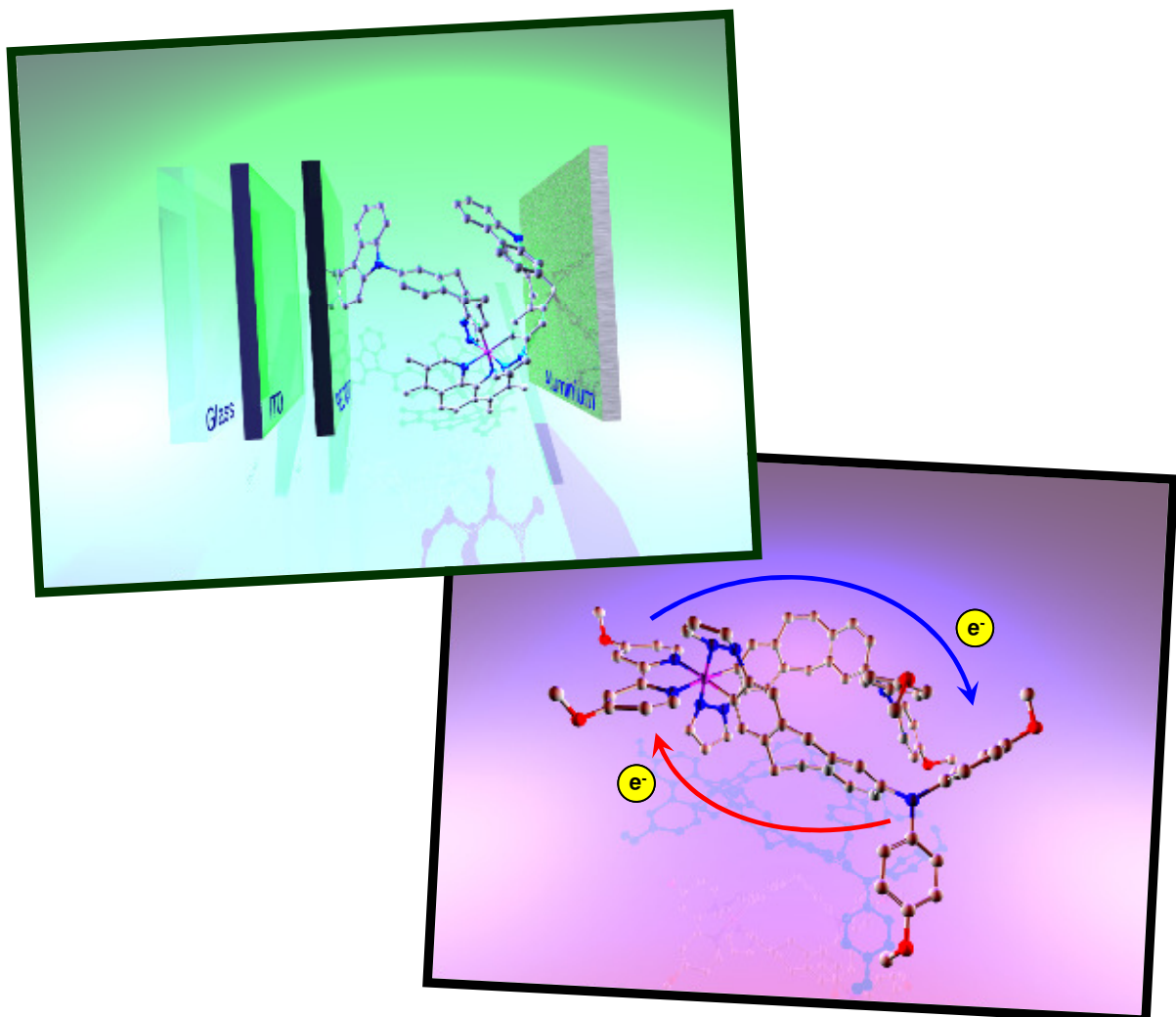
Doktorurkunde ausgehändigt am: _____

Die vorliegende Arbeit wurde in der Zeit von Juli 2004 bis August 2009 am Institut für
Organische Chemie der Universität Würzburg angefertigt.

Mein besonderer Dank gilt

Herrn Prof. Dr. Christoph Lambert

für die Vergabe des vielseitigen Themas, die intensive Betreuung und Förderung und
das mit vielen Anregungen und Diskussionen verbundene Interesse an dieser Arbeit.



*Man muss das Unmögliche versuchen,
um das Mögliche zu erreichen.*

Hermann Hesse

(1877-1962)

meinen Eltern

Contents

1	Introduction	1
1.1	Charge Separation in Transition Metal Complexes	2
1.1.1	Introduction	2
1.1.2	Marcus Theory	3
1.1.3	State of the Art	5
1.2	Transition Metal Complexes in Organic Light Emitting Devices	11
1.2.1	Introduction	11
1.2.2	Design and Functionality of OLEDs	11
1.2.3	Materials for OLEDs	12
1.2.4	Transition Metal Complexes as Triplet Emitters	14
1.2.5	State of the Art	17
1.3	Project Aim	19
2	Cyclometalated Transition Metal Complexes	22
2.1	Structure and Energy Levels	22
2.2	Cationic Iridium Complexes	25
2.2.1	Synthesis	26
2.2.1.1	The Ligands	26
2.2.1.2	The Cationic Ir(III) Complexes	28
2.2.2	Redox Properties	29

2.2.3 Steady State Spectroscopy	34
2.2.3.1 Steady State Absorption Spectroscopy	34
2.2.3.2 Emission Spectroscopy	38
2.2.3.2.1 Emission Spectroscopy at RT	38
2.2.3.2.2. Emission Spectroscopy at 77 K	43
2.2.4 Transient Absorption Spectroscopy	47
2.2.4.1 Transient Absorption Spectroscopy at RT	47
2.2.4.2 Temperature-Dependent Transient Absorption Spectroscopy	54
2.2.5 LEC Studies	58
2.3 Neutral Platinum and Iridium Complexes	60
2.3.1 Synthesis	61
2.3.1.1 The Acetylacetone Compounds	61
2.3.1.2 The Homoleptic Ir(ppz _{TAA}) ₃ Compound	63
2.3.2 Redox Properties	64
2.3.3 Spectroscopy	66
2.3.3.1 Steady State Absorption Spectroscopy	66
2.3.3.2 Steady State Emission Spectroscopy at RT and 77K	67
2.3.3.3 Transient Absorption Spectroscopy	70
2.4 Summary	72

3	Experimental Section	74
3.1	Apparatus and Methods	74
3.1.1	General Analytical Methods	74
3.1.2	Electrochemistry	75
3.1.3	UV/Vis/NIR Spectroscopy	75
3.1.4	Transient Absorption Spectroscopy	76
3.1.5	Fluorescence Spectroscopy	78
3.1.6	LECs: Fabrication and Measurements	79
3.1.7	Synthesis	80
3.2	Synthesis	82
3.2.1	General Experimental Procedures	82
3.2.2	Synthesis of the Cationic Iridium Complexes	85
3.2.2.1	Synthesis of the Ligands	85
3.2.2.2	Synthesis of the Complexes	96
3.2.3	Synthesis of Neutral Transition Metal Complexes	124
3.2.3.1	Synthesis of the Acetylacetone Compounds	124
3.2.3.2	Synthesis of the Homoleptic Ir(ppz _{TAA}) ₃ Complex	130
4	Literature	131

5	Table of Formulas	140
5.1	Reference Compounds	140
5.2	Cationic Complexes	141
5.3	Neutral Complexes	145
5.4	Dimers	146
5.5	Ligands and Precursors	147
 Appendix		148
Zusammenfassung		148
Danksagung		151

Abbreviations

ATP	adenosine triphosphate
bdppe	<i>cis</i> -1,2- <i>bis</i> (diphenylphosphino)ethylene
bpy	2,2'-bipyridyl
CR	charge recombination
CS	charge separation
¹ CS	excited singlet charge separated
³ CS	excited triplet charge separated
CT	charge transfer
¹ CT	excited singlet charge transfer
³ CT	excited triplet charge transfer
CV	cyclic voltammetry / cyclic voltammogram
CW	continuous white light
CZ	carbazole
DA	donor-acceptor
dba	<i>trans,trans</i> -dibenzylideneacetone
DMF	dimethylformamide
EA	ethylacetate
ET	electron transfer
ETL	electron transporting layer
Fc	ferrocene
HTL	hole transporting layer
ISC	intersystem crossing
LEC	light emitting electrochemical cell
LEL	light emitting layer
MeCN	acetonitrile
2-MeTHF	2-methyltetrahydrofuran
¹ MLCT	singlet metal-to-ligand charge transfer
³ MLCT	triplet metal-to-ligand charge transfer
NADPH	nicotinamide adenine dinucleotide phosphate
OD	optical density
OLED	organic light emitting device
PE	petrol ether

PES	potential energy surface
PET	photoinduced electron transfer
PhCN	benzonitrile
PMT	photomultiplier
ppy	phenylpyridyl
ppz	2-phenylpyrazole
S ₀	singlet ground state
S ₁	excited singlet state
SEC	spectroelectrochemistry
T	triplet state
TAA	triarylamine
TTA	triplet-triplet-annihilation
TBAH	tetrabutylammonium hexafluorophosphate
THF	tetrahydrofuran
tmp	3,4,7,8-tetramethyl-1,10-phenanthroline
UV	ultraviolet
Vis	visible

1 Introduction

Energy is the basic necessity for life. About 85 % of our energy comes from fossil fuels, a resource that is not regenerative. With increasing world population the reserves of fossil fuels are progressively decreasing. Therefore it is important to find alternative energy sources as soon as possible.

Nature shows impressively how to store and convert optical energy by photoinduced electron transfer (PET) reactions. Initiated by sunlight the natural photosynthesis utilises sequential multi step electron transfer between chlorophyll and quinone moieties, which are well-organised in a protein matrix to produce a long-lived charge-separated state.¹⁻⁴ This reaction is supported by two large protein systems, Photosystem I and II. Photosystem I provides the reducing potential by producing nicotinamide adenine dinucleotide phosphate (NADPH). Photosystem II accelerates the production of the oxidising equivalents which are necessary for the production of O₂ from H₂O. The electron flow between these two systems creates a proton gradient that advances the transport of protons across the membrane resulting in the synthesis of the high-energy biological fuel adenosine triphosphate (ATP) to restore the charge balance of the membrane. The charges are separated with remarkable efficiency without losses from back electron transfer, achieved by an evolutionarily optimised, complicated arrangement of functional molecular components that separate the charge to a large distance. This principle of optimised electron transfer is currently the objective of extensive studies to capture and store solar energy.

A model reaction center for PET must at least consist of an electron donor chromophore that absorbs visible light and an additional electron acceptor linked via a bridging unit that controls their electronic interactions. The ability of these so-called “antenna systems” to exhibit fluorescence and the flexible interaction between the redox centers make them also interesting for supramolecular luminescence-based systems, capable of sensing the environment.^{5,6} Furthermore, molecules that employ reversible ultrafast electron transfer reactions can be useful to produce light intensity dependent optical switches.⁷

In the context of PET, transition metal complexes play a dominant role.¹⁻³ In this work, we concentrate on donor-acceptor substituted Ir(III) complexes as this type

of complexes are currently used as triplet emitters in OLEDs. We will present the synthesis and photophysical characterisation of a series of such compounds.

The following chapter is divided into three parts: the first part describes basic aspects of electron transfer theory and charge separation in some detail. The second part deals with the construction and functionality of OLEDs and especially with the use of transition metal complexes in OLEDs. In the third part the design of the complexes presented in this work is outlined followed by the aim of this project.

1.1 Charge separation in transition metal complexes

1.1.1 Introduction

Inner sphere electron transfer (ET) proceeds via covalently linked redox centers, the oxidant (acceptor, A) and the reductant (donor, D). By photoinduced excitation of a DA-compound the resulting excited state ((DA)^{*}) produces a charge separated (CS) state D⁺A⁻ that decays subsequently by charge recombination (CR) (Figure 1.1).⁸ The first and now generally accepted theory of ET was developed by Rudolph A. Marcus which describes the dependence of ET rates on parameters associated with structure and medium.⁹⁻¹³

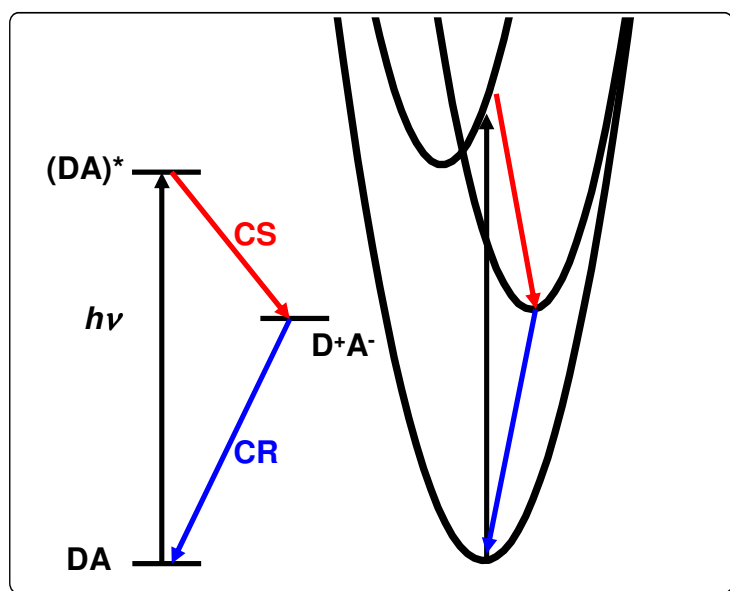


Figure 1.1 The typical energy diagram for a donor-acceptor (DA) dyad. Excitation into the lowest excited state can be followed by charge separation (CS) if the CS state is lower in energy. Charge recombination (CR) into the ground state follows.

1.1.2 Marcus Theory

The potential energy surface of DA-dyads depends both on nuclear and solvent coordinates. This leads to a multidimensional potential-energy surface (PES) that can be simplified by introducing a reaction coordinate that allows to consider only a one-dimensional profile.¹⁴ In a diabatic approach one can represent the system by Gibb's free energy profiles using harmonic potentials for reactants (DA) and products (D^+A^-) (Figure 1.2). In this model it is assumed that the DA and D^+A^- states are weakly coupled (diabatic model).

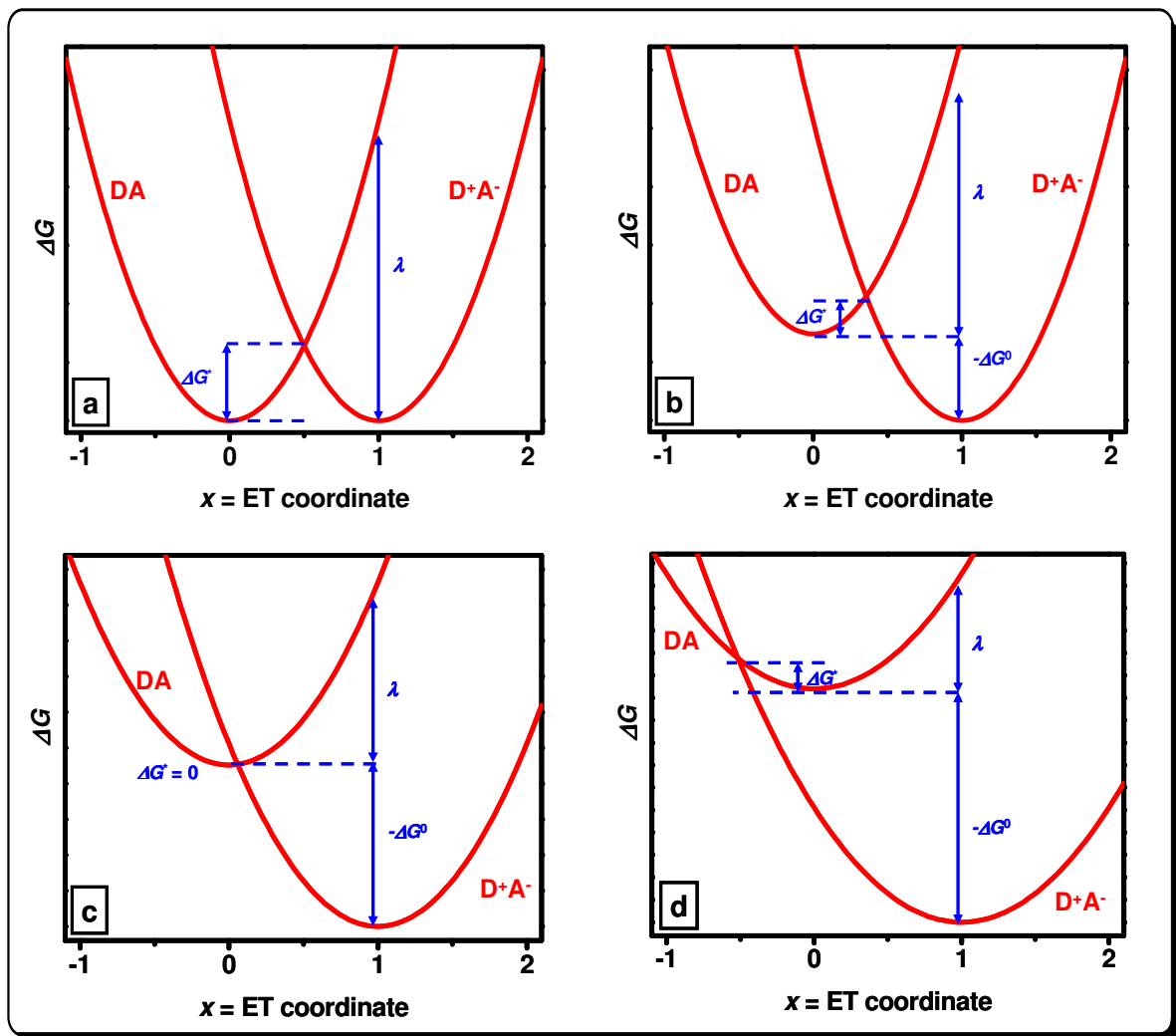


Figure 1.2 The energy profiles for diabatic (weak coupling) ET reactions ($DA \rightarrow D^+A^-$) depending on the free energy difference ΔG^0 : a) $-\Delta G^0 = 0$: self-exchange reaction; b) $-\Delta G^0 < \lambda$: Marcus normal region; c) $-\Delta G^0 = \lambda$: optimal conditions; d) $-\Delta G^0 > \lambda$: Marcus inverted region.

The two minima of the parabolas in Figure 1.2 differ by free energy difference ΔG^0 . According to Marcus' theory of electron transfer, the rate can be expressed by

$$k_{ET} = 4\pi^2 hc^2 V^2 \sqrt{\frac{1}{4\pi hc \lambda kT}} \exp\left[-\frac{hc(\lambda + \Delta G^0)^2}{4\lambda_o kT}\right] \quad (1.1)$$

Where V (in cm^{-1}) is the electronic coupling between reactant and product state and λ (in cm^{-1}) is the reorganisation energy (= force constant of the harmonic potentials in Fig 1.2) which comprises two parameters, the solvent (outer) reorganisation energy λ_o and the inner reorganisation energy λ_v .¹⁵

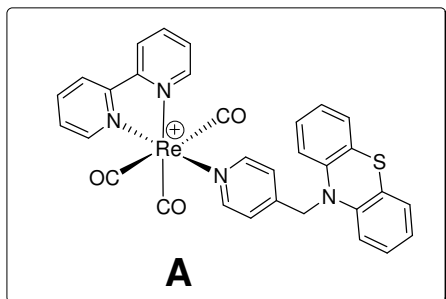
$$\lambda = \lambda_o + \lambda_v \quad (1.2)$$

The inner reorganisation energy arises from changes of vibrations of the nuclei in the reactant and product states which differ in the average bond lengths. This parameter is solvent-independent and only depends on the structure of the chromophore. The outer reorganisation energy depends on the solvent and is the energy needed to reorient the solvent dipoles. The ET barrier ΔG^* can be derived from the reorganisation energy λ and the free energy difference ΔG^0 by

$$\Delta G^* = \frac{(\lambda + \Delta G^0)^2}{4\lambda} \quad (1.3)$$

Figure 1.1 shows four kinetic regimes for ET reactions depending on the driving force range.¹⁴ Figure 1.2 a) shows the situation for ET where $\Delta G^0 = 0$. For this self-exchange reaction a significant Gibb's energy of activation $\Delta G^* = \lambda/4$ is needed. In the second example (Fig 1.2 b) the energy of the product is lowered by $|\Delta G^0|$ while the activation barrier ΔG^* decreases. This regime where $-\Delta G^0 < \lambda$ is called the “Marcus normal region” and is most often found for CS processes (see Figure 1.1). Under optimal conditions ΔG^* is zero when $-\Delta G^0 = \lambda$ (see Figure 1.2 c). The fourth case is for strongly exergonic reactions with $-\Delta G^0 > \lambda$ where again ΔG^* rises and, thus, ET is slowed down with increasing driving force. This region is called the “Marcus inverted region”, whose existence was first proved by Miller and Closs using steroid bridged D-A systems in 1984.¹⁶ This effect has now been well-established in innumerable DA systems after long controversy and is often found for CR processes

(see Figure 1.1).¹⁶⁻²⁵ An inverted region has also been observed in inorganic transition metal complexes for the intramolecular electron transfer between two ligands.^{26,27}



For example, in the $[(2,2'\text{bpy})\text{Re}^{\text{l}}(\text{CO})_3(\text{py-PTZ})]^+$ complex (**A**) metal-to-ligand charge transfer (MLCT) excitation is followed by intramolecular electron transfer to form a charge separated state $[(2,2'\text{bpy}^{\bullet-})\text{Re}^{\text{l}}(\text{CO})_3(\text{py-PTZ}^{\bullet+})]^+$. Transient absorption measurements show that the back electron transfer to the ground state ($k = 4 \times 10^7 \text{ s}^{-1}$) is dominated by a nonradiative process that corresponds to a long-range electron transfer from the bpy-radical anion to the py-PTZ-radical cation. Charge recombination in the Marcus inverted region ensures a slow recombination rate from an energy rich CS state. In contrast, charge separation is expected to be in the Marcus normal region with $-\Delta G^0 < \lambda$ to facilitate fast charge separation.

1.1.3 State of the Art

After photoinduced electron transfer from excitation of a locally excited state D^*A or DA^* into a charge separated state D^+A^- two scenarios are conceivable. If locally excited triplet states are lower in energy (Fig 1.3 a) than the D^+A^- state, realaxation (quenching) into the triplet state ${}^3\text{DA}^*$ or D^3A^* is possible which shortens the lifetime of the D^+A^- CS state. If however the local triplet states are higher in energy than the D^+A^- state may decay into the ground state by charge recombination (Fig 1.3 b). Furthermore, one has to take into account that the CS state may be present in both triplet and singlet forms.

The energy of the CS states depends on the polarity of the solvent and on the redox potential differences between donor and acceptor. In polar solvents and with small redox potential differences the CS states are lower in energy so that CR can occur from both CS states, the spin-forbidden ${}^3\text{CS}$ and the spin-allowed ${}^1\text{CS}$ state (Figure 1.3 b).⁸

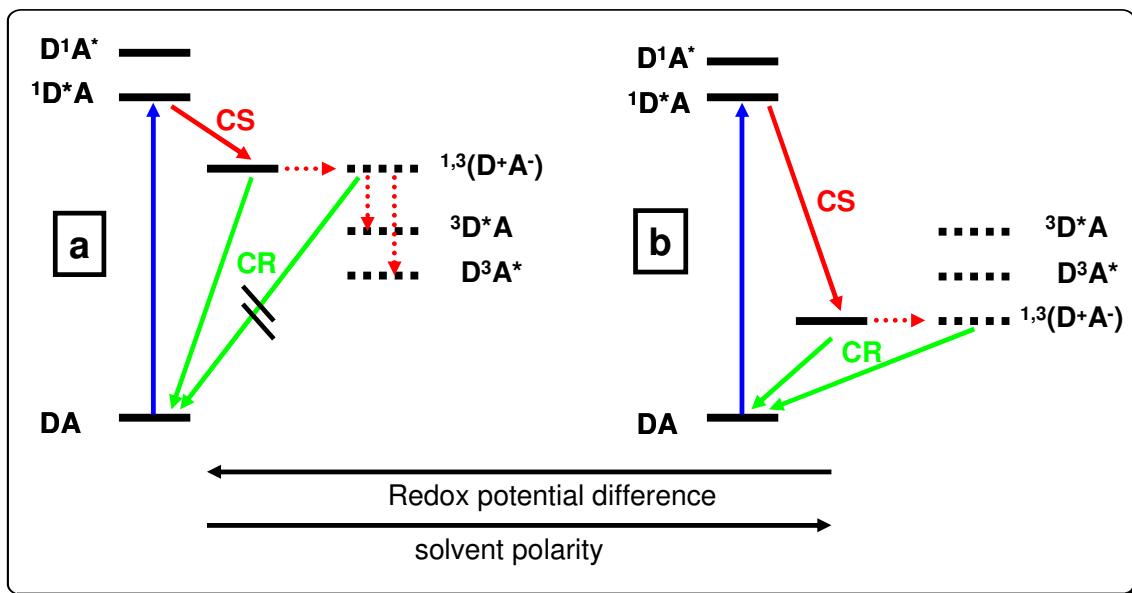
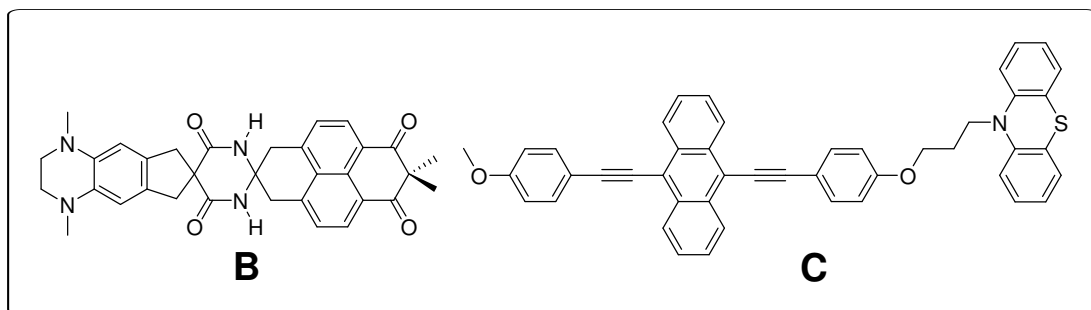


Figure 1.3 Possible population of CS and CR in dyads with varying solvent polarity. Dotted lines show ISC between the triplet states.

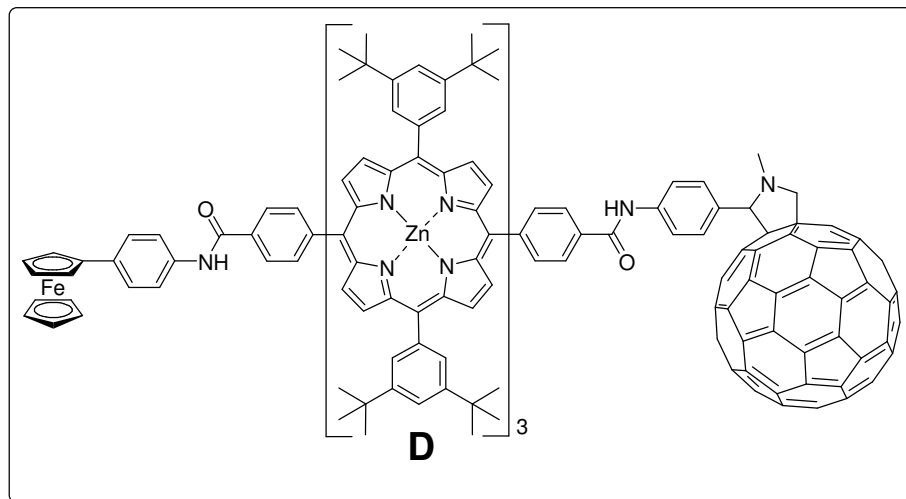
In the following, some examples of long-lived charge-separated states will be reported. Beginning with the classical fully organic and organometallic Zn-compounds I will lead over to less popular transition metal complexes and finally concentrate on the Ir(III) compounds.

There is a large number of fully organic triads and upper homologues mainly based on tetrapyrrolic and/or fullerene units.^{1-3,8,28-37} Photoexcitation of **B** leads to virtually quantitative population of a ³CS state where an electron is transferred from the diaminobenzene donor to the naphthalenediketone acceptor. CS follows with the lifetime of 3.35 μ s in THF.³⁰ Nanosecond flash photolysis experiments of **C** gave transient absorptions assignable to the phenothiazine radical cation and bis(phenylethynyl)anthracene radical anion. The decay of the transient state is 36 μ s.³⁶

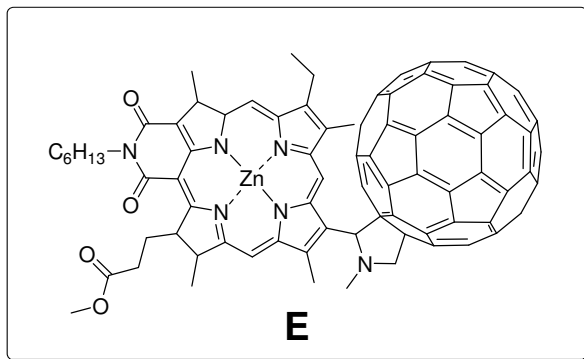


In addition to the fully organic compounds, metal-organic complexes became of interest during the last years because they accelerate the ISC rate to the ³CS state due to the heavy-atom effect. Some impressive examples of long-lived CS states in

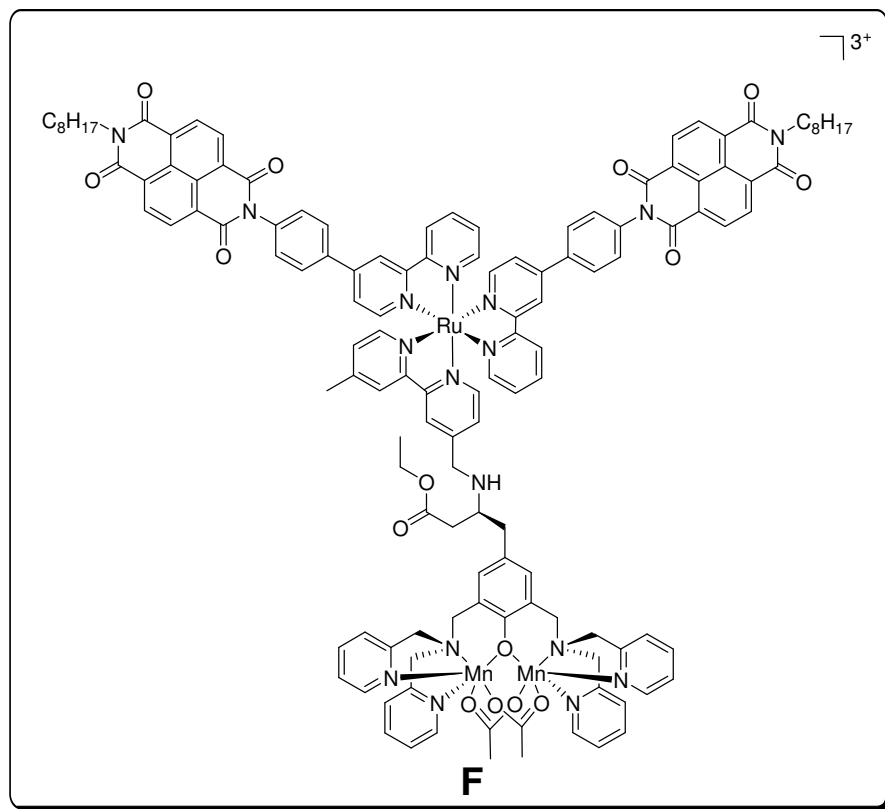
the millisecond range have been reported in systems based on tetrapyrrolic and/or fullerene units using Zn or Sn as metal center.^{28,29,38-47}



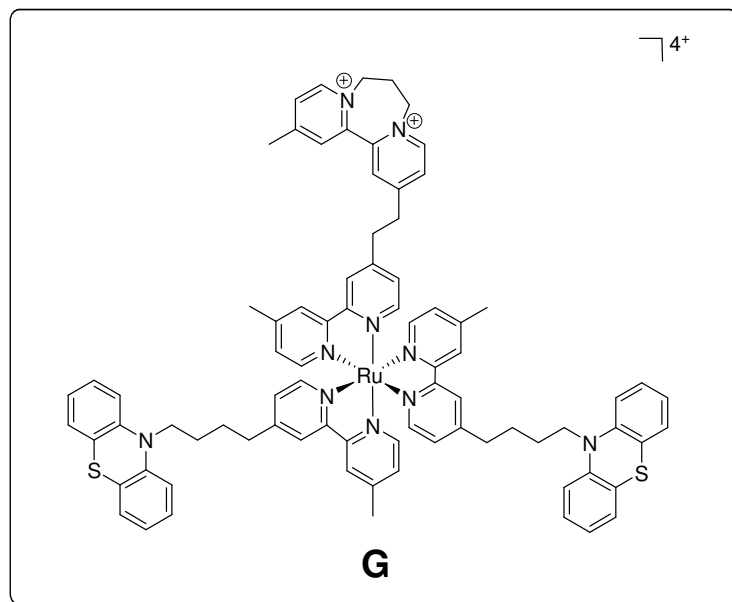
The formation of a CS state **Fc^{•+}-(ZnP)₃-C₆₀^{•-}** in triad **D** was confirmed by transient absorption spectroscopy. The CS state decays with a long lifetime of 0.53 s in DMF at 163 K.^{39,40} Ohkubo *et al.* showed that even compact dyads, as compound **E**, can display long-lived CS states. The Zinc Chlorin-C₆₀ dyad forms a ¹CS state within 10 ps that undergoes intersystem crossing to a longer-lived ³CS state lower in energy. CR is surprisingly slow with a lifetime of 230 μ s at room temperature in PhCN that increases dramatically at low temperatures (-150 °C) up to 2 h.^{8,47}



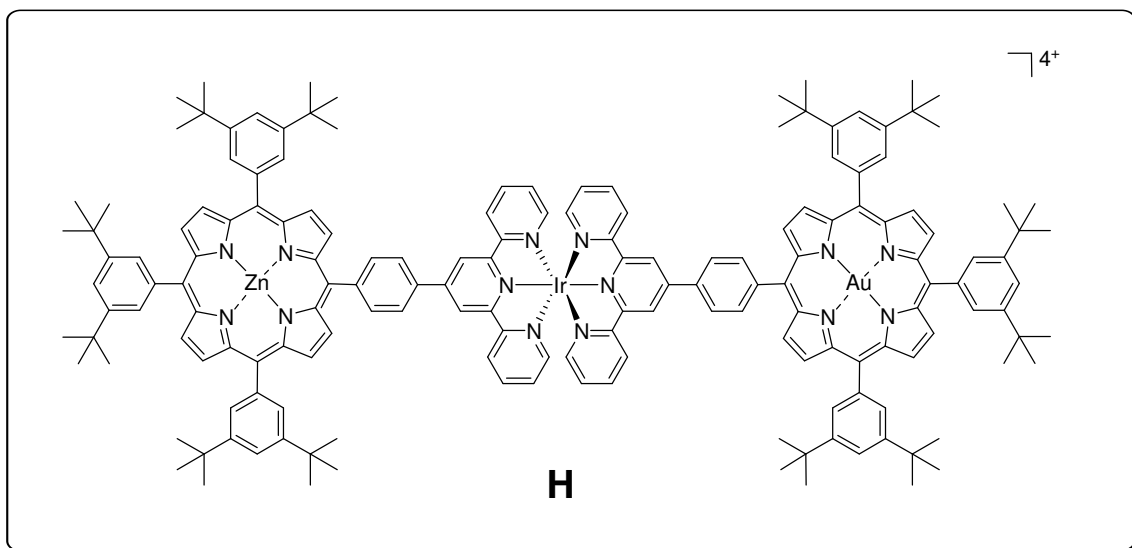
While Zn is the most usual transition metal used for such compounds, also complexes using lower d⁵, d⁶ or d⁷ elements have become of interest during the last years. Borgström *et al.*⁴⁸ designed a triad in which a manganese complex plays the role of the donor (**F**). The complex was reported to exhibit a light-induced CS process with the direct formation of the oxidised Mn₂^{II,III} dimer complex and the reduced naphthalenediimide acceptor moieties. The CS state is very long-lived with a lifetime of 600 μ s at room temperature in dichloromethane.



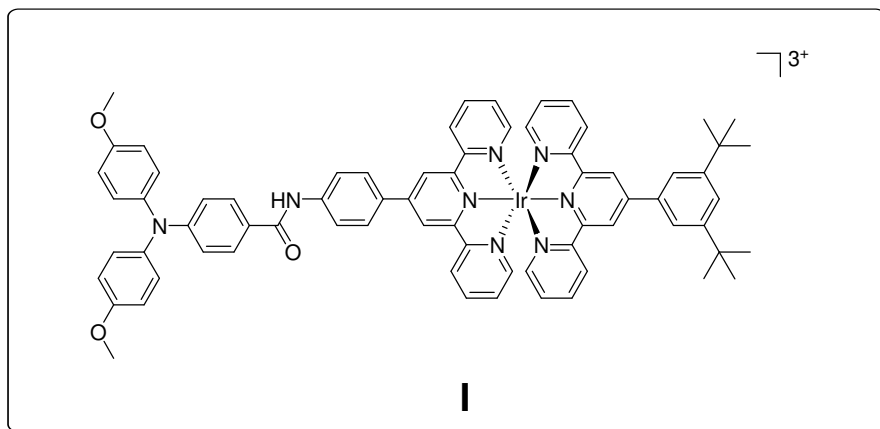
One compound that undergoes very fast and virtually complete ISC to the long lived ${}^3\text{MLCT}$ state is complex **G** published by Weber *et al.*^{49,50} The compound is based on a ruthenium(II)trisbipyridine $[\text{Ru}(\text{bpy})_3]^{2+}$ moiety, covalently linked to a N,N' -diquaternary-2,2'-bipyridinium salt (diquat, DQ^{2+}) electron acceptor and two phenothiazine (PTZ) donors. The chromophore absorbs into its MLCT state and subsequent formation of a species where the PTZ moiety is oxidised to PTZ^+ and diquat is reduced from DQ^{2+} to DQ^+ . In the following years triads based on transition metal compounds, especially $[\text{Ru}(\text{bpy})_3]^{2+}$, were studied intensely.^{32,41-44,49-62}



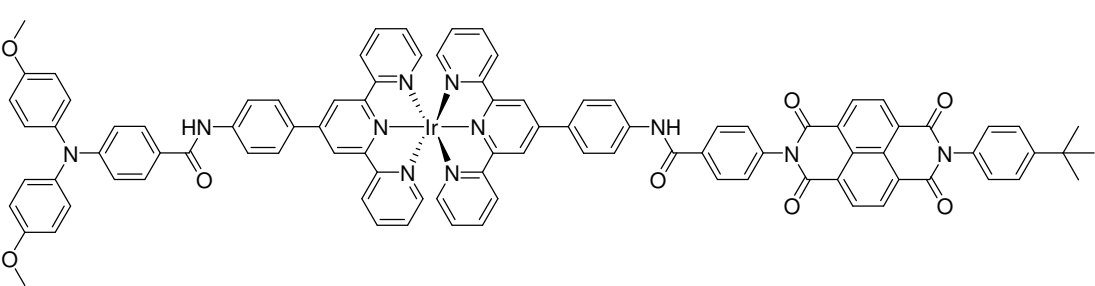
Also Flamingni *et al.* successfully studied long-lived CS states of ruthenium complexes. But due to the presence of a relatively low lying (1.9 eV for ruthenium(II)*bisterpyridine*) $^3\text{MLCT}$ state located on the Ru-core an energy transfer process from the porphyrin to the Ru(II) complex could efficiently compete with the desired electron transfer process. Using Ir(III) instead of Ru(II) this effect could be reduced because its $^3\text{MLCT}$ is higher in energy.^{32,41-44,56,57,63} Therefore, in 2000, they investigated triad **H** with an Ir(III)*bis*-terpyridine central complex with an excited state higher in energy (2.5 eV). The lifetime of the CS state is 450 ns.^{44,63}



Flamigni's latest compounds, **I** and **J**, show the influence of the acceptor unit on charge separation. The lifetime of the CS state of the donor-substituted **I** only is 70 ps. Much in contrast, **J** is one of the most successful examples of charge separation system based on transition metal compounds with a lifetime of 120 μs .^{41,43} Transient absorption analyses of the CS state of **J** show characteristic features of the triarylamine radical cation and the naphthalene bisimide radical anion.



1 Introduction



J

1.2 Transition Metal Complexes in Organic Light Emitting Devices

1.2.1 Introduction

In 1987 Tang *et. al.* invented a new electroluminescent device using organic materials as the emitting component. The new double-layer structure enabled a driving voltage below 10 V which was the key step for the development of commercially available organic light emitting devices (OLEDs).^{64,65} Friend *et. al.* introduced thin-film technologies with poly(*p*-phenylene-vinylene) (PVV) as light-emitting polymers in single-layer devices.⁶⁶ Since that time, the development of organic electronics proceeded rapidly and now OLEDs have become a strong competitor to traditional liquid-crystal technology. The attractive features of this new technology are the thin film structure, low weight, the possibility to fabricate on flexible substrates, high brightness at low voltages, large viewing angle, no need for background lighting and cheap production and maintenance.⁶⁷

1.2.2 Design and Functionality of OLEDs

Figure 1.4 shows the basic and simplified set-up of an OLED. Hole injection takes place from the anode into the highest occupied molecular orbital (HOMO) of the hole transporting layer (HTL). On the opposite side, electrons are injected (when applying a driving voltage of 5 to 10 V) from the metal cathode into the lowest unoccupied molecular orbital (LUMO) of the electron transporting layer (ETL). Now, the electrons from the one side and the holes from the other side hop via the LUMOs and HOMOs towards each other. When the two carriers of opposite charge meet they can recombine and build excitons. Excitons are neutral excited states that can diffuse through the material until they decay radiatively or nonradiatively.^{65,67-69} The HOMOs and LUMOs of the different organic layers must be adjusted keenly to avoid charge carrier trapping, unfavourable space charges and irregular hole and electron transports that may reduce the efficiency of OLEDs dramatically.

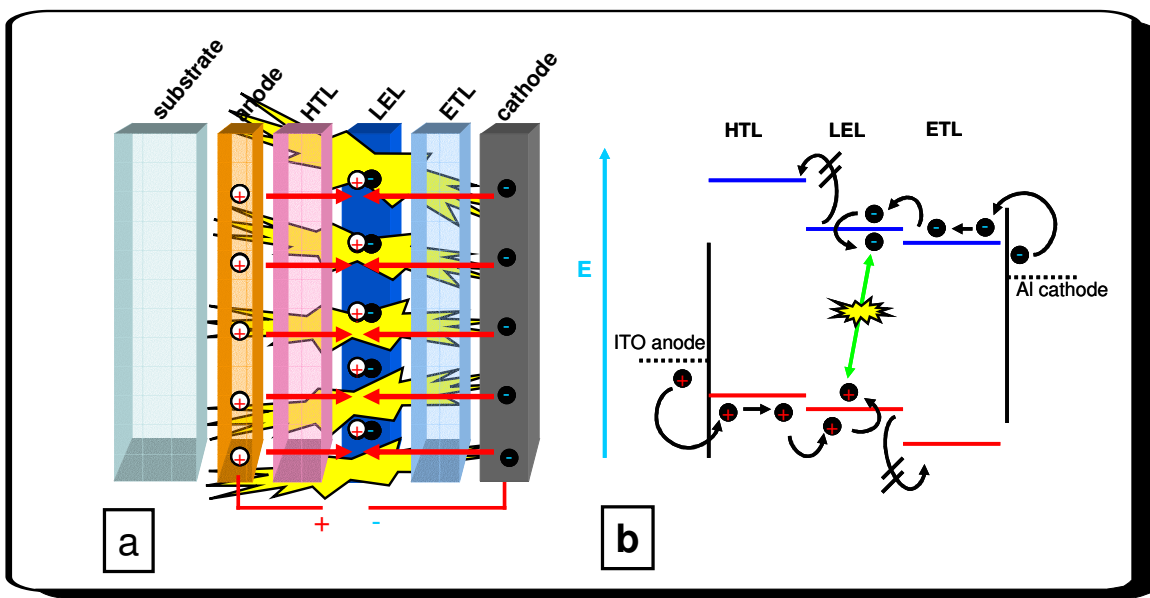
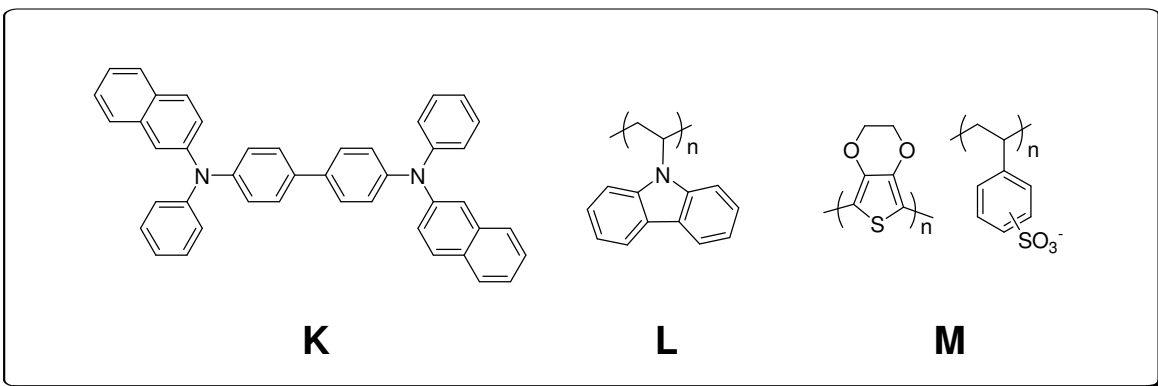


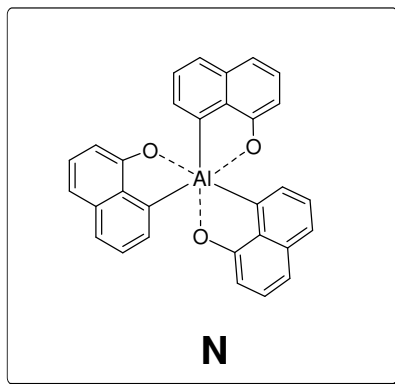
Figure 1.4 a) Basic set-up of a three-layer OLED structure. HTL = hole transporting layer; LEL = light emitting layer; ETL = electron transporting layer; b) Energy profile for a three-layer OLED. Lowest unoccupied molecular orbitals (LUMOs) are given in blue, highest occupied molecular orbitals (HOMOs) in red.

1.2.3 Materials for OLEDs

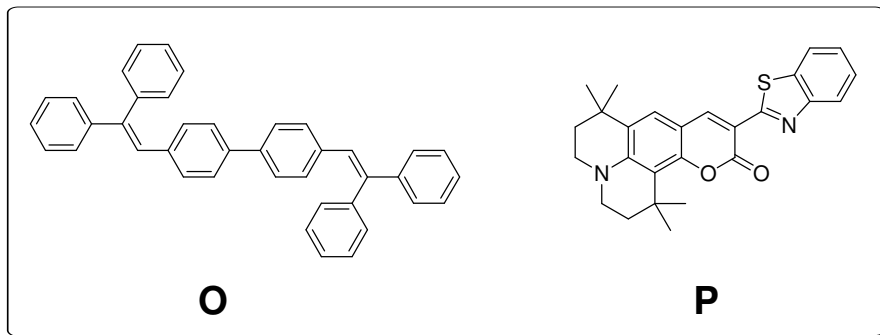
After years of intensive research the erstwhile OLED device structure has been improved considerably but is far from being optimal. The set-up of OLEDs in ongoing developments is much more complicated than the traditional one. Nowadays, additional layers are used, like the hole blocking layer which prevents holes to move to the cathode without recombining with electrons to form excitons or layers to improve hole and electron injection (HTL, ETL).⁶⁹⁻⁷¹ The anode is a transparent semiconducting layer that consists of a composite of SnO_2 and In_2O_3 , usually called ITO, coated on a glass substrate. ITO is used because of its low work function for hole injection into the HTL. The HTL usually consists of an organic compound with a HOMO as high in energy as the anode (to guarantee hole injection from the anode) and a HOMO-LUMO difference higher than that of the emitter in order to ensure favourable energetics for exciton formation. Hole conductors are electron donators, the most commonly used are triarylamine- and carbazole-derivates (i.e. **K** and **L**).^{64,67,72-77}



Nowadays, nearly all fabricated OLEDs have one additional layer between ITO and HTL to improve hole injection and substrate smoothness and to avoid the diffusion of indium into the HTL. For this purpose, PEDOT (poly(ethylenedioxythiophene)) doped with polystyrenesulfonic acid (PSS) **M** has been established.⁶⁹⁻⁷¹ The cathode mostly consists of a metal or a composition of metals that reduces the work function of electron injection into the ETL. Materials often used are Al, Mg, Ca, Al/LiF or Ag/MgAg.^{69,78-80} Electron transporters are characterised by a high electron affinity and should therefore be good electron acceptors. The most common electron transporter is Alq₃, **N**.

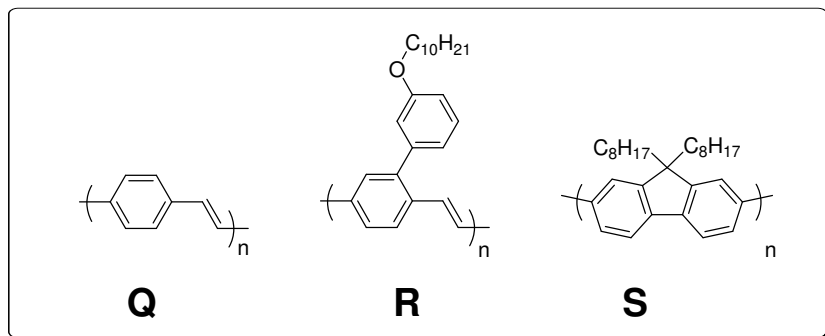


The emitters required are organic electroluminescent materials with high fluorescent quantum yields. Depending on their molecular weight they devide OLEDs in two groups, the SMOLEDs (small molecular organic light emitting devices) and the PLEDs (polymer light emitting devices). SMOLEDs are made of small molecules that can be thermally evaporated and therefore they can be coated by vapour deposition. Established small emitting molecules are, for example, the stilbene **O** (blue emitter at 480 nm) and the coumarin **P** (green emitter at 550 nm).⁸¹⁻⁸³



PLEDs have several advantages compared to SMOLEDs. They are easier in fabrication because they only consist of two polymer-films (conducting and emitting polymer) sandwiched between two electrodes. They operate at lower voltage, are more power-efficient and their manufacturing costs are lower because the polymers can be coated by ink-jet printing methods or solution processing (spin-coating).^{65,67}

Because light-emitting polymers have received remarkable attention during the last years there are lots of interesting compounds known by now.^{64-67,84-88} The most popular one is the poly(*p*-phenylenevinylene), PPV (**Q**) first used by Tang *et al.* in 1987.⁶⁴ However, its application was limiting because of its very low solubility. Therefore, soluble substituted PPV compounds were fabricated (i.e. **R**).⁸⁶ Polyfluorenes also are very promising materials because of their thermal stability, high photoluminescence and electroluminescence efficiency and their emission in the blue region (**S**).^{88,89}



1.2.4 Transition Metal Complexes as Triplet Emitters

OLEDs based on luminescent transition metal complexes found an increasing interest during the last couple of years.^{70,89-103} Figure 1.5 shows the effect of triplet harvesting in transition metal complexes and classical organic emitters. Compared with the typical organic molecular OLED emitters, transition metal compounds exhibit

faster and therefore more efficient intersystem crossing rates due to strong spin-orbit-coupling.

The excitons generated in the LEL (see Figure 1.4) are statistically formed with respect to their spin orientations as depicted in Figure 1.5. In this way, 25 % of the excitons are of singlet character, 75 % of triplet character. In this way, the lowest excited singlet and triplet states are populated. Organic molecules exhibit an efficient $S_1 \rightarrow S_0$ fluorescence while phosphorescence $T_1 \rightarrow S_0$ is usually negligible. The remaining 75 % triplet excitons are lost. Their energy is transferred into heat because of the small $T_1 \rightarrow S_0$ rate. Due to spin-orbit-coupling in heavy transition metal complexes the ISC rate into the lowest T_1 state is very efficient, thus no singlet emission can be observed. Besides, the radiative $T_1 \rightarrow S_0$ rate can become sufficiently high so that phosphorescence can occur. Thus, both singlet and triplet excitons contribute to the population of the lowest T_1 state. This implicates a maximal efficiency of light emission that is four times higher compared with singlet emitters.⁶⁹

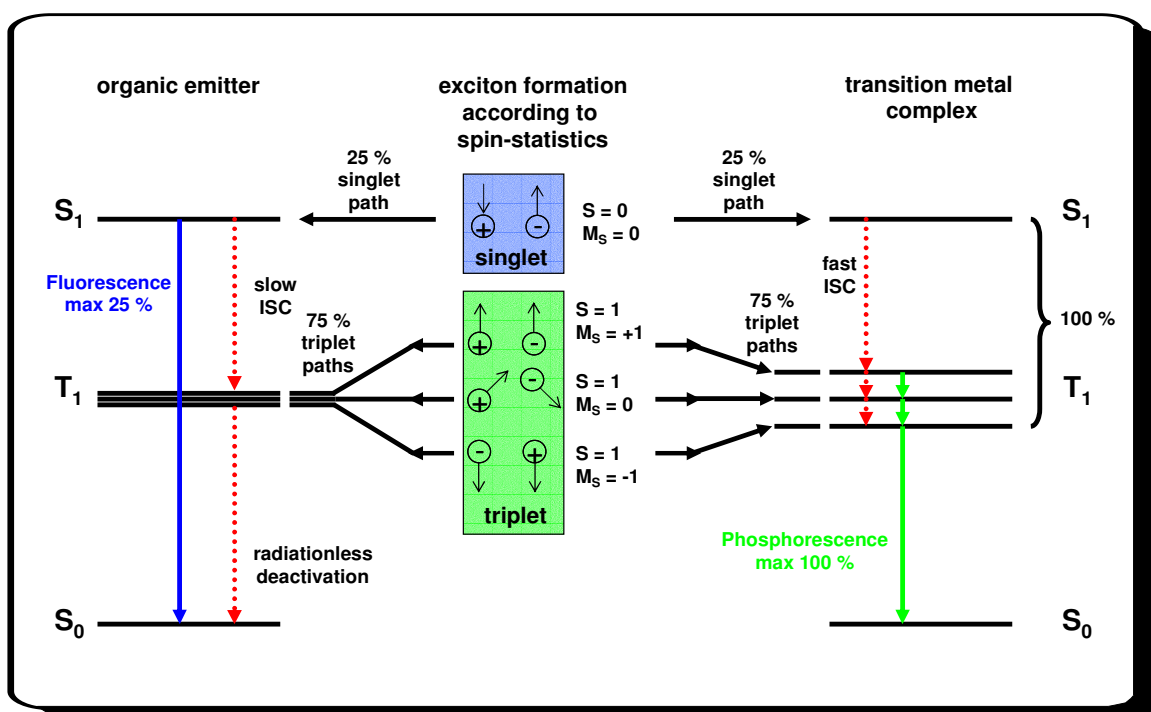
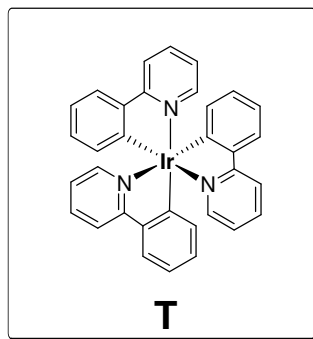


Figure 1.5 Diagram explaining the effect of triplet harvesting.⁶⁹

The spin-orbit coupling is a weak relativistic effect of the interaction of electron spin and its motion around the atomic nucleus. With increasing atomic number the number of nuclear charges increase and consequently the spin-orbit coupling also increases.¹⁰⁴ Phosphorescence is in principle a forbidden deactivation process

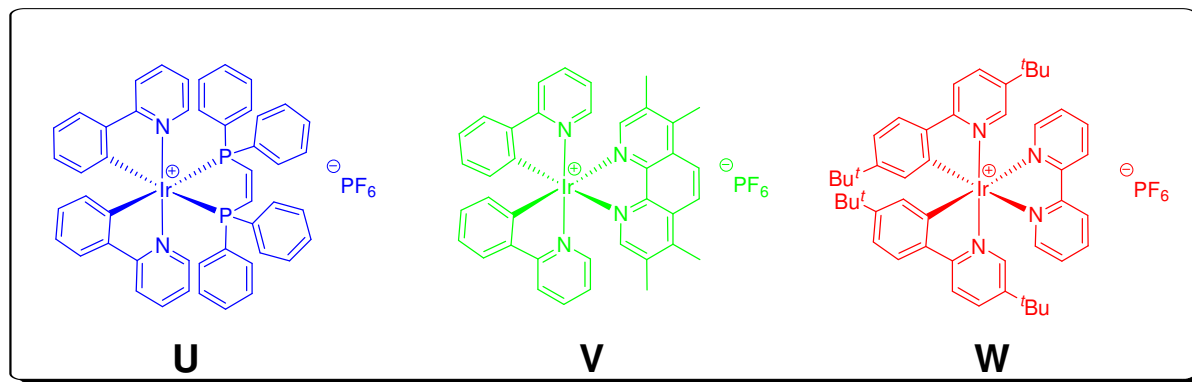
because of spin selection rules. It only gains allowance in organo-transition metal complexes, in which singlet and triplet states may be partially mixed due to spin-orbit coupling. Compared to organic molecules transition metal complexes can exhibit a ISC rate that is about 100 times faster. Thus, with increasing spin-orbit coupling the attribution of defined spin-multiplicities becomes diffuse. Especially for 4d- and 5d-complexes the exact classification of the states is nearly impossible. In praxis, it is useful to discriminate by the lifetimes of the transient states. Phosphorescence, caused by the decay of a triplet state have a much longer (in the μs -regime) lifetime than fluorescence from a singlet state.¹⁰⁵

Particularly neutral *tris*-orthometalated iridium complexes have been studied extensively and have successfully been used for OLED applications.^{71,94,102,106-112}. The green emitting *fac*-*tris*(2-phenylpyridine) iridium, Ir(ppy)₃ (**T**), is the most popular and most commonly used green phosphorescent emitter for OLED applications.^{67,69,113}



Recently, mixed ligand cationic iridium complexes (with PF₆⁻ or ClO₄⁻ as counterions) have become a new alternative to these neutral complexes.^{96,99,100,103,114-119} These ion pairs can easily be used for the fabrication of solid-state light emitting electrochemical cells (LECs) that have several advantages compared with OLEDs.^{103,109} The device fabrication of LECs is easier than that of OLEDs because no multilayer structure is required. The complexes are directly spin-coated onto a hole-injecting material. When applying an electric field, the negatively charged mobile counterions migrate to the anode. As a consequence of these space charges the electric field at the electrode is higher which enhances the electron injection at low voltages.^{68,120-124} The luminescent transition metal complexes can be synthesised and purified easily compared to polymers. They show excellent electrochemical, photochemical and thermal stability. Their excited states have high photoluminescence efficiencies and long lifetimes. Furthermore, the emission colour of LECs can readily be tuned by modification of the coordinating ligands.

Lowry *et al.* published a series of cationic iridium(III) luminophores with a high colour versatility depending on the modification of the ligands.¹¹⁷ The blue emitting Ir complex has a *cis*-1,2-bis(diphenylphosphino)ethylene ligand (**U**). The replacement of the cyclometalating ligand by 3,4,7,8-tetramethyl-1,10-phenanthroline gives a green emitting complex (**V**). The substitution of the C^N ligand by *tert*-butyl substituents results in a bipyridyl complex that emits in the red region (**W**).



1.2.5 State of the Art

Although the usage of phosphorescent emitters has led to an improvement of the quantum efficiency of OLEDs, there is a loss of efficiency by triplet-triplet-annihilation (TTA) of the complexes at high chromophore concentration. Because of their long transient lifetime the probability of saturation of the phosphorescent sites is increased. Consequently, there is a higher interaction between the triplets that leads to a loss of triplet excitons into the ground state as shown in Equation 1.4.¹²⁵⁻¹²⁹

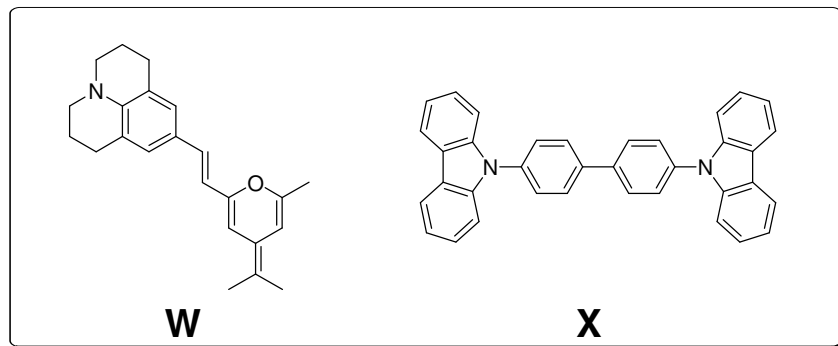


³(DA)* represents the triplet excited state, ¹(DA)* the singlet excited state and DA the ground state of the molecule. The TTA depends on the phosphorescence lifetime and the concentration of phosphorescent sites. To impede TTA the lifetimes should be chosen accurately because lifetimes which are too long promote the TAA.^{125,128}

To avoid this waste of triplet excitons, Baldo *et. al.* explored OLEDs charged with low concentrations of a fluorescent dye (**W**) additional to the triplet emitter **T** in order to transfer the excessive amount of triplets that are formed after electrical excitation into a singlet excited state of the fluorescent dye.¹²⁶ Thus, the triplets that

1 Introduction

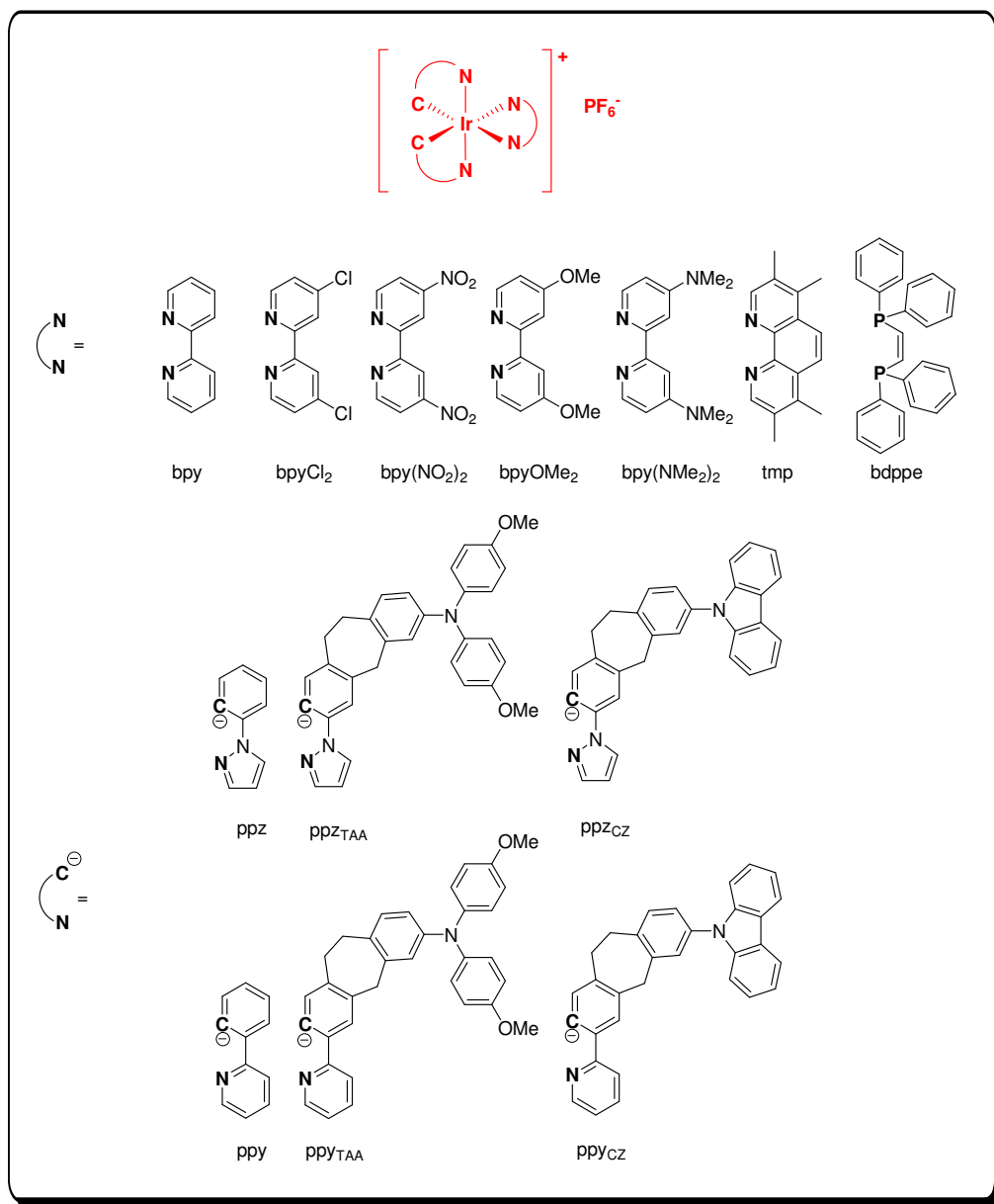
are formed after electrical excitation are not wasted, but transferred to the singlet excited state of the fluorescent dye.



To reduce the amount of TTA the triplet emitters are usually doped into a suitably selected matrix material. Therefore the triplet energy of the matrix material has to lie at higher energies than that of the triplet emitter. Otherwise, the emission of the dopants also would be quenched. The most commonly used emitter layer for OLEDs is $\text{Ir}(\text{ppy})_3$ (**S**) doped into the hole transporting polymer PPV (**Q**).⁸⁴⁻⁸⁸ Baldo *et al.* described devices with increased efficiency using 4,4'-*N,N*-dicarbazole-biphenyl (CBP) (**X**) as host for $\text{Ir}(\text{ppy})_3$.^{69,107}

1.3 Project Aim

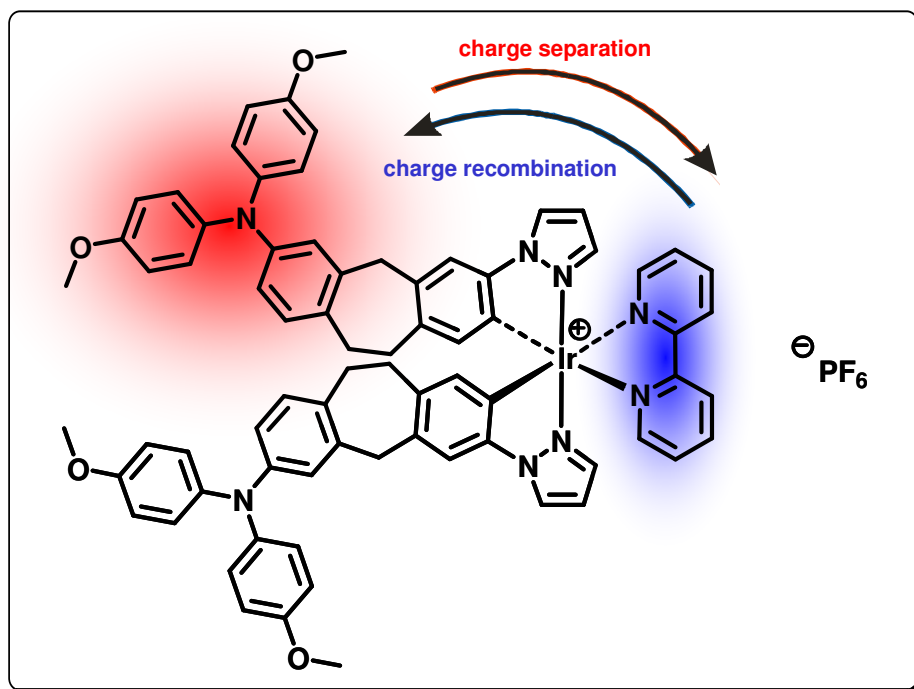
One goal of this work is to connect the cyclometalated iridium triplet emitters directly with two equivalent donor components in order to construct relatively small and simple (donor_2)-acceptor ($\text{D}_2\text{-A}$) molecules which may display long-lived CS states. Triarylamine (TAA) and carbazole (CZ) were chosen as the donor units (D) because of their high lying triplet states (TAA: 3.05 eV, CZ: 3.04 eV).¹³⁰⁻¹³³ These donor units are directly linked to the cyclometalating C^N ligands phenylpyrazole and phenylpyridine. Bidentate N^N and P^P donor ligands shall be used as acceptor (A) units (Scheme 1.1 and 1.2).



Scheme 1.1 (Donor_2)-acceptor molecules with triarylamine (TAA) and carbazole as donor units and N^N and P^P ligands as acceptor units.

Furthermore, as TAA and CZ are well-known hole conducting compounds, their direct connection to the triplet emitter can serve as a matrix for the triplet excited complexes to avoid triplet-triplet-annihilation. The directly attached hole transport units will also influence charge injection in LEC and ion mobility, both aspects that are crucial for LEC device performance.

Thus, a new series of cationic phenylpyrazole (ppz) and phenylpyridine (ppy) iridium complexes depicted in Scheme 1.1 were synthesised.¹³⁴ TAA and CZ are linked to the phenylpyrazole / phenylpyridine via a methylene and an ethylene bridge in order to minimise conformational flexibility of the hole transport moieties. Ppy and ppz substituted Ir-complexes have been investigated extensively during the last years, especially for their application in the field of organic light-emitting diodes.^{99,103,110,135-137} Therefore, the cationic phenylpyrazole iridium complex was chosen because of its strong emission in the blue and green region.^{103,135} The phenylpyridine complexes were chosen because of their higher quantum yields and because of their similarity to published D-A-Ir compounds.³²



Scheme 1.2 Example of a (donor)₂-acceptor molecule with triarylamine (TAA) as donor and bipyridyl (bpy) as acceptor.

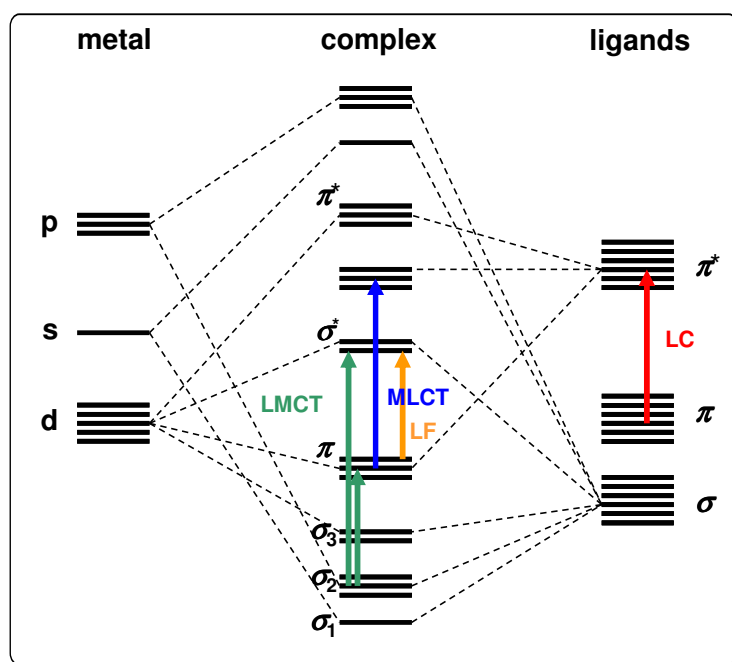
The goal of this project is primarily to describe the photophysical (absorption and emission spectroscopy, time resolved fluorescence spectroscopy) and

electrochemical (cyclic voltammetry and spectroelectrochemistry) properties of such complexes and to characterise their excited states by transient absorption spectroscopy. The luminescent compounds shall also be tested whether they might be useful for LEC applications.

2 Cyclometalated Transition Metal Complexes

2.1 Structure and Energy Levels

For a better understanding of the spectroscopic measurements some important facts about the structure and especially about the energy levels of Ir(III) complexes have to be discussed. First, the photoluminescence behaviour of these compounds is determined by the properties of their emitting states which is therefore closely related to their molecular orbitals.



Scheme 2.1 MO scheme of an octahedral transition metal complex including π -interactions as well as σ -interactions. The most common transitions are demonstrated.¹⁰⁵

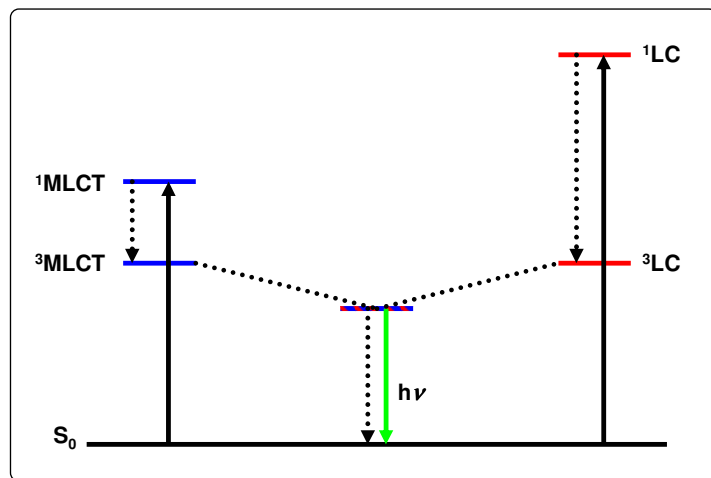
The most important transitions in octahedral complexes are illustrated in Scheme 2.1. The ligand field (LF) transitions take place between orbitals with d-character. There are two types of charge transfer (CT) transitions, the ligand-to-metal-CT (LMCT) and the metal-to-ligand-CT (MLCT) transition. The MLCT transitions occur between occupied metal orbitals and unoccupied ligand orbitals, whereas in LMCT transitions the direction is opposite. In addition to these transitions there are typical spin-allowed $\pi-\pi^*$ ligand-centered (LC) transitions.¹⁰⁵

Iridium (III) has the electronic configuration [Xe] 6s⁰ 4f¹⁴ 5d⁶. The complexes show a high ligand-field stabilization energy and therefore less thermally accessible nonemissive ³MC (metal-centered) states. This is the reason why *bis*-cyclometalated Ir(III) compounds more and more replace the Ru(II) complexes in their function as triplet emitters and in other photochemical and photophysical investigations.^{98,117,138-140}

³MLCT and ³LC transitions are commonly observed in most of the presently investigated mixed-ligand complexes. The ³MLCT transition arises from the promotion of an electron coming from one filled d-orbital of the metal into a vacant π -orbital of the neutral N⁺N ligand. The ³LC transition typically results from the excitation of electrons between the occupied and the vacant π -orbitals of the cyclometalating C⁺N ligand (Scheme 2.1).

Caused by spin-orbit coupling, fast ISC enables the formation of a triplet state with mixed LC/MLCT character in which *a* and *b* refer to the contributions of the ³MLCT and ³LC states, respectively. (Scheme 2.2, Equation 1.5).^{117,138}

$$\Psi_{T_1} = a \Psi_{\text{MLCT}} + b \Psi_{\text{LC}} \quad (1.5)$$



Scheme 2.2 Formation of a mixed excited triplet state containing of ³MLCT and ³LC transitions assuming $a \approx b$.

This excited-state mixing occurs when the overlap between ³MLCT and ³LC is sufficient. This can be controlled by a deliberate adjustment of the energy of the lowest excited states by substituent effects or different ligands.¹¹⁷ Also the environment influences whether the ³LC or the ³MLCT is the lowest excited state.

2 Cyclometalated Transition Metal Complexes

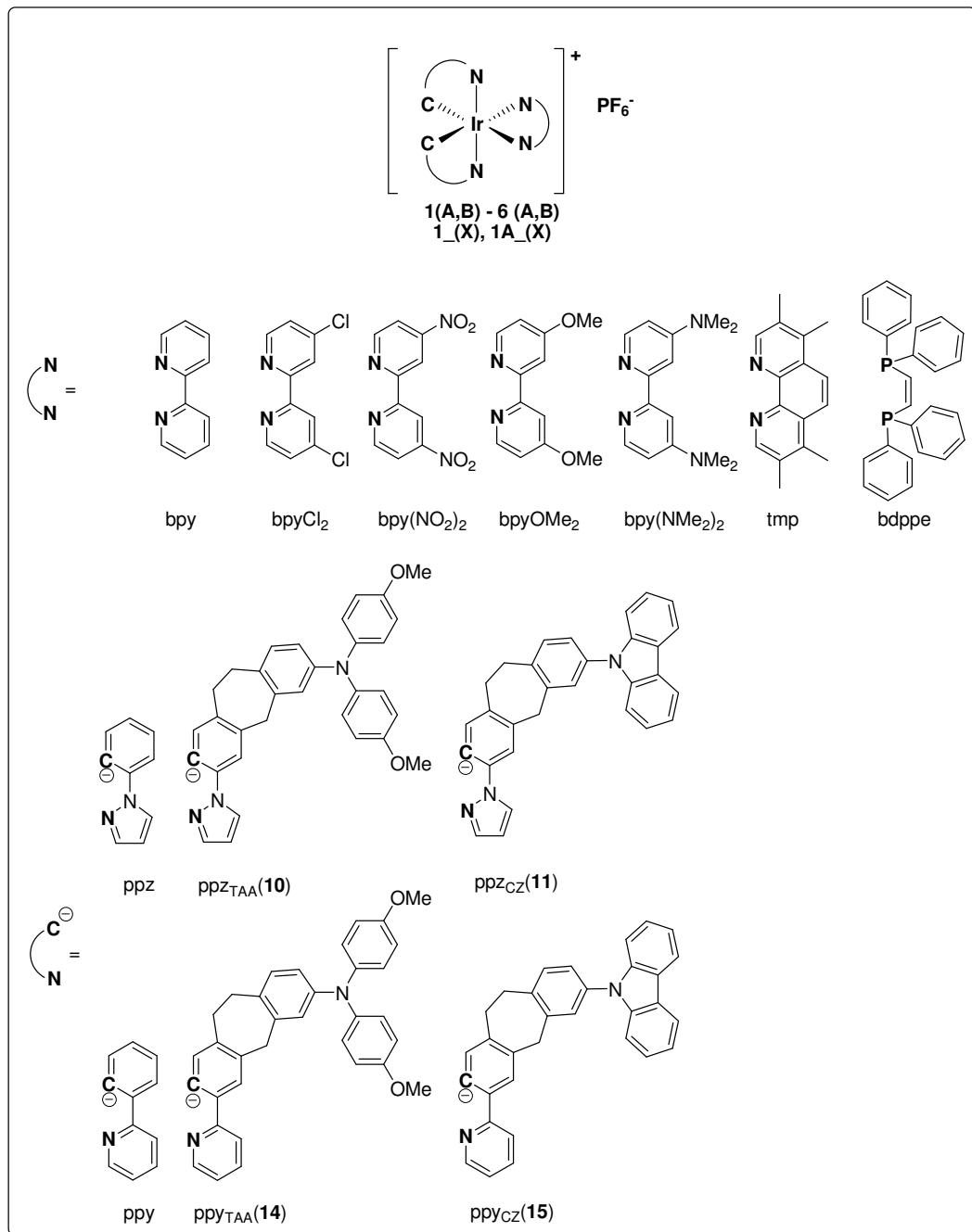
The $^3\text{MLCT}$ state is stabilised in solutions and glasses at RT, while at low temperatures this order is reversed. Due to the enhanced rigidity of the host at low temperatures, the $^3\text{MLCT}$ state moves up to an energy that is similar to that of the ^3LC what causes the LC/MLCT mixing.

The emission bands of the $^3\text{MLCT}$ transitions are broad and featureless with lower energies than the blue-shifted structured ^3LC transitions. $^3\text{MLCT}$ transitions are typical of solutions at room temperature. By lowering the temperature the energy of the $^3\text{MLCT}$ rises and superimposes or even crosses the ^3LC transition (Scheme 2.2). For this reason phosphorescence spectra of most of the iridium mixed-ligand complexes show mixed excited states at low temperatures. The energy of this mixed excited state can be controlled by an accurate adjustment of metal and ligand orbitals.^{94,99,102,115,116,138,141-147}

All complexes of the type $(\text{C}^{\text{N}})^2\text{Ir}(\text{N}^{\text{N}})$ show C_2 symmetry as confirmed by ^1H NMR measurements. The NMR spectra indicate that only a single isomer is present, because no detectable impurities due to a mixture were found. For the *cis*-1,2-bis(diphenylphosphino)ethylene (bdppe) complexes the C_2 symmetry is broken. The phosphorus atoms are not equivalent. This asymmetry has consequences for the ^1H and ^{13}C NMR signals as shown in the experimental section.¹⁴⁸⁻¹⁵⁰

2.2 Cationic Iridium Complexes

Our goal was the synthesis of the compounds depicted in Scheme 2.3. Complexes **1 – 6** are serving as references complexes without hole transporting component. **A** identifies the triarylamine (TAA) substituted compounds, **B** the carbazole (CZ) substituted ones. **1 – 3** are the phenylpyrazole complexes and **4 – 6** the phenylpyridyl complexes. **1_(X)** and **1A_(X)** describe the phenylpyrazole references and TAA-substituted complexes with differently substituted bipyridyl ligands.

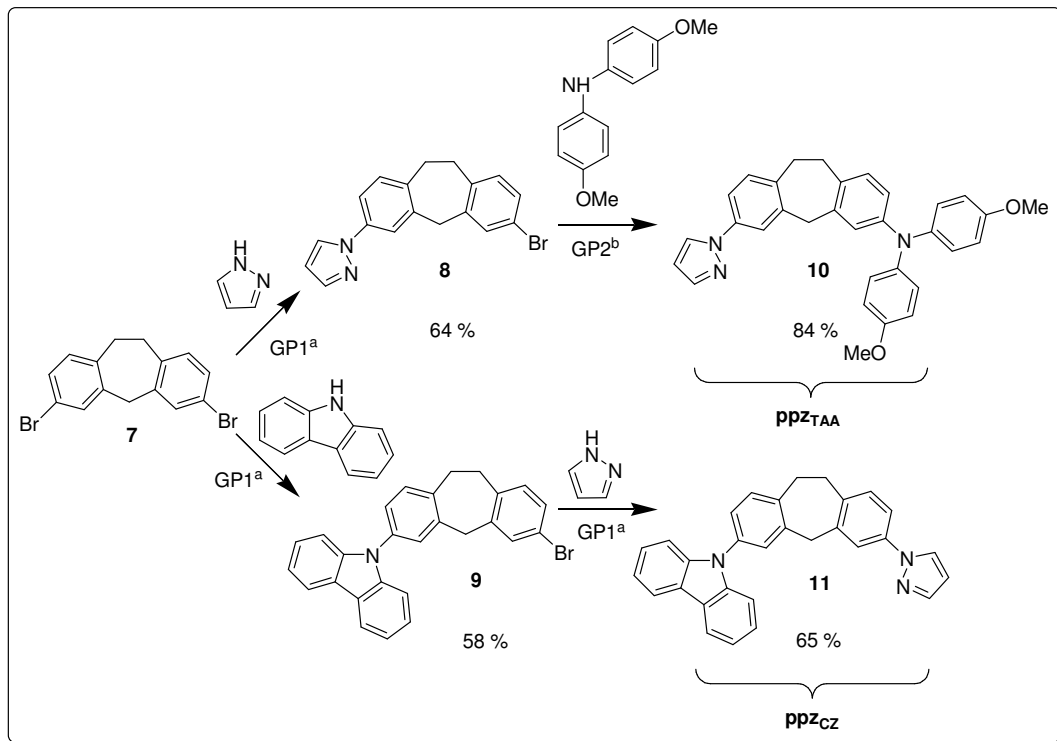


Scheme 2.3 Synthesised compounds.

2.2.1 Synthesis

2.2.1.1 The Ligands

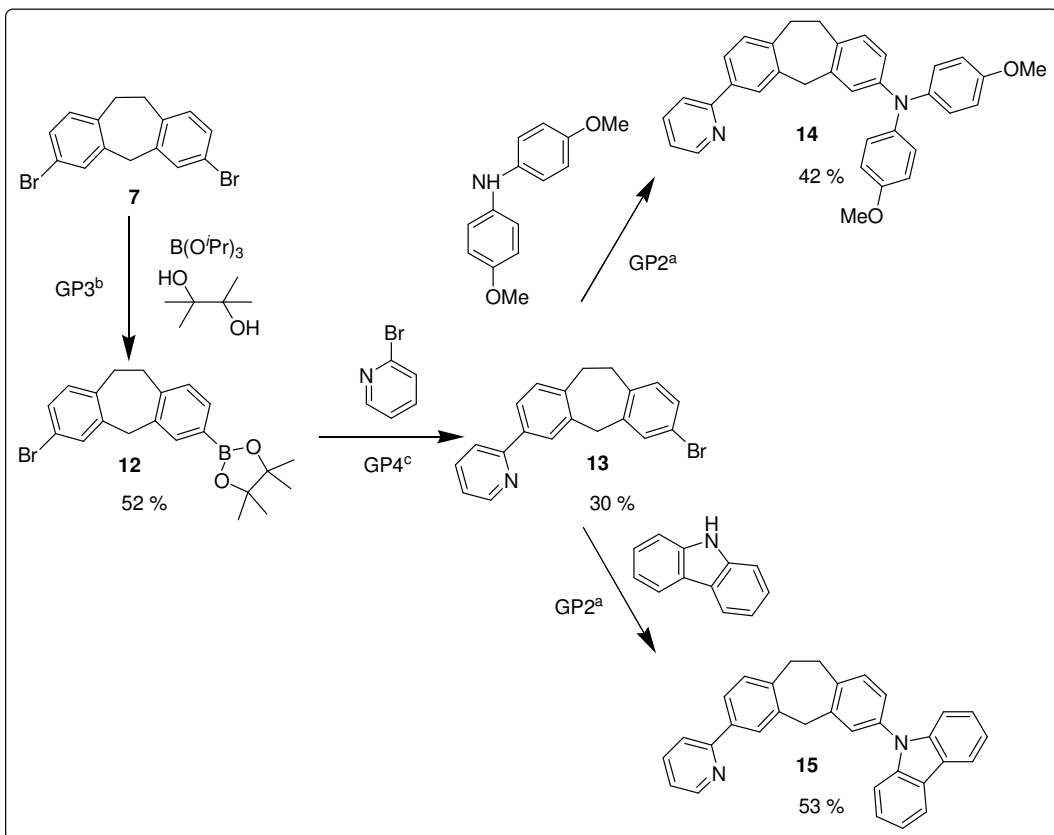
The triarylamine- and carbazole-substituted cyclometalating phenylpyrazole and phenylpyridyl ligands for the complexes **1**, **1A**, **1B** to **6**, **6A**, **6B** were synthesised from 3,7-dibromo-10,11-dihydro-5*H*-dibenzo[a,d]cycloheptene **7** (Scheme 2.4).^{134,151} Carbazole and pyrazole were attached via copper catalysed couplings to yield **8** and **9**.¹⁵² The triarylamine-substituted ligand **10** was obtained by palladium-catalysed Buchwald-Hartwig amination with 4,4'-dimethoxydiphenylamine.¹⁵³⁻¹⁵⁷ The carbazole-substituted ligand **11** was obtained by copper-catalysed amination with phenylpyrazole. Several attempts to couple **8** directly to carbazole gave no product and the two different synthetic routes to synthesise **10** and **11** had to be followed.



Scheme 2.4 Synthesis of the triarylamine- and carbazole-substituted phenylpyrazole ligands.

^a GP1: arylamine, CuI, *trans*-1,2-cyclohexanediamine, potassium phosphate; dioxane, 110 °C, 24 h. ^b GP2: arylamine, Pd₂(dba)₃·CHCl₃, NaO*t*Bu, *P**t*Bu₃; toluene, 80 °C, 12 h.

The triarylamine- and carbazole-substituted cyclometalating phenylpyridyl ligands for the complexes **4**, **4A**, **4B** to **6**, **6A**, **6B** also were synthesised from 3,7-dibromo-10,11-dihydro-5H-dibenzo[a,d]cycloheptene **7** (Scheme 2.5).¹⁵¹

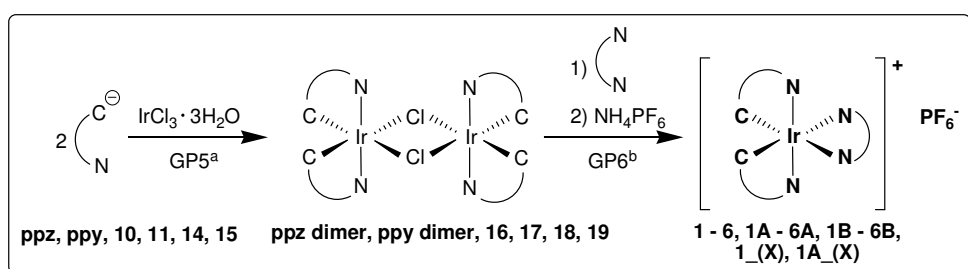


Scheme 2.5 Synthesis of the triarylamine- and carbazole-substituted ligands. ^a GP2: arylamine, $Pd_2(dba)_3 \cdot CHCl_3$, $NaO'Bu$, $P'Bu_3$; toluene, $80\text{ }^\circ C$, 12 h. ^b GP3: arylhalide, $nBuLi$, triisopropylborate, pinacol, Et_2O , reflux, 24 h. ^c GP4: arylhalide, Cs_2CO_3 , $Pd(PPh_3)_4$, dioxane, reflux, 24 h.

The pinacoborane **12** was obtained by lithiation of **7** followed by reaction with pinacol.¹⁵⁸⁻¹⁶⁰ The pyridyl-substituted compound **13** then was obtained by a palladium-catalysed Suzuki coupling with bromopyridine.¹⁶⁰ This precursor was used to prepare the two ligands **14** and **15** by palladium-catalysed Buchwald-Hartwig-amination with 4,4'-dimethoxydiphenylamine and carbazole, respectively.¹⁵³⁻¹⁵⁵

2.2.1.2 The Cationic Ir(III) Complexes

The dichloro-bridged Ir(III) dimers were synthesised following the classical method published by Nonoyama *et al.*. Thus, the reaction of the cyclometalating ligands **10**, **11**, **14**, **15** were treated with $\text{IrCl}_3 \cdot 3\text{H}_2\text{O}$ in 2-ethoxyethanol/water 3:1 at 100 °C for 12 h (Scheme 2.6).¹⁶¹ The synthesis of the dichloro-bridged dimers with phenylpyrazole and phenylpyridyl as precursor for the reference complexes **1 – 6** are known in literature.^{103,117,161}



Scheme 2.6 Synthesis of the cyclometalated complexes **1 – 6, 1A – 6A, 1B – 6B**. ^a GP5: $\text{IrCl}_3 \cdot 3\text{H}_2\text{O}$, 2-ethoxyethanol : $\text{H}_2\text{O} = 3 : 1$, 100 °C, 12 h. ^b GP6: CH_2Cl_2 , reflux, 12 h.

The mixed-ligand complexes (see Table 2.1) then were prepared in dry dichloromethane by reaction of the corresponding dichloro-bridged iridium(III) dimer (**16 – 19**) with neutral (N^\wedgeN , P^\wedgeP) ligand, followed by metathesis with NH_4PF_6 .^{100,103,114,117}

Table 2.1 Synthesised complexes **1 – 6, 1A – 6A, 1B – 6B**.

ligands	ppz		ppy	
bpy	$[\text{Ir}(\text{ppz})_2\text{bpy}]\text{PF}_6$	1 ¹⁰³	$[\text{Ir}(\text{ppy})_2\text{bpy}]\text{PF}_6$	4 ⁹⁵
	$[\text{Ir}(\text{ppz}_{\text{TAA}})_2\text{bpy}]\text{PF}_6$	1A ¹³⁴	$[\text{Ir}(\text{ppy}_{\text{TAA}})_2\text{bpy}]\text{PF}_6$	4A
	$[\text{Ir}(\text{ppz}_{\text{CZ}})_2\text{bpy}]\text{PF}_6$	1B	$[\text{Ir}(\text{ppy}_{\text{CZ}})_2\text{bpy}]\text{PF}_6$	4B
tmp	$[\text{Ir}(\text{ppz})_2\text{tmp}]\text{PF}_6$	2	$[\text{Ir}(\text{ppy})_2\text{tmp}]\text{PF}_6$	5 ¹⁰⁰
	$[\text{Ir}(\text{ppz}_{\text{TAA}})_2\text{tmp}]\text{PF}_6$	2A	$[\text{Ir}(\text{ppy}_{\text{TAA}})_2\text{tmp}]\text{PF}_6$	5A
	$[\text{Ir}(\text{ppz}_{\text{CZ}})_2\text{tmp}]\text{PF}_6$	2B	$[\text{Ir}(\text{ppy}_{\text{CZ}})_2\text{tmp}]\text{PF}_6$	5B
bdppe	$[\text{Ir}(\text{ppz})_2\text{bdppe}]\text{PF}_6$	3	$[\text{Ir}(\text{ppy})_2\text{bdppe}]\text{PF}_6$	6
	$[\text{Ir}(\text{ppz}_{\text{TAA}})_2\text{bdppe}]\text{PF}_6$	3A	$[\text{Ir}(\text{ppy}_{\text{TAA}})_2\text{bdppe}]\text{PF}_6$	6A
	$[\text{Ir}(\text{ppz}_{\text{CZ}})_2\text{bdppe}]\text{PF}_6$	3B	$[\text{Ir}(\text{ppy}_{\text{CZ}})_2\text{bdppe}]\text{PF}_6$	6B

Table 2.1 shows the synthesised complexes with varying neutral (N^N , P^P) ligands 2,2'-bipyridyl (bpy), 3,4,7,8-tetramethyl-1,10-phenanthroline (tmp) and *cis*-1,2-bis(diphenylphosphino)ethylene (bdppe), which are all commercially available. To probe the influence of the electron density of the bpy ligand on the photophysical properties in detail, complexes **1** and **1A** were modified by attaching substituents with different donor- and acceptor- character (Table 2.2).

Table 2.2 Synthesised complexes **1_(X)** and **1A_(X)** with different substituents.

[Ir(ppz) ₂ bpy]PF ₆	1 ¹⁰³	[Ir(ppz _{TAA}) ₂ bpy]PF ₆	1A
[Ir(ppz) ₂ bpy(NO ₂) ₂]PF ₆	1_NO₂	[Ir(ppz _{TAA}) ₂ bpy(NO ₂) ₂]PF ₆	1A_NO₂
[Ir(ppz) ₂ bpyCl ₂]PF ₆	1_Cl	[Ir(ppz _{TAA}) ₂ bpyCl ₂]PF ₆	1A_Cl
[Ir(ppz) ₂ bpy(OMe) ₂]PF ₆	1_OMe ¹⁰³	[Ir(ppz _{TAA}) ₂ bpy(OMe) ₂]PF ₆	1A_OMe
[Ir(ppz) ₂ bpy(NMe ₂) ₂]PF ₆	1_NMe₂	[Ir(ppz _{TAA}) ₂ bpy(NMe ₂) ₂]PF ₆	1A_NMe₂

The bpy ligands 4,4'-dinitro-2,2'-bipyridyl (bpy(NO₂)₂), 4,4'-dichloro-2,2'-bipyridyl (bpyCl₂) and 4,4'-dimethoxy-2,2'-bipyridyl (bpy(OMe)₂) are all commercially available except of bpy(NMe₂)₂. This ligand was synthesised according to literature by refluxing 4,4'-dichloro-2,2'-bipyridyl in DMF for one week.^{162,163}

2.2.2 Redox Properties

The electrochemical properties of the *bis*-cyclometalated complexes were examined by using cyclic voltammetry. All compounds were measured in acetonitrile containing 0.1 M tetrabutylammonium hexafluorophosphate at 100 mV s⁻¹ scan rate. A summary of the redox potentials vs ferrocene/ferrocenium is listed in Tables 2.3, 2.4 and 2.5. All complexes show one reduction that can be assigned to the reduction of the neutral (N^N , P^P) ligands, an interpretation supported by DFT calculations by Thompson *et al.*¹⁰³ The bpy can be reduced a higher potential than the tmp and the bdppe ligands.

2 Cyclometalated Transition Metal Complexes

Table 2.3 Redox properties of the cyclometalated ppz-complexes and their ligands in acetonitrile.

	$E_{1/2}^{\text{Ox}}$ (Ir) / mV	$E_{1/2}^{\text{Ox}}$ (CZ) / mV	$E_{1/2}^{\text{Ox}}$ (TAA) / mV	$E_{1/2}^{\text{Red}}$ (N^N, P^P) / mV	$\Delta E_{1/2} = E^{\text{Ox}} - E^{\text{Red}}$ / mV
ppz_{TAA} (10)			180 ^r		
ppz_{CZ} (11)		890 ⁱ			
1	935 ^r			-1800 ^r	2735
1A	900 ⁱ		230 ^r	-1800 ^r	2030
1B	910 ⁱ	910 ⁱ		-1800 ^r	2710
2	890 ^r			-2010 ^r	2900
2A	800 ⁱ		180 ^r	-2050 ^r	2230
2B	840 ⁱ	840 ⁱ		-2010 ^r	2850
3	1150 ⁱ			-2330 ^r	3480
3A	920 ⁱ		240 ^r	-2310 ^r	2550
3B	1040 ⁱ	950 ⁱ		-2300 ^r	3250

^rreversible, ⁱirreversible

Furthermore, all of the complexes exhibit one oxidation wave at about 0.90 V that is associated with the *bis*-cyclometalated phenyl-Ir moiety.^{94,102,139,141,142,164-168}

The data of the literature-known complexes **1**, **1_OMe** and **4** are consistent with the literature;^{93,97,99,101-103} redox potentials of **2**, **3**, **5** and **6** are not published. The carbazole- and triarylamine-substituted complexes show one additional oxidation wave, respectively, compared to the reference compounds (Figure 2.1).

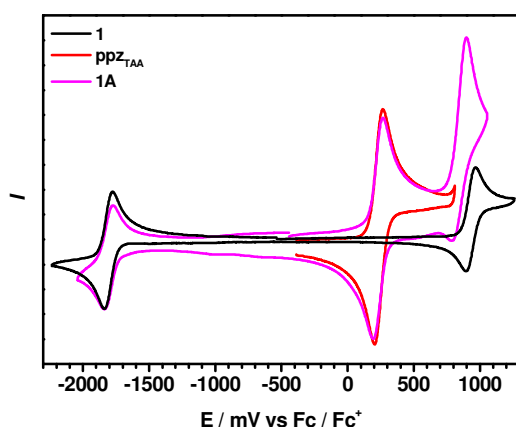


Figure 2.1 CV of the complexes **1**, **1A** and the free ligand in 0.1 M MeCN/TBAH, $v = 100 \text{ mVs}^{-1}$.

The characteristic oxidation waves of the triarylamines are in the region 0.18 – 0.24 V and are all reversible under thin layer conditions.¹⁶⁹⁻¹⁷¹

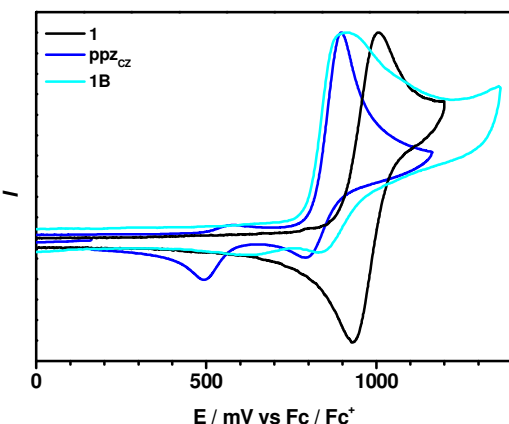


Figure 2.2 CV of the oxidation waves of the complexes **1**, **1B** and the free ligand in 0.1 M MeCN/TBAH, $v = 100 \text{ mVs}^{-1}$.

On the contrary, the oxidation waves of the carbazole substituted compounds are all irreversible as also reported in literature.¹⁷² The redox potentials of the carbazole complexes (0.84 – 0.95 V) is quite in the same region as the oxidation of the phenyl-Ir moiety. Figure 2.2 shows the superposition of the two oxidation waves. There are only minor deviations between the redox potentials of the ppz and the ppy complexes. (Table 2.3 and 2.4)

Table 2.4 Redox properties of the cyclometalated ppy-complexes and their ligands in acetonitrile.

	$E^{\text{Ox}}_{1/2}$ (Ir) / mV	$E^{\text{Ox}}_{1/2}$ (CZ) / mV	$E^{\text{Ox}}_{1/2}$ (TAA) / mV	$E^{\text{Red}}_{1/2}$ (N ⁺ N, P ⁺ P) / mV	$\Delta E_{1/2} = E^{\text{Ox}} - E^{\text{Red}}$ / mV
ppy_{TAA} (14)			230 ^r		
ppy_{CZ} (15)		880 ⁱ			
4	870 ^r			-1770 ^r	2640
4A	830 ⁱ		230 ^r	-1780 ^r	2010
4B	875 ⁱ	880 ⁱ		-1760 ^r	2635
5	820 ^r			-1970 ^r	2790
5A	770 ⁱ		230 ^r	-2050 ^r	2280
5B	740 ⁱ	890 ⁱ		-2010 ^r	2750
6	1100 ⁱ			-2290 ⁱ	3390
6A	930 ⁱ		240 ^r	-2340 ⁱ	2580
6B	935 ⁱ	800 ⁱ		-2300 ⁱ	3100

^r reversible, ⁱ irreversible

2 Cyclometalated Transition Metal Complexes

The oxidation potential that can be assigned to the oxidation of the Ir-phenyl moiety is reduced compared to the ppz-complexes. Therefore the redox potential differences also have smaller values.

As expected, there is a difference in the reduction potentials of the differently substituted bpy complexes (Figure 2.3). The compounds with the most negative reduction potential are **1(A)_{NMe₂}** with $E_{\text{Red}}^{1/2} = -2.19$ and -2.22 V. These values increase by attaching substituents with decreasing donor strength and even further by using electron acceptors, such as NO₂ and Cl. Consequently, the least negative reduction potential can be observed for the NO₂-bpy complexes with -0.85 and -0.99 V which are both irreversible. This increase of reduction potential goes along with a lowering of the energy of the ligand π^* orbital, an effect that increasingly destabilises the Ir(III) core leading to an increase of the iridium centered oxidation potential for the reference compounds **1(X)**.

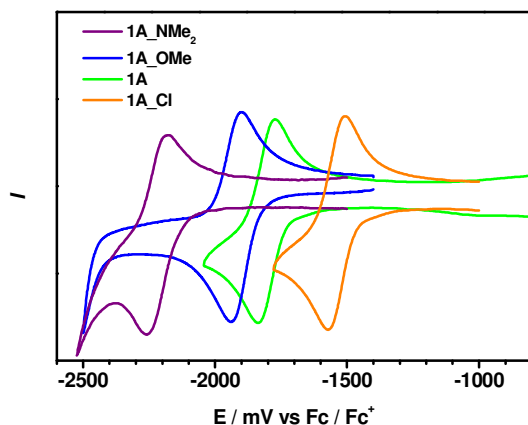


Figure 2.3 Reduction potential waves of the substituted complexes **1A_(X)** in 0.1 M MeCN/TBAH, $v = 100$ mVs⁻¹.

However, this effect cannot be observed for the TAA substituted compounds **1A_(X)** because the iridium centered oxidation is preceded by the oxidation of the two TAA moieties in these cases.^{114,173-179} The redox potential difference $\Delta E_{1/2}$ directly yields an estimate for the energy of the charge separated state which, thus, decreases in the series **1A_(X)** with X = NMe₂ to X = NO₂.

Table 2.5 Redox properties of the cyclometalated bpy-complexes and their ligands in acetonitrile.

	$E_{1/2}^{\text{Ox}}$ (Ir) / mV	$E_{1/2}^{\text{Ox}}$ (TAA) / mV	$E_{1/2}^{\text{Red}}$ (bpy) / mV	$\Delta E_{1/2} = E^{\text{Ox}} - E^{\text{Red}}$ / mV
1_NO₂	1030 ⁱ		-850 ⁱ -970 ⁱ -1580 ⁱ	1880
1_Cl	970 ⁱ		-1540 ^r	2510
1	960 ⁱ		-1800 ^r	2760
1_OMe	990 ^r		-1900 ^r	2890
1_NMe₂	770 ⁱ		-2190 ^r	2960
1A_NO₂	870 ⁱ	240 ^r	-990 ⁱ -1140 ⁱ -1570 ⁱ	1230
1A_Cl	920 ⁱ	290 ^r	-1540 ⁱ	1830
1A	900 ⁱ	230 ^r	-1800 ^r	2030
1A_OMe	910 ⁱ	240 ^r	-1920 ^r	2160
1A_NMe₂	920 ⁱ	230 ^r	-2220	2450

^r reversible, ⁱ irreversible

2.2.3 Steady State Spectroscopy

2.2.3.1 Steady State Absorption Spectroscopy

The absorption spectra of all complexes and the ligands are given in Figures 2.4 – 2.8. All complexes show the characteristic intense bands for the spin-allowed $^1\pi-\pi^*$ ligand-centered (LC) transition in the C^N and N^N ligands between 35000 and 40000 cm⁻¹. The absorption bands between 15000 and 24000 cm⁻¹ can be assigned to the spin-forbidden 3 MLCT absorption transitions caused by spin-orbit coupling associated with the iridium center.^{94,102,103,110,145-147,166,180-182} Figure 2.5 shows the UV-spectra of **1**, **1A**, **1B** with the corresponding transitions (inset).

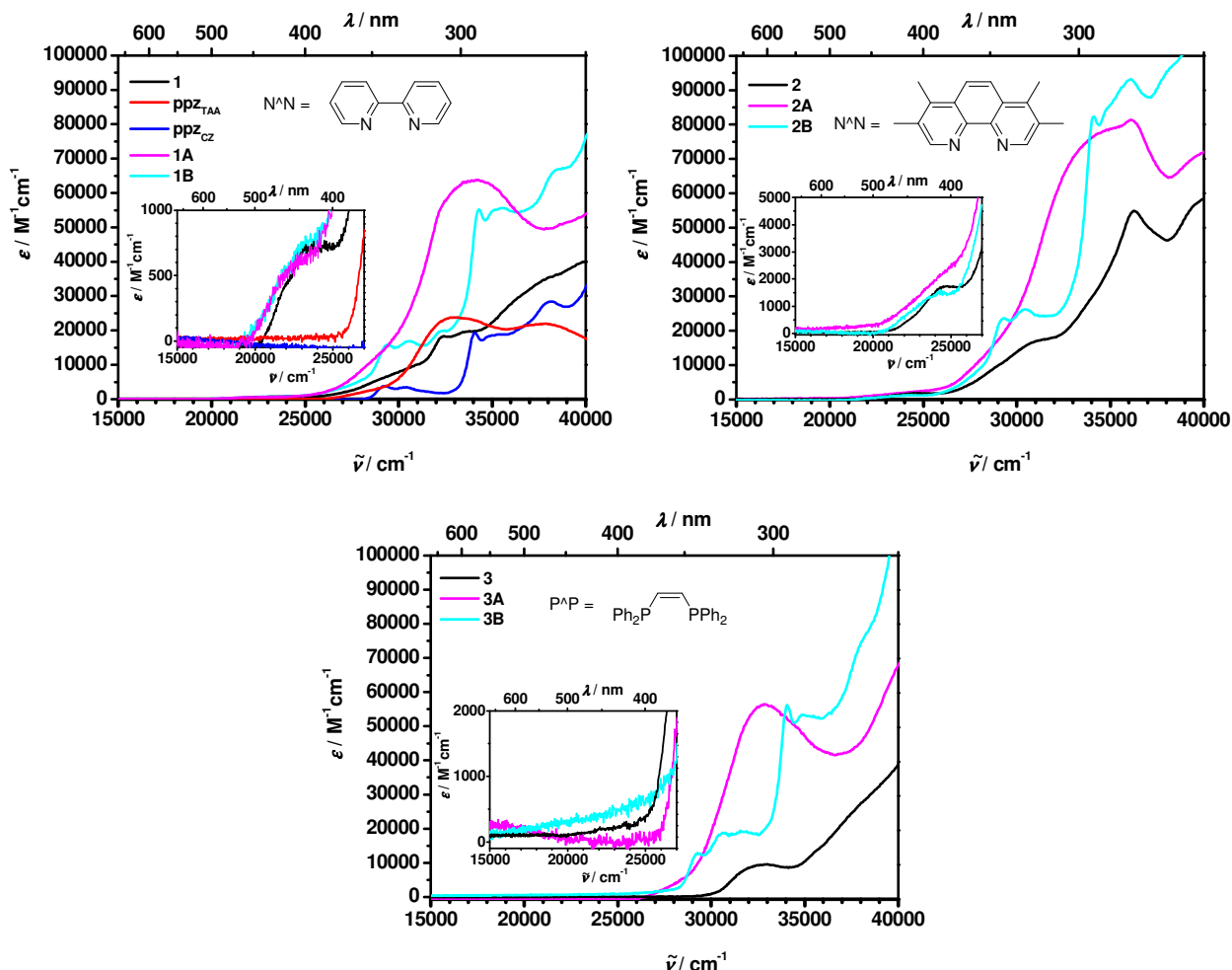


Figure 2.4 Absorption spectra of **1** – **3**, **1A** – **3A**, **1B** – **3B** and the ligands in acetonitrile solution at 298 K.

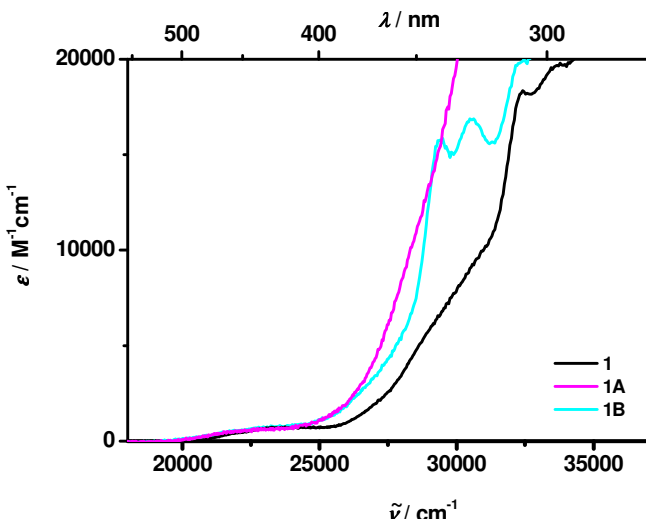


Figure 2.5 Absorption spectra of **1**, **1A** and **1B** with the corresponding transitions.

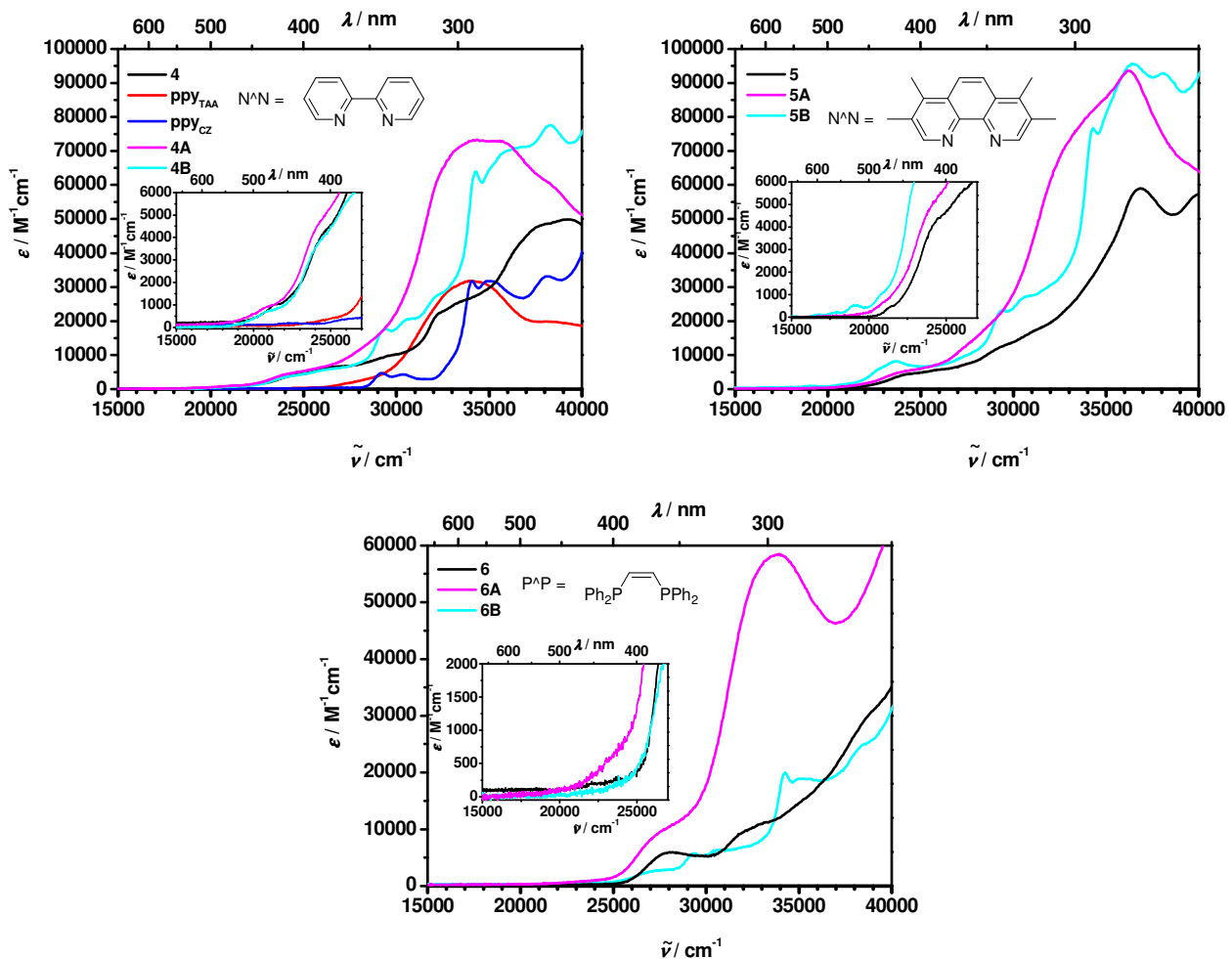


Figure 2.6 Absorption spectra of **4 - 6**, **4A - 6A**, **4B - 6B** and the ligands in acetonitrile solution at 298 K.

2 Cyclometalated Transition Metal Complexes

For the bdppe complexes it is remarkable that the $^1\text{MLCT}$ and $^3\text{MLCT}$ transitions show a significant decrease in signal intensity. This phenomenon can be ascribed to the *cis*-arranged, strong π -accepting ligand which lowers the electron density at the iridium (see chapter 2.1).^{150,183}

The moderately intense bands between 24000 cm^{-1} and 35000 cm^{-1} are based on two factors. Firstly, the intensity of these bands in comparison to those of the free ligands is higher because the complexes have two cyclometalating ligands. The band shapes are similar to those of the free ligands and can be attributed to the characteristic localised transitions of the triarylamine and carbazole subunits.^{151,171,172} Secondly, the intensity of these bands is increased because they add to the typical spin-allowed metal-to-ligand charge-transfer ($^1\text{MLCT}$) $d\pi(\text{Ir}) \rightarrow \pi^*$ absorption bands in this spectral region.^{103,116}

The absorption spectra of the ppz and ppy complexes are shown in Figure 2.4 and 2.6 in acetonitrile solution. Measurements in CH_2Cl_2 , 2-MeTHF and THF showed practically no differences. The observed $^3\text{MLCT}$ and $^1\text{MLCT}$ transitions have the same intensity as the reference compounds without the hole transporting component. As expected, the absorption coefficients of the typical ^3LC transitions in the complexes have about twice the intensity as the free ligands because the complexes comprise two of these ligands.

The absorption spectra of the substituted bpy complexes **1_(X)** and **1A_(X)** are shown in Figure 2.7. As known from studies on similar ruthenium complexes, the $^3\text{MLCT}$ bands of the iridium complexes shift to longer wavelengths when the substituents are electron-withdrawing (see Figure 2.8).^{174-176,178,184} The acceptor substituted compounds exhibit the greater withdrawing effect on the ring π -system, resulting in a lowering of the π^* -orbital energy. This effect can clearly be observed at the $^3\text{MLCT}$ transitions of the substituted complexes (Figure 2.7 and 2.8). The $^3\text{MLCT}$ band of **1_NO₂** is keenly shifted to lower energies (18400 cm^{-1}) compared to the donor-substituted **1_OMe** (24100 cm^{-1}).

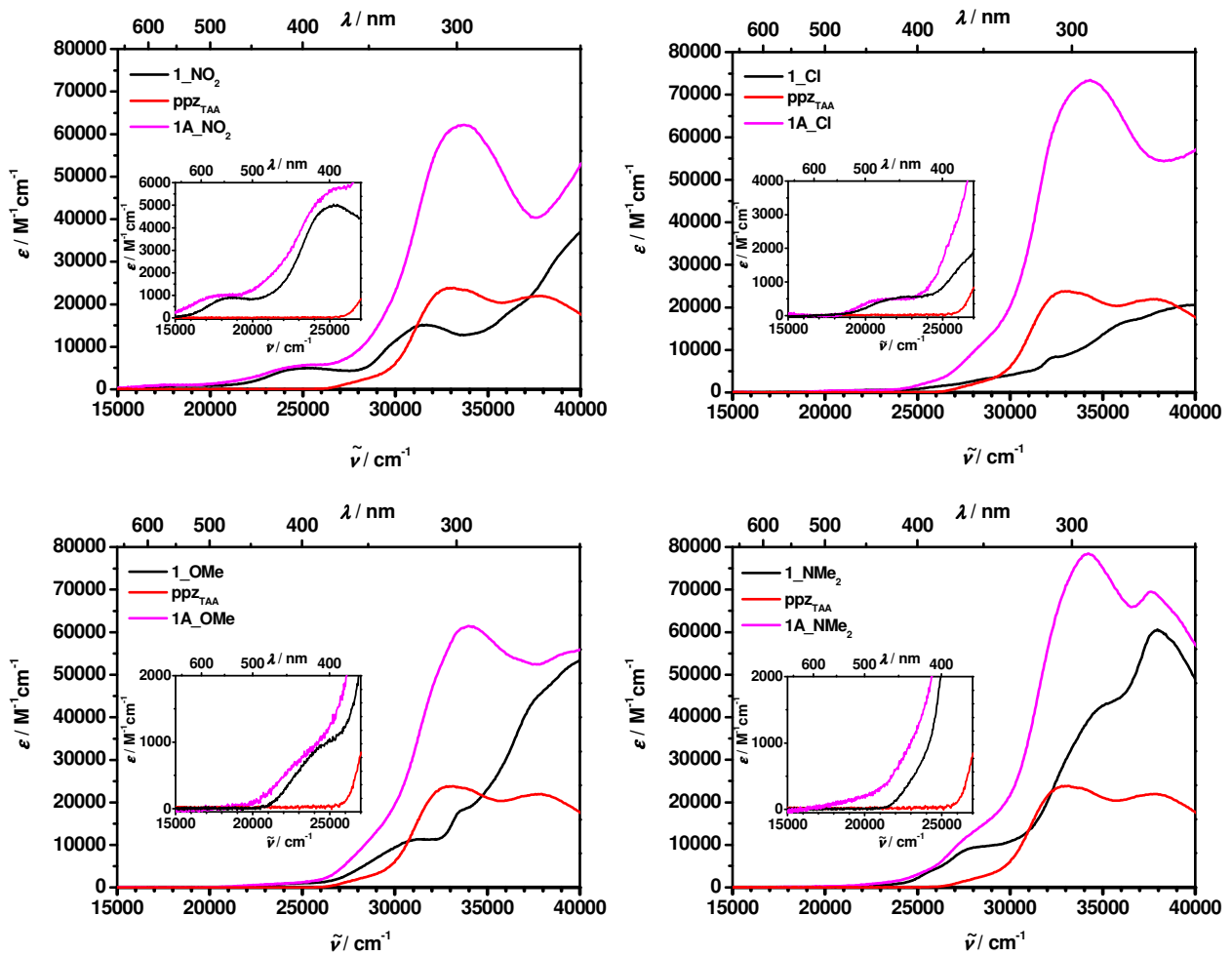


Figure 2.7 Absorption spectra of the differently substituted bpy complexes in acetonitrile solution at 298 K.

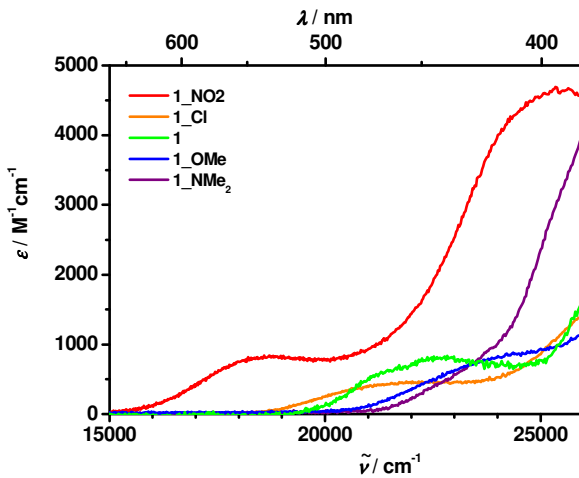


Figure 2.8 Magnification of absorption spectra of $\mathbf{1A}_{(\text{X})}$ in 2-MeTHF in the region of the MLCT bands.

2.2.3.2 Emission Spectroscopy

2.2.3.2.1 Emission Spectroscopy at RT

The emission data, excitation wavelengths and energies of all complexes and free ligands are listed in Table 2.6 a,b and c. The literature-known reference complexes **1**, **1_OMe**, **4** and **5** all show a strong luminescence in the green to red region with quantum yields between 4 and 49 % in 2-MeTHF at RT in agreement with literature data.⁹³⁻¹⁰³

However, at room temperature the triarylamine-substituted complexes only show weak fluorescence from the triarylamine ligand (Figure 2.9 b). There is obviously a very fast quenching process which inhibits luminescence from the Ir core. Much in contrast, the carbazole substituted compounds show a strong and slightly red-shifted luminescence in comparison to their reference compounds (Figure 2.9 a and 2.10).

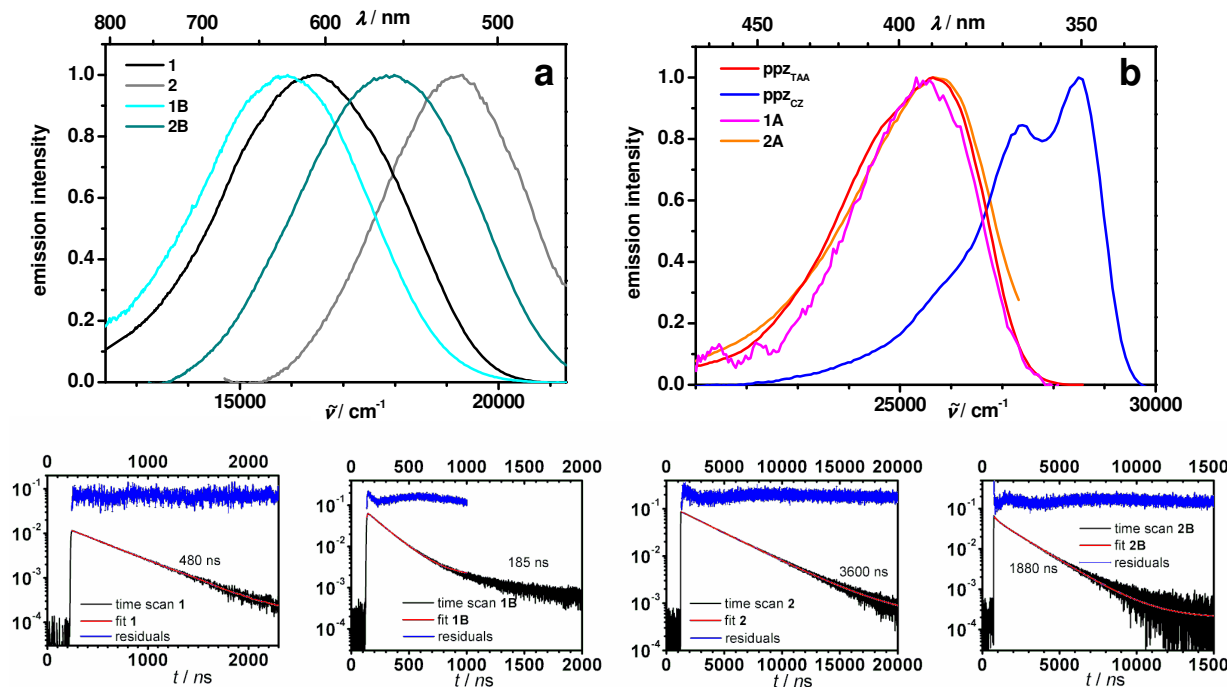


Figure 2.9 Emission spectra and time scans of **1**, **2**, **1A**, **2A**, **1B**, **2B** and the ligands in 2-MeTHF solution at 298 K. ^aexcitation: 28200 cm⁻¹ (355 nm); ^bexcitation 33300 cm⁻¹ (300 nm).

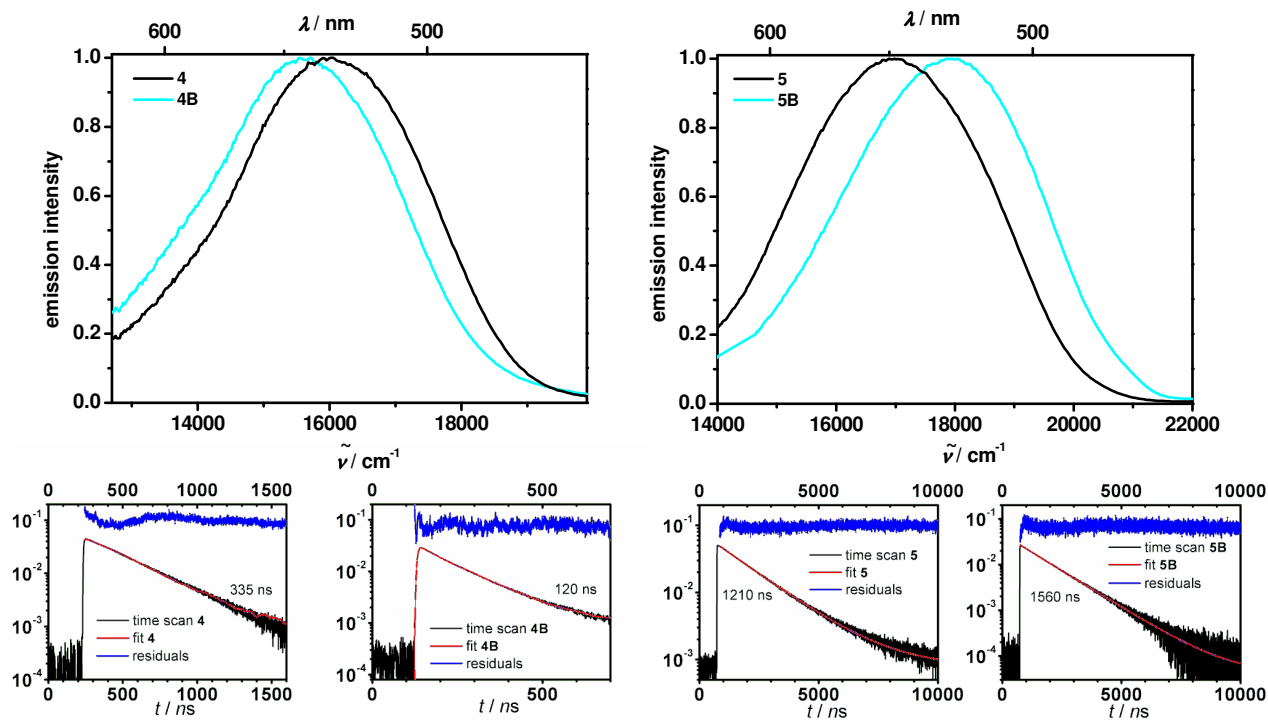


Figure 2.10 Emission spectra and time scans of **4**, **5**, **4B** and **5B** in 2-MeTHF solution at 298 K. Excitation: 28200 cm⁻¹ (355 nm).

The bdppe_ppz complexes **3**, **3A** and **3B** all do not luminesce at RT while the corresponding ppy complex **6** only shows weak emission in the blue-green region with quantum yields of 4 %. Attachment of the hole transporting components also leads to an emission quenching, thus **6A** and **6B** do not emit at RT.

Both quantum yields and luminescence decay lifetimes of the carbazole complexes are smaller than that of the reference complexes which points towards an additional luminescence quenching process. The luminescent decay lifetimes of the triarylamine complexes could not be determined because of their weak emission quantum yields ($\Phi < 1\%$). The triarylamine ligand **ppz_{TAA}** has a quantum yield of $\Phi = 6\%$ and the carbazole ligand **ppz_{CZ}** $\Phi = 26\%$ in CH₂Cl₂. The quantum yields of all illuminating complexes and their reference compounds vary significantly in different solvents. The tmp complexes show the highest quantum yields with a hypsochromic shifted emission compared to the other complexes.

2 Cyclometalated Transition Metal Complexes

Table 2.6a Emission properties of **1(A,B) – 3(A,B)** and their free ligands.

	medium (T/K)	$\tilde{\nu}_{\text{em}}$ /cm ⁻¹	τ /ns	Φ_{em} /%	k_r ^c /10 ⁶ s ⁻¹	k_{nr} ^d /10 ⁶ s ⁻¹
ppz_{TAA}	CH ₂ Cl ₂ (298) ^a	25600		6		
ppz_{CZ}	CH ₂ Cl ₂ (298) ^a	28500		26		
1	2-MeTHF (298) ^b	16400	480	19	0.40	1.7
	CH ₂ Cl ₂ (298) ^b	17100	650	55	0.85	0.7
	CH ₃ CN (298) ^b	16400	215	17	0.79	3.9
	2-MeTHF (77) ^b	19200	5130			
1A	2-Me-THF (298) ^a	25500	-	< 1	-	-
	2-MeTHF (77) ^b	18500	3050			
1B	2-MeTHF (298) ^b	15800	185	8	0.44	5.0
	CH ₂ Cl ₂ (298) ^b	16400	360	19	0.52	2.2
	CH ₃ CN (298) ^b	15600	145	5	0.34	6.5
	2-MeTHF (77) ^b	18700	3380			
2	2-MeTHF (298) ^b	18600	3600	31	0.09	0.2
	CH ₂ Cl ₂ (298) ^b	19200	4160	27	0.06	0.2
	CH ₃ CN (298) ^b	18400	880	19	0.22	0.9
	2-MeTHF (77) ^b	21100/19600/ 18300	18300			
2A	2-Me-THF (298) ^a	25500	-	< 1	-	-
	2-MeTHF (77) ^b	21000/19600/ 18200	10000			
2B	2-MeTHF (298) ^b	17900	1880	25	0.13	0.4
	CH ₂ Cl ₂ (298) ^b	18100	1670	25	0.15	0.5
	CH ₃ CN (298) ^b	17500	1160	16	0.14	0.7
	2-MeTHF (77) ^b	21000/19600/ 18200	9200			
3	2-MeTHF (298)	-	-	-	-	-
	2-MeTHF (77) ^b	-	-	-	-	-
3A	2-MeTHF (298) ^a	-	-	-	-	-
	2-MeTHF (77) ^b	-	-	-	-	-
3B	2-MeTHF (298)	-	-	-	-	-
	2-MeTHF (77) ^b	-	-	-	-	-

^aexcitation: 28200 cm⁻¹ (355 nm), ^bexcitation: 40000 cm⁻¹ (416 nm), ^ccalculated by $k_r = \Phi/\tau$, ^dcalculated with $k_{\text{nr}} = (1-\Phi)/\tau$

Table 2.6b Emission properties of **4(A,B) – 6(A,B)** and their free ligands.

	medium	$\tilde{\nu}_{\text{em}}$	τ	Φ_{em}	k_r^{c}	k_{nr}^{d}
	(T/K)	/cm ⁻¹	/ns	/%	/10 ⁶ s ⁻¹	/10 ⁶ s ⁻¹
ppy_{TAA}	CH ₂ Cl ₂ (298) ^a	25400		3		
ppy_{CZ}	CH ₂ Cl ₂ (298) ^a	28600		29		
4	2-MeTHF (298) ^b	16100	335	9	0.27	2.7
	CH ₂ Cl ₂ (298) ^b	16000	590	27	0.46	1.2
	CH ₃ CN (298) ^b	15900	225	10	0.44	4.0
	2-MeTHF (77) ^b	19800/19100	4500			
4A	2-Me-THF (298) ^a	25400	-	< 1	-	-
	2-MeTHF (77) ^b	18800	3500			
4B	2-MeTHF (298) ^b	15700	120	8	0.67	7.7
	CH ₂ Cl ₂ (298) ^b	15900	320	16	0.50	2.6
	CH ₃ CN (298) ^b	15500	130	6	0.46	7.2
	2-MeTHF (77) ^b	19200/18000	3400			
5	2-MeTHF (298) ^b	18000	1210	42	0.35	0.5
	CH ₂ Cl ₂ (298) ^b	18200	1830	56	0.31	0.2
	CH ₃ CN (298) ^b	18100	1790	48	0.27	0.3
	2-MeTHF (77) ^b	21000/19600	6000			
5A	2-Me-THF (298) ^a	25500	-	< 1	-	-
	2-MeTHF (77) ^b	20600/19300	5100			
5B	2-MeTHF (298) ^b	16900	1560	28	1.79	4.6
	CH ₂ Cl ₂ (298) ^b	17600	1380	39	2.83	4.4
	CH ₃ CN (298) ^b	16800	1190	29	2.44	6.0
	2-MeTHF (77) ^b	20600/19300	4800			
6	2-MeTHF (298) ^b	18500	370/1800	4	-	-
	CH ₂ Cl ₂ (298) ^b	18600	52/1620	5	-	-
	CH ₃ CN (298) ^b	18400	100/1430	3	-	-
	2-MeTHF (77) ^b	18700	35900/4320			
6A	2-Me-THF (298) ^a	-	-	-	-	-
	2-MeTHF (77) ^b	-	-	-	-	-
6B	2-MeTHF (298) ^b	-	-	-	-	-
	2-MeTHF (77) ^b	-	-	-	-	-

^aexcitation: 28200 cm⁻¹ (355 nm), ^bexcitation: 40000 cm⁻¹ (416 nm), ^ccalculated by $k_r = \Phi/\tau$, ^dcalculated by $k_{\text{nr}} = (1 - \Phi)/\tau$

2 Cyclometalated Transition Metal Complexes

Table 2.6c Emission properties of **1_(X)** and **1A_(X)** and their free ligand.

	medium	$\tilde{\nu}_{\text{em}}$	τ	Φ_{em}	k_r^{c}	k_{nr}^{d}
	(T/K)	/cm ⁻¹	/ns	/%	/10 ⁶ s ⁻¹	/10 ⁶ s ⁻¹
ppz_{TAA}	CH ₂ Cl ₂ (298) ^a	25600		6		
1_NO₂	2-MeTHF (298)	-	-	-	-	-
	2-MeTHF (77)	-	-	-	-	-
1A_NO₂	2-MeTHF (298)	-	-	-	-	-
	2-MeTHF (77)	-	-	-	-	-
1_Cl	2-MeTHF (298) ^b	15400	55	3	0.55	18
	CH ₂ Cl ₂ (298) ^b	15700	185	7	0.38	5.0
	CH ₃ CN (298) ^b	15400	45	3	0.67	22
	2-MeTHF (77) ^b	18300	4200			
1A_Cl	2-MeTHF (298)	-	-	-	-	-
	2-MeTHF (77) ^b	18400	2500	-	-	-
1	2-MeTHF (298) ^b	16400	480	19	0.40	1.7
	CH ₂ Cl ₂ (298) ^b	17100	650	55	0.85	0.7
	CH ₃ CN (298) ^b	16400	215	17	0.79	3.9
	2-MeTHF (77) ^b	19200	5130			
1A	2-Me-THF (298) ^a	25500	-	< 1	-	-
	2-MeTHF (77) ^b	18500	3100	-	-	-
1_OMe	2-MeTHF (298) ^b	17200	535	4	0.08	1.8
	CH ₂ Cl ₂ (298) ^b	17300	765	9	0.12	1.2
	CH ₃ CN (298) ^b	17000	115	8	0.69	8.0
	2-MeTHF (77) ^b	20600	7200			
1A_OMe	2-MeTHF (298)	-	-	-	-	-
	2-MeTHF (77) ^b	19400	4100	-	-	-
1_NMe₂	2-MeTHF (298) ^b	19000	2975	30	0.10	0.2
	CH ₂ Cl ₂ (298) ^b	19200	2990	37	0.12	0.2
	CH ₃ CN (298) ^b	19200	1695	27	0.16	0.4
	2-MeTHF (77) ^b	19900/21400	12400			
1A_NMe₂	2-MeTHF (298)	-	-	-	-	-
	2-MeTHF (77) ^b	19900/21200	12600	-	-	-

^aexcitation: 28200 cm⁻¹ (355 nm), ^bexcitation: 40000 cm⁻¹ (416 nm), ^ccalculated by $k_r = \Phi/\tau$, ^dcalculated by $k_{\text{nr}} = (1 - \Phi)/\tau$

The emission data of the substituted complexes are listed in Table 2.6. All the reference compounds **1_(X)** with exception of the NO_2 substituted complex show emission in the green-red region, except the NO_2 substituted complex. The quantum yields vary between naught for **1_NO₂** and 55 % for **1_OMe**. Thus, for light emitting applications such as OLEDs **1_NMe₂** might be an interesting candidate as it emits green light with a quantum yield of ca. 30 – 40 %. Much in contrast, the triarylamine-substituted compounds show no emission at RT due to a quenching process caused by the formation of a charge separated state. The quantum yields are estimated to be almost unity for these processes (see Experimental section). The emission spectra of the reference compounds are given in Figure 2.11. The donor-substituted complexes emit in the green and yellow region, the unsubstituted and Cl-substituted complexes in the orange and red region.

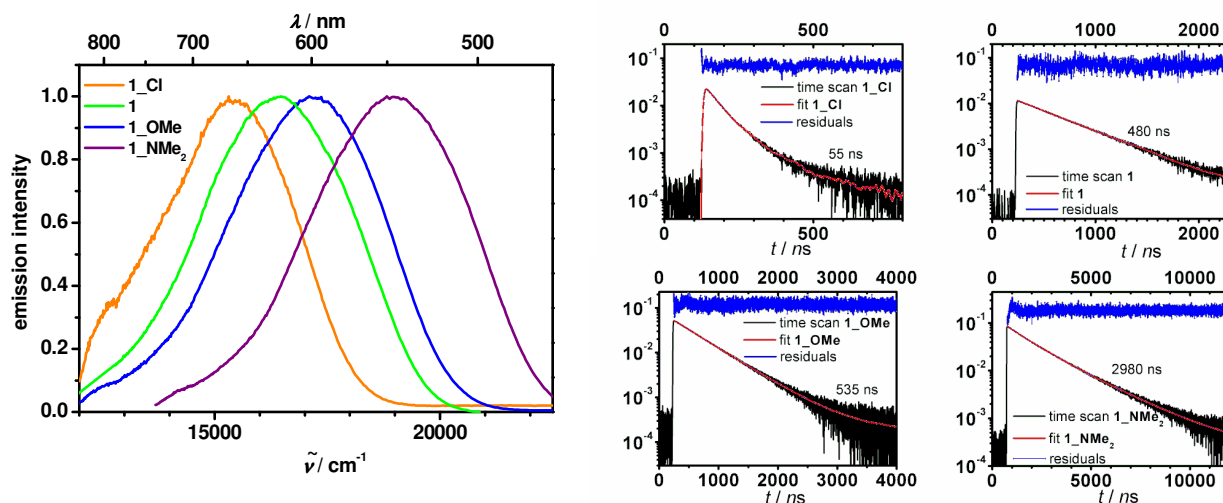


Figure 2.11 Emission spectra and time scans with monoexponential fits of the substituted **1_(X)** reference complexes in 2-MeTHF solution at 298 K. Excitation: 28200 cm^{-1} (355 nm).

Time resolved measurements (see Figure 2.11) proved the emission decays to be monoexponential with lifetimes at RT in the 50 – 3000 ns range. This long lifetime is consistent with the emission being phosphorescence.

2.2.3.2.2 Emission Spectroscopy at 77 K

The emission spectra of the complexes at 77 K in a rigid matrix are shown in Figure 2.12 and 2.13. The emission maxima and lifetimes are given in Table 2.6. All complexes (except the bdppe and NO₂ complexes) show intense and long-lived luminescence at 77 K with monoexponential decay in the μ s regime which indicates the phosphorescent nature of the luminescence. The lifetimes of the CZ and TAA substituted complexes are shorter compared to that of the corresponding reference compounds which is caused by an additional quenching process. Interestingly, unlike at RT, at 77 K the TAA substituted complexes also show emission spectra differing from the spectra recorded at RT.

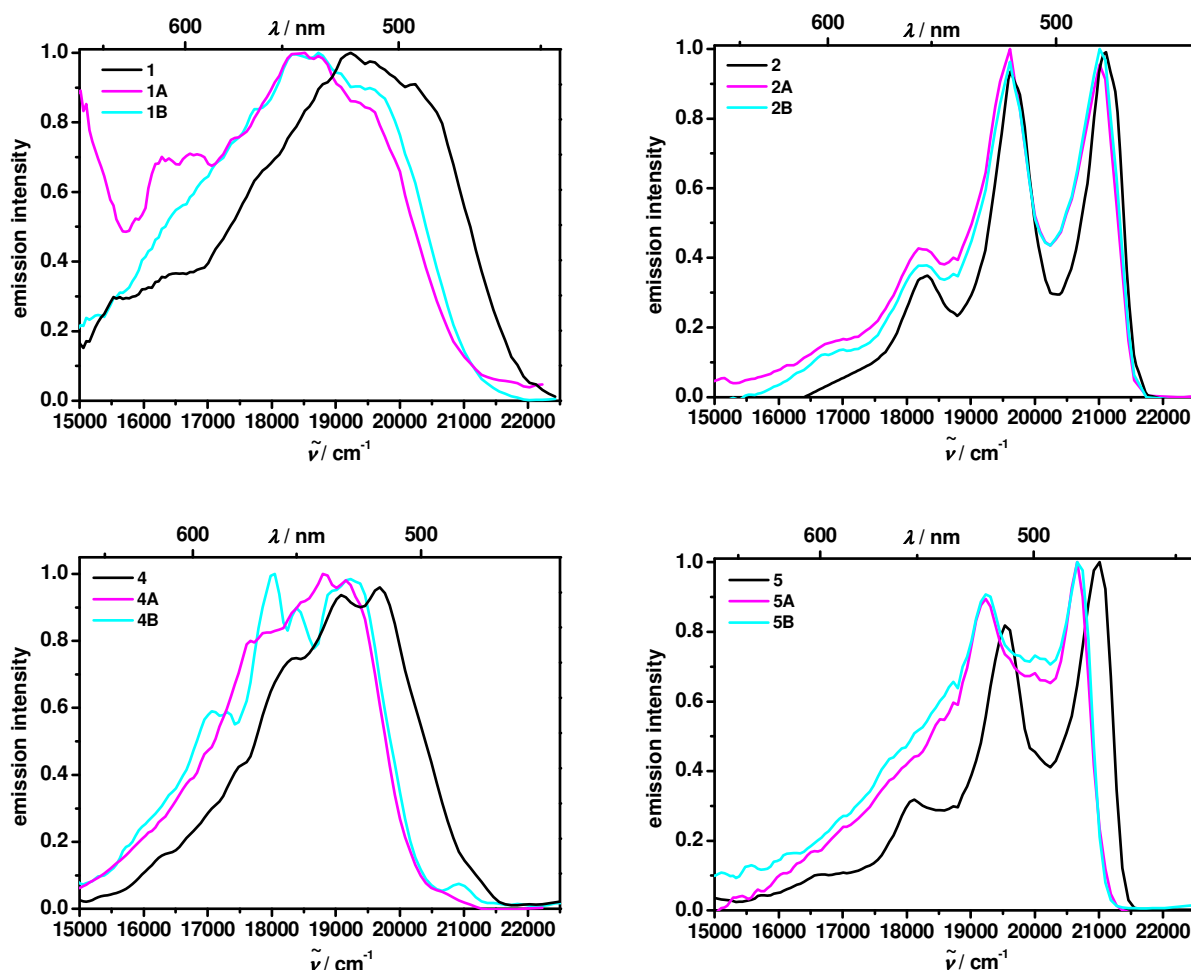


Figure 2.12 Emission spectra of **1**, **2**, **4**, **5**, **1A**, **2A**, **4A**, **5A**, **1B**, **2B**, **4B** and **5B** in 2-MeTHF glass matrix at 77 K. Excitation: 28200 cm^{-1} (355 nm).

The emission maxima of the carbazole-compounds and the references are blue-shifted compared to the emission maxima at RT. This shift by about 2700 cm^{-1} is due to the inhibition of the solvent reorganisation in a rigid matrix. Mixed-ligand transition-metal complexes such as the reference compounds show two characteristic excited

states: The metal-to-ligand CT ($^3\text{MLCT}$) transition and the $\pi\text{-}\pi^*$ ligand-centered (^3LC) transition (see Chapter 2.1, Scheme 2.2). The emission bands for the $^3\text{MLCT}$ transitions exhibit a broad and featureless emission with lower energies than the blue-shifted structured ^3LC transitions. $^3\text{MLCT}$ transitions are typical of solutions at room temperature. By reducing the temperature the energy of the $^3\text{MLCT}$ rises and superimposes or even crosses the ^3LC transition. For this reason phosphorescence spectra of most of the Iridium mixed-ligand complexes at low temperatures have mixed excited states at low temperatures.

The broad and structureless blue-shifted emission spectra of **1(A,B)** and **4(A,B)** suggests a combined $^3\text{MLCT}$ and $^3\pi\text{-}\pi^*$ LC transition with a higher $^3\text{MLCT}$ participation. For the tmp complexes **2(A,B)** and **5(A,B)** the spectra are more blue-shifted and structured due to a higher percentage of $^3\pi\text{-}\pi^*$ LC transitions.^{94,99,102,115,116,138,141-147}

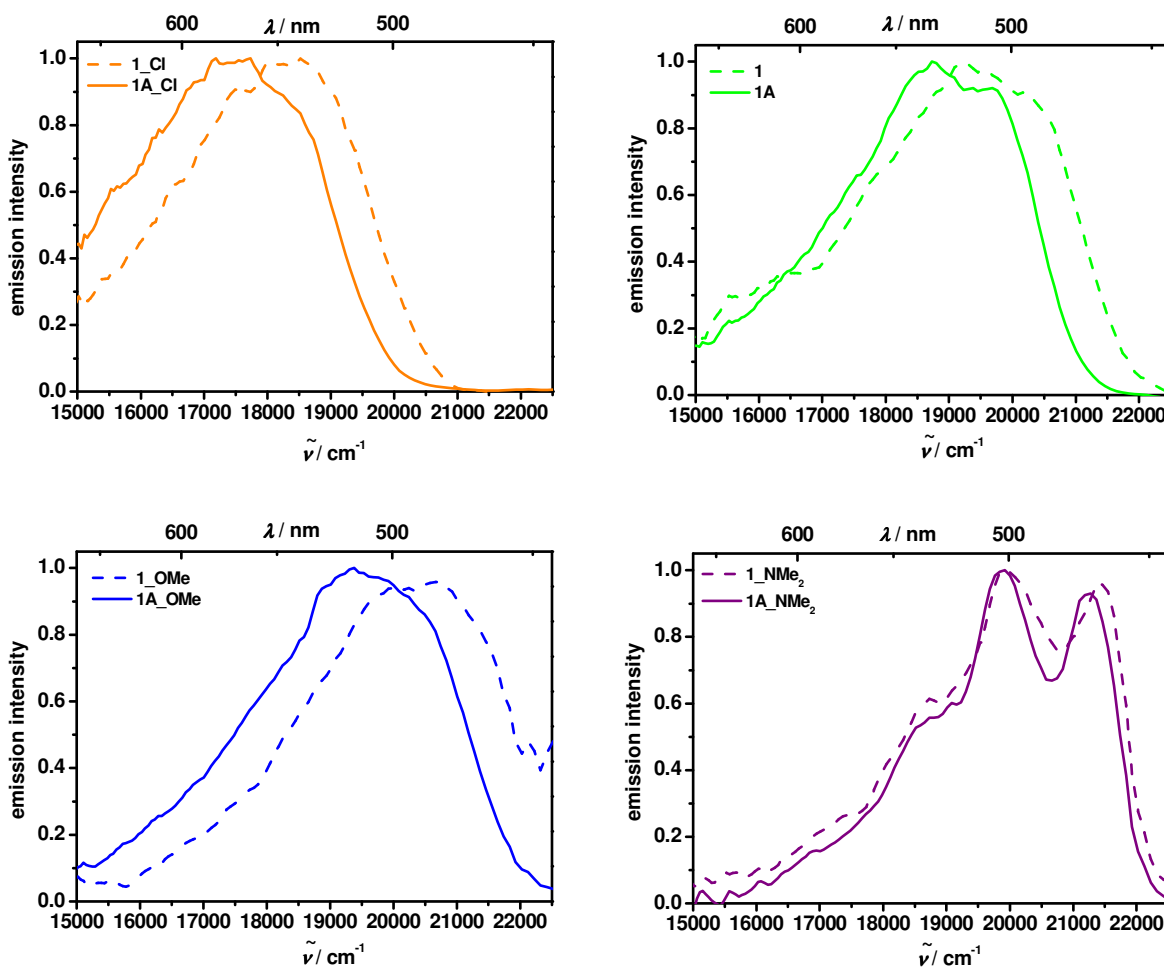
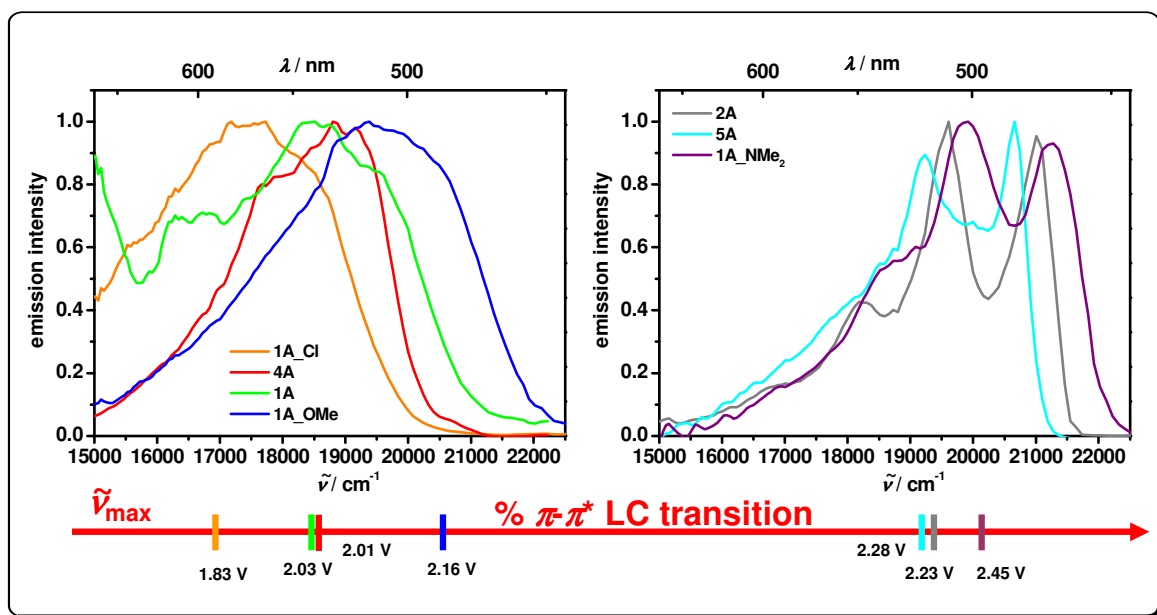


Figure 2.13 Emission spectra of the **1_(X)** and **1A_(X)** complexes in 2-MeTHF glass matrix at 77 K. Excitation: 28200 cm^{-1} (355 nm).

Furthermore, the bands of the **1A_(X)** complexes are slightly shifted to lower energies than those of the **1_X** compounds for X = Cl, H and OMe. While the bands of these complexes are broad and almost featureless, those of **1_NMe₂** and **1A_NMe₂** are practically identical and show vibronic fine structure. This effect is in direct correlation with the redox potential differences $\Delta E_{1/2}$ as depicted in Scheme 2.6. The higher the redox potential difference the higher is the percentage of ^3LC transition and the more pronounced is the vibronic fine structure and the hypsochromic shift. For **1A**, **4A** and **5A**, **2A** the overall trend is inverse what may be caused by the similar $\tilde{\nu}_{\text{max}}$ and $\Delta E_{1/2}$ values.



Scheme 2.6 Differences between phosphorescence spectra changing the percentage of $^3\pi-\pi^*$ LC transition and correlation with $\Delta E_{1/2}$ (see Table 2.3 – 2.5).

2.2.4 Transient Absorption Spectroscopy

2.2.4.1 Transient Absorption Spectroscopy at RT

We assume that the missing luminescence of the TAA complexes at RT is due to charge transfer quenching from the triarylamine to the N⁺N ligand. To prove this assumption transient absorption spectroscopy was measured for all complexes at RT in 2-MeTHF. The transient absorption data are listed in Table 2.7, the spectra are shown in Figures 2.14 and 2.15.

All reference compounds show absorption bands that decay with the same lifetimes, respectively. These bands can be assigned to the ³Ir(C^N)₂(bpy) states as they are in good accordance with the luminescence lifetimes at RT. The lifetimes of these triplet states increase with increasing donor strength of the substituents on the bpy ligands.

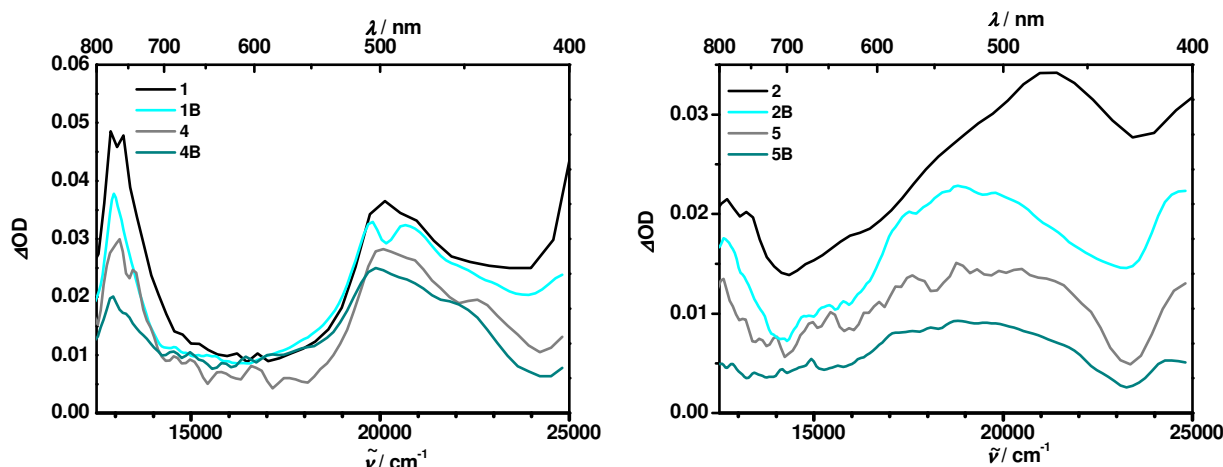


Figure 2.14 Transient absorption spectra of **1 – 5** and **1B – 5B** in 2-MeTHF with excitation at 28200 cm^{-1} (355 nm).

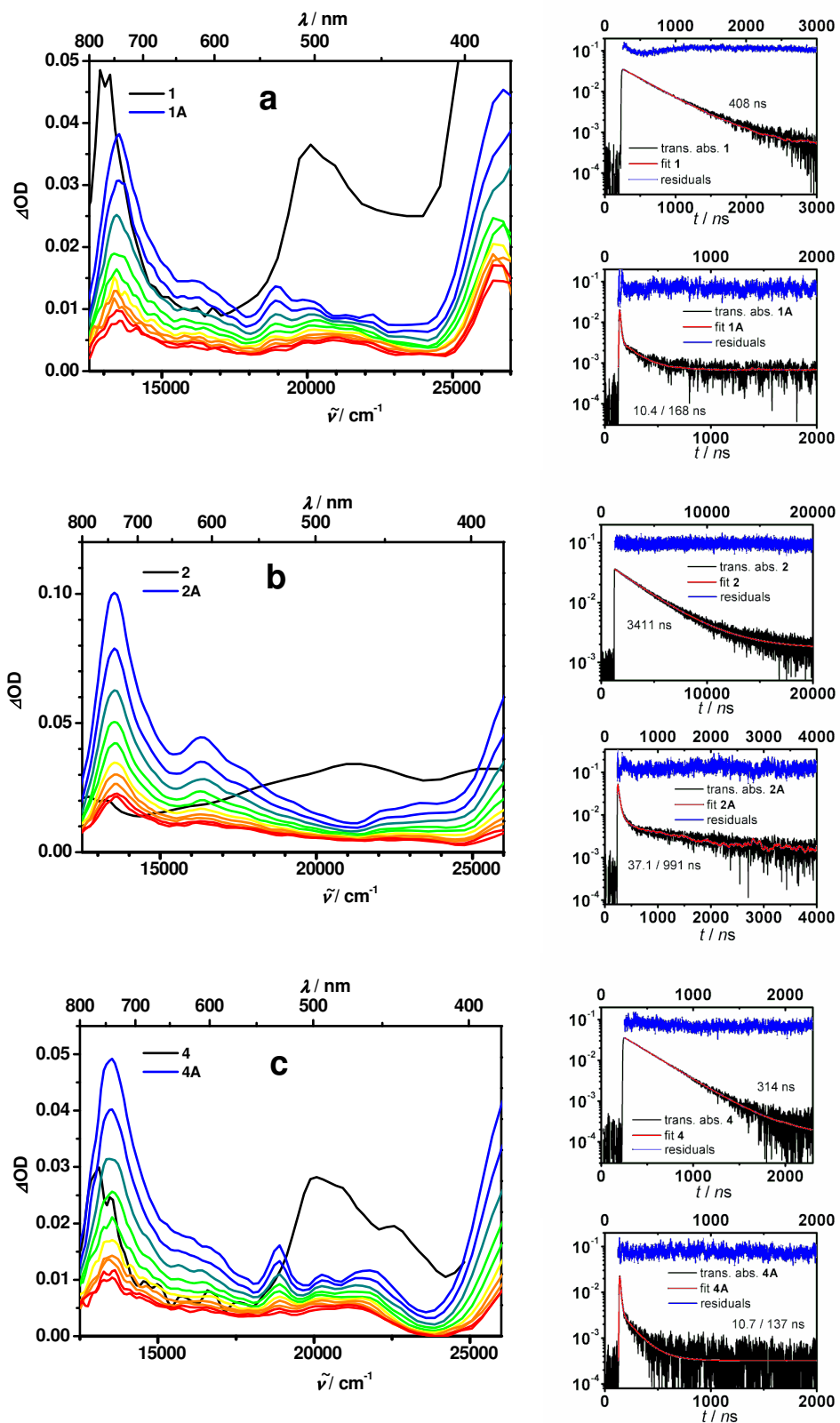
The transient absorption spectra of the CZ compounds are nearly identical to their reference compounds (Figure 2.14). The transient signals decay with the same lifetimes which are slightly shorter than their luminescence lifetimes at RT. For the CZ compounds where a distinctly higher k_{nr} is observed (Table 2.6) than for the reference complexes, the redox potential differences ΔE (Table 2.3 and 2.4) are higher than the energy of the excited state as determined from the onset of the absorption maximum lying at about $\Delta E = 2.5\text{ eV}$. Thus, charge separation should be slightly unfavourable but might still be the reason for partial luminescence quenching.

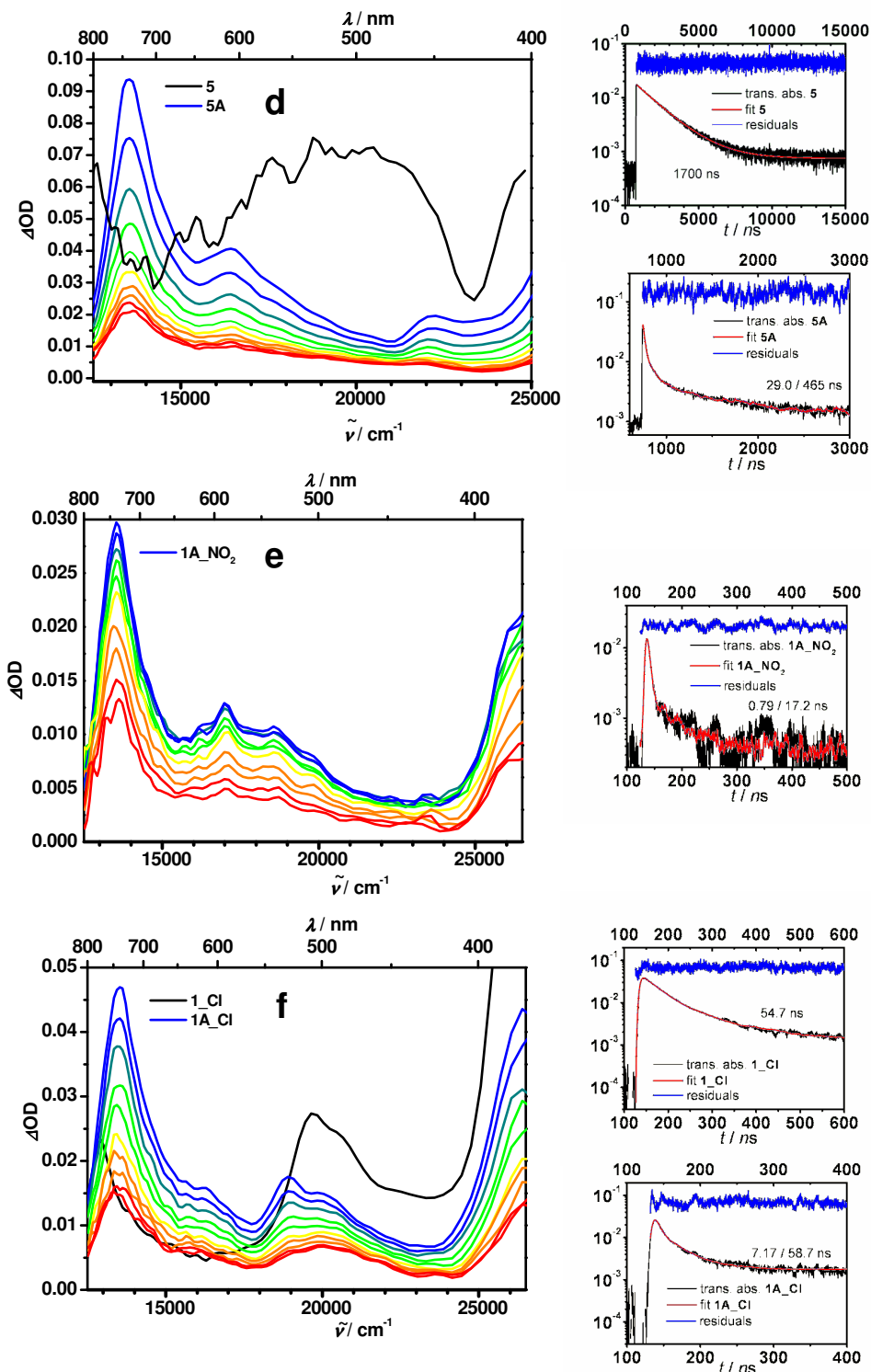
2 Cyclometalated Transition Metal Complexes

Table 2.7 Transient absorption properties of the cationic Ir(III) complexes in 2-MeTHF and in O₂ saturated solution.

	medium (T/K)	$\tilde{\nu}$ scan ^c /cm ⁻¹	τ (relative amplitudes)	
			/ns	
1	2-MeTHF (298) ^a	20000	408	
1A	2-MeTHF (293) ^b	16100	10.4 (31) / 168 (1)	
	2-MeTHF/O ₂ (293) ^b	16100	6.77	
1B	2-MeTHF (293) ^a	20000	167	
	2-MeTHF/O ₂ (293) ^a	20000	24.4	
2	2-MeTHF (298) ^a	20000	3411	
2A	2-MeTHF (293) ^b	16100	37.2 (5) / 991 (1)	
	2-MeTHF/O ₂ (293) ^b	16100	19.1 (15) / 116 (1)	
2B	2-MeTHF (293) ^a	20000	1712	
	2-MeTHF/O ₂ (293) ^a		16.6	
4	2-MeTHF (298) ^a	20000	314	
4A	2-MeTHF (293) ^b	16100	10.7 (9) / 137 (1)	
	2-MeTHF/O ₂ (293) ^b	16100	5.35 (6) / 38.7 (1)	
4B	2-MeTHF (293) ^a	20000	132	
	2-MeTHF/O ₂ (293) ^a		24.2	
5	2-MeTHF (298) ^a	20000	1700	
5A	2-MeTHF (293) ^b	16100	29.0 (10) / 465 (1)	
	2-MeTHF/O ₂ (293) ^b	16100	6.80 (10) / 35.5 (1)	
5B	2-MeTHF (293) ^a	20000	1512	
	2-MeTHF/O ₂ (293) ^a		18.5	
1_NO₂	2-MeTHF (298) ^a	-	-	
1A_NO₂	2-MeTHF (293) ^b	16100	0.79 (39) / 17.2 (1)	
	2-MeTHF/O ₂ (293) ^b	16100	0.86 (37) / 11.7 (1)	
1_Cl	2-MeTHF (298) ^a	20000	54.7	
1A_Cl	2-MeTHF (293) ^b	16100	7.17 (7) / 58.7 (1)	
	2-MeTHF/O ₂ (293) ^b	16100	3.60 (7) / 11.7 (1)	
1_OMe	2-MeTHF (298) ^a	20000	452	
1A_OMe	2-MeTHF (293) ^b	16100	14.1 (5) / 270 (1)	
	2-MeTHF/O ₂ (293) ^b	16100	4.53 (4) / 24.4 (1)	
1_NMe₂	2-MeTHF (298) ^a	20000	2789	
1A_NMe₂	2-MeTHF (293) ^b	16100	37.0 (20) / 239 (1)	
	2-MeTHF/O ₂ (293) ^b	16100	6.40 (18) / 18.9 (1)	

^aexcitation: 28200 cm⁻¹ [355 nm], ^bexcitation: 40000 cm⁻¹ [416 nm], ^c wavenumber at which the transient decay was measured.





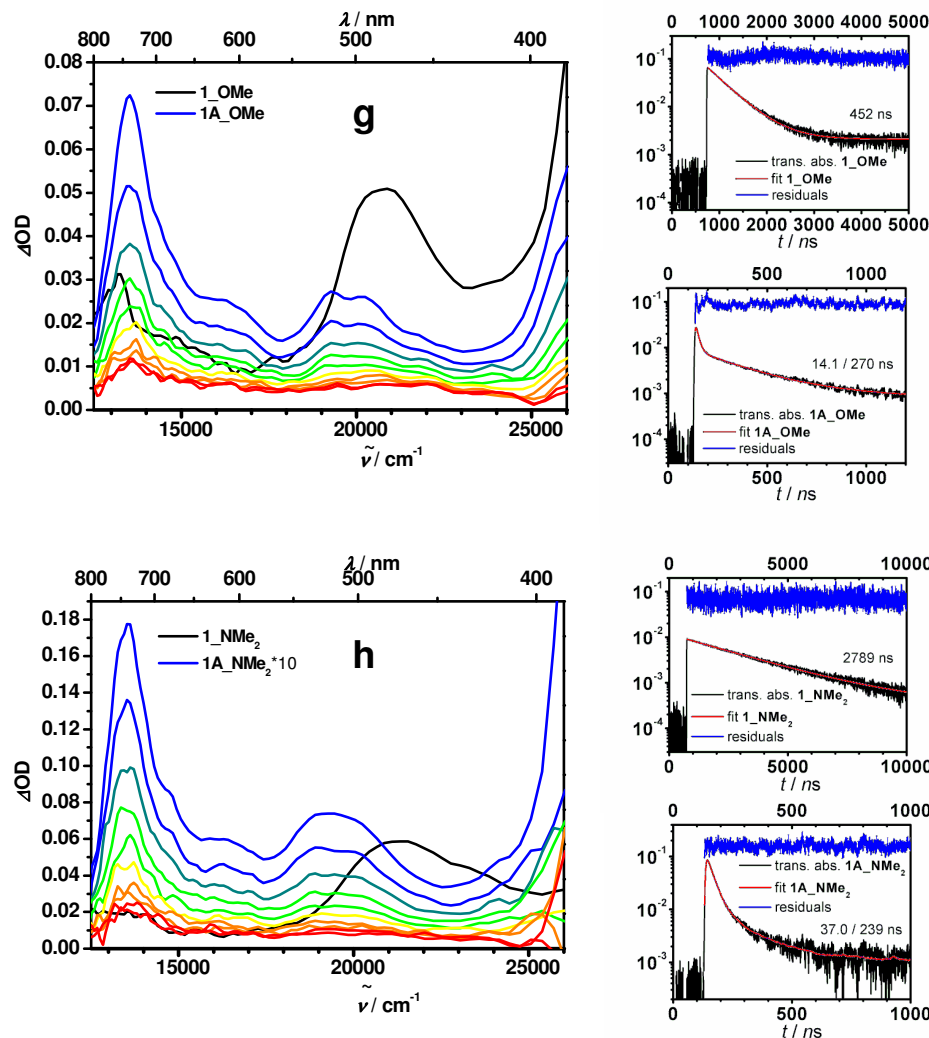


Figure 2.15 Left hand side: Transient absorption spectra of the TAA complexes **1A-X**, **2(A)**, **4(A)**, **5(A)** and references in 2-MeTHF with excitation at 24000 cm^{-1} (416 nm). Early spectra are shown in blue/green and late spectra are shown in orange/red colours. a) **1A**: 0 – 30 ns, b) **2A** 0 – 100 ns, c) **4A** 0-30 ns, d) **5A** 0 – 90 ns, e) **1A-NO₂**: 0 – 10 ns, f) **1A-Cl**: 0 – 20 ns, g) **1A-OMe**: 0 – 50 ns, h) **1A-NMe₂**: 0 – 100 ns. For comparison the reference compounds are given in black. Right hand side: Time scans and fits at 16100 cm^{-1} (620 nm) for the TAA compounds and 20000 cm^{-1} (500 nm) for the references.

The transient absorption spectra of the TAA substituted complexes differ strongly from their corresponding reference compounds. All the TAA complexes show a strong transient absorption at 13500 cm^{-1} and between $17000 - 21000\text{ cm}^{-1}$. These features decay biexponentially with the same time constants. Thus, it can be assumed that the transient state is a CS state which results from a charge transfer quenching from the TAA to the bpy ligands of the initially populated MLCT states. Therefore, the transient absorption spectra of the CS states are expected to display characteristic features of the spectra of the isolated radical anions and cations. For comparison, the spectra of these ion species were generated by oxidation and

reduction of the donor-substituted complexes in acetonitrile by spectroelectrochemistry (Figure 2.16 and 2.17).

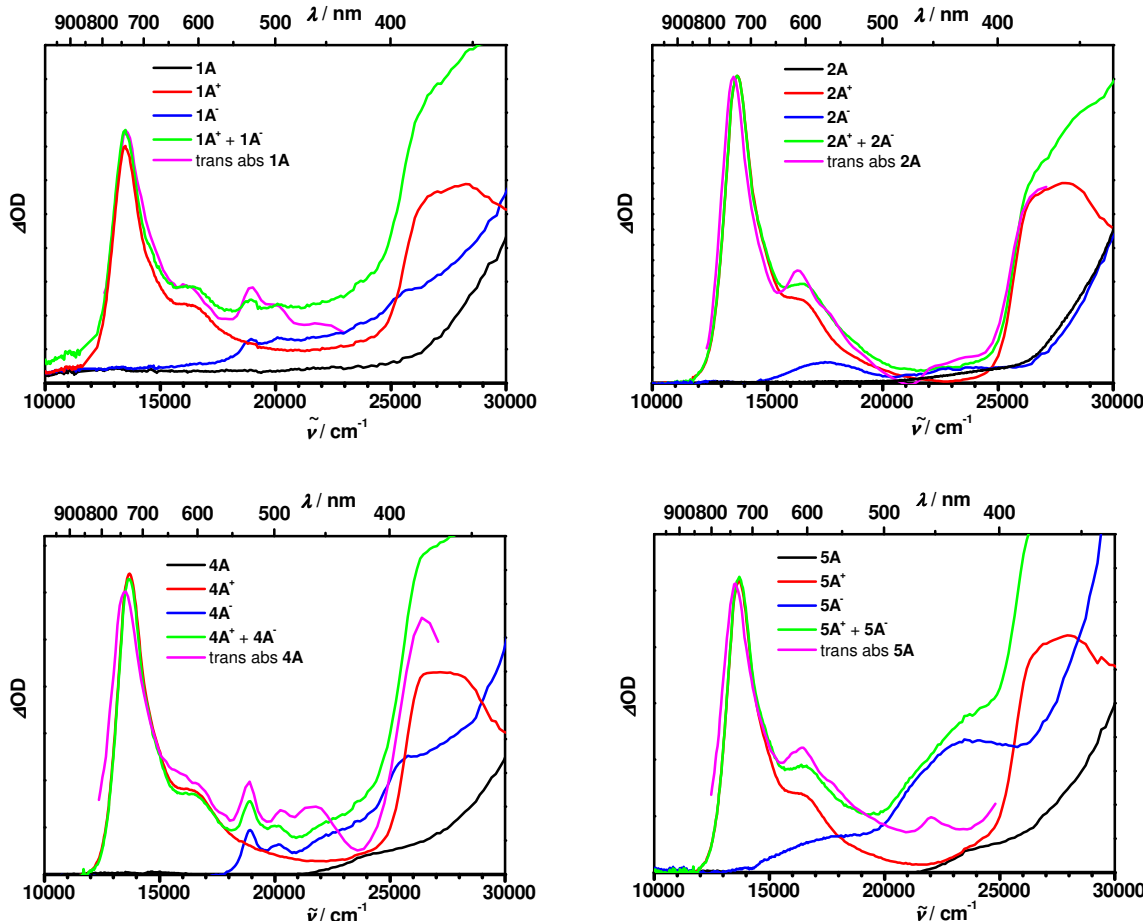


Figure 2.16 Absorption spectra of radical cations and radical anions of the compounds **1A – 5A**. The green lines show the superimposed spectra of cations and anions. The pink lines shows the transient absorption spectra of **1A – 5A** in 2-MeTHF with excitation at 24000 cm^{-1} (416 nm).

Superposition of the spectra of the radical cations and anions with the transient spectra clearly proves that the transient spectra are due to the formation of a CS state in which on triarylamine group is oxidised (the intense band at 13500 cm^{-1} is typical of triarylamine cations¹⁶⁹) and the N^{N} ligand is reduced ($17000 - 21000\text{ cm}^{-1}$ depending on the ligand¹⁸⁵).

The transient spectra of the Cl- and NO_2 -substituted complexes can only be compared to the spectra of the triarylamine cations. The radical anion spectra could not be determined accurately by spectroelectrochemistry because of the irreversibility of the reduction of the acceptor substituted bpy.

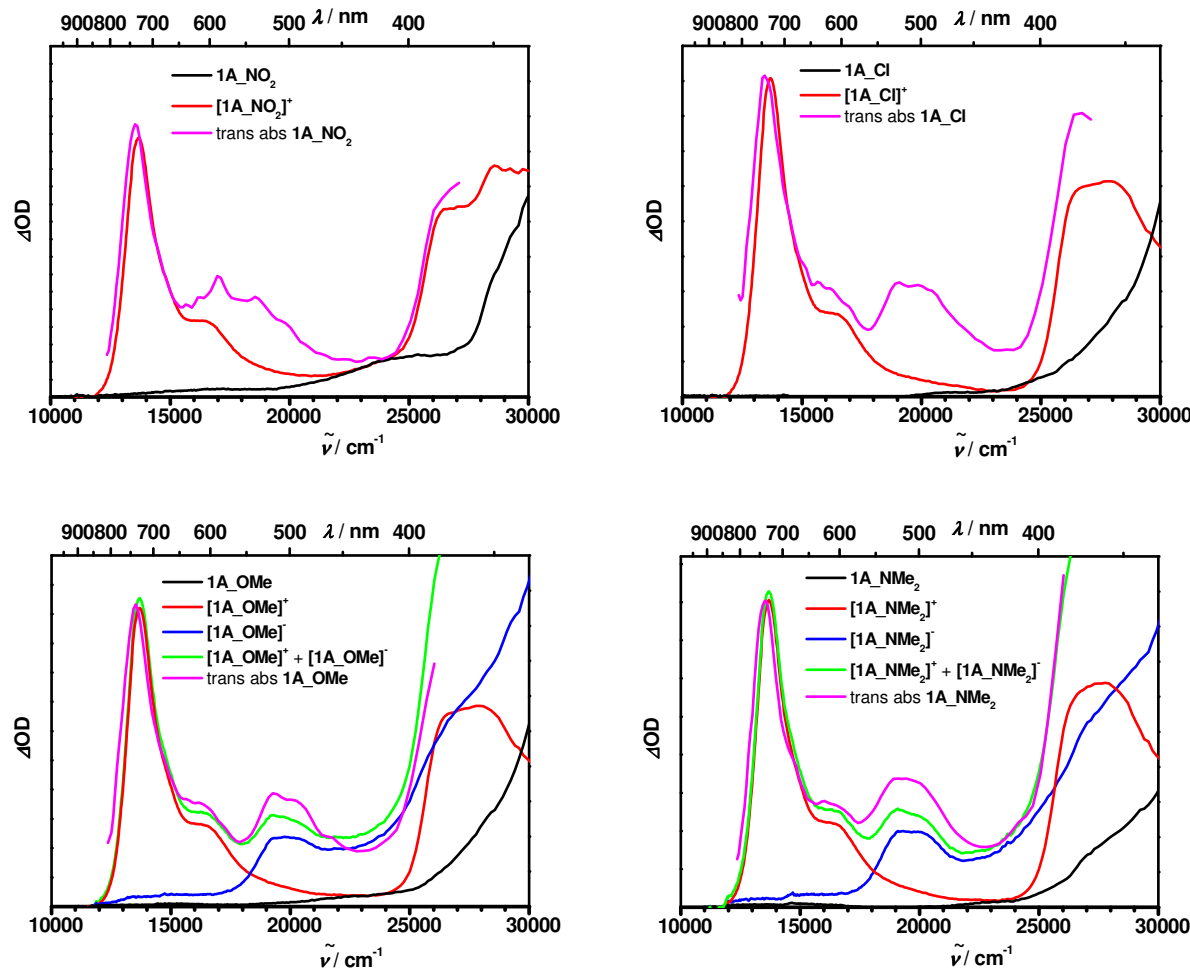


Figure 2.17 Absorption spectra of radical cations and radical anions of the substituted compounds. The green lines show the superimposed spectra of cations and anions. The pink lines shows the transient absorption spectra in 2-MeTHF with excitation at 24000 cm⁻¹ (416 nm).

Thus, while the formation of a CS state as the consequence of a photoinduced electron transfer process from one triarylamine to the bpy ligand is evident, the biexponential decay to the ground state warrants further interpretation. A biexponential decay indicates the presence of two transient species. The fact that all the transient spectra do not change significantly while decaying further indicates that these two transient species have all the same CS character. A biexponential decay is in agreement with a branched kinetic relaxation mechanism as proposed by Hayashi and Nagakura^{186–188} (see Figure 2.18). According to this model, charge separation leads to the initial formation of a singlet ¹CS which is in equilibrium with its triplet ³CS counterpart. Owing to a non-negligible zero field splitting (ZFS) caused by spin-orbit coupling to the iridium core,⁶⁹ we have to deal with three non-degenerate triplet states (T_I , T_{II} , T_{III}). Furthermore, the singlet and triplet CS states are non-degenerate

because of magnetic exchange interaction J which is related to the CS energies by $2J = E(^1\text{CS}) - E(^3\text{CS})$.¹⁸⁹ However, the ZFS as well as J are small compared to the other state energy differences and we can neglect this fact for the moment. Charge recombination to the singlet ground state occurs predominantly from the ^1CS state. While the short component of the decay is mainly associated with k_2 (see Figure 2.18), it is the long component which is associated with k_{-1} . A biphasic decay is expected provided that the formation of the equilibrium is low compared to the decay of the ^1CS state to the singlet ground state.

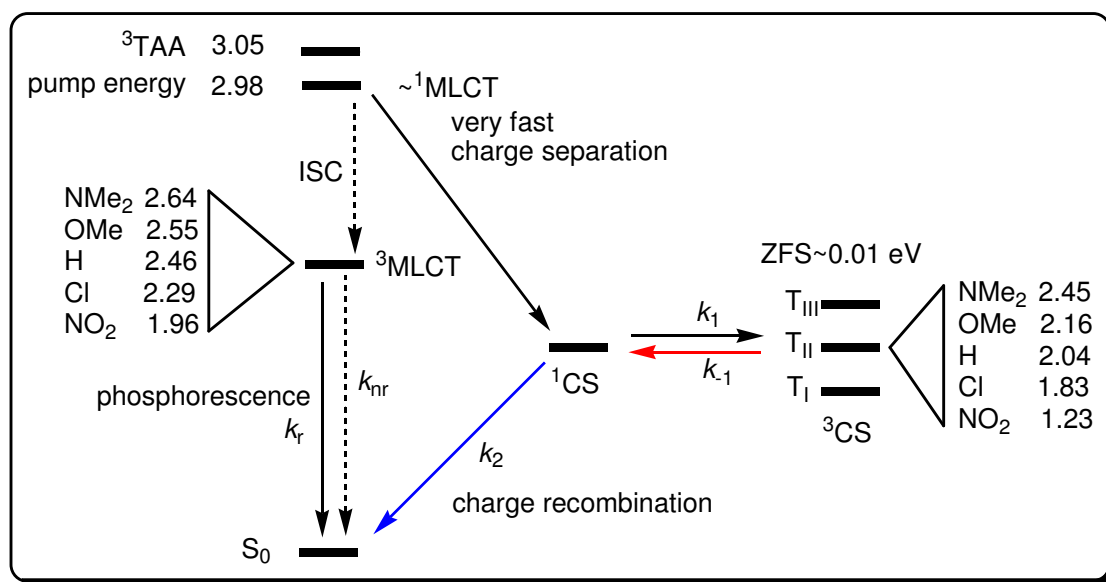


Figure 2.18 Formation of the charge separated (CS) states leading to the almost degenerate equilibrium $^1\text{CS} \rightleftharpoons ^3\text{CS}$. The energies of the $^3\text{MLCT}$ state were determined by the cut-on of the lowest energy band in 2-MeTHF (see Figure 2.8).

2.2.4.2 Temperature-Dependent Transient Absorption Spectroscopy

In order to support the proposed model temperature dependent transient absorption measurements of the differently substituted bpy complexes **1A_(X)**, in the -50 to + 30 °C range as well as measurements with oxygen saturated solutions were accomplished in 2-MeTHF.

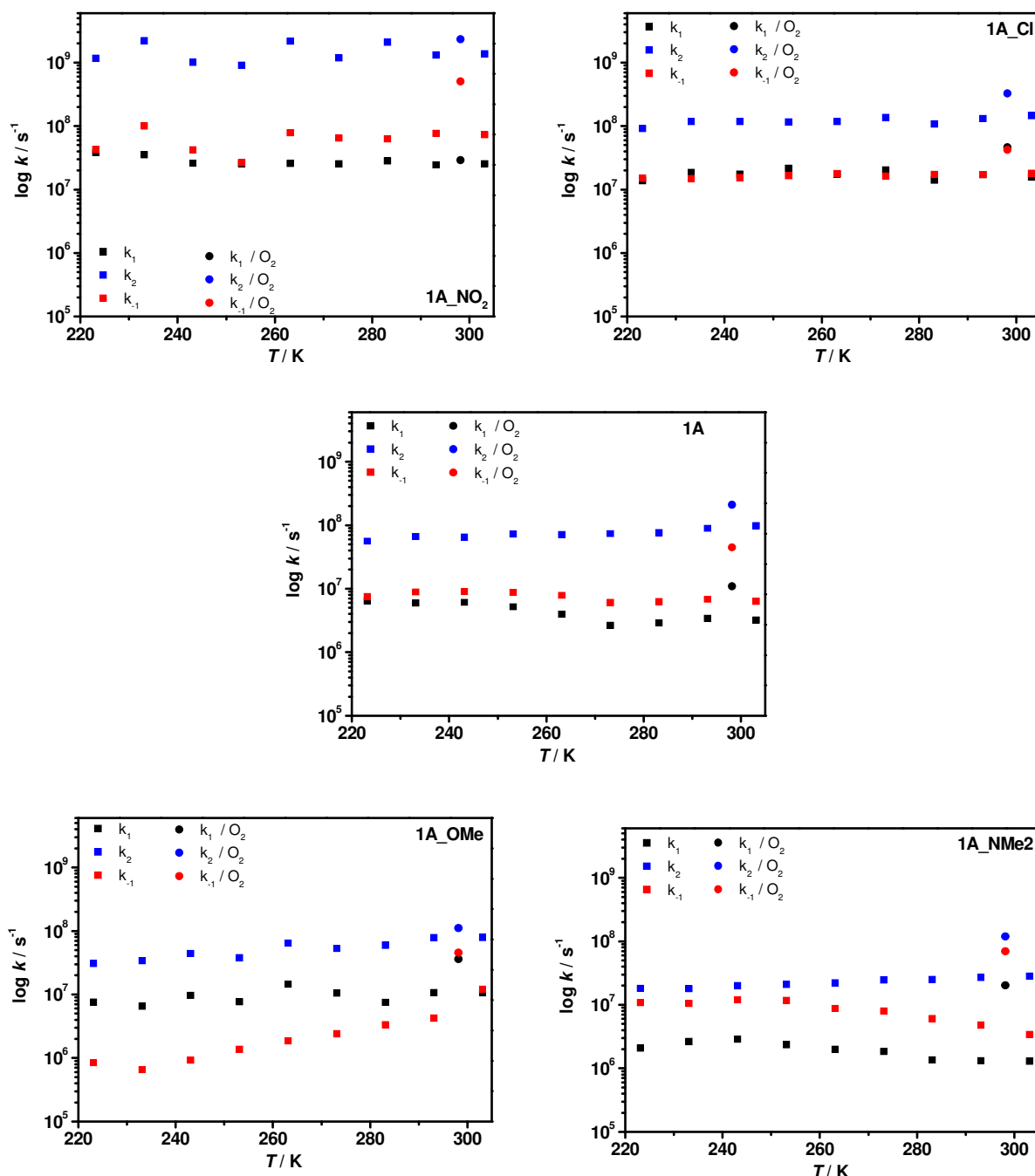


Figure 2.19 Temperature dependence of rate constants of **1A_(X)** complexes determined by transient absorption measurements in 2-MeTHF with excitation at 24000 cm^{-1} (416 nm). The circles refer to measurements in oxygen-saturated solution at RT.

The two lifetimes of each compound were estimated by transient absorption measurements at 13700 cm^{-1} , 16100 cm^{-1} and 18800 cm^{-1} as explained in Chapter 3.1.4 and their average values were determined. The individual rate constants of these experiments were calculated from the two lifetimes and their relative amplitudes by solving the appropriate differential equations as given in Ref¹⁹⁰ and are given in Figure 2.19. From these plots it is evident that the rate constants of all complexes with exception of $X = \text{OMe}$ are practically independent on the temperature

in the given range. For k_2 this is not surprising if one assumes the applicability of Marcus equation 1.1 for charge recombination where ΔG^0 ($=\Delta E_{1/2}$ from Table 2.4) is the free energy difference between donor and acceptor state. Because both the solvent reorganisation energy and the free energy depend on the temperature (mainly through the temperature dependence of the refractive index of the solvent), these effects may cancel out and lead to temperature independent rate constants in small temperature intervals as previously observed in other cases.^{8,13-15,191,192}

The fact that neither k_1 nor k_{-1} depend on the temperature leads to the equilibrium constant $K = k_1/k_{-1}$ being also independent on the temperature. This is consistent with an isoenergetic ($\Delta H_R = 0$) equilibrium of the ${}^1\text{CS}$ and the ${}^3\text{CS}$ states with an equilibrium constant near unity as indeed observed for all complexes except X = OMe (see Figure 2.20).

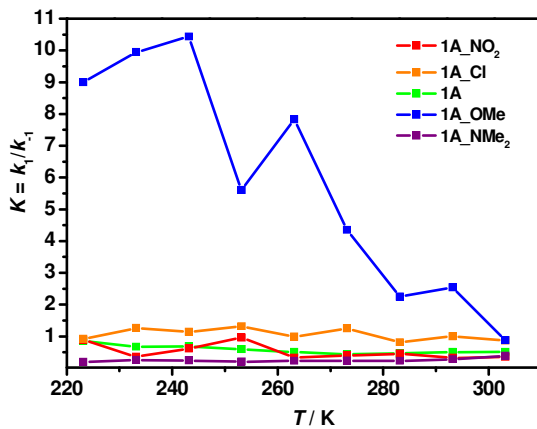


Figure 2.20 Temperature dependence of $K = k_1/k_2$ of $\mathbf{1A}_{\text{(X)}}$ complexes. The scattering in the data reflect the accuracy of the measurements.

Furthermore, pump-probe measurements at RT in oxygen-saturated 2-MeTHF led to an increase of all rate constants but particularly of k_{-1} . This effect may be due to bimolecular reaction of ${}^3\text{CS}$ with ${}^3\text{O}_2$ yielding ${}^1\text{O}_2$ and/or due to the enhancement of intersystem crossing because of the paramagnetic properties of ${}^3\text{O}_2$.¹⁸⁸ In both cases the apparent rate constant k_{-1} represents the enhanced depopulation of ${}^3\text{CS}$ via $k_{-1} = k[\text{O}_2]$. These rate constants are given in Figure 2.19 as circles at RT. The quenching by O_2 supports the assumption that a triplet CS state is involved in the kinetic scheme.

Plotting the individual rate constants vs. the free energy difference of charge recombination (taken as the redox potential difference $\Delta E_{1/2}$ from Table 2.5) shows

that k_2 decreases with increasing free energy drift as expected for an electron transfer process in the Marcus inverted region. The other rate constants k_1 and k_{-1} show a more complex behaviour (Figure 2.21).

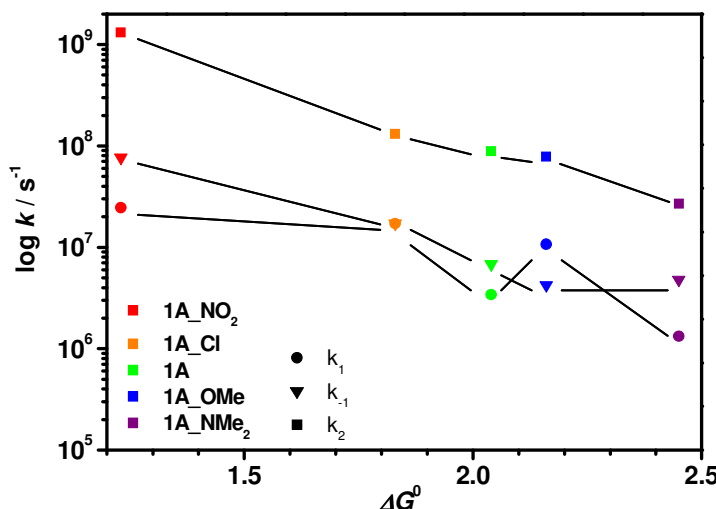


Figure 2.21 Relationship between ΔG_{CR} (from Table 2.5 in MeCN) and the rate constants of **1A_(X)** complexes determined by transient absorption measurements in 2-MeTHF at 293 K with excitation at 24000 cm^{-1} (416 nm).

From the Marcus plot and the data in Table 2.7 it is obvious that **1A_NMe₂** shows the longest living ¹CS state. However, for possible practical application in solar energy conversion the spin state is not relevant and, thus, one should also consider the lifetime of the ³CS state and its relative amplitude. For these reasons, **1A_OMe** is clearly superior as it shows a longer lifetime of the slower component with distinctly higher amplitude (ca 20 %) than **1A_NMe₂**.

As mentioned before, **1A_OMe** is the only complex that shows a significant temperature dependence of the rate constants. In general, the rate constants rise with rising temperature. This effect is most pronounced for k_{-1} which is consistently smaller than k_1 and which changes by one order of magnitude when going from -50 °C to + 30 °C. This makes the equilibrium constant K to rise from ca 1 to 10 when lowering the temperature in the above mentioned range (see Figure 2.20). The change of K goes along with a non-negligible energy difference ΔH_R between ¹CS and ³CS which might be induced by spin-orbit coupling and which lowers the energy of one triplet component T₁ and/or by a magnetic exchange coupling J that makes the ³CS more stable than the ¹CS. Another interpretation which is based on DFT computation in the group of Prof. M. Kaupp suggests an acquisition of conformers of the OMe positions which might be responsible for this temperature dependence.

2.2.5 LEC Studies

To prove the electroluminescent properties, two-layer LECs were constructed with **1**, **1B**, **2**, **2B**, **5** and **5B**. The fabricated LECs (see Chapter 3.1.6) show Emission in the green to yellow region as shown in Figure 2.22. In comparison to the emission spectra in 2-MeTHF they show a blue-shifted emission (see Table 2.6). The spectra do not depend on the applied voltage. At a voltage of 5 V the luminescence starts after 30 minutes. As it is increased, the delay decreases and at a voltage of 7 V the devices show visible emission without any delay.

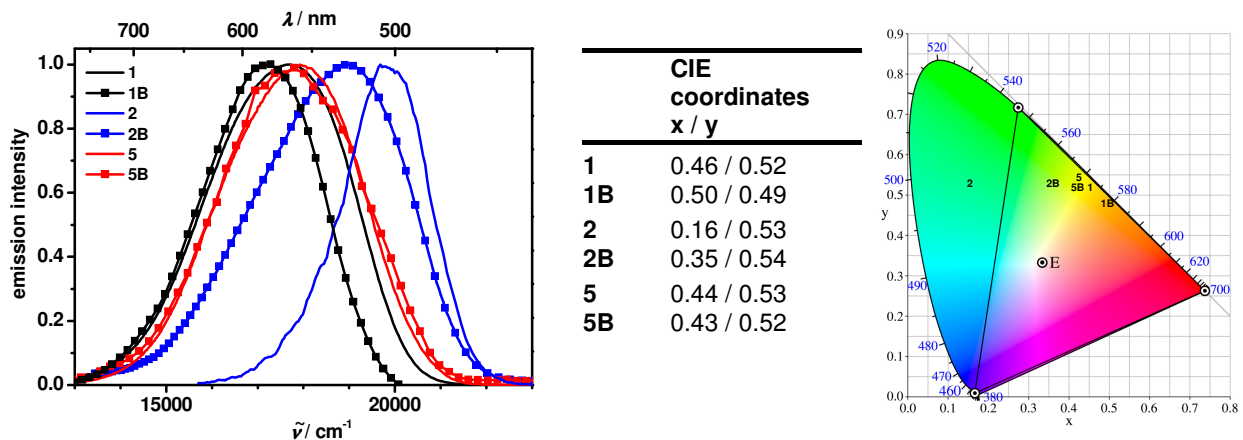


Figure 2.22 Left hand side: emission spectra of the LEC devices of **1**, **1B**, **2**, **2B**, **5** and **5B** at a constant bias of 5 V. Right hand side: CIE (Commission Internationale de l'Éclairage) coordinates and CIE scheme with **1**, **1B**, **2**, **2B**, **5** and **5B**.

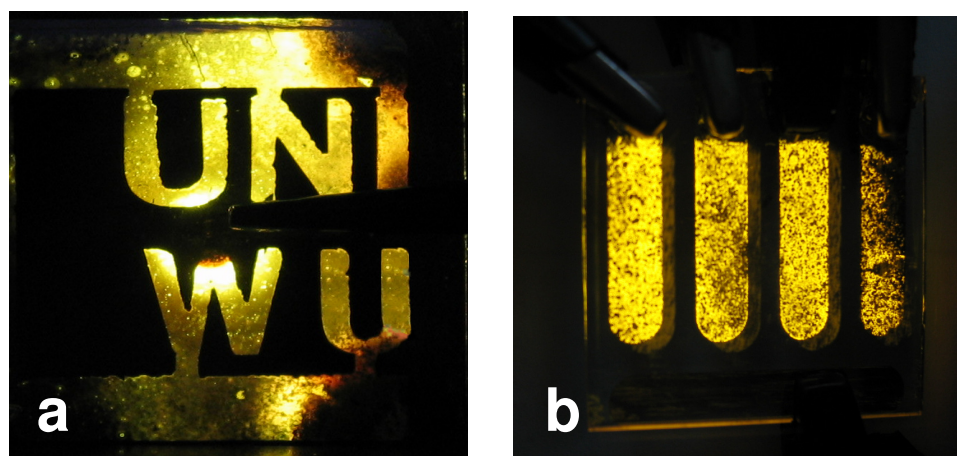


Figure 2.23 fabricated LECs with **1B**. Picture **a** shows a LEC with the emblem of the University of Würzburg. **B** shows a prototype device with four 3 mm stripes.

The fabricated LECs with **1B** and **2B** show a red shifted emission compared to their reference compounds **1** and **2**. For **5** and **5B**, no differences could be observed. The Commission Internationale de l'Éclairage coordinates show for **1**, **5** and **5B** a yellow, for **1B** an orange and for **2** and **2B** a green luminescence.

Further measurements (like current – voltage plots and luminescence intensity) could not be done because of the unbalanced coatings of the devices.

2.3 Neutral Platinum and Iridium Complexes

Prior to the synthesis and analysis of the cationic Ir(III) complexes described in Chapter 2.2 the synthesis of some neutral transition metal complexes was planned. As acetylacetonate Pt(II) and Ir(III) complexes are of particular interest due to their promising use in electroluminescent devices^{69,78,106,108,111,112,193,194}, the compounds given in Figure 2.24 were synthesised. The aim was to describe the photophysical and electrochemical properties of these complexes and whether they might be suitable for OLED applications when attaching triarylamine (TAA) as hole conducting compound. TAA was connected directly or via a CH₂ bridge to the acetylacetonate (acac) in order to probe the influence of the different kinds of connection on the photophysics of the complexes.

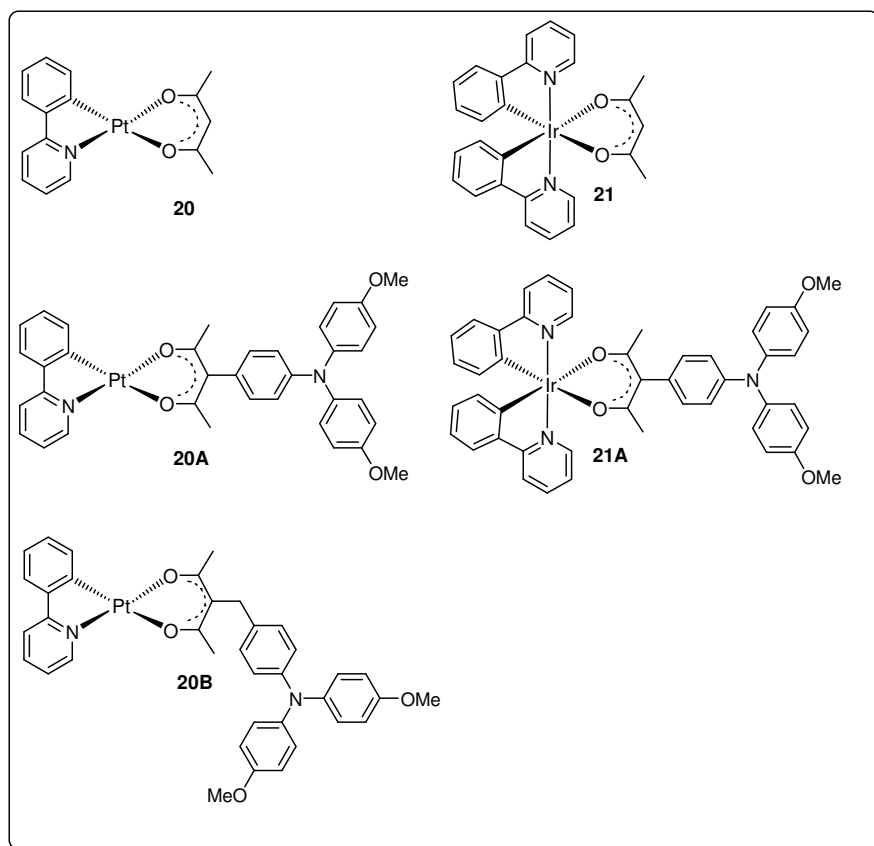
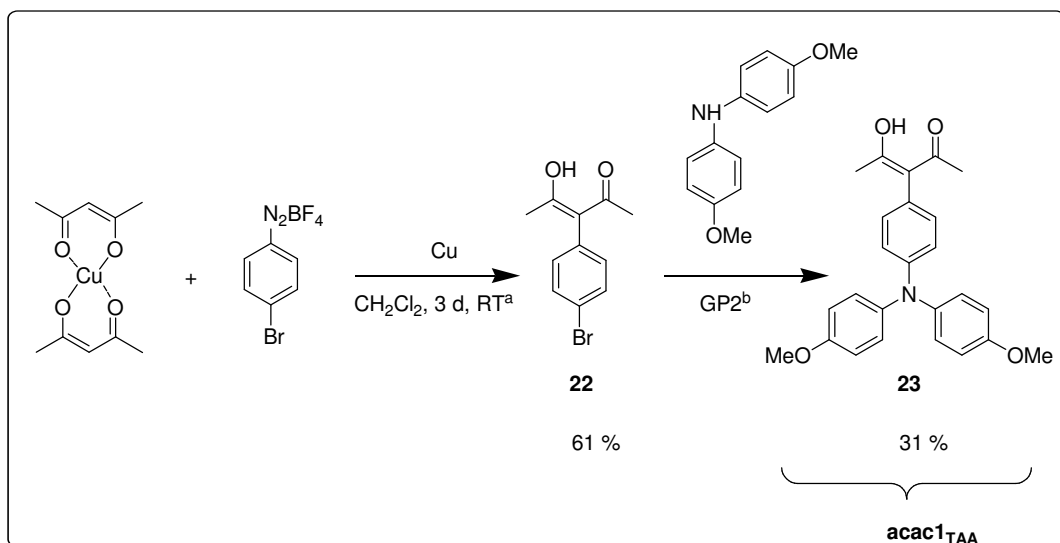


Figure 2.24 (C^N)Pt(O²⁻) and (C^N)₂Ir(O²⁻) complexes **20**, **21**, **20A**, **21A**, **20B** and **21B**.

2.3.1 Synthesis

2.3.1.1 The Acetylacetone Compounds

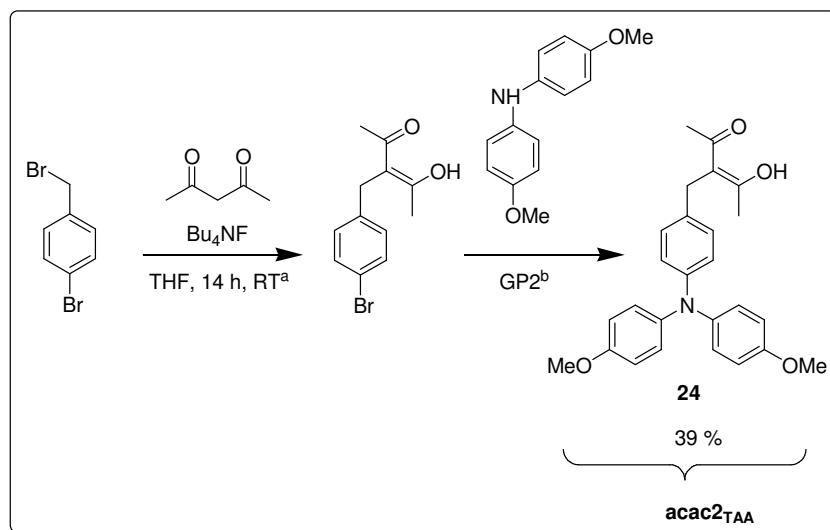
The triarylamine-substituted β -diketonato Pt(II) and Ir(III) complexes **20B** and **21B** only differ from **20A** and **21A** in the additional CH₂-bridge between TAA and acetylacetone complexes (Table 2.8). The triarylamine-substituted acetylacetone ligand **acac1_{TAA}** (**23**) was synthesised from compound **22** by palladium-catalysed Buchwald-Hartwig amination with 4,4'-dimethoxydiphenylamine.¹⁵³⁻¹⁵⁷ Compound **22** was obtained by reaction of copper(II)pentane-2,4-dithionate¹⁹⁵ with the *p*-bromophenyldiazoniumtetrafluoroborat in a Meerwein arylation according to literature (Scheme 2.6).^{195,196}



Scheme 2.6 Synthesis of the triarylamine-substituted acetylacetone ligand **23**. ^a Lit: ^{195,196}, ^b GP2: Arylamine, Pd₂(dba)₃·CHCl₃, NaO*t*Bu, P*t*Bu₃; toluene, 80 °C, 12 h.

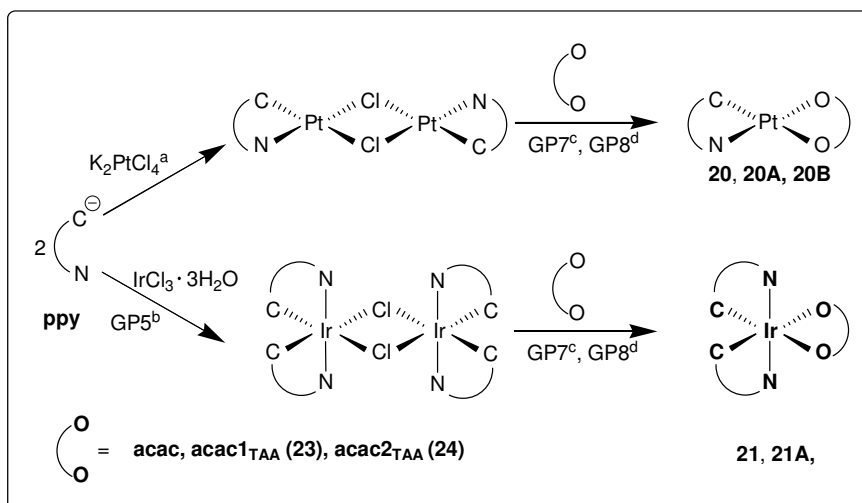
Acetylacetone ligand **acac2_{TAA}** (**24**) with the inserted CH₂-group also was prepared by palladium-catalysed Buchwald-Hartwig amination with 3-(4-bromobenzyl)pentane-2,4-dione and 4,4'-dimethoxydiphenylamine (Scheme 2.7).^{153-157,197,198}

The β -diketonato Pt(II) and Ir(III) complexes **20**, **20A** and **20B** and **21** and **21A** (Table 2.7) were synthesised from their dichloro-bridged dimers (Scheme 2.8), following literature-known reactions.^{161,193}



Scheme 2.7 Synthesis of the triarylamine-substituted acetylacetone ligand **24**. ^a Lit.: ^{197,198}, GP2: arylamine, $\text{Pd}_2(\text{dba})_3 \cdot \text{CHCl}_3$, NaO^tBu , P^tBu_3 ; toluene, 80°C , 12 h.

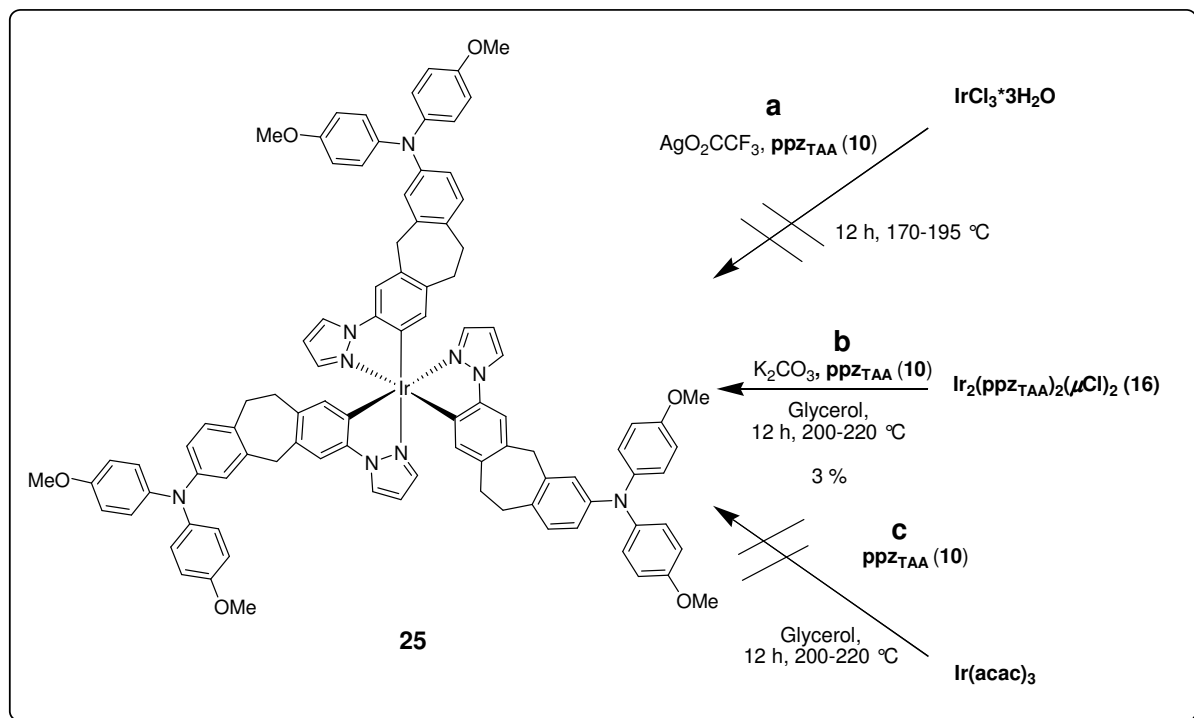
Complex **20B** was prepared following the classical method for the synthesis of compounds **20** and **21** by refluxing the corresponding reactants in 2-ethoxyethanol with Na_2CO_3 as the base.^{112,161,193} However, this synthesis did not work for compounds **20A** and **21A**. Thus, **20A** and **21A** were synthesised by a modified method heating the ligands with the corresponding dimer in dichloromethane with tetrabutylammonium hydroxide.¹⁰⁸ However, this route did not work sufficiently for the synthesis of the missing $[\text{Ir}(\text{ppy})_2(\text{acac2}_{\text{TAA}})]$ compound. Only traces could be detected in the mass spectrum. **20A** and **21A** could only be characterised by ^1H and ^{13}C NMR spectroscopy, the mass spectra (MALDI and ESI) gave unsatisfactory results with differing mass signals.



Scheme 2.8 Synthesis of the cyclometalated complexes **20**, **20A**, **20B**, **21** and **21A**. ^a Lit.: ¹⁹³, ^b GP5: $\text{IrCl}_3 \cdot 3\text{H}_2\text{O}$, 2-ethoxyethanol : $\text{H}_2\text{O} = 3 : 1$, 100°C , 12 h, ^c GP7: 2-ethoxyethanol, Na_2CO_3 , 100°C , 16 h, ^d GP8: CH_2Cl_2 , tetrabutylammonium hydroxide, reflux, 12 h.

2.3.1.2 The Homoleptic Ir(ppz_{TAA})₃ Complex (**25**)

Compared to the cationic and mixed-ligand Ir(III) complexes, *facial* homoleptic compounds are studied most intensely for OLED application^{106,107,110,199} as, for example, the *fac* tris(2-phenylpyridine) iridium, Ir(ppy)₃ (**S**) compound (see Chapter 1.2.3). Due to their uniform structure they are easier in synthesis and, compared to the cationic compounds, their solubility is better. For this reason, the synthesis of the *fac* Ir(ppz_{TAA})₃ was planned in order to analyse the photophysical properties.



Scheme 2.9 Approaches for the synthesis of complex **25**.

Different routes were tested for the synthesis of complex **25** (Scheme 2.9). The reaction of $\text{IrCl}_3 \cdot 3\text{H}_2\text{O}$ and the cyclometalating ligand with silver trifluoroacetate^{199,200} (**a**) as well as the reaction of $\text{Ir}(\text{acac})_3$ with ppz_{TAA} in glycerol²⁰¹ (**c**) gave no product. Only little product could be obtained by refluxing the ligand with K_2CO_3 in glycerol (**b**). This route could be enhanced by heating in the microwave oven for 2 h to get **25** in 3 % yield. For comparison, $\text{Ir}(\text{ppz})_3$ was synthesised according to literature.¹¹⁰

2.3.2 Redox Properties

The electrochemical properties of the neutral β -diketonate complexes and the homoleptic $\text{Ir}(\text{ppz}_{\text{TAA}})_3$ compound were examined by using cyclic voltammetry. All compounds were measured in acetonitrile containing 0.1 M tetrabutylammonium hexafluorophosphate at 100 mV s⁻¹ scan rate. A summary of the redox potentials vs ferrocene/ferrocenium is listed in Table 2.8.

All the Pt complexes described show irreversible redox properties, analogous to literature-known compounds.¹⁹³ The CV of **20B** is shown in Figure 2.25 to demonstrate that the two oxidation waves at 0.27 and 0.88 V are irreversible as well as the reduction at -2.38 V. Similar to the cationic complexes, the reduction is localized on the C^N ligand while the oxidation at ~0.27 V occurs at the TAA and the second oxidation signal at the metal center. This square planar metal center can easily be attacked by nucleophilic solvents which explains the irreversibility of the oxidation.¹⁹³

	$E^{\text{Ox}}_{1/2}$ (Pt / Ir) / mV	$E^{\text{Ox}}_{1/2}$ (TAA) / mV	$E^{\text{Red}}_{1/2}$ / mV
20	550 ⁱ 1070 ⁱ		-2400 ^r
20A	990 ⁱ	280 ⁱ	-2200 ⁱ
20B	880 ⁱ	270 ⁱ	-2380 ⁱ
21	1030 ^r		-1950 ^r
21A	980	230	-1870

Table 2.8 Redox properties of the acac compounds **20(A,B)** and **21(A)** in acetonitrile.
ⁱreversible, ^rirreversible.

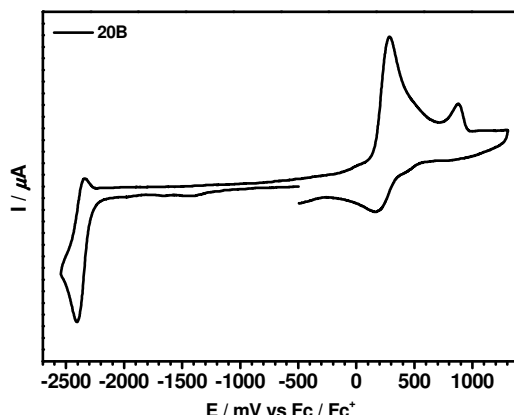


Figure 2.25 CV of **20A** in 0.1 M MeCN/TBAH, $v = 100 \text{ mVs}^{-1}$.

For **21** the oxidation and reduction is reversible, for **21A** the reversibility could not be checked under thin layer conditions because the compound is not stable under CV conditions.

	$E^{\text{Ox}}_{1/2}$ (Ir) / mV	$E^{\text{Ox}}_{1/2}$ (TAA) / mV
25	310 ^r	180 ^r
Ir(ppz) ₃	340 ^r	
ppz _{TAA}		180 ^r

Figure 2.25 Redox properties of the homoleptic TAA complex **25** in acetonitrile. ^r reversible, ⁱ irreversible.

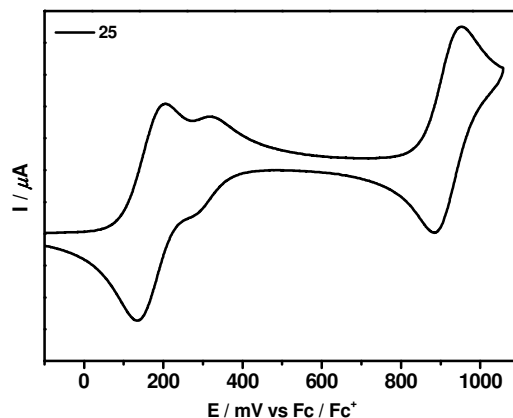


Figure 2.26 CV of **25** in 0.1 M MeCN/TBAH, $v = 100 \text{ mV/s}$.

The electrochemical properties of the homoleptic Ir(ppz_{TAA})₃ complex is depicted in Figure 2.26. The data of the literature-known complexes Ir(ppz)₃ is consistent with

the literature describing only one reversible oxidation wave resulting from the oxidation of the Ir-phenyl moiety.¹¹⁰ The two additional oxidation waves of **25** are caused by single and double oxidation of the TAA part.

2.2.3 Spectroscopy

2.2.3.1 Steady State Absorption Spectroscopy

The absorption spectra of the acac complexes are given in Figure 2.27. Intense bands are observed between 35000 and 40000 cm⁻¹ that can be assigned to the spin-allowed $^1\pi\text{-}\pi^*$ ligand-centered (LC) transitions in the C^N ligands. The low-energy transitions (insets Figure 2.27) can be assigned to the spin-forbidden $^3\text{MLCT}$ absorption transitions.^{111,112,193} These absorption bands are covered by more intense bands for the directly linked acac_{TAA} compounds. These transitions are charge-transfer (CT) bands caused by a charge transfer process within the ligands.¹⁵¹ As discussed for the cationic complexes, the moderately intense bands between 24000 cm⁻¹ and 35000 cm⁻¹ can be attributed to the characteristic localised transitions of the triarylamine subunits^{151,171} and the typical spin-allowed metal-to-ligand charge-transfer ($^1\text{MLCT}$) $d\pi(\text{Ir})\rightarrow\pi^*$ absorption.^{103,116}

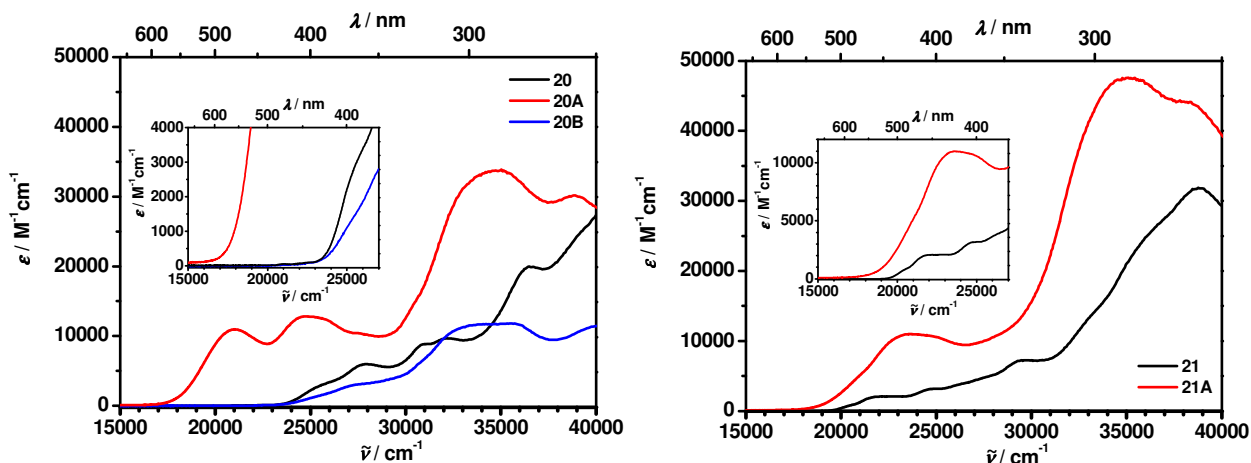


Figure 2.27 Absorption spectra of **20**, **20A**, **20B** and **21**, **21A**, **21B** in acetonitrile solution at 298 K.

In the *fac* Ir(III)phenylpyrazole (**25**) the $^1\pi\text{-}\pi^*$ transitions of the phenylpyrazole ligand can be found between 30000 and 40000 cm⁻¹ (Figure 2.28). The $^1\text{MLCT}$ and $^3\text{MLCT}$ can be observed between 22000 cm⁻¹ and 27000 cm⁻¹ (inset).¹¹⁰

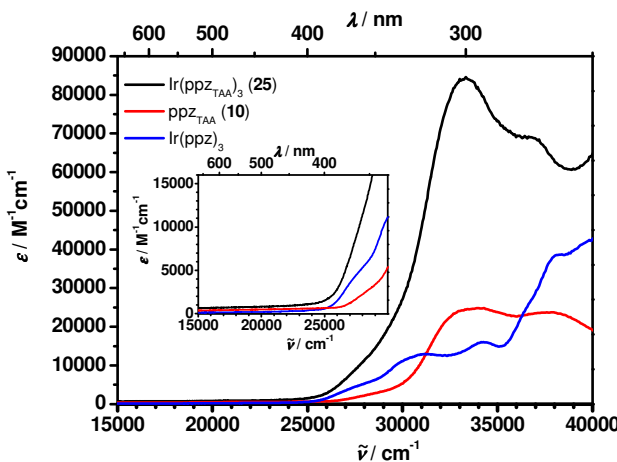


Figure 2.28 Absorption spectra of **25**, the reference and the free ligand in acetonitrile solution at 298 K.

2.3.2.2 Steady State Emission Spectroscopy at RT and 77K

The emission data, excitation wavelengths and energies of all complexes and are listed in Table 2.9. The literature-known reference complexes **20** and **21** show luminescence in agreement with literature data.^{110-112,193}

Compared to the reference compounds, the TAA substituted complexes show only weak or no fluorescence at RT. The emission band of **21A** is completely different than that of **21** which indicates that this compound does not emit from the triplet ³Ir state as proposed for **21** due to the long lifetimes. Besides, the quantum yield of **21A** is nearly naught, which shows that an additional quenching process might take place. Compound **20B** shows luminescence that is nearly identical with that of its reference. However, the low quantum yield suggests an additional quenching process which inhibits luminescence from the Ir core.

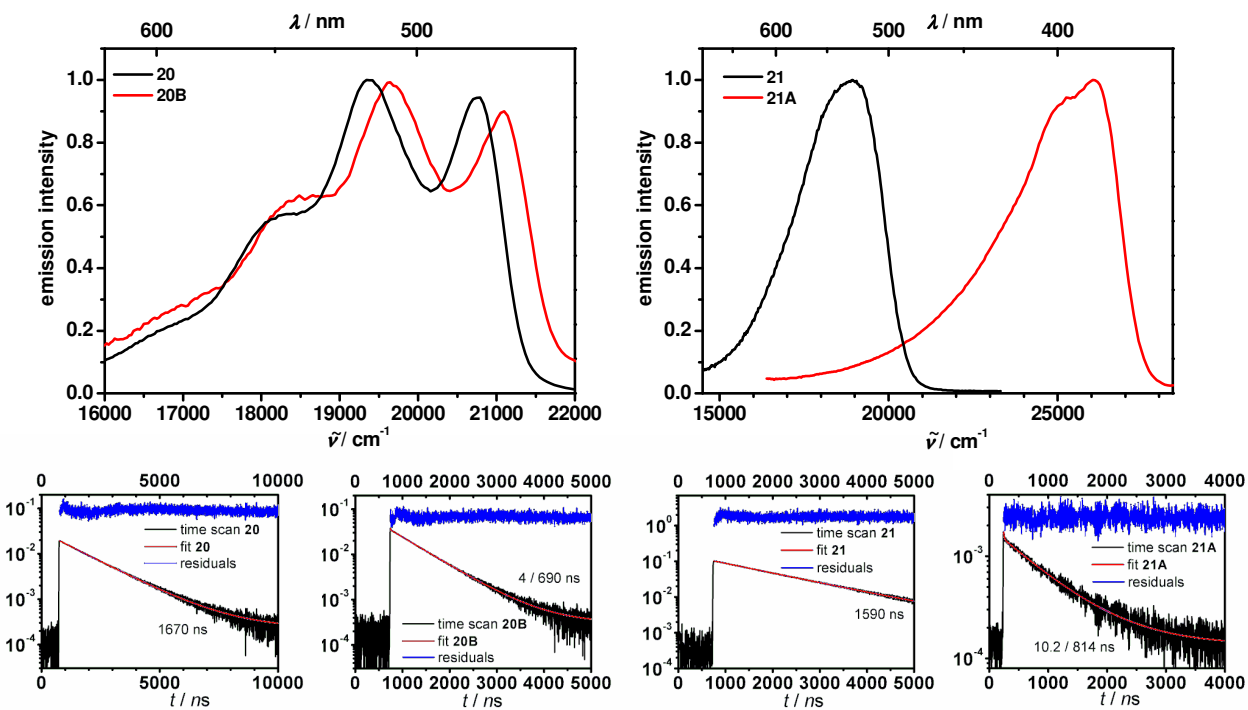


Figure 2.29 Emission spectra and time scans of **20**, **20B**, **21** and **21A** in 2-MeTHF solution at 298 K. Excitation 28200 cm^{-1} (355 nm), for **21A**: 33300 cm^{-1} (300 nm).

Table 2.9 Emission properties of **20**, **20A**, **20B** and **21**, **21A**.

	medium (T/K)	$\tilde{\nu}_{\text{em}}$ /cm ⁻¹	τ (relative amplitudes) /ns	Φ_{em} /%
20	2-MeTHF (298) ^a	20900	1670	15 ^a
	CH ₂ Cl ₂ (298) ^b	20700	-	23
	2-MeTHF (77) ^b	20900	9200	26
20A	2-MeTHF (298)	-	-	-
	2-MeTHF (77)	-	-	-
20B	2-MeTHF (298) ^c	20800	4 (1) /690 (12)	2
	MeCN (298) ^c	21000	-	2
	CH ₂ Cl ₂ (298) ^c	21000	-	5
	2-MeTHF (77) ^c	20900	7360	
21	2-MeTHF (298) ^b	18900	1590	36
	CH ₂ Cl ₂ (298) ^b	19100	-	37
	2-MeTHF (77) ^b	19700	4630	
21A	2-MeTHF (298) ^c	26000	10.2 (1) /814 (300)	< 1
	CH ₂ Cl ₂ (298) ^c	25500	-	< 1
	2-MeTHF (77) ^c	20200	4030	
25	2-MeTHF (298)	-	-	-
	2-MeTHF (77) ^c	-	16300	-

^a data from literature¹⁹³, ^bexcitation: 28200 cm^{-1} (355 nm), ^cexcitation: 40000 cm^{-1} (416 nm).

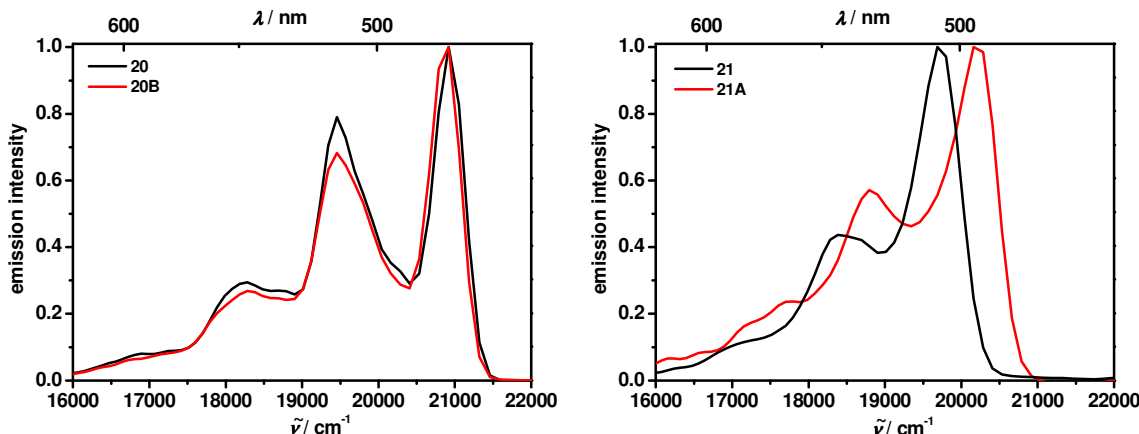
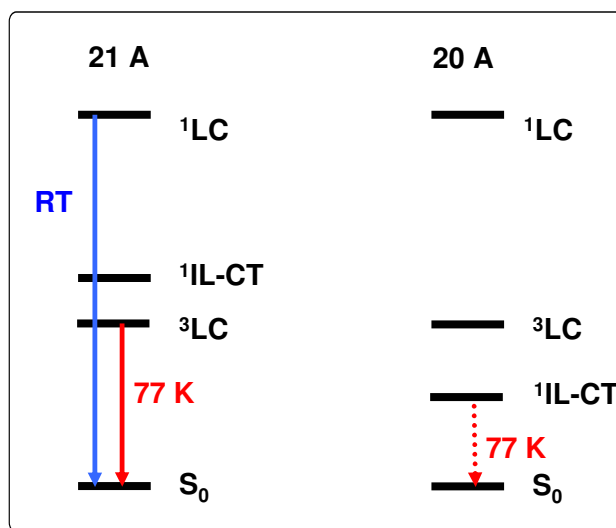


Figure 2.30 Emission spectra of the ppz-complexes in 2-MeTHF solution at 77 K. Excitation: 28200 cm^{-1} (355 nm) for the references, 40000 cm^{-1} (416 nm) for the TAA compounds.

The phosphorescence spectra of the complexes at 77 K in a rigid 2-MeTHF matrix are shown in Figure 2.30. The emission maxima and lifetimes are given in Table 2.7. At RT, as well as at low temperatures, compound **20A** exhibits no emission that may be caused by the population of an IL-CT state that decays rationless (see Scheme 2.10). The other complexes show intense and long-lived luminescence at 77 K with a lifetime in the μs regime which indicates the phosphorescent nature of the luminescence. Similar to the cationic complexes, the TAA compound **21A** shows long-lived phosphorescence differing from the emission spectrum recorded at RT. This emission seems to be caused by phosphorescence from a local ${}^3\text{LC}$ state that is lower in energy and populated at low temperatures (Scheme 2.10).



Scheme 2.10 Emission of **20A** and **21A** at RT and 77 K.

All emission maxima at 77 K are blue-shifted compared to the emission maxima at RT. This shift is due to inhibition of solvent reorganisation in the rigid matrix. The spectra of the platinum and iridium complexes **20(B)** and **21(A)** show a vibronic finestructure that suggests a high percentage of ^3LC transition as described for the cationic complexes in Chapter 2.2.3.2.2.

The phosphorescence spectrum of **25** is depicted in Figure 2.31. As known from literature, $\text{Ir}(\text{ppz})_3$ is a very weak emitter at RT but is phosphoresces intensely at 77 K with two maxima at 24400 cm^{-1} and 22200 cm^{-1} in 2-MeTHF. The highly structured emission with ^3LC transition character has a lifetime of $\tau = 14 \mu\text{s}$.¹¹⁰ The similar structure of the phosphorescence spectrum of **25** also suggests a $^3\text{Ir}(\text{ppz}_{\text{TAA}})_3$ state.

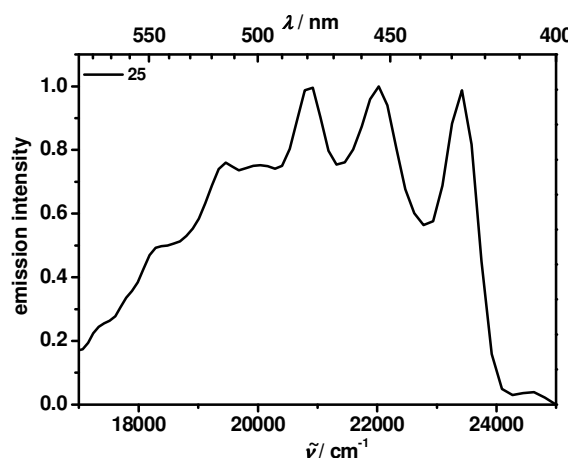


Figure 2.31 Emission spectrum of **25** in 2-MeTHF solution at 77 K. Excitation: 40000 cm^{-1} (416 nm).

2.3.3.3 Transient Absorption Spectroscopy

The transient absorption spectra together with the time scans are shown in Figures 2.32 and 2.33. Both, **20A** and **21A** show no transient signals, maybe caused by charge-transfer quenching due to the direct linkage between donor and acceptor. Compared to the reference complexes, the transient absorption spectrum of the TAA substituted complex **20B** does not differ from its corresponding reference compound. The absorption bands of both compounds decay with the same lifetimes, respectively. These bands can be assigned to the $^3\text{Pt}(\text{N}^{\text{N}})(\text{acac})$ states as they are in good accordance with the luminescence lifetimes at RT. However, the transient signals of **20B** decay with lifetimes that are slightly shorter than their luminescence

lifetimes at RT, so a partial luminescence quenching is taking place. The transient spectrum of **21** is shown in Figure 2.33 and can be assigned to the $^3\text{Ir}(\text{N}^{\wedge}\text{N})_2(\text{acac})$ state, because the transient lifetime with 1580 ns is in good agreement with the luminescence lifetime of 1590 ns. For $\text{Ir}(\text{ppz}_{\text{TAA}})_3$ (**25**) and its reference compound no transient signals could be detected.

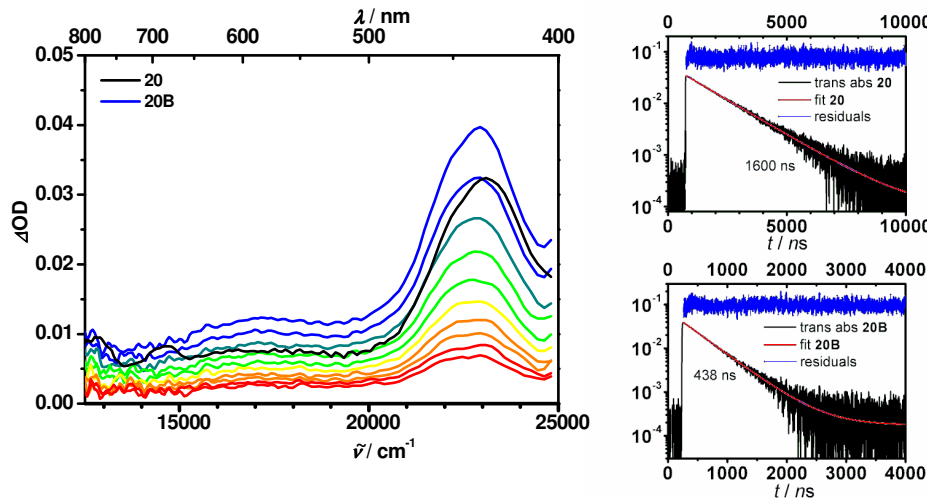


Figure 2.32 Left hand side: Transient absorption spectra of **20B** with excitation at 24000 cm^{-1} (416 nm). Early spectra are shown in blue/green and late spectra are shown in orange/red colours (0 – 1000 ns). For comparison the reference compound **20** is given in black. Right hand side: Time scans and fits at 20000 cm^{-1} (500 nm).

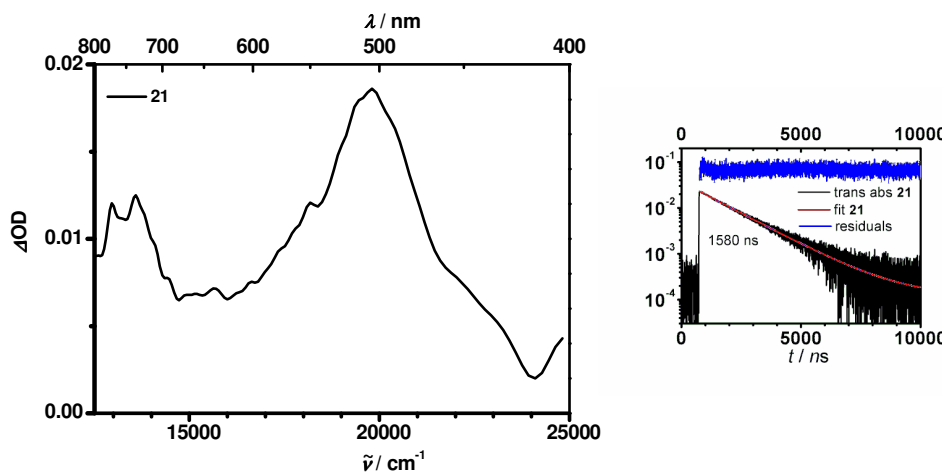


Figure 2.33 Left hand side: Transient absorption spectrum of **21** with excitation at 24000 cm^{-1} (416 nm). Right hand side: Time scan and fit at 20000 cm^{-1} (500 nm).

2.4 Summary

In the first part of this work we presented the synthesis and photophysical properties of a series of transition metal donor-acceptor Ir(III)complexes of the type $[(C^N)_2Ir(N^N)][PF_6]$. The Ir(III) was connected with hole conducting donor-moieties like carbazole (CZ) and triarylamine (TAA) linked via a methylene and ethylene bridge to the cyclometalating C^N ligands phenylpyrazole (ppz) and phenylpyridine (ppy). Bidentate N^N and P^P ligands like 2,2'-bipyridyl (bpy), 3,4,7,8-tetramethyl-1,10-phenanthroline (tmp) and *cis*-1,2-*bis*(diphenylphosphino)ethylene (bdppe) were used as acceptor units. In order to analyse the influence of the electron density of the bpy ligand, TAA-complexes with acceptor- and donor-substituted bpy acceptor units were synthesised. Therefore, 4,4'-dinitro-2,2'-bipyridyl, 4,4'-dichloro-2,2'-bipyridyl, 4,4'-dimethoxy-2,2'-bipyridyl and 4,4'-dimethylamino-2,2'bipyridyl were used as neutral N^N ligands. In order to compare the photophysical properties, all reference compounds without hole conducting component were synthesised.

All the carbazole compounds, except the bdppe complexes, exhibit emission and transient absorption properties similar to their reference compounds that make them interesting for OLED (organic light emitting device) applications. LEC (light emitting electrochemical cell) studies show a red shifted luminescence.

The triarylamine compounds do not luminesce at RT but they exhibit an intense, blue-shifted and long-lived luminescence at 77 K in a rigid matrix. The transient absorption spectra differ strongly from that of their reference compounds. The spectra display characteristic features of the spectra of the isolated radical anions and cations supported by spectroelectrochemical measurements. Thus, it can be assumed that the transient states are charge separated (CS) states in which the positive charge is localised at the TAA donor units and the negative charge at the N^N acceptor units. The decays of the transient states are biexponentially what indicates the presence of two transient states, the ¹CS and the ³CS state.

To understand this behaviour the differently substituted bipyridyl-complexes were synthesised and analysed. Temperature dependent transient absorption measurements showed that all rate constants are indepentend of the temperature, except for the complex with OMe substituents at the bpy ligand. The equilibrium constant $K = k_1 / k_2$ is nearly one for all complexes. For the OMe-compound it

decreases with increasing temperature. Plotting the rate constants vs. the free energy differences (determined by cyclovoltammetry measurements) shows that all constants are decreasing with increasing donor strength of the bpy ligand. DFT calculations on the OMe-compound are already in work.

In the second part of this work, neutral Ir(III) and Pt(II) complexes of the type $[(O^{\wedge}O)Ir(N^{\wedge}N)_2]$ and $[(O^{\wedge}O)Pt(N^{\wedge}N)]$ were introduced. There, TTA was connected directly or via a CH_2 bridge to acetetylacetone (acac = $O^{\wedge}O$) in order to probe the influence of the different kinds of connection on the photophysics of the complexes. As the bidentate $N^{\wedge}N$ ligand 2,2'-bipyridyl (bpy) was chosen. All the corresponding reference compounds without triarylamine were obtained in order to compare with the TAA substituted analogs. Furthermore, the homoleptic *fac* $Ir(N^{\wedge}N)_3$ complex with triarylamine connected via a methylene and ethylene bridge to phenylpyrazole as introduced in the first part of this work was synthesised.

The synthesis of the Ir(III) compound with the TAA substituted acac ligand connected via the CH_2 group was not successful. All the neutral triarylamine-substituted β -diketonato Pt(II) and Ir(III) complexes do not luminesce at RT, except the Pt(II)-complex with CH_2 bridge. This compound shows transient state characteristics that are in good agreement with the luminescence lifetimes at RT and that are similar to the reference compound, what suggests to a $^3Pt(N^{\wedge}N)(O^{\wedge}O)$ state. The complexes without the CH_2 bridging unit show no transient signals what may be caused by charge-transfer quenching due to the direct linkage between donor and acceptor unit.

The homoleptic *fac* $Ir(N^{\wedge}N)_3$ complex exhibits no emission at RT and no transient signals. At 77 K it shows a highly structured emission with 14 μs lifetime. Compared to the literature-known reference compound this emission is caused by the population of a $^3Ir(ppz)_3$ state.

Our findings are important for designing complexes with stronger acceptor units (i.e. naphthaleneimide) for long CS states lifetimes to be used as photosynthesisers in solar cells and other optoelectronic devices. Besides, LEC and OLED studies on the carbazole complexes are still of interest to analyse the degree of triplet-triplet-annihilation in these devices.

3 Experimental Section

3.1 Apparatus and Methods

3.1.1 General Analytical Methods

NMR spectroscopy

- Bruker Avance 400 FT-Spectrometer (^1H : 400.1 MHz; ^{13}C : 100.6 MHz)
- Bruker Anance DMX 600 FT-Spectrometer (^1H : 600.13 MHz; ^{13}C : 150.92 MHz)

All ^1H and ^{13}C spectra were recorded at 295 K. The signal of the solvent was used as the internal reference and the chemical shifts are given in ppm (δ -scale). Multiplicities were denoted as s (singlet), d (doublet), t (triplet), m (multiplet). NMR-spectroscopy data are quoted as follows: chemical shift (multiplicity, number of protons).

Mass spectroscopy

- Finnigan MAT 90
- Bruker Daltonik microTOF focus

Mass spectra were recorded at the Institute of Organic Chemistry, University of Würzburg. For ESI-spectra 10 μM solutions of the sample in chloroform were prepared.

Melting points

Melting points are uncorrected and were determined by using a Tottoli melting point apparatus from Büchi.

3.1.2 Electrochemistry

- Electrochemical workstation BAS CV-50 W including software version 2.0
- EG & G potentiostat / galvanostat model 363
- JASCO V-570 UV/Vis/NIR spectrometer

Cyclic voltammograms

were measured under an argon atmosphere in dry and oxygen-free solvents with 0.1 M tetrabutylammonium hexafluorophosphate (TBAH) as supporting electrolyte. The concentration of the solute was about 0.5 mM. A conventional three electrode setup consisting of a platinum disc working electrode, a Ag/AgCl pseudoreference electrode and a platinum wire counter electrode was used. The redox potentials were referenced against the ferrocene/ferrocenium redox couple as an internal standard.

Spectroelectrochemistry

The spectroelectrochemical measurements were carried out in a thin-layer cell with a gold minigrid working electrode.²⁰² The potential applied to the electrode was varied in steps of 50 – 100 mV and an UV/Vis/NIR spectrum was recorded ca. 1 min after each potential change.

3.1.3 UV/Vis/NIR Spectroscopy

- JASCO V-570 UV/Vis/NIR spectrometer

All solvents were of spectroscopic grade and were used without further purification. The 2-MeTHF was degassed, stored under inert gas and used freshly until decomposition products that interfere emission measurements could be observed. Absorption spectra were recorded with a JASCO V-570 UV/vis/NIR spectrometer in 1 cm quartz cuvettes.

3.1.4 Transient Absorption Measurements

- Edinburgh LP 920 Laser Flash spectrometer with a 300 W ozone-free Xe arc lamp including a photomultiplier (Hamamatsu R955) and a digital storage oscilloscope (Tektronix TDS3012B)
- Continuum Minilite II Nd:YAG laser operating at 10 Hz, 8 ns pulse duration, ca. 57 mW average power at 28200 cm^{-1}

Nanosecond transient absorption spectra were acquired on an Edinburgh LP 920 Laser Flash spectrometer. All solvents were of spectroscopic grade and used without purification. Measurements were carried out in a 1 cm quartz cell. The samples were degassed by bubbling through inert gas for 5 min. The samples were excited with 5 ns laser pulses at 24000 cm^{-1} (416 nm) or 28200 cm^{-1} (355 nm). The excitation pulse was produced by a Continuum Minilite II Nd:YAG laser operating at 10 Hz and the probe pulse was provided by a pulsed Xe flash lamp. For experiments at 24000 cm^{-1} the THG of the fundamental of 9400 cm^{-1} (1064 nm) was shifted to lower energy by means of a 50 cm Raman shifter which was charged with hydrogen (50 bar). The corresponding energy was selected by a Pellin-Broca prism. The 24000 cm^{-1} pump energy was used in order to avoid ionization of the triarylamine moieties.¹⁵¹ The instrument response (ca. 8 ns) of the setup was determined by measuring the scattered light using an empty quartz cell. The decay curves were deconvoluted with the IRF using the corresponding spectrometer software. Residuals and autocorrelation function (without any significant structure) served as the main criteria in the evaluation of the fit.¹⁵¹ Measurements were performed at different concentrations ($1.1\text{--}1.8 \times 10^{-4}\text{ mol l}^{-1}$) and laser power (1.8 mJ – 3.2 mJ).

The blueprints of the fabricated apparatus for the temperature dependent measurements are shown in Figures 3.1 and 3.2. The cuvette, fixed in an extra cuvette fixture, is scoured with ethanol that is tempered by an external cryostate (Ultra-Kryomat® R410 LAUDA). To avoid condensation of air moisture, the cuvette is placed in a vacuum sealed chamber filled with argon (Figure 3.1). In each side glass windows are inserted, exactly adjusted to keep the correct angle conditions for probe and laser light (Figure 3.2).²⁰³ To avoid condensation of moisture at the windows, they are wrapped by heating elements.

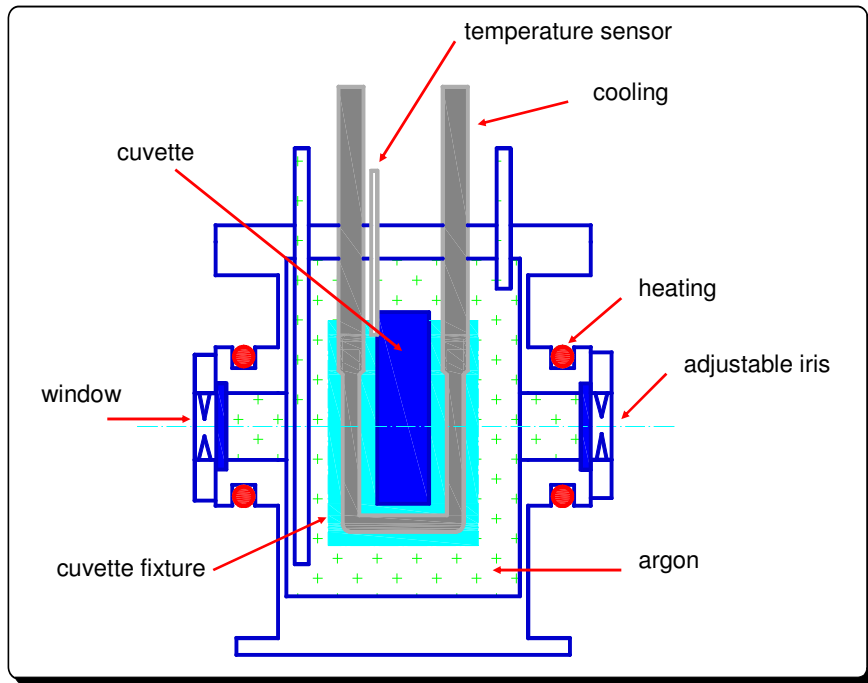


Figure 3.1 General plan of the apparatus for the temperature-dependent measurements.

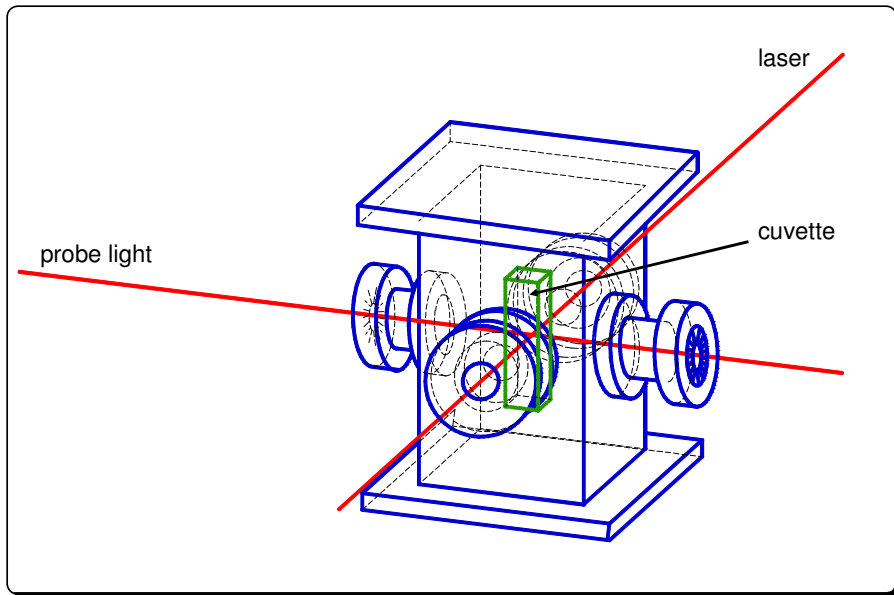


Figure 3.2 Detailed drawing of the apparatus including the directions of probe and laser light.

3.1.4 Fluorescence Spectroscopy

- Photon Technology International fluorescence spectrometer QM-2000-4 including a cooled photomultiplier (R928 P) and a 75 W xenon short arc lamp
- Edinburgh LP 920 Laser Flash spectrometer with a 300 W ozone-free Xe arc lamp including a photomultiplier (Hamamatsu R955) and a digital storage oscilloscope (Tektronix TDS3012B)
- Continuum Minilite II Nd:YAG laser operating at 10 Hz, 8 ns pulse duration, ca. 57 mW average power at 28200 cm^{-1}

Steady state fluorescence spectra at RT

The spectra were recorded in 1 cm quartz cells. All solvents were of spectroscopic grade and were used without further purification. The concentration was ca. $10^{-5} - 10^{-6}\text{ M}$ and oxygen was removed by bubbling inert gas through the solutions for about 5 minutes before each measurement. The fluorescence quantum yields were determined relative to Rhodamine 101.²⁰⁴

Fluorescent lifetime measurements

The spectra were recorded in 1 cm quartz cells. The analysis of the decay curves was performed in the same manner as those of the transient absorption measurements.

Steady state emission experiments at 77 K

The samples were dissolved in 2-MeTHF, filtered, filled in an EPR quartz tube and cooled down with liquid N₂ in an EPR dewar vessel. The wavelength dependence of the detector was corrected with the known spectrum of N,N'-Dimethylamino-m-nitrobenzene (N,N'- DMANB).²⁰⁵ The analysis of the decay curves was performed in the same manner as those of the transient absorption measurements.

3.1.6 LECs: Fabrication and Measurements

Fabrication

The LECs were fabricated similar to literature.¹⁰³ In Figure 3.1 the basic set-up of a LEC is shown.

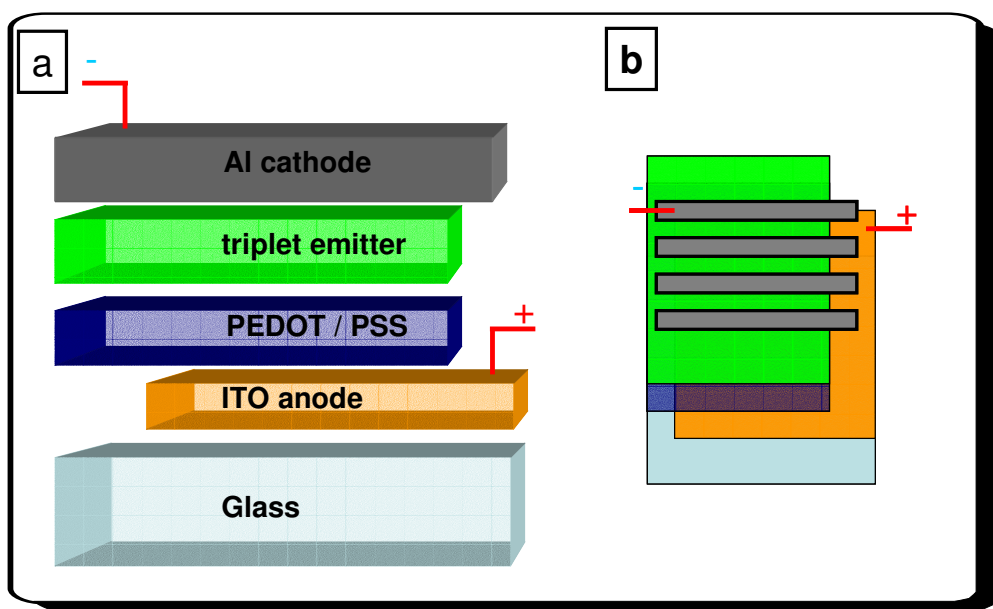


Figure 3.1 Basic set-up of fabricated LECs: a) front view b) sloped top view

Indium/tin oxide (ITO) on glass (25×25 mm) with a resistivity of 20Ω were etched at the left side (ca 5×25 mm) with tin / HCl. Then, the substrates were masked with adhesive tape where the ITO should remain. Then, a suspension of 50 g tin-dust and 10 ml H_2O were coated on the substrates. HCl 20 wt% was added and after 10 min the ITO was removed. The substrates were cleaned with soap solution, water, acetone, isopropanole and heated at $140^\circ C$ for 24 h. Then, poly(3,4-ethylenedioxythiophene) / poly-(styrenesulfonate) (PEDOT / PSS) was filtered and spin-coated onto the substrates (2000 rpm / 60 s). The substrate was heated for 2 h at $140^\circ C$ to remove the residual solvent. Films of the complexes were then spin-coated from a filtered acetonitrile solution ($200 \mu l$ of a 30 mg ml^{-1} solution) onto the substrates (6000 rpm / 45 s). The PEDOT / PSS and emitter layer had to be scratched off at the right side with a scalpel (ca 2.5×25 mm) for contacting the ITO.

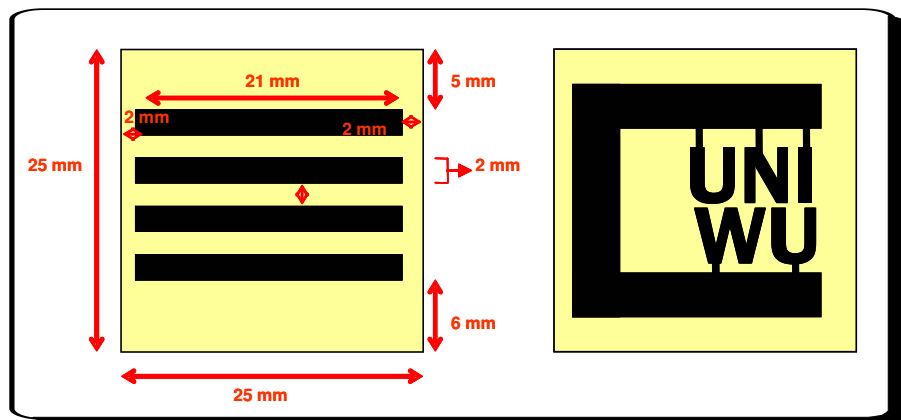


Figure 3.1 dimensions and basic set-up of fabricated masks for vapour-deposition of the aluminium.

Aluminium cathodes (100 \AA) were vapor-deposited in a BOC Edwards 306/500 deposition system ($1 \times 10^6 \text{ mbar}$, deposition rate 0.2 nms^{-1}) through a shadow mask (dimensions and set-up see Figure 3.2) that defined four devices per substrate with the dimension of $2 \times 21 \text{ mm}$ each. The shadow mask was fabricated in the GEISS AG from aluminum on a Laser Trumpf TCL 4050.

Measurements

- Photon Technology International fluorescence spectrometer detector
- EG & G potentiostat / galvanostat model 363

The voltage was applied by a Gamry Instruments Reference 600 Potentiostat/Galvanostat/ZRA and the resulting luminescence was recorded with the PTI fluorescence spectrometer detector.

3.1.7 Synthesis

All chemicals were of standard quality and were used without further purification. All experiments were carried out under inert-gas conditions (nitrogen, dried with Sicapent from MERCK, oxygen was removed by copper oxide catalyst R3-11 from BASF) in flame-dried Schlenk tubes. If necessary, the solvents were purified and
80

3 Experimental Section

dried by standard procedures and kept under inert gas atmosphere. Flash column chromatography was carried out using silica gel (32 – 63 μm) from MP Biomedicals. $\text{IrCl}_3 \cdot n\text{H}_2\text{O}$ was purchased from Heraeus, *N,N*-dimethylamino-*m*-nitrobenzene (*N,N*-DMANB), 2-phenylpyrazole and *cis*-1,2-*bis*(diphenylphosphino)ethylene from ACROS organics. The *N^N* cyclometalating ligands 4,4'-dichloro-2,2'-bipyridyl, 4,4'-dimethoxy-2,2'-bipyridyl, 4,4'-dinitro-2,2'-bipyridyl were purchased from Carbosynth. 3,4,7,8-tetramethyl-1,10-phenanthroline and 2,2'-bipyridyl were ordered from ALDRICH. The ITO substrates were acquired from Delta-Technologies and poly(3,4-ethylenedioxythiophene) / poly-(styrenesulfonate) (PEDOT/PSS) from H.C.Starck. *Fac* $\text{Ir}(\text{ppz})_3$ ¹¹⁰ and 4,4'-dimethylamino-2,2'-bipyridyl ($\text{bpy}(\text{NMe}_2)_2$)^{162,163} were synthesised according to literature methods.

3.2 Synthesis

3.2.1 General Experimental Procedures

General procedure for the copper catalysed amination of aryl halides with Cul (GP1).¹⁵²

Amine (1.00 equiv), Cul (2 – 5 mol%), *trans*-1,2-cyclohexanediamine (4 - 10 mol%), potassium phosphate (2.10 equiv) and the aryl halide were suspended in dry dioxane under nitrogen atmosphere and stirred at 110 °C for 24 – 72 h. The solvent was evaporated; the resulting solid was suspended in dichloromethane and washed with water. The aqueous phase was extracted with dichloromethane and the combined organic extracts were dried over MgSO₄. The crude product was purified by flash column chromatography.

General procedure for the palladium catalyzed amination of aryl halides (GP2).¹⁵³⁻¹⁵⁷

A solution of the aryl halide (1.00 equiv), the aryl amine (1.10 equiv), Pd₂(dba)₃·CHCl₃ (8 mol%), sodium *tert*-butoxide (2.50 equiv), P^tBu₃ (12 mol% of a 1.00 M solution in toluene) in dry toluene were stirred under a nitrogen atmosphere at 80 °C for 12 h. The solvent was evaporated and the resulting solid was diluted with dichloromethane and washed with water. The aqueous phase was extracted with dichloromethane and the combined organic extracts were dried over MgSO₄. The crude product was purified by flash column chromatography.

General procedure for the synthesis of pinacol borane by lithiation (GP3).¹⁵⁸⁻¹⁶⁰

A solution of aryl halide (1.00 equiv) in THF was cooled to –78 °C and while stirred *n*BuLi (1.00 – 1.20 equiv of a 1.60 M solution in hexane) was dropped to the solution within 0.5 h. Subsequently, triisopropyl borate (2.00 equiv) was added and the mixing was stirred for 2 h while the temperature slowly increased up to 25 °C. After quenching with 5 w% HCl and extracting with Et₂O pinacol (3.30 equiv) was added and the solution was stirred at 45 °C for 12 h. The solvent was evaporated and the resulting solid was purified by flash column chromatography.

General procedure for the palladium catalyzed Suzuki-coupling (GP4).¹⁶⁰

The arylboronester (1.00 equiv) was dissolved in dioxane and the aryl halide (1.20 equiv), Cs₂CO₃ (1.50 equiv) and Pd(PPh₃)₄ (0.04 equiv) were added. The mixing was stirred at 110 °C for 24 h. The solvent was evaporated under reduced pressure and the resulting solid was diluted with dichloromethane and was purified by flash column chromatography.

General procedure for the synthesis of cyclometalated Ir(III) dichloro-bridged dimers (C[^]N)₂Ir(μ-Cl)₂Ir(C[^]N)₂ (GP5).^{103,161}

IrCl₃·3 H₂O was mixed together with 2 – 2.5 equiv of the cyclometalating ligand in a 3 : 1 mixture of 2-ethoxyethanol and deionized water. The solution was heated to 110 °C under inert gas atmosphere. After cooling to room temperature the dimers were precipitated by pouring into water. The precipitate was filtered, washed twice with water, and dried. The dimers were used for the following reaction without further purification.

General procedure for the synthesis of (C[^]N)₂Ir(N[^]N)⁺PF₆⁻ complexes (GP6).^{93-98,100-103,110,114,117,136,137,144,164,206-208}

The dichloro-bridged iridium dimer (C[^]N)₂Ir(μ-Cl)₂Ir(C[^]N)₂ and 2.0 equiv of the diimine ligand were mixed together in dichloromethane. The solution was then refluxed for 12 h under inert gas atmosphere. After cooling to room temperature the solvent was evaporated and the resulting solid was dissolved in methanol. After filtration of the solution, counterion exchange from Cl⁻ to PF₆⁻ was accomplished via metathesis reaction in which the complexes were precipitated from the filtered methanol solution with an ammonium hexafluorophosphate salt solution in methanol. The resulting precipitate was filtered, washed twice with water and methanol, and dried.

General procedure for the synthesis of the β-diketonato Pt(II) and Ir(III) complexes (GP7).^{103,112,161}

The μ-dichloro-bridged phenylpyridyl Pt(II)¹⁹³ or Ir(III) dimer^{103,161} and 3 equiv of the chelating diketone derivative were mixed together with 10 equiv of Na₂CO₃ in 2-ethoxyethanol at 100 °C for 16 h under inert gas atmosphere. After cooling to room

3 Experimental Section

temperature the reaction mixture was diluted with water. The aqueous phase was extracted with dichloromethane and the combined organic extracts were dried over MgSO₄. The crude product was purified by flash column chromatography.

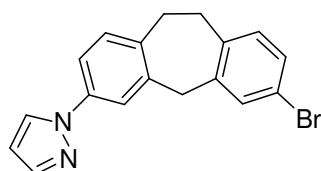
General procedure for the synthesis of the β -diketonato Pt(II) and Ir(III) complexes (GP8).¹⁰⁸

The μ -dichloro-bridged phenylpyridyl Pt(II)¹⁹³ or Ir(III) dimer^{103,161} and 2 equiv of the chelating diketone derviate were dissolved in dichloromethane under inert gas atmosphere. Tetrabutylammonium hydroxide (2 equiv of a 0.80 M solution in methanol) was added and the mixing was stirred for 24 h under reflux. After cooling to room temperature the reaction mixture was diluted with water. The aqueous phase was extracted with dichloromethane and the combined organic extracts were dried over MgSO₄. The crude product was purified by flash column chromatography.

3.2.2 Synthesis of the Cationic Iridium Complexes

3.2.2.1 Synthesis of the Ligands

3-Pyrazolyl-7-bromo-10,11-dihydro-5H-dibenzo[a,d]-cycloheptene (8)



Following GP1: 3,7-Dibromo-10,11-dihydro-5*H*-dibenzo[*a,d*]cycloheptene **7**¹⁵¹ (1.00 g; 2.84 mmol), 1*H*-pyrazole (193 mg; 2.84 mmol), CuI (54.1 mg; 280 μ mol), *trans*-1,2-cyclohexanediamine (13.7 μ l; 1.14 mmol), potassium phosphate (1.27 g; 5.97 mmol), dioxane (2 ml); 20 h at 110 °C, flash chromatography (CH_2Cl_2 : PE = 1:1).

Formula: $\text{C}_{18}\text{H}_{15}\text{BrN}_2$ [339.23].

Yield: 307 mg (910 μ mol; 64 %) of a colourless solid.

Melting point: 145 °C.

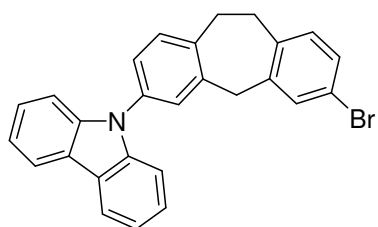
$^1\text{H NMR}$ (400.1 MHz, CDCl_3): δ = 7.86 (d, $^3J_{\text{HH}} = 2.5$ Hz, 1H); 7.68 (d, $^3J_{\text{HH}} = 1.4$ Hz, 1H); 7.53 (d, $^3J_{\text{HH}} = 2.2$ Hz, 1H); 7.40 (dd, $^3J_{\text{HH}} = 8.2$ Hz, $^4J_{\text{HH}} = 2.4$ Hz, 1H); 7.32 (d, $^3J_{\text{HH}} = 2.0$ Hz, 1H); 7.24 (dd, $^3J_{\text{HH}} = 8.1$ Hz, $^4J_{\text{HH}} = 2.2$ Hz, 1H); 7.16 (d, $^3J_{\text{HH}} = 8.2$ Hz, 1H); 6.97 (d, $^3J_{\text{HH}} = 8.1$ Hz, 1H); 6.42 (dd, $^3J_{\text{HH}} = 2.4$ Hz, $^4J_{\text{HH}} = 1.9$ Hz, 1H); 4.09 (s, 2H); 3.18 – 3.09 (-, 4H).

$^{13}\text{C NMR}$ (100.6 MHz, CDCl_3): δ = 141.0 (tert.); 140.6 (quart.); 139.6 (quart.); 138.5 (quart.); 138.1 (quart.); 137.3 (quart.); 131.9 (tert.); 131.4 (tert.); 130.8 (tert.); 129.9 (tert.); 126.8 (tert.); 120.1 (tert.); 119.6 (quart.); 117.6 (tert.); 107.5 (tert.); 40.7 (sec.); 32.0 (sec.); 31.9 (sec.).

HRMS (70 eV, EI): m/z calcd for $[\text{M}^+] = \text{C}_{18}\text{H}_{15}\text{BrN}_2^{+}$: 338.04136; found: 338.04081 ($\Delta = 1.49$ ppm).

3 Experimental Section

3-Bromo-7-carbazolyl-10,11-dihydro-5H-dibenzo-[a,d]cycloheptene (9)



Following GP1: 3,7-Dibromo-10,11-dihydro-5*H*-dibenzo[*a,d*]cycloheptene **7** (1.10 g; 3.12 mmol), carbazole (261 mg, 1.56 mmol), Cul (29.8 mg, 160 μ mol), *trans* -1,2-cyclohexanediamine (37.6 μ l; 130 μ mol), potassium phosphate (796 mg; 3.75 mmol), dioxane (3 ml); 40 h at 110 °C, flash chromatography (CH_2Cl_2 : PE = 1:1).

Formula: $\text{C}_{27}\text{H}_{20}\text{BrN}$ [438.36].

Yield: 400 mg (910 μ mol; 58 %) of a colourless solid.

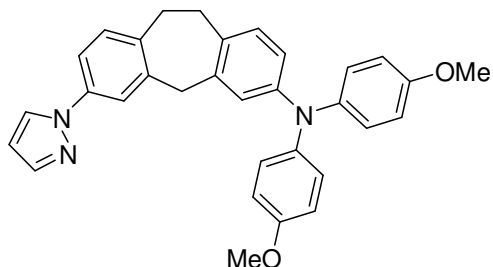
Melting point: 96 °C.

$^1\text{H NMR}$ (600.1 MHz, CDCl_3): δ = 8.12 (d, $^3J_{\text{HH}} = 7.9$ Hz, 2H); 7.39 – 7.34 (-, 5H); 7.32 (-, 3H); 7.30 – 7.25 (-, 3H); 7.04 (d, $^3J_{\text{HH}} = 8.1$ Hz, 1H); 4.12 (s, 2H); 3.21 – 3.19 (-, 4H).

$^{13}\text{C NMR}$ (150.9 MHz, CDCl_3): δ = 141.1 (quart.); 140.8 (quart.); 139.9 (quart.); 138.4 (quart.); 138.3 (quart.); 135.7 (quart.); 131.9 (tert.); 131.4 (tert.); 131.3 (tert.); 129.9 (tert.); 127.7 (tert.); 126.0 (tert.); 125.6 (tert.); 123.4 (quart.); 120.4 (tert.); 119.9 (tert.); 119.7 (quart.); 110.0 (tert.); 40.6 (sec.); 32.2 (sec.); 32.0 (sec.).

HRMS (70 eV, EI): m/z calcd for $[\text{M}^+] = \text{C}_{27}\text{H}_{20}\text{BrN}^+$: 437.07736; found: 437.07704 ($\Delta = 0.75$ ppm).

3-Pyrazolyl-7-(4,4'-dimethoxydiphenylamino)-10,11-dihydro-5*H*-dibenzo[a,d]-cycloheptene (10)



Following GP2: 3-Pyrazolyl-7-bromo-10,11-dihydro-5*H*-dibenzo[a,d]-cycloheptene **8** (690 mg, 2.03 mmol), 4,4'-dimethoxydiphenylamine (513 mg, 2.24 mmol), Pd₂(dba)₃·CHCl₃ (168 mg, 160 μmol), sodium *tert*-butoxide (489 mg, 5.09 mmol), P^tBu₃ (240 μl, 240 μmol), toluene (5 ml), flash chromatography (CH₂Cl₂ : PE = 1:1).

Formula: C₃₂H₂₉N₃O₂ [487.59].

Yield: 836 mg (1.71 mmol; 84 %) of a colourless solid.

Melting point: 165 °C.

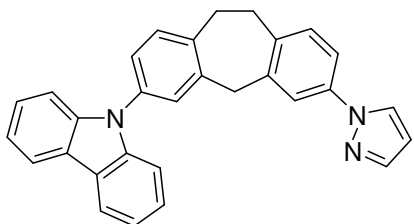
¹H NMR (600.1 MHz, d₆-acetone): δ = 7.91 (-, 1H); 7.65 (-, 1H); 7.47 (-, 1H); 7.44 (-, 1H); 7.20 (-, 1H); 6.97 (AA', 4H); 6.94 (-, 1H); 6.80 (BB', 4H); 6.78 (-, 1H); 6.70 (-, 1H); 6.43 (-, 1H); 4.00 (s, 2H); 3.77 (s, 6H), 3.18 – 3.09 (-, 4H).

¹³C NMR (150.9 MHz, d₆-acetone): δ = 156.0 (quart.); 147.2 (quart.); 141.6 (quart.); 140.9 (tert.); 140.8 (quart.); 139.4 (quart.); 138.5 (quart.); 138.1 (quart.); 131.8 (quart.); 130.8 (tert.); 130.6 (tert.); 126.9 (tert.); 126.4 (tert.); 122.0 (tert.); 120.0 (tert.); 119.8 (tert.); 117.3 (tert.); 114.8 (tert.); 107.5 (tert.); 55.7 (prim.); 41.2 (sec.); 32.5 (sec.); 32.0 (sec.).

HRMS (70 eV, EI): *m/z* calcd for [M⁺] = C₃₂H₂₉N₃O₂⁺: 487.22543; found: 487.22532 (Δ = 0.22 ppm).

3 Experimental Section

3-Pyrazolyl-7-carbazolyl-10,11-dihydro-5H-dibenzo-[a,d]cycloheptene (11)



Following GP1: 3-Bromo-7-carbazolyl-10,11-dihydro-5H-dibenzo[a,d]cycloheptene **9** (767 mg, 1.75 mmol), 1*H*-pyrazole (119 mg, 1.75 mmol), CuI (33.3 mg, 170 μ mol), *trans*-1,2-cyclohexanediamine (84.1 μ l; 700 μ mol), potassium phosphate (780 mg; 3.67 mmol), dioxane (2 ml); 20 h at 110 °C, flash-chromatography (CH_2Cl_2 : PE = 1:1).

Formula: $\text{C}_{30}\text{H}_{23}\text{N}_3$ [425.52].

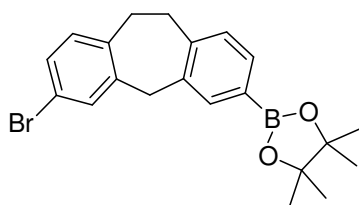
Yield: 480 mg (1.13 mmol; 65 %) of a colourless solid.

Melting point: 170 °C.

$^1\text{H NMR}$ (600.1 MHz, d_6 -acetone): δ = 8.12 (-, 3H); 7.87 (-, 1H); 7.69 (-, 1H); 7.56 (-, 1H); 7.56 (-, 1H); 7.35 – 7.30 (-, 7H); 7.26 (-, 2H); 6.50 (-, 1H); 4.23 (s, 2H); 3.32 – 3.27 (-, 4H).

$^{13}\text{C NMR}$ (150.9 MHz, d_6 -acetone): δ = 141.1 (quart.); 141.0 (tert.); 140.1 (quart.); 140.0 (quart.); 138.6 (quart.); 138.5 (quart.); 137.7 (quart.); 135.6 (quart.); 131.3 (tert.); 130.7 (tert.); 127.8 (tert.); 126.9 (tert.); 126.0 (tert.); 125.6 (tert.); 123.3 (quart.); 120.4 (tert.); 120.2 (tert.); 119.9 (tert.); 117.6 (tert.); 110.0 (tert.); 110.0 (tert.); 107.6 (tert.); 41.1 (sec.); 32.5 (sec.); 32.0 (sec.).

HRMS (70 eV, EI): m/z calcd for $[\text{M}^+]$ = $\text{C}_{30}\text{H}_{23}\text{N}_3^{+}$: 425.18865; found: 425.18833 (Δ = 0.75 ppm).

3-Pinacolborane-7-bromo-10,11-dihydro-5H-dibenzo[a,d]-cycloheptene (12)

Following GP3: 3,7-Dibromo-10,11-dihydro-5H-dibenzo[a,d]cycloheptene **7** (1.00 g, 2.84 mmol), *n*BuLi (1.78 ml, 1.6 M in hexane, 2.84 mmol), THF (3.50 ml); 1 h at -78 °C, triisopropyl borate (1.32 ml, 5.68 mmol); 2 h from -78 °C to RT, pinacol (1.11 g, 9.37 mmol), diethylether (50 ml); 12 h at 45 °C, flash chromatography (CH₂Cl₂ : PE = 1:1).

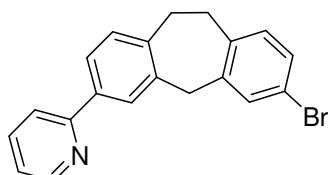
Formula: C₂₁H₂₄BrBO₂ [399.13].

Yield: 590 mg (1.47 mmol, 52 %) of a colourless solid.

Melting point: 132 °C.

¹H NMR (600.1 MHz, d₆-acetone): δ = 7.59 (s, 1H); 7.50 (-, 2H); 7.27 (-, 1H); 7.14 (-, 1H); 7.08 (-, 1H); 4.18 (s, 2H); 3.17 (-, 4H); 1.31 (s, 12 H).

¹³C NMR (150.9 MHz, d₆-acetone): δ = 143.5 (quart.); 143.0 (quart.); 139.6 (quart.); 139.0 (quart.); 136.4 (tert.); 136.3 (quart.); 134.2 (tert.); 132.6 (tert.); 132.5 (tert.); 130.3 (tert.); 130.0 (tert.); 119.9 (quart.); 84.5 (quart.); 40.4 (sec.); 33.1 (sec.); 32.5 (sec.); 25.4 (prim.).

3-Pyridine-7-bromo-10,11-dihydro-5H-dibenzo[a,d]-cycloheptene (13)

Following GP4: 3-Pinacolborane-7-bromo-10,11-dihydro-5H-dibenzo[a,d]cycloheptene **12** (430 mg, 1.08 mmol), 2-bromopyridine (123 μl, 1.29 mmol), Pd(PPh₃)₄

3 Experimental Section

(49.8 mg, 43.1 μmol), Cs_2CO_3 (527 mg, 1.62 mmol), dioxane (5 ml); 12 h at 80 °C, flash chromatography (PE : EA = 2:1).

Formula: $\text{C}_{20}\text{H}_{16}\text{BrN}$ [350.25].

Yield: 112 mg (320 μmol , 30 %) of a colourless solid.

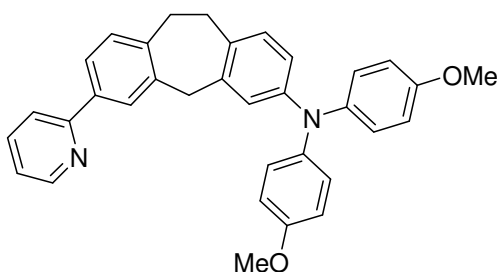
Melting point: 118 °C.

$^1\text{H NMR}$ (600.1 MHz, d_6 -acetone): δ = 8.63 (-, 1H); 8.02 (s, 1H); 7.87 (-, 2H); 7.81 (-, 1H); 7.48 (s, 1H); 7.26 (-, 3H); 7.11 (-, 1H); 4.24 (s, 2H); 3.18 (-, 4H).

$^{13}\text{C NMR}$ (150.9 MHz, d_6 -acetone): δ = 161.5 (quart.); 154.4 (tert.); 146.7 (quart.); 144.8 (quart.); 143.7 (quart.); 143.5 (quart.); 142.1 (quart.); 141.6 (tert.); 136.3 (tert.); 136.3 (tert.); 134.9 (tert.); 134.2 (tert.); 132.2 (tert.); 129.8 (tert.); 126.9 (tert.); 124.6 (tert.); 123.7 (quart.); 44.6 (sec.); 36.5 (sec.); 36.35 (sec).

HRMS (70 eV, EI): m/z calcd for $[\text{M}^+ - \text{H}] = \text{C}_{20}\text{H}_{15}\text{BrN}^+$: 348.03737; found: 348.03682 ($\Delta = 4.08$ ppm).

3-Pyridine-7-(4,4'-dimethoxydiphenylamino)-10,11-dihydro-5*H*-dibenzo[a,d]-cycloheptene (14)



Following GP2: 3-Pyridine-7-bromo-10,11-dihydro-5*H*-dibenzo[a,d]cycloheptene **13** (230 mg, 660 μmol), 4,4'-dimethoxydiphenylamine (181 mg, 790 μmol), $\text{Pd}_2(\text{dba})_3 \cdot \text{CHCl}_3$ (27.2 mg, 26.3 μmol), P^tBu_3 (39.4 μl , 39.4 μmol), sodium *tert*-butoxide (94.7 mg, 990 μmol), toluene (5 ml); 12 h at 80 °C, flash chromatography (PE : EA = 2:1).

Formula: $\text{C}_{34}\text{H}_{30}\text{N}_2\text{O}_2$ [498.61].

Yield: 132 mg (280 μmol , 42 %) of a colourless solid.

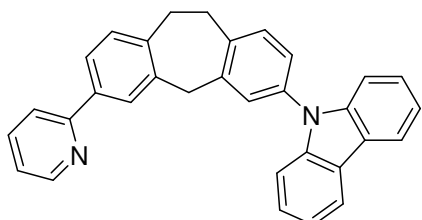
Melting point: 80 °C.

$^1\text{H NMR}$ (600.1 MHz, d_6 -acetone): δ = 8.61 (-, 1H); 8.95 (-, 1H); 7.89 (-, 2H); 7.80 (-, 1H); 7.26 (-, 1H); 7.24 (-, 1H); 6.99 – 6.95 (-, 5H); 6.87 – 6.84 (-, 5H); 6.67 (-, 1H); 4.10 (s, 2H); 3.79 (s, 6H); 3.21 – 3.12 (-, 4H).

$^{13}\text{C NMR}$ (150.9 MHz, d_6 -acetone): δ = 161.6 (quart.); 166.7 (quart.); 154.4 (tert.); 151.8 (quart.); 146.2 (quart.); 145.3 (quart.); 144.7 (quart.); 144.3 (quart.); 141.9 (quart.); 141.5 (tert.); 136.7 (quart.); 135.0 (tert.); 134.8 (tert.); 132.1 (tert.); 130.9 (tert.); 129.6 (tert.); 126.9 (tert.); 126.7 (tert.); 124.6 (tert.); 124.5 (tert.); 119.5 (tert.); 59.4 (prim.); 45.2 (sec.); 36.9 (sec.); 36.1 (sec).

HRMS (70 eV, EI): m/z calcd for $[\text{M}^+]$ = $\text{C}_{34}\text{H}_{30}\text{N}_2\text{O}_2^{+}$: 498.23018; found: 498.22998 (Δ = 0.40 ppm).

3-Pyridine-7-carbazolyl-10,11-dihydro-5*H*-dibenzo-[a,d]cycloheptene (15)



Following GP2: 3-Pyridine-7-bromo-10,11-dihydro-5*H*-dibenzo[*a,d*]cycloheptene **13** (70.0 mg, 200 μmol), carbazole (36.8 mg, 220 μmol), $\text{Pd}_2(\text{dba})_3 \cdot \text{CHCl}_3$ (8.27 mg, 7.99 μmol), P^tBu_3 (12.0 μl , 12.0 μmol), sodium *tert*-butoxide (28.8 mg, 300 μmol), toluene (5 ml); 12 h at 80 °C, flash chromatography (PE : EA = 2:1).

Formula: $\text{C}_{32}\text{H}_{24}\text{N}_2$ [436.55].

Yield: 46.0 mg (110 μmol , 53 %) of a colourless solid.

Melting point: 95 °C.

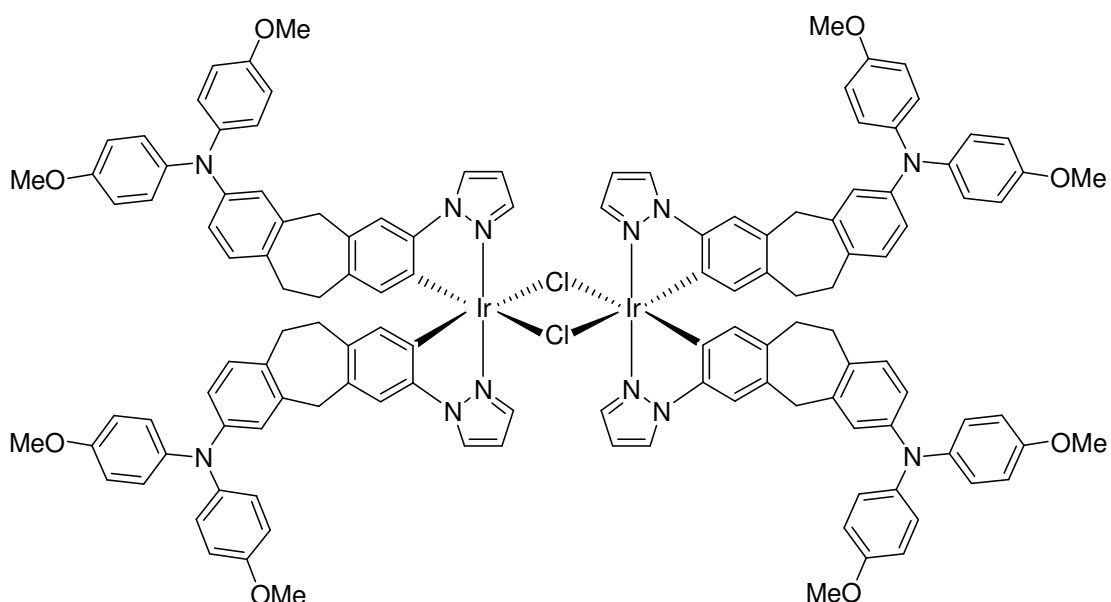
3 Experimental Section

¹H-NMR (600.1 MHz, d₆-acetone): δ = 7.72 (-, 1H); 7.31 (-, 2H); 7.17 (-, 1H); 7.03 (-, 1H); 7.00 (-, 1H); 6.92 (-, 1H); 6.66 (-, 1H); 6.58 (-, 1H), 6.52 – 6.47 (-, 5H); 6.42 (-, 1H); 6.39 – 6.36 (-, 3H); 3.51 (s, 2H); 2.50 – 2.44 (-, 4H).

¹³C-NMR (150.9 MHz, d₆-acetone): δ = 157.9 (quart.); 150.7 (tert.); 142.4 (quart.); 142.1 (quart.); 141.5 (quart.); 140.4 (quart.); 140.2 (quart.); 138.5 (quart.); 138.0 (tert.); 136.5 (quart.); 132.5 (tert.); 131.2 (tert.); 128.6 (tert.); 128.5 (tert.); 127.2 (tert.); 126.2 (tert.); 126.2 (tert.); 124.4 (quart.); 123.3 (tert.); 121.4 (tert.); 121.0 (tert.); 121.0 (tert.); 110.9 (tert.); 41.3 (sec.); 33.1 (sec.); 33.1 (sec).

HRMS (70 eV, EI): *m/z* calcd for [M⁺ -H] = C₃₂H₂₃N₂⁺: 435.18558; found: 435.18404 (Δ = 3.53 ppm).

Dimer (16) Ir₂(ppz_{TAA})₂(μ -Cl)₂

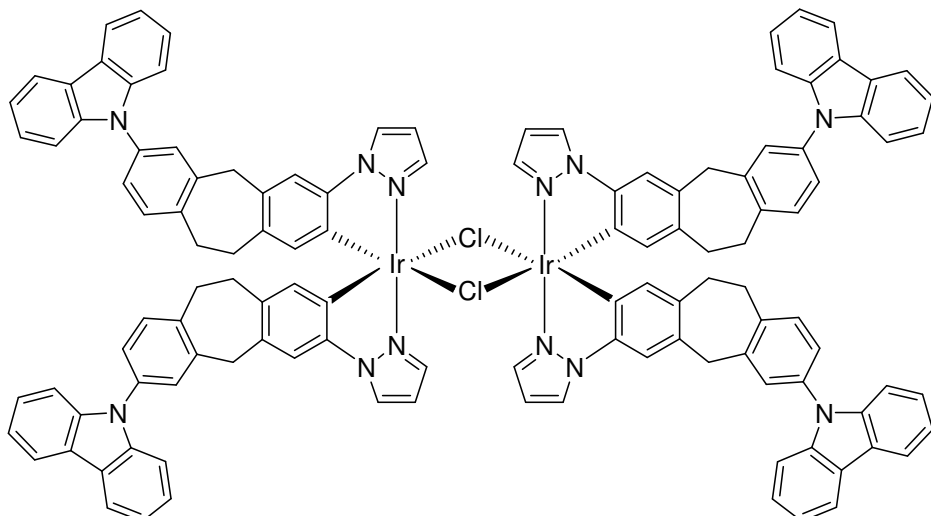


Following GP5: 3-Pyrazolyl-7-(4,4'-dimethoxydiphenylamino)-10,11-dihydro-5*H*-dibenzo[a,d]-cycloheptene **10** (231 mg, 470 μ mol), IrCl₃·3H₂O (80.0 mg, 230 μ mol), ethoxyethanol : water = 3:1 (3 ml); 14 h at 80 °C. The product was used for the following reaction without further purification.

Formula: C₁₂₈H₁₁₂Cl₂Ir₂N₁₂O₈ [2401.67].

Yield: 267 mg (110 μ mol, 49 %) of a pale yellow solid.

Dimer (17) Ir₂(ppzcz)₂(μ -Cl)₂



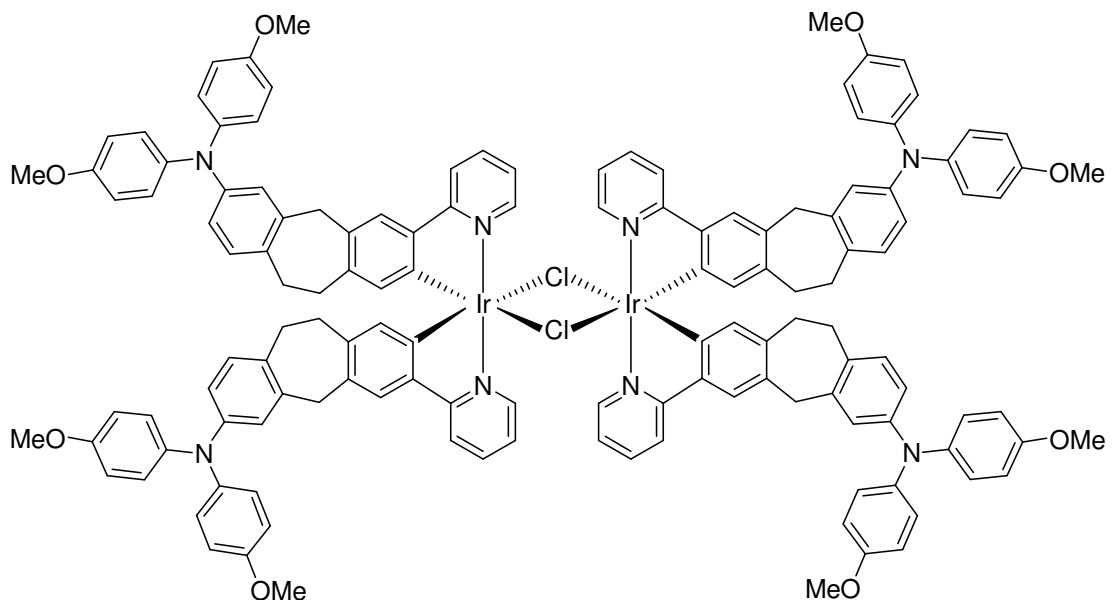
Following GP5: 3-Pyrazolyl-7-carbazolyl-10,11-dihydro-5H-dibenzo[a,d]cycloheptene **11** (200 mg, 470 μ mol), IrCl₃·3H₂O (80.0 mg, 230 μ mol), ethoxyethanol : water = 3:1 (3 ml); 14 h at 80 °C. The product was used for the following reaction without further purification.

Formula: C₁₂₀H₈₈Cl₂Ir₂N₁₂ [2153.40].

Yield: 218 mg (100 μ mol, 54 %) of a grey solid.

3 Experimental Section

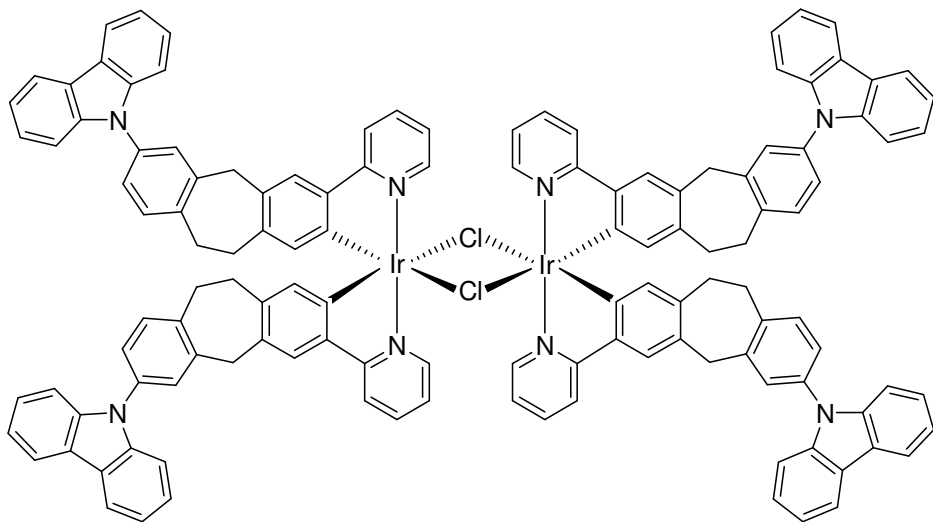
Dimer (18) $\text{Ir}_2(\text{ppy}_{\text{TAA}})_2(\mu\text{-Cl})_2$



Following GP5: 3-Pyridine-7-(4,4'-dimethoxydiphenylamino)-10,11-dihydro-5*H*-dibenzo[a,d]-cycloheptene **14** (181 mg, 360 μmol), $\text{IrCl}_3 \cdot 3\text{H}_2\text{O}$ (64 mg, 180 μmol), ethoxyethanol : water = 3:1 (3 ml); 14 h at 80 $^{\circ}\text{C}$. The product was used for the following reaction without further purification.

Formula: $\text{C}_{136}\text{H}_{116}\text{Cl}_2\text{Ir}_2\text{N}_8\text{O}_8$ [2445.77].

Yield: 86.0 mg (35.2 μmol , 39 %) a grey solid.

Dimer (19) $\text{Ir}_2(\text{ppycz})_2(\mu\text{-Cl})_2$ 

Following GP5: 3-Pyridine-7-carbazolyl-10,11-dihydro-5*H*-dibenzo-[*a,d*]cycloheptene **15** (117 mg, 270 μmol), $\text{IrCl}_3 \cdot 3\text{H}_2\text{O}$ (47.3 mg, 130 μmol), ethoxyethanol : water = 3:1 (3 ml); 14 h at 80 $^{\circ}\text{C}$. The product was used for the following reaction without further purification.

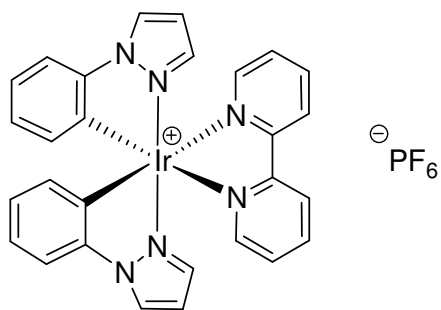
Formula: $\text{C}_{128}\text{H}_{92}\text{Cl}_2\text{Ir}_2\text{N}_8$ [2197.49].

Yield: 180 mg (54.6 μmol , 41 %) of a grey solid.

3 Experimental Section

3.2.2.2 Synthesis of the Complexes

Complex (1) [Ir(ppz)₂(bpy)]PF₆



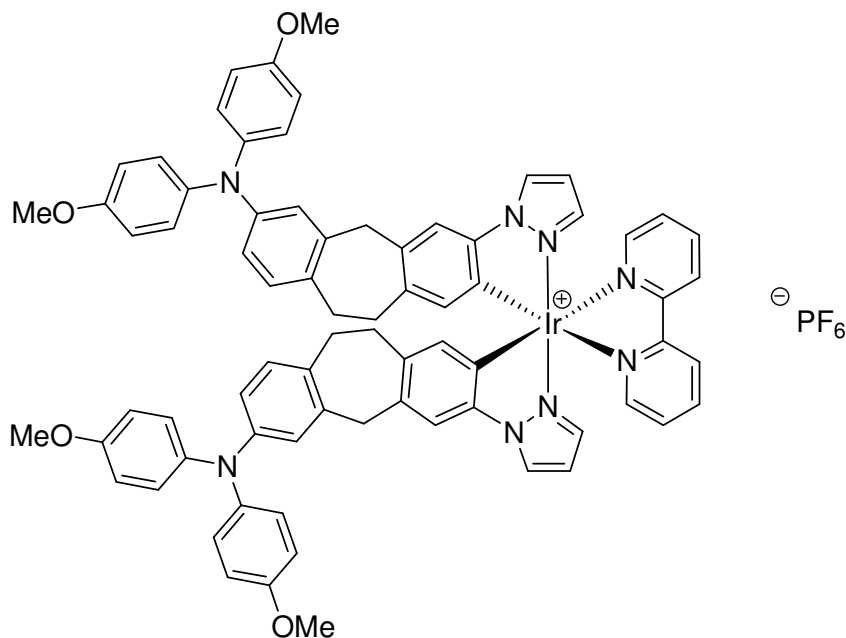
Following GP6: Phenylpyrazole dimer¹⁰³ (136 mg, 132 μ mol), 2,2'-bipyridyl (41.3 mg, 265 μ mol), CH₂Cl₂ (2.00 ml); 14 h at 50 °C.

Formula: C₂₈H₂₂F₆IrN₆P [779.70].

Yield: 152 mg (195 μ mol, 74 %) of a yellow solid.¹⁰³

Melting point: 289 °C.

¹H NMR (600.1 MHz, d₆-chloroform): δ = 8.67 (-, 2H); 8.17 (-, 2H); 8.10 (-, 4H); 7.42 (-, 2H); 7.28 (-, 2H); 7.06 (-, 2H); 6.88 (-, 4H); 6.55 (-, 2H); 6.31 (-, 2H).¹⁰³

Complex (1A) $[\text{Ir}(\text{ppz}_{\text{TAA}})_2(\text{bpy})]\text{PF}_6$ 

Following GP6: Dimer **16** (80.0 mg, 33.3 μmol), 2,2'-bipyridyl (10.4 mg, 66.7 μmol), CH_2Cl_2 (2.00 ml); 14 h at 50 $^{\circ}\text{C}$.¹³⁴

Formula: $\text{C}_{74}\text{H}_{64}\text{F}_6\text{IrN}_8\text{O}_4\text{P}$ [1466.53].

Yield: 37.0 mg (25.2 μmol , 38 %) of a pale green solid.

Melting point: 209 $^{\circ}\text{C}$.

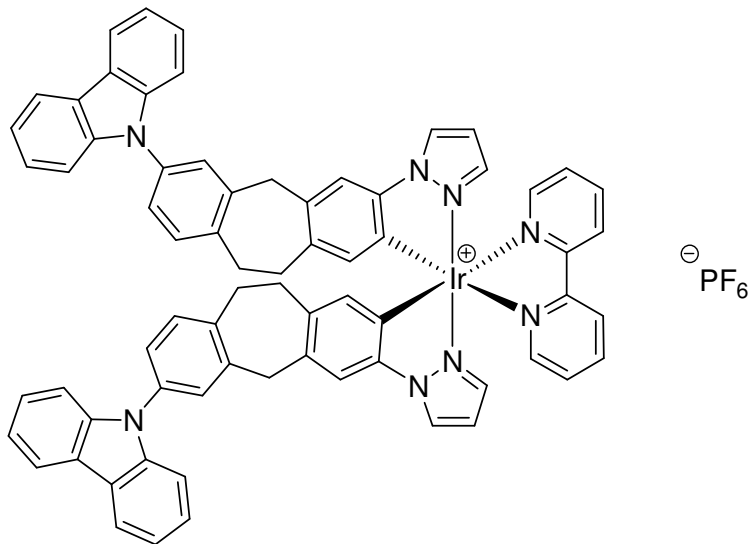
$^1\text{H NMR}$ (600.1 MHz, $d_8\text{-THF}$): δ = 8.75 (-, 2H); 8.42 (-, 2H); 8.20 (-, 2H); 8.16 (-, 2H); 7.53 (-, 2H); 7.29 (s, 2H); 7.01 (-, 2H); 6.94 (AA', 8H); 6.90 (-, 2H); 6.87 (BB', 8H); 6.71 (-, 2H); 6.65 (-, 2H); 6.60 (-, 2H); 6.05 (s, 2H); 3.86 – 3.91 (-, 4H); 3.73 (s, 12H); 2.85 – 2.97 (-, 8H).

$^{13}\text{C NMR}$ (150.9 MHz, $d_8\text{-THF}$): δ = 157.4 (quart.); 156.6 (quart.); 151.4 (tert.); 147.7 (quart.); 142.2 (quart.); 142.1 (quart.); 140.4 (tert.); 140.1 (quart.); 139.1 (quart.); 138.7 (tert.); 134.51 (tert.); 134.49 (quart.); 132.5 (quart.); 130.7 (tert.); 130.5 (quart.); 128.6 (tert.); 127.8 (tert.); 126.7 (tert.); 125.6 (tert.); 122.4 (tert.); 120.2 (tert.); 115.1 (tert.); 112.9 (tert.); 108.5 (tert.); 55.4 (prim.); 41.5 (sec.); 33.4 (sec.); 32.7 (sec.).

ESI pos. (high resolution): calcd for $[\text{M}^+] = \text{C}_{74}\text{H}_{64}\text{IrN}_8\text{O}_4^+$: 1319.46510; found: 1319.46508 ($\Delta = 0.01$ ppm).

3 Experimental Section

Complex (1B) $[\text{Ir}(\text{ppz}_{\text{CZ}})_2(\text{bpy})]\text{PF}_6$



Following GP6: Dimer **17** (83.0 mg, 38.5 μmol), 2,2'-bipyridyl (12.0 mg, 77.1 μmol), CH_2Cl_2 (2 ml); 14 h at 50 °C.

Formula: $\text{C}_{70}\text{H}_{52}\text{F}_6\text{IrN}_8\text{P}$ [1342.40].

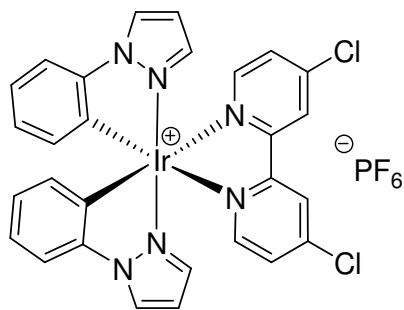
Yield: 53.0 mg (39.5 μmol , 51 %) of a pale yellow solid.

Melting point: 271 °C.

$^1\text{H NMR}$ (600.1 MHz, $d_8\text{-THF}$): $\delta = 8.92$ (-, 2H); 8.65 (-, 2H); 8.37 (-, 4H); 8.28 (-, 4H); 7.71 (-, 2H); 7.56 (-, 4H); 7.48 (-, 12H); 7.37 (-, 4H); 7.21 (-, 2H); 6.73 (-, 2H); 6.30 (s, 2H); 4.13 – 4.23 (-, 4H); 3.01 – 3.28 (-, 8H).

$^{13}\text{C NMR}$ (150.9 MHz, $d_8\text{-THF}$): $\delta = 157.7$ (quart.); 151.7 (tert.); 142.7 (quart.); 142.0 (quart.); 141.7 (quart.); 140.7 (tert.); 140.2 (quart.); 139.2 (tert.); 138.9 (quart.); 136.5 (quart.); 134.9 (quart.); 134.4 (tert.); 132.1 (tert.); 131.2 (quart.); 128.9 (tert.); 128.3 (tert.); 128.2 (tert.); 126.6 (tert.); 126.0 (tert.); 125.8 (tert.); 124.4 (quart.); 121.0 (tert.); 120.6 (tert.); 113.3 (tert.); 110.6 (tert.); 108.9 (tert.); 41.4 (sec.); 33.5 (sec.); 33.3 (sec.).

ESI pos. (high resolution): calcd for $[\text{M}^+] = \text{C}_{70}\text{H}_{52}\text{IrN}_8^+$: 1195.39154; found: 1195.39154 ($\Delta = 0.00$ ppm).

Complex (1_Cl) [Ir(ppz)₂(bpy-Cl₂)]PF₆

Following GP6: Phenylpyrazole dimer¹⁰³ (100 mg, 97.3 μ mol), 4,4'-dichloro-2,2'-bipyridyl (43.8 mg, 190 μ mol), CH₂Cl₂ (2.00 ml); 14 h at 50 °C.

Formula: C₂₈H₂₀Cl₂F₆IrN₆P [848.59].

Yield: 71.0 mg (83.7 μ mol, 43 %) of a yellow solid.

Melting point: 234 °C.

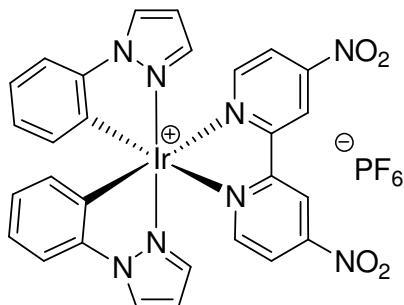
¹H NMR (400.1 MHz, d₆-acetone): δ = 9.05 (-, 2H); 8.71 (-, 2H); 8.22 (-, 2H); 7.84 (-, 2H); 7.63 (-, 2H); 7.42 (-, 2H); 7.07 (-, 2H); 6.87 (-, 2H); 6.71 (-, 2H); 6.31 (-, 2H).

¹³C NMR (100.6 MHz, d₆-acetone): δ = 158.6 (quart.); 153.4 (tert.); 148.5 (quart.); 144.5 (quart.); 140.4 (tert.); 134.3 (tert.); 132.6 (quart.); 130.1 (tert.); 129.4 (tert.); 127.9 (tert.); 126.9 (tert.); 124.7 (tert.); 113.3 (tert.); 109.6 (tert.).

ESI pos. (high resolution): calcd for [M⁺] = C₂₈H₂₀Cl₂IrN₆⁺: 701.07269; found: 701.07270 (Δ = 0.01 ppm).

3 Experimental Section

Complex (1_{NO₂}) [Ir(ppz)₂(bpy-(NO₂)₂)]PF₆



Following GP6: Phenylpyrazole dimer¹⁰³ (100 mg, 97.3 μmol), 4,4'-dinitro-2,2'-bipyridyl (47.8 mg, 190 μmol), dichloromethane (2.00 ml); 14 h at 50 °C.

Formula: C₂₈H₂₀F₆IrN₈O₄P [869.69].

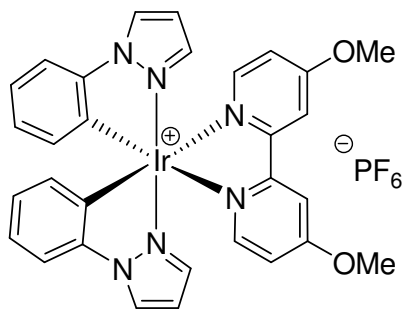
Yield: 49.0 mg (56.3 μmol, 29 %) of a brown solid.

Melting point: 231 °C.

¹H NMR (400.1 MHz, d₆-acetone): δ = 9.90 (-, 2H); 8.75 (-, 2H); 8.71 (-, 2H); 8.51 (-, 2H); 7.67 (-, 2H); 7.42 (-, 2H); 7.11 (-, 2H); 6.92 (-, 2H); 6.72 (-, 2H); 6.32 (-, 2H).

¹³C NMR (100.6 MHz, d₆-acetone): δ = 159.8 (quart.); 156.7 (quart.); 155.4 (tert.); 144.3 (quart.); 140.6 (tert.); 134.2 (tert.); 131.9 (quart.); 129.7 (tert.); 128.1 (tert.); 125.2 (tert.); 123.8 (tert.); 120.7 (tert.); 113.5 (tert.); 109.8 (tert.).

ESI pos. (high resolution): calcd for [M⁺] = C₂₈H₂₀IrN₈O₄⁺: 723.12079; found: 723.12080 (Δ = 0.01 ppm).

Complex (1-OMe) [Ir(ppz)₂(bpy-(OMe)₂)]PF₆

Following GP6: Phenylpyrazole dimer¹⁰³ (100 mg, 97.3 μ mol), 4,4'-dimethoxy-2,2'-bipyridyl (42.1 mg, 190 μ mol), CH₂Cl₂ (2.00 ml); 14 h at 50 °C.

Formula: C₃₀H₂₆F₆IrN₆O₂P [839.75].

Yield: 66.0 mg (78.6 μ mol, 40 %) of a pale green solid.¹⁰³

Melting point: 267 °C.

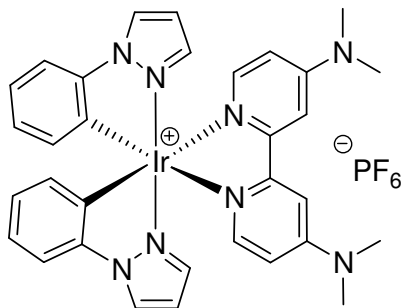
¹H NMR (400.1 MHz, d₆-acetone): δ = 8.69 (-, 2H); 8.34 (-, 2H); 8.00 (-, 2H); 7.61 (-, 2H); 7.25 (-, 4H); 7.04 (-, 2H); 6.84 (-, 2H); 6.70 (-, 2H); 6.34 (-, 2H), 4.10 (s, 6H).

¹³C NMR (100.6 MHz, d₆-acetone): δ = 169.4 (quart.); 159.4 (quart.); 153.1 (tert.); 144.7 (quart.); 139.7 (tert.); 134.5 (tert.); 134.4 (quart.); 129.1 (tert.); 127.7 (tert.); 124.2 (tert.); 114.8 (tert.); 113.1 (tert.); 112.4 (tert.); 109.5 (tert.); 57.6 (prim.).

ESI pos. (high resolution): calcd for [M⁺] = C₃₀H₂₆IrN₆O₂⁺: 693.17177; found: 693.17177 (Δ = 0.00 ppm).

3 Experimental Section

Complex (1_NMe₂) [Ir(ppz)₂(bpy-(NMe₂)₂)]PF₆



Following GP6: Phenylpyrazole dimer¹⁰³ (72.0 mg, 70.0 μmol), 4,4'-bis(dimethylamino)-2,2'-bipyridyl¹⁶² (33.9 mg, 140 μmol), CH₂Cl₂ (2.00 ml); 14 h at 50 °C.

Formula: C₃₂H₃₂F₆IrN₈P [865.83].

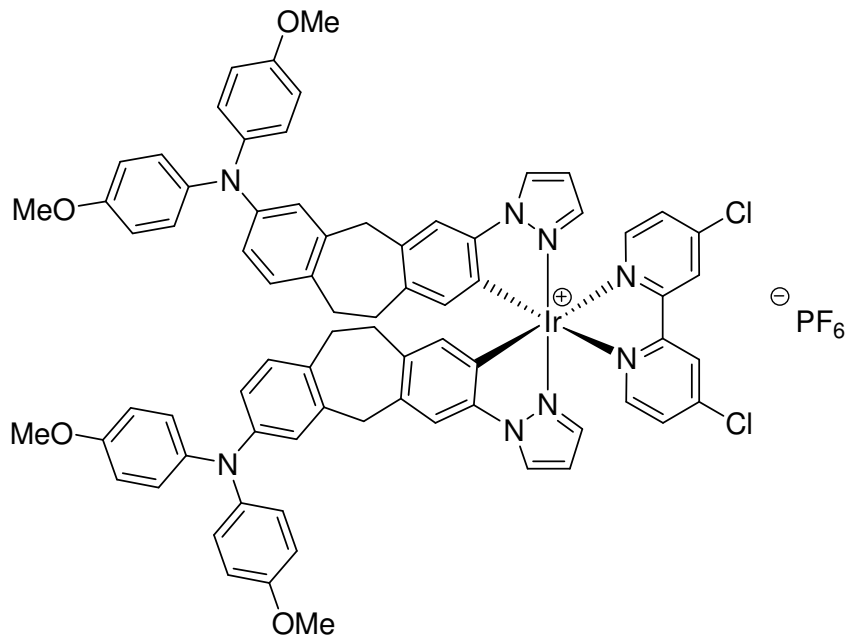
Yield: 48.0 mg (55.4 μmol , 41 %) of a pale blue solid.

Melting point: 357 °C.

¹H NMR (400.1 MHz, d₆-acetone): δ = 8.66 (-, 2H); 7.76 (-, 2H); 7.62 (-, 2H); 7.58 (-, 2H); 7.16 (-, 2H); 7.00 (-, 2H); 6.81 (-, 2H); 6.75 (-, 2H); 6.70 (-, 2H); 6.36 (-, 2H); 3.21 (s, 12H).

¹³C NMR (100.6 MHz, d₆-acetone): δ = 138.06 (quart.); 156.5 (quart.); 150.4 (tert.); 145.0 (quart.); 139.2 (tert.); 135.6 (quart.); 134.6 (tert.); 128.7 (tert.); 127.5 (tert.); 123.7 (tert.); 112.8 (tert.); 110.2 (tert.); 109.2 (tert.); 106.8 (tert.); 40.1 (prim.).

ESI pos. (high resolution): calcd for [M⁺] = C₃₂H₃₂IrN₈⁺: 719.23504; found: 719.23503 (Δ = 0.00 ppm).

Complex (1A_Cl) [Ir(ppz_{TAA})₂(bpy-Cl₂)]PF₆

Following GP6: Dimer **16** (70.0 mg, 29.2 μmol), 4,4'-dichloro-2,2'-bipyridyl (13.1 mg, 58.3 μmol), CH₂Cl₂ (2.00 ml); 14 h at 50 °C.

Formula: C₇₄H₆₂Cl₂F₆IrN₈O₄P [1535.42].

Yield: 21.0 mg (13.7 μmol , 24 %) of a pale green solid.

Melting point: 239 °C.

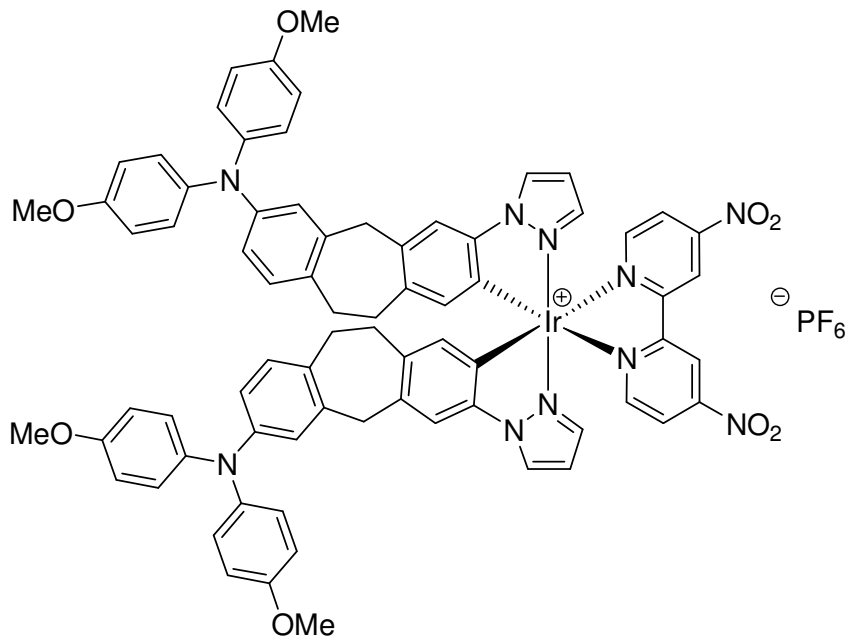
¹H NMR (600.1 MHz, d₆-acetone): δ = 9.03 (-, 2H); 8.63 (-, 2H); 8.27 (-, 2H); 7.78 (-, 2H); 7.45 (s, 2H); 7.35 (-, 2H); 6.96 (AA', 8H); 6.90 (-, 2H); 6.87 (BB', 8H); 6.70 (-, 2H); 6.65 (-, 2H); 6.63 (-, 2H); 6.03 (s, 2H); 3.88 (-, 4H); 3.78 (s, 12H); 2.96 – 2.80 (-, 8H).

¹³C NMR (150.9 MHz, d₆-acetone): δ = 158.3 (quart.); 156.9 (quart.); 153.2 (tert.); 148.1 (quart.); 147.9 (quart.); 142.4 (quart.); 142.2 (quart.); 140.5 (quart.); 139.7 (tert.); 138.9 (quart.); 135.1 (quart.); 134.9 (tert.); 132.6 (quart.); 131.2 (tert.); 129.74 (tert.); 129.73 (quart.); 128.6 (tert.); 127.3 (tert.); 126.5 (tert.); 122.2 (tert.); 120.1 (tert.); 115.6 (tert.); 113.5 (tert.); 109.1 (tert.); 55.8 (prim.); 41.4 (sec.); 33.5 (sec.); 32.6 (sec.).

ESI pos. (high resolution): calcd for [M⁺] = C₇₄H₆₂Cl₂IrN₈O₄⁺: 1387.38715; found: 1387.38716 (Δ = 0.00 ppm).

3 Experimental Section

Complex (1A₂-NO₂) [Ir(ppz_{TAA})₂(bpy-(NO₂)₂)]PF₆



Following GP6: Dimer **16** (70.0 mg, 29.2 μmol), 4,4'-dinitro-2,2'-bipyridyl (14.4 mg, 58.3 μmol), CH₂Cl₂ (2.00 ml); 14 h at 50 °C.

Formula: C₇₄H₆₂F₆IrN₁₀O₈P [1556.53].

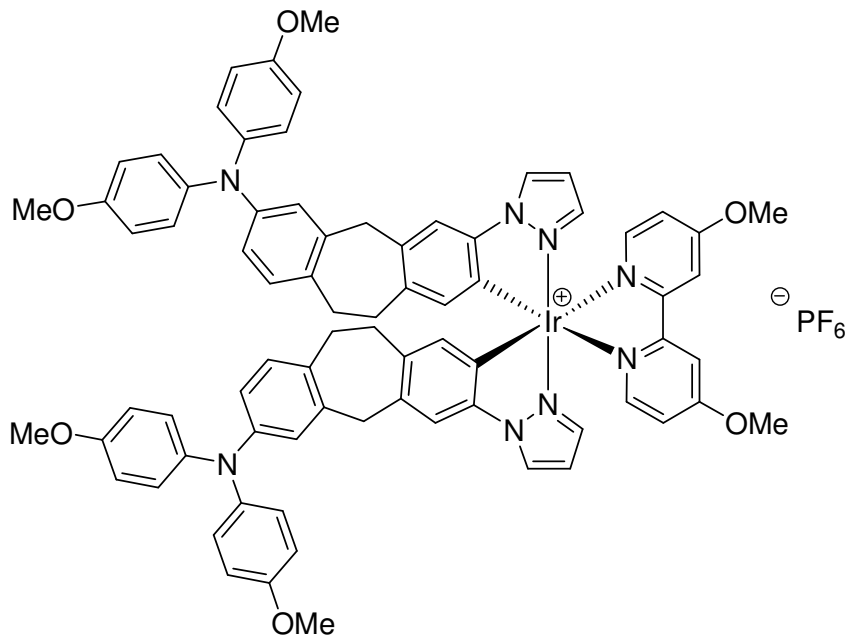
Yield: 14.0 mg (8.99 μmol , 15 %) of a dark green solid.

Melting point: 205 °C.

¹H NMR (600.1 MHz, d₆-acetone): δ = 9.88 (-, 2H); 8.77 (-, 2H); 8.66 (-, 2H); 8.47 (-, 2H); 7.49 (s, 2H); 7.35 (-, 2H); 6.97 (AA', 8H); 6.91 (-, 2H); 6.88 (BB', 8H); 6.71 (-, 2H); 6.66 (-, 4H); 6.03 (s, 2H); 3.91 (-, 4H); 3.78 (s, 12H); 2.86 – 2.79 (-, 8H).

¹³C NMR (150.9 MHz, d₆-acetone): δ = 159.6 (quart.); 157.1 (quart.); 156.4 (quart.); 155.4 (tert.); 148.0 (quart.); 142.30 (quart.); 142.26 (quart.); 140.5 (quart.); 140.0 (tert.); 139.3 (quart.); 135.7 (quart.); 134.8 (tert.); 132.7 (quart.); 131.3 (tert.); 129.1 (quart.); 129.0 (tert.); 127.4 (tert.); 123.6 (tert.); 122.2 (tert.); 120.4 (tert.); 120.2 (tert.); 115.8 (tert.); 113.8 (tert.); 109.4 (tert.); 55.9 (prim.); 41.4 (sec.); 33.6 (sec.); 32.6 (sec.).

ESI pos. (high resolution): calcd for [M⁺] = C₇₄H₆₂IrN₁₀O₈⁺: 1409.43525; found: 1409.43526 (Δ = 0.01 ppm).

Complex (1A_OMe) [Ir(ppz_{TAA})₂(bpy-(OMe)₂)]PF₆

Following GP6: Dimer **16** (70.0 mg, 29.2 μmol), 4,4'-dimethoxy-2,2'-bipyridyl (12.6 mg, 58.3 μmol), CH₂Cl₂ (2.00 ml); 14 h at 50 °C.

Formula: C₇₆H₆₈F₆IrN₈O₆P [1526.45].

Yield: 43.0 mg (28.2 μmol , 48 %) of a pale yellow solid.

Melting point: 257 °C.

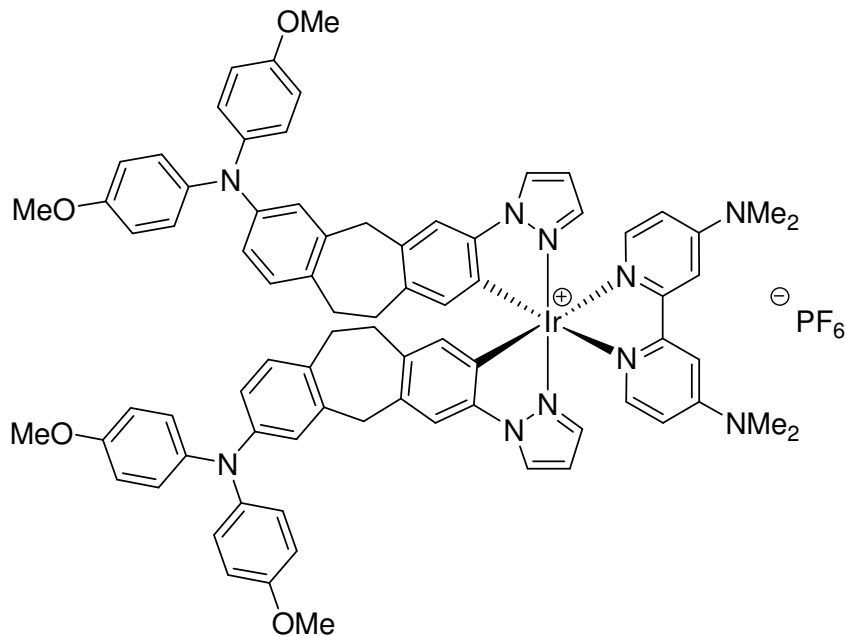
¹H NMR (600.1 MHz, d₆-acetone): δ = 8.61 (-, 2H); 8.32 (-, 2H); 8.05 (-, 2H); 7.43 (s, 2H); 7.20 (-, 2H); 7.19 (-, 2H); 6.96 (AA', 8H); 6.89 (-, 2H); 6.86 (BB', 8H); 6.70 (-, 2H); 6.64 (-, 4H); 6.06 (s, 2H); 4.08 (s, 6H); 3.87 (-, 4H); 3.78 (s, 12H); 2.96 – 2.84 (-, 8H).

¹³C NMR (150.9 MHz, d₆-acetone): δ = 169.1 (quart.); 159.2 (quart.); 157.0 (quart.); 153.0 (tert.); 148.0 (quart.); 142.7 (quart.); 142.3 (quart.); 140.7 (quart.); 139.1 (tert.); 138.8 (quart.); 135.1 (tert.); 134.7 (quart.); 132.8 (quart.); 131.3 (tert.); 131.1 (quart.); 128.4 (tert.); 127.3 (tert.); 122.3 (tert.); 120.2 (tert.); 115.7 (tert.); 114.6 (tert.); 113.4 (tert.); 112.2 (tert.); 109.1 (tert.); 57.5 (prim.); 55.9 (prim.); 41.5 (sec.); 33.5 (sec.); 32.7 (sec.).

ESI pos. (high resolution): calcd for [M⁺] = C₇₆H₆₈IrN₈O₆⁺: 1379.48622; found: 1379.48623 (Δ = 0.01 ppm).

3 Experimental Section

Complex (1A_NMe₂) [Ir(ppz_{TAA})₂(bpy-(NMe₂)₂)]PF₆



Following GP6: Dimer **16** (70.0 mg, 29.1 μmol), 4,4'-*bis*-(dimethylamino) -2,2'-bipyridyl¹⁶² (14.1 mg, 58.3 μmol), CH₂Cl₂ (2.00 ml); 14 h at 50 °C.

Formula: C₇₈H₇₄F₆IrN₁₀O₄P [1552.67].

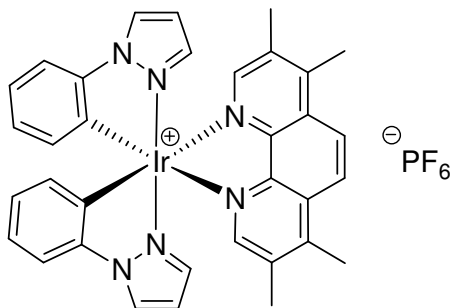
Yield: 48.0 mg (30.9 μmol , 37 %) of a pale blue solid.

Melting point: 212 °C.

¹H NMR (600.1 MHz, d₆-acetone): δ = 8.57 (-, 2H); 7.74 (-, 2H); 7.65 (-, 2H); 7.40 (s, 2H); 7.09 (-, 2H); 6.95 (AA', 8H); 6.88 (-, 2H); 6.86 (BB', 8H); 6.70 (-, 2H); 6.68 (-, 2H); 6.63 (-, 4H); 6.07 (s, 2H); 3.86 (-, 4H); 3.77 (s, 12 H); 3.19 (s, 12H); 2.88 – 2.78 (-, 8H).

¹³C NMR (150.9 MHz, d₆-acetone): δ = 157.9 (quart.); 157.0 (quart.); 156.2 (quart.); 150.3 (tert.); 147.9 (quart.); 143.0 (quart.); 142.3 (quart.); 140.8 (quart.); 138.61 (tert.); 138.55 (quart.); 135.3 (tert.); 134.2 (quart.); 132.8 (quart.); 132.7 (quart.); 131.3 (tert.); 128.0 (tert.); 127.3 (tert.); 122.3 (tert.); 120.2 (tert.); 115.7 (tert.); 113.2 (tert.); 110.0 (tert.); 108.8 (tert.); 106.6 (tert.); 55.9 (prim.); 41.5 (sec.); 39.9 (prim.); 33.5 (sec.); 32.8 (sec.).

ESI pos. (high resolution): calcd for [M⁺] = C₇₈H₇₄IrN₁₀O₄⁺: 1405.54949; found: 1405.54949 (Δ = 0.00 ppm).

Complex (2) [Ir(ppz)₂(tmp)]PF₆

Following GP6: Phenylpyrazole dimer¹⁰³ (100 mg, 97.3 μ mol), 3,4,7,8-tetramethyl-1,10-phenanthroline (46.0 mg, 19.0 mmol), CH₂Cl₂ (2.00 ml); 14 h at 50 °C.

Formula: C₃₄H₃₀F₆IrN₆P [859.82].

Yield: 62.0 mg (72.1 μ mol, 37 %) of a yellow solid.

Melting point: 251 °C.

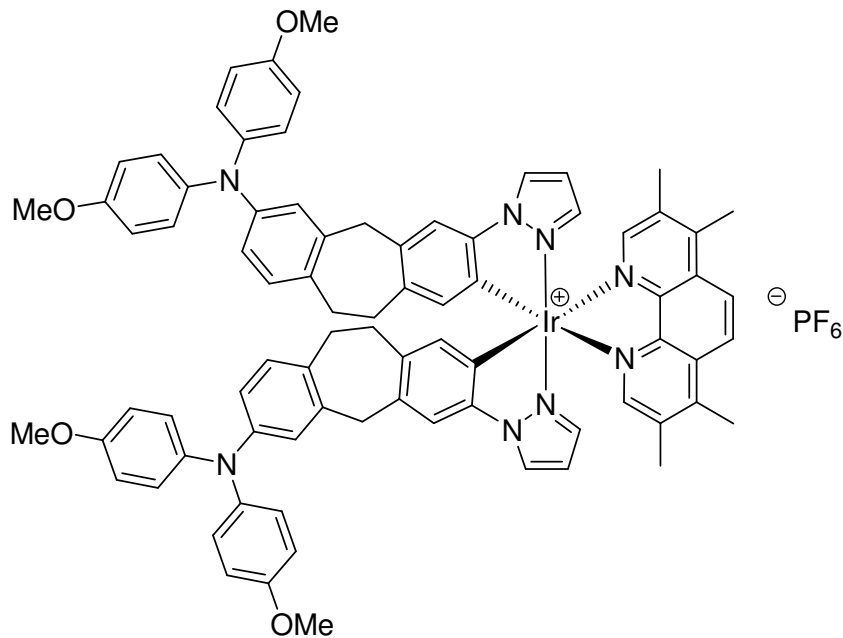
¹H NMR (600.1 MHz, d₆-acetone): δ = 8.68 (-, 2H); 8.52 (-, 2H); 8.30 (-, 2H); 7.65 (-, 2H); 7.08 (-, 4H); 6.91 (-, 2H); 6.58 (-, 2H); 6.44 (-, 2H); 2.91 (s, 6H); 2.43 (2, 6H).

¹³C NMR (150.9 MHz, d₆-acetone): δ = 152.7 (tert.); 147.6 (quart.); 147.3 (quart.); 144.6 (quart.); 139.6 (tert.); 136.0 (quart.); 134.3 (tert.); 133.5 (quart.); 130.9 (quart.); 128.9 (tert.); 127.6 (tert.); 125.4 (tert.); 124.2 (tert.); 112.9 (tert.); 109.1 (tert.); 18.2 (prim.); 15.3 (prim.).

ESI pos. (high resolution): calcd for [M⁺] = C₃₄H₃₀IrN₆⁺: 713.21324; found: 713.21324 (Δ = 0.00 ppm).

3 Experimental Section

Complex (2A) [Ir(ppz_{TAA})₂(tmp)]PF₆



Following GP6: Dimer **16** (75.0 mg, 31.2 μmol), 3,4,7,8-tetramethyl-1,10-phenanthroline (14.8 mg, 62.5 μmol), CH₂Cl₂ (2.00 ml); 14 h at 50 °C.

Formula: C₈₀H₇₂F₆IrN₈O₄P [1546.66].

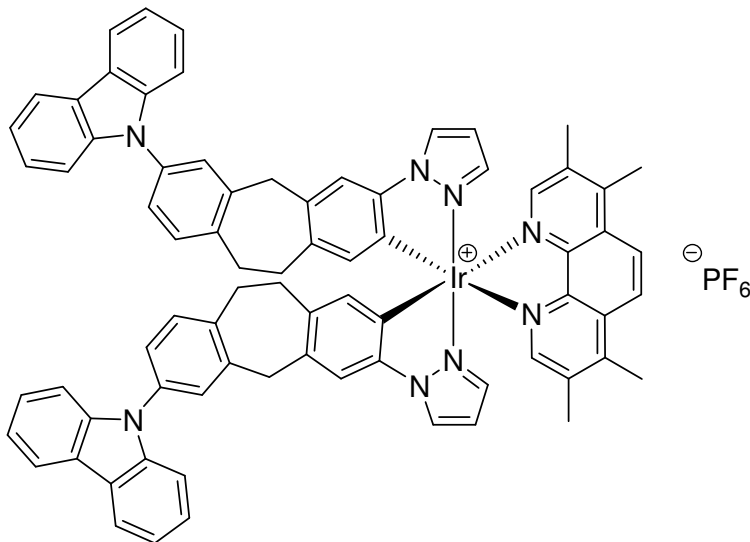
Yield: 40.0 mg (25.9 μmol , 41 %) of a green solid.

Melting point: 214 °C.

¹H NMR (600.1 MHz, d₈-THF): δ = 8.58 (-, 2H); 8.55 (-, 2H); 8.34 (s, 2H); 7.45 (s, 2H); 7.09 (AA', 8H); 7.00 (-, 4H); 6.93 (BB', 8H); 6.89 (-, 2H); 6.80 (-, 2H); 6.59 (-, 2H); 6.31 (s, 2H); 3.98 – 4.15 (-, 4H); 3.88 (s, 12H); 3.00 – 3.19 (-, 14H); 2.52 (s, 6H).

¹³C NMR (150.9 MHz, d₈-THF): δ = 156.6 (quart.); 152.1 (tert.); 147.7 (quart.); 147.2 (quart.); 147.1 (quart.); 142.5 (quart.); 142.2 (tert.); 140.2 (quart.); 138.9 (tert.); 138.7 (quart.); 135.6 (quart.); 134.6 (quart.); 134.5 (quart.); 132.6 (quart.); 130.9 (tert.); 130.6 (quart.); 130.5 (quart.); 127.7 (tert.); 126.7 (tert.); 125.0 (tert.); 122.5 (tert.); 120.3 (tert.); 115.2 (tert.); 112.9 (tert.); 108.4 (tert.); 55.4 (prim.); 41.5 (sec.); 33.4 (sec.); 33.0 (sec.); 17.8 (prim.); 14.8 (prim.).

ESI pos. (high resolution): calcd for [M⁺] = C₈₀H₇₂IrN₈O₄⁺: 1399.52770; found: 1399.52770 (Δ = 0.00 ppm).

Complex (2B) [Ir(ppzCz)₂(tmp)]PF₆

Following GP6: Dimer **17** (90.0 mg, 41.8 μmol), 3,4,7,8-tetramethyl-1,10-phenanthroline (19.7 mg, 83.6 μmol), CH₂Cl₂ (2.00 ml); 14 h at 50 °C.

Formula: C₇₆H₆₀F₆IrN₈P [1422.52].

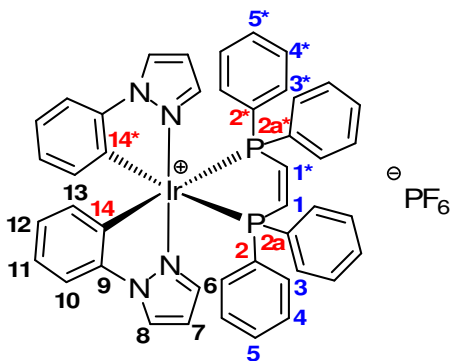
Yield: 48.0 mg (33.7 μmol , 40 %) of a yellow solid.

Melting point: 263 °C.

¹H NMR (600.1 MHz, d₈-THF): δ = 8.58 (-, 2H); 8.56 (s, 2H); 8.36 (s, 2H); 8.27 (-, 4H); 7.55 (-, 4H); 7.47 (-, 12H); 7.35 (-, 4H); 7.07 (-, 2H); 6.61 (-, 2H); 6.43 (s, 2H); 4.38 (-, 4H); 3.47 – 3.14 (-, 8H); 2.99 (s, 6H); 2.52 (s, 6H).

¹³C NMR (150.9 MHz, d₈-THF): δ = 152.0 (tert.); 147.3 (quart.); 147.0 (quart.); 142.7 (quart.); 141.9 (quart.); 141.6 (quart.); 139.9 (quart.); 139.0 (tert.); 138.7 (quart.); 136.2 (quart.); 135.5 (quart.); 134.7 (tert.); 134.1 (quart.); 131.9 (tert.); 131.1 (quart.); 130.6 (quart.); 128.1 (tert.); 127.7 (tert.); 126.4 (tert.); 125.7 (tert.); 125.0 (tert.); 124.1 (quart.); 120.7 (tert.); 120.3 (tert.); 112.9 (tert.); 110.4 (tert.); 108.5 (tert.); 41.2 (sec.); 33.5 (sec.); 32.9 (sec.); 17.8 (prim.); 14.8 (prim.).

ESI pos. (high resolution): calcd for [M⁺] = C₇₆H₆₀IrN₈⁺: 1275.45414; found: 1275.45414 (Δ = 0.00 ppm).

Complex (3) [Ir(ppz)₂(bdppe)]PF₆

Following GP6: Phenylpyrazole dimer¹⁰³ (60.0 mg, 58.4 μmol), *cis*-1,2-bis(diphenylphosphino)ethylene (46.3 mg, 120 μmol), CH₂Cl₂ (2.00 ml); 14 h at 50 °C.

Formula: C₄₄H₃₆F₆IrN₄P₃ [1019.91].

Yield: 46.0 mg (45.1 μmol , 39 %) of a colourless solid.

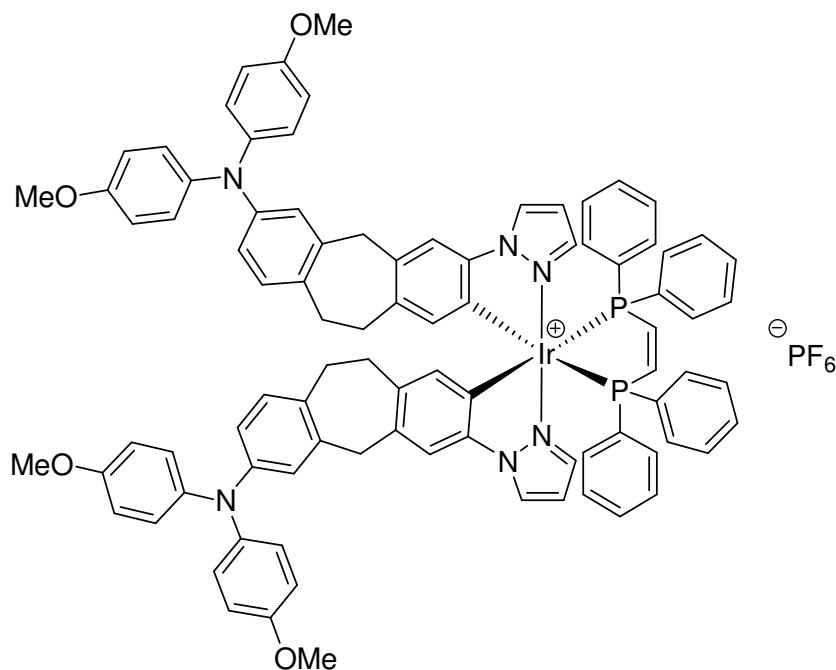
Melting point: 310 °C.

¹H NMR (600.1 MHz, d₈-THF): δ = 8.23 (s, 1H, H1 or H1*); 8.68 (s, 1H, H1 or H1*); 8.16 (-, 2H, H8); 7.99 (-, 4H, H3 or H3*); 7.64 (-, 2H, H5 or H5*); 7.58 (-, 4H, H4 or H4*); 7.46 (-, 2H, H12); 7.20 (-, 2H, H5 or H5*); 7.08 (-, 6H, H11 and H4 or H4*); 6.94 (-, 2H, H13); 6.73 (-, 4H, H3 or H3*); 6.44 (-, 2H, H10); 6.33 (-, 2H, H6); 6.16 (-, 2H, H7).

¹³C NMR (150.9 MHz, d₈-THF): δ = 150.2 (tert., C1 or C1*); 150.0 (tert., C1 or C1*); 142.4 (quart., C9); 141.1 (tert., C8); 140.4 (quart., C2 or C2* or C2a or C2a* or C14 or C14*); 139.7 (quart., C2 or C2* or C2a or C2a* or C14 or C14*); 135.0 (tert., C10); 134.0 (tert., C3 or C3*); 133.2 (tert., C5 or C5*); 131.7 (quart., C2 or C2* or C2a or C2a* or C14 or C14*); 131.4 (quart., C2 or C2* or C2a or C2a* or C14 or C14*); 131.2 (tert., C5 or C5*); 130.8 (tert., C4 or C4*); 130.7 (tert., C3 or C3*); 129.8 (quart., C2 or C2* or C2a or C2a* or C14 or C14*); 129.7 (tert., C4 or C4*); 129.5 (quart., C2 or C2* or C2a or C2a* or C14 or C14*); 128.6 (tert., C6); 127.7 (tert., C13); 125.4 (tert., C11); 113.3 (tert., C12); 109.7 (tert., C7).

ESI pos. (high resolution): calcd for $[M^+] = C_{44}H_{36}IrN_4P_2^+$: 873.20156; found: 873.20156 ($\Delta = 0.00$ ppm).

Complex (3A) $[Ir(ppz_{TAA})_2(bdppe)]PF_6$



Following GP6: Dimer **16** (100 mg, 41.6 μmol), *cis*-1,2-*bis*(diphenylphosphino)ethylene (33.0 mg, 83.3 μmol), CH_2Cl_2 (2.00 ml); 14 h at 50 °C.

Formula: $C_{90}H_{78}F_6IrN_6O_4P_3$ [1706.75].

Yield: 63.0 mg (36.9 μmol , 44 %) of a grey solid.

Melting point: 194 °C.

$^1\text{H NMR}$ (600.1 MHz, d_8 -THF): $\delta = 8.78$ (-, 1H); 8.67 (-, 1H); 8.05 (-, 4H); 8.01 (-, 2H); 7.46 (-, 6H); 7.28 (-, 2H); 7.21 (-, 2H); 7.10 – 7.00 (-, 14H); 6.94 – 6.88 (-, 10H); 6.78 (-, 6H); 6.36 (-, 2H); 6.30 (-, 2H); 6.12 (-, 2H); 4.12 – 3.97 (-, 4H); 3.87 (s, 12H); 3.20 – 3.05 (-, 8H).

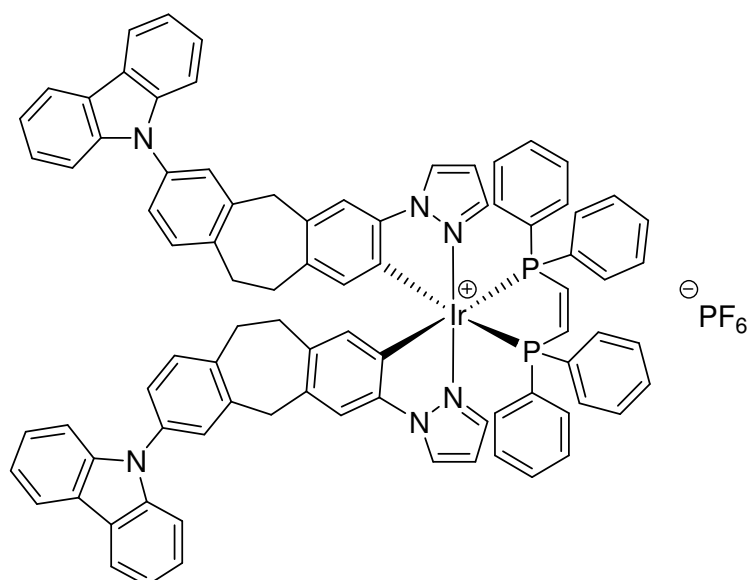
$^{13}\text{C NMR}$ (150.9 MHz, d_8 -THF): $\delta = 156.6$ (quart.); 149.7 (tert.); 149.5 (tert.); 147.7 (quart.); 142.1 (quart.); 140.2 (tert.); 140.1 (quart.); 138.7 (quart.); 137.0 (quart.); 135.9 (quart.); 135.4 (tert.); 133.6 (tert.); 132.19

3 Experimental Section

(tert.); 132.21 (quart.); 131.6 (quart.); 131.3 (quart.); 130.9 (tert.); 130.5 (tert.); 130.2 (tert.); 130.0 (tert.); 129.6 (quart.); 129.2 (quart.); 129.0 (tert.); 128.8 (quart.); 127.3 (tert.); 126.7 (tert.); 126.6 (quart.); 122.4 (tert.); 120.2 (tert.); 115.1 (tert.); 113.3 (tert.); 108.6 (tert.); 55.4 (prim.); 41.3 (sec.); 33.4 (sec.); 33.0 (sec.).

ESI pos. (high resolution): calcd for $[M^+] = C_{90}H_{78}IrN_6O_4P_2^+$: 1559.51602; found: 1559.51602 ($\Delta = 0.00$ ppm).

Complex (3B) $[Ir(ppz_{cz})_2(bdppe)]PF_6$



Following GP6: Dimer **17** (100 mg, 46.4 μmol), *cis*-1,2-bis(diphenylphosphino)ethylene (36.8 mg, 92.9 μmol), CH_2Cl_2 (2.00 ml); 14 h at 50 °C.

Formula: $C_{86}H_{66}F_6IrN_6P_3$ [1582.61].

Yield: 68.0 mg (43.0 μmol , 46 %) of a colourless solid.

Melting point: 207 °C.

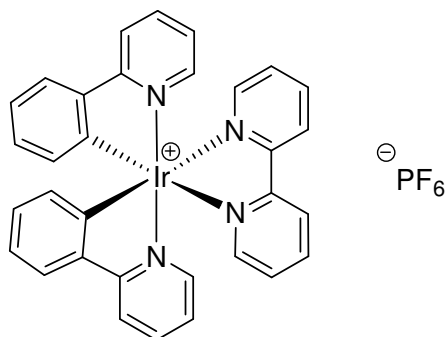
$^1\text{H NMR}$ (600.1 MHz, d_8 -THF): $\delta = 8.31$ (-, 2H); 8.13 (-, 4H); 7.80 (-, 4H); 7.61 (-, 2H); 7.54 (-, 4H); 7.42 - 7.23 (-, 20H); 7.13 (-, 2H); 7.00 (s, 2H); 6.95

(-, 4H); 6.56 (-, 4H); 6.20 (-, 4H); 5.94 (-, 2H); 4.20 (-, 4H); 3.43 – 3.07 (-, 8H).

¹³C NMR (150.9 MHz, d₈-THF): δ = 149.9 (tert.); 149.4 (tert.); 141.8 (quart.); 141.5 (quart.); 140.9 (quart.); 140.4 (quart.); 140.3 (tert.); 139.6 (quart.); 138.6 (quart.); 136.3 (quart.); 135.6 (quart.); 135.4 (tert.); 133.6 (tert.); 132.3 (tert.); 132.1 (tert.); 131.8 (quart.); 130.5 (tert.); 130.3 (tert.); 130.0 (tert.); 129.0 (tert.); 128.2 (tert.); 127.5 (tert.); 126.9 (quart.); 126.4 (tert.); 125.8 (tert.); 124.1 (quart.); 120.8 (tert.); 120.7 (quart.); 120.3 (quart.); 120.4 (tert.); 113.4 (tert.); 110.4 (quart.); 110.3 (tert.); 108.7 (tert.); 41.1 (sec.); 33.6 (sec.); 32.9 (sec.).

ESI pos. (high resolution): calcd for [M⁺] = C₈₆H₆₆IrN₆P₂⁺: 1435.44246; found: 1435.44246 (Δ = 0.00 ppm).

Complex (4) [Ir(ppy)₂(bpy)]PF₆



Following GP6: Phenylpyridyl dimer ¹⁰² (100 mg, 93.3 μ mol), 2,2'-bipyridyl (29.1 mg, 187 μ mol), CH₂Cl₂ (2.00 ml); 14 h at 50 °C.

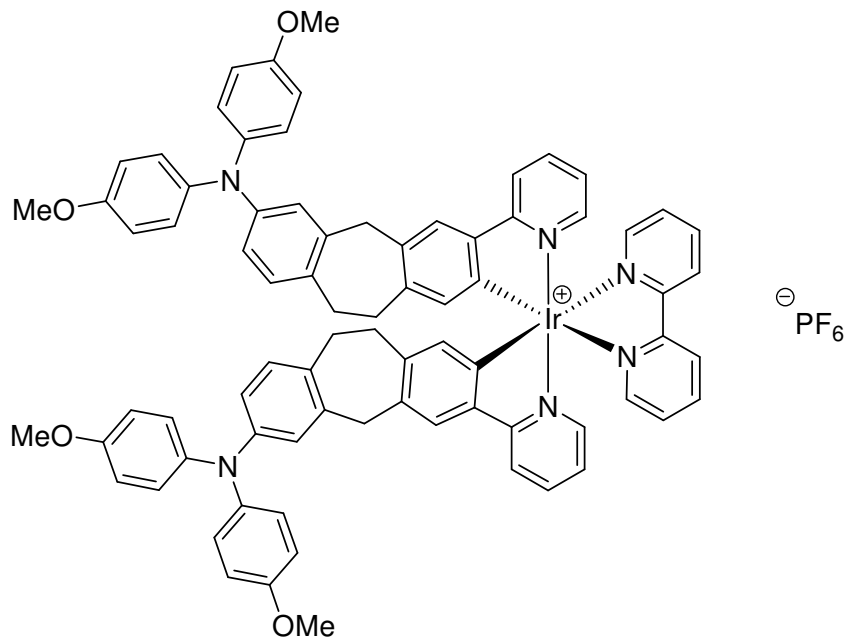
Formula: C₃₂H₂₄F₆IrN₄P [801.74 g/mol]

Yield: 117 mg (146 μ mol, 78 %) of a pale yellow solid.^{93,94,96,97,100,102,117}

Melting point: >300 °C.

3 Experimental Section

$^1\text{H NMR}$ (600.1 MHz, d_6 -acetone): $\delta = 8.85$ (-, 2H); 8.30 (-, 2H); 8.24 (-, 2H); 8.11 (-, 2H); 7.96 (-, 2H); 7.90 (-, 2H); 7.83 (-, 2H); 7.71 (-, 2H), 7.16 (-, 2H); 7.04 (-, 2H); 6.92 (-, 2H); 6.35 (-, 2H).¹⁰²

Complex (4A) $[\text{Ir}(\text{ppy}_{\text{TAA}})_2(\text{bpy})]\text{PF}_6$ 

Following GP6: Dimer **18** (72.0 mg, 29.4 μmol), 2,2'-bipyridyl (9.20 mg, 58.9 μmol), CH_2Cl_2 (2.00 ml); 14 h at 50 °C.

Formula: $\text{C}_{78}\text{H}_{66}\text{F}_6\text{IrN}_6\text{O}_4\text{P}$ [1488.58].

Yield: 32.0 mg (21.5 μmol , 37 %) of a pale yellow solid.

Melting point: 205 °C.

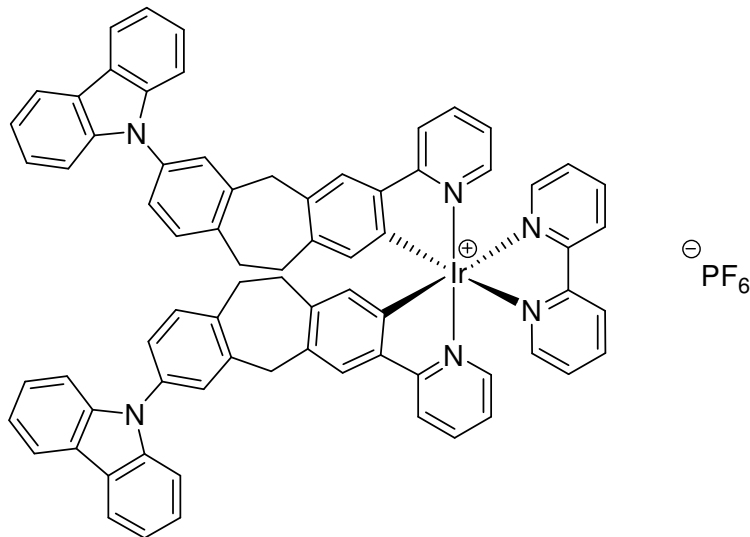
H NMR (600.1 MHz, $d_8\text{-THF}$): $\delta = 8.91$ (-, 2H); 8.32 (-, 2H); 8.16 (-, 4H); 7.92 (-, 2H); 7.75 (-, 2H); 7.72 (s, 2H); 7.64 (-, 2H); 7.14 (-, 2H); 7.10 – 6.91 (-, 20H); 6.78 (-, 2H); 6.20 (s, 2H); 3.89 (-, 4H); 3.73 (s, 12H); 2.95 – 2.80 (-, 8H).

^{13}C NMR (150.9 MHz, $d_8\text{-THF}$): $\delta = 168.9$ (quart.); 157.0 (quart.); 156.7 (quart.); 151.2 (tert.); 149.8 (tert.); 147.8 (quart.); 143.5 (quart.); 142.8 (quart.); 142.3 (quart.); 140.51 (quart.); 140.47 (tert.); 138.8 (tert.); 133.9 (quart.); 133.3 (tert.); 132.7 (quart.); 130.7 (tert.); 129.1 (tert.); 126.8 (tert.); 126.7 (quart.); 126.2 (tert.); 126.1 (tert.); 123.6 (tert.); 122.7 (tert.); 120.3 (tert.); 120.1 (tert.); 115.3 (tert.); 55.5 (prim.); 41.6 (sec.); 33.9 (sec.); 32.9 (sec.).

ESI pos. (high resolution): calcd for $[\text{M}^+] = \text{C}_{78}\text{H}_{66}\text{IrN}_6\text{O}_4^+$: 1341.47460 found: 1341.47460 ($\Delta = 0.00$ ppm).

3 Experimental Section

Complex (4B) $[\text{Ir}(\text{ppy}_{\text{CZ}})_2(\text{bpy})]\text{PF}_6$



Following GP6: Dimer **19** (62.0 mg, 28.2 μmol), 2,2'-bipyridyl (8.81 mg, 56.4 μmol), CH_2Cl_2 (2.00 ml); 14 h at 50 °C.

Formula: $\text{C}_{74}\text{H}_{54}\text{F}_6\text{IrN}_6\text{P}$ [1364.44].

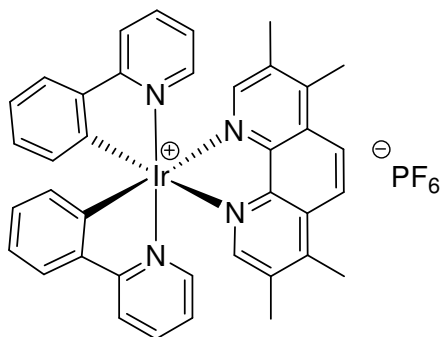
Yield: 38.0 mg (27.9 μmol , 49 %) of a pale yellow solid.

Melting point: 242 °C.

$^1\text{H NMR}$ (600.1 MHz, d_8 -THF): δ = 8.92 (-, 2H); 8.33 (-, 2H); 8.25 (-, 4H); 8.21 (-, 2H); 8.18 (-, 2H); 7.96 (-, 2H); 7.83 (s, 2H); 7.80 (-, 2H); 7.67 (-, 2H); 7.57 (s, 2H); 7.49 – 7.45 (-, 12H); 7.37 – 7.32 (-, 4H); 7.16 (-, 2H); 6.30 (s, 2H); 4.36 (4H); 3.32 (8H).

$^{13}\text{C NMR}$ (150.9 MHz, d_8 -THF): δ = 169.0 (quart.); 157.2 (quart.); 151.4 (tert.); 150.1 (tert.); 149.8 (quart.); 143.5 (quart.); 143.4 (quart.); 142.2 (quart.); 142.1 (quart.); 140.7 (tert.); 140.2 (quart.); 139.2 (tert.); 136.6 (quart.); 133.7 (quart.); 133.6 (tert.); 132.0 (tert.); 129.4 (tert.); 128.5 (tert.); 126.7 (tert.); 126.5 (tert.); 126.3 (tert.); 126.0 (tert.); 124.5 (quart.); 124.1 (tert.); 121.1 (tert.); 120.7 (tert.); 120.4 (tert.); 110.7 (tert.); 41.6 (sec.); 33.7 (sec.); 33.6 (sec.).

ESI pos. (high resolution): calcd for $[\text{M}^+]$ = $\text{C}_{74}\text{H}_{54}\text{IrN}_6^+$: 1217.40104 found: 1217.40103 (Δ = 0.01 ppm).

Complex (5) [Ir(ppy)₂(tmp)]PF₆

Following GP6: Phenylpyridyl dimer¹⁰⁰ (120 mg, 112 μ mol), 3,4,7,8-tetramethyl-1,10-phenanthroline (52.9 mg, 224 μ mol), CH₂Cl₂ (2.00 ml); 14 h at 50 °C.

Formula: C₃₆H₃₂F₆IrN₄P [881.87 g/mol].

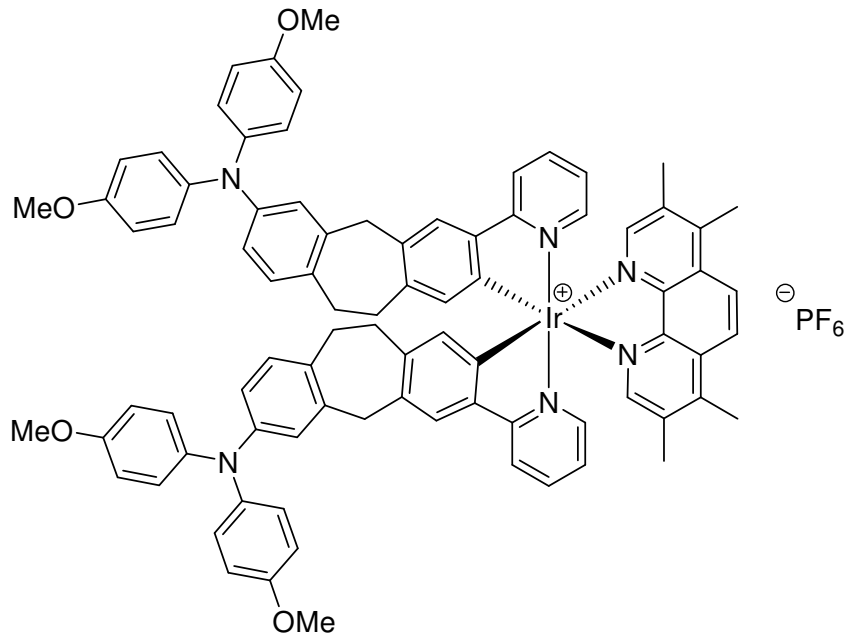
Yield: 143 mg (162 μ mol, 72 %) of a yellow solid.^{95,96,100}

Melting point: >300 °C.

¹H NMR (600.1 MHz, d₈-THF): δ = 8.52 (s, 2H); 8.21 (-, 2H); 8.13 (s, 2H); 7.89 (-, 4H); 7.66 (-, 2H); 7.07 (-, 2H); 6.96 (-, 4H); 6.44 (-, 2H); 2.89 (s, 6H); 2.40 (s, 6H).¹⁰⁰

3 Experimental Section

Complex (5A) [Ir(ppy_{TAA})₂(tmp)]PF₆



Following GP6: Dimer **18** (62.0 mg, 28.2 μmol), 3,4,7,8-tetramethyl-1,10-phenanthroline (8.81 mg, 56.4 μmol), CH₂Cl₂ (2.00 ml); 14 h at 50 °C.

Formula: C₈₄H₇₄F₆IrN₆O₄P [1568.71].

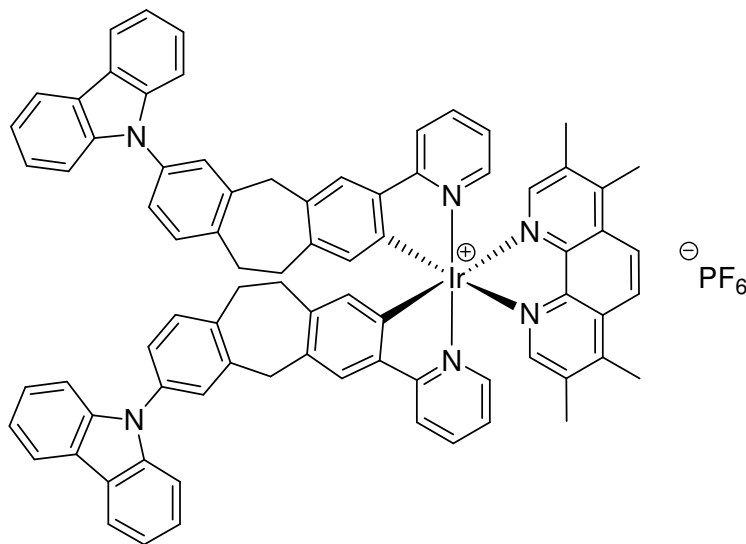
Yield: 52.0 mg (33.2 μmol , 47 %) of a pale yellow solid.

Melting point: 230 °C.

¹H NMR (600.1 MHz, d₈-THF): δ = 8.56 (s, 2H); 8.14 (-, 4H); 7.84 (-, 2H); 7.73 (s, 2H); 7.59 (-, 2H); 7.28 (-, 2H); 7.09 (AA', 8H); 6.99 (-, 2H); 6.92 (BB', 10H); 6.78 (-, 2H); 6.29 (s, 2H); 4.09 (-, 4H); 3.88 (s, 12H); 3.18 – 2.92 (-, 14H); 2.46 (s, 6H).

¹³C NMR (150.9 MHz, d₈-THF): δ = 169.2 (quart.); 156.8 (quart.); 152.0 (tert.); 150.0 (tert.); 147.9 (quart.); 147.6 (quart.); 146.7 (quart.); 143.5 (quart.); 143.2 (quart.); 142.6 (quart.); 141.0 (quart.); 138.7 (tert.); 136.2 (quart.); 133.9 (quart.); 133.7 (tert.); 133.1 (quart.); 131.1 (quart.); 130.9 (tert.); 127.0 (tert.); 126.3 (tert.); 126.2 (quart.); 125.4 (tert.); 123.8 (tert.); 123.0 (tert.); 120.7 (tert.); 120.1 (tert.); 115.5 (tert.); 55.7 (prim.); 41.8 (sec.); 34.1 (sec.); 33.1 (sec.); 18.2 (prim.); 15.2 (prim.).

ESI pos. (high resolution): calcd for [M⁺] = C₈₄H₇₄IrN₆O₄⁺: 1421.53720 found: 1421.53719 (Δ = 0.01 ppm).

Complex (5B) [Ir(ppy_{cz})₂(tmp)]PF₆

Following GP6: Dimer **19** (60.0 mg, 27.3 μmol), 3,4,7,8-tetramethyl-1,10-phenanthroline (12.9 mg, 54.6 μmol), CH₂Cl₂ (2.00 ml); 14 h at 50 °C.

Formula: C₈₀H₆₂F₆IrN₆P [1444.57].

Yield: 29.0 mg (20.1 μmol , 37 %) of a pale yellow solid.

Melting point: 235 °C.

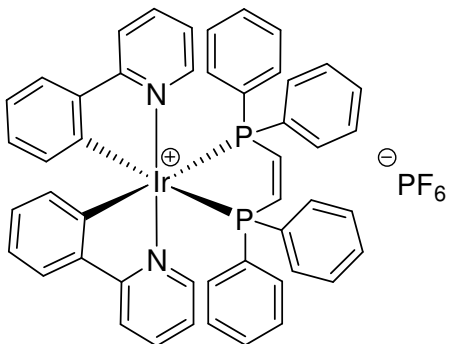
¹H NMR (600.1 MHz, d₈-THF): δ = 8.56 (s, 2H); 8.27 (-, 4H); 8.15 (-, 4H); 7.87 (-, 4H); 7.64 (-, 2H); 7.58 (-, 2H); 7.48 (-, 12H); 7.36 (-, 4H); 7.18 (-, 2H); 7.03 (-, 2H); 4.47 (-, 4H); 3.39 – 3.08 (-, 8H); 2.98 (s, 6H); 2.48 (s, 6H).

¹³C NMR (150.9 MHz, d₈-THF): δ = 151.9 (tert.); 150.1 (tert.); 149.9 (quart.); 147.6 (quart.); 146.5 (quart.); 143.4 (quart.); 143.2 (quart.); 142.3 (quart.); 142.1 (quart.); 140.1 (quart.); 138.7 (tert.); 136.4 (quart.); 136.2 (quart.); 133.8 (tert.); 133.5 (quart.); 131.9 (tert.); 131.0 (quart.); 128.3 (tert.); 126.6 (tert.); 126.2 (tert.); 125.9 (tert.); 125.3 (tert.); 124.3 (quart.); 123.8 (tert.); 121.0 (tert.); 120.9 (quart.); 120.6 (tert.); 120.1 (tert.); 110.6 (tert.); 41.4 (sec.); 33.5 (sec.); 33.5 (sec.); 18.1 (prim.); 15.0 (prim.).

ESI pos. (high resolution): calcd for [M⁺] = C₈₀H₆₂IrN₆⁺: 1297.46364 found: 1297.46364 (Δ = 0.00 ppm).

3 Experimental Section

Complex (6) [Ir(ppy)₂(bdppe)]PF₆



Following GP6: Dimer **18** (108 mg, 0.10 mmol), *cis*-1,2-*bis*(diphenylphosphino)ethylene (79.8 mg, 200 μ mol), CH₂Cl₂ (2.00 ml); 14 h at 50 °C.

Formula: C₄₈H₃₈F₆IrN₂P₃ [1041.96].

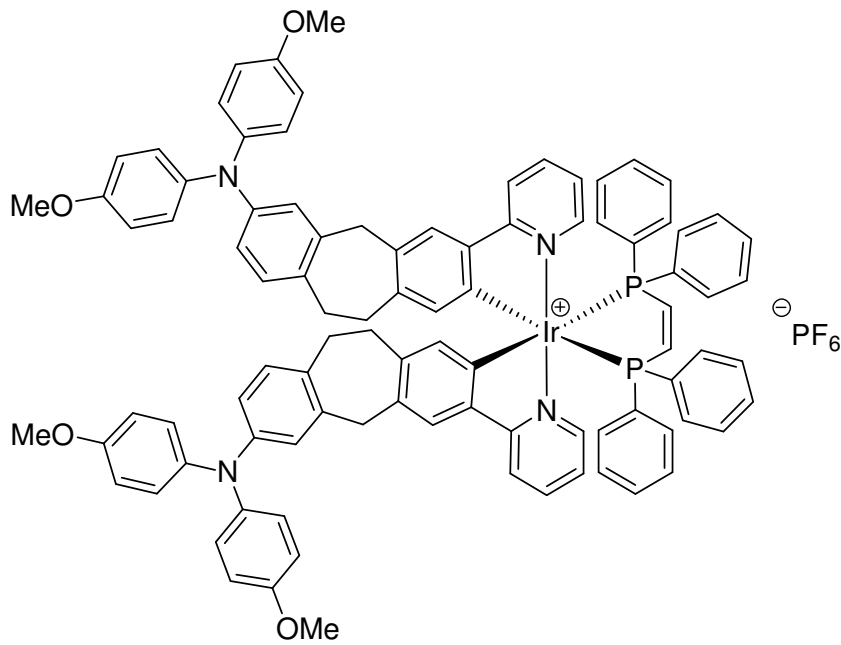
Yield: 79.0 mg (75.8 μ mol, 38 %) of a pale yellow solid.

Melting point: 357 °C.

¹H NMR (600.1 MHz, d₆-acetone): δ = 8.87 (s, 1H); 8.78 (s, 1H); 7.97 (-, 4H); 7.79 (-, 2H); 7.76 (-, 2H); 7.64 (-, 4H); 7.59 (-, 2H); 7.52 (-, 4H); 7.09 (-, 4H); 7.00 (-, 2H); 6.93 (-, 4H); 6.64 (-, 4H); 6.50 (-, 2H); 6.38 (-, 2H).

¹³C NMR (150.9 MHz, d₆-acetone): δ = 168.7 (quart.); 158.1 (quart.); 157.4 (quart.); 154.3 (tert.); 149.9 (tert.); 149.6 (tert.); 144.9 (quart.); 139.2 (tert.); 134.0 (tert.); 132.9 (tert.); 132.8 (tert.); 131.3 (quart.); 131.1 (tert.); 131.0 (quart.); 130.8 (tert.); 130.61 (tert.); 130.55 (tert.); 129.4 (tert.); 129.2 (quart.); 128.9 (quart.); 126.3 (tert.); 124.6 (tert.); 124.2 (tert.); 121.6 (tert.).

ESI pos. (high resolution): calcd for [M⁺] = C₄₈H₃₈IrN₂P₂⁺: 895.21106; found: 895.21105 (Δ = 0.02 ppm).

Complex (6A) $[\text{Ir}(\text{ppy}_{\text{TAA}})_2(\text{bdppe})]\text{PF}_6$ 

Following GP6: Dimer **18** (50.0 mg, 20.4 μmol), *cis*-1,2-*bis*(diphenylphosphino)ethylene (16.2 mg, 40.9 μmol), CH_2Cl_2 (2.00 ml); 14 h at 50 °C.

Formula: $\text{C}_{94}\text{H}_{80}\text{F}_6\text{IrN}_4\text{O}_4\text{P}_3$ [1728.79].

Yield: 18.0 mg (10.4 μmol , 25 %) of a pale yellow solid.

Melting point: 203 °C.

$^1\text{H NMR}$ (600.1 MHz, d_8 -THF): $\delta = 8.89$ (-, 1H); 8.79 (-, 1H); 8.04 (-, 4H); 7.74 (-, 2H); 7.63 (-, 4H); 7.59 (s, 2H); 7.56 (-, 4H); 7.13 (-, 2H); 7.07 (-, 8H); 7.00 (-, 2H); 6.95 – 6.90 (-, 16H); 6.78 (-, 2H); 6.70 (-, 4H); 6.48 (-, 2H); 6.20 (-, 2H); 4.14 – 3.96 (-, 4H); 3.86 (s, 12H); 3.15 – 2.91 (-, 8H).

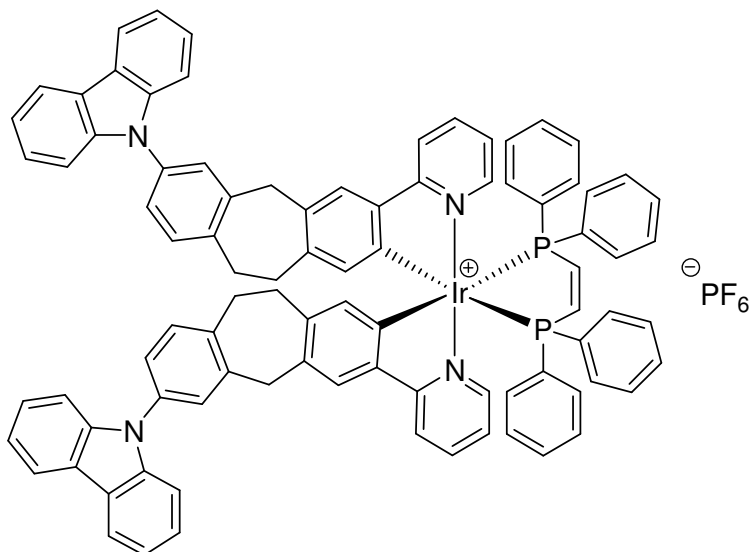
$^{13}\text{C NMR}$ (150.9 MHz, d_8 -THF): $\delta = 168.6$ (quart.); 156.6 (quart.); 155.5 (quart.); 154.8 (quart.); 153.8 (tert.); 149.6 (tert.); 149.4 (tert.); 147.7 (quart.); 143.0 (quart.); 142.6 (quart.); 142.1 (quart.); 140.4 (quart.); 138.2 (tert.); 135.1 (quart.); 133.7 (tert.); 133.6 (tert.); 132.2 (quart.); 131.9 (tert.); 131.3 (quart.); 131.0 (quart.); 130.8 (tert.); 130.6 (tert.); 130.0 (tert.); 129.8 (tert.); 129.1 (quart.); 128.8 (tert.); 128.4 (quart.); 126.7 (tert.); 126.3 (tert.); 123.2 (tert.); 122.5

3 Experimental Section

(tert.); 120.6 (tert.); 120.2 (tert.); 115.1 (tert.); 55.4 (prim.); 41.4 (sec.); 33.8 (sec.); 33.0 (sec.).

ESI pos. (high resolution): calcd for $[M^+] = C_{94}H_{80}IrN_4O_4P_2^+$: 1581.52552; found: 1581.52553 ($\Delta = 0.01$ ppm).

Complex (6B) $[Ir(ppy_{cz})_2(bdppe)]PF_6$



Following GP6: Dimer **19** (30.0 mg, 13.6 μmol), *cis*-1,2-*bis*(diphenylphosphino)ethylene (10.8 mg, 27.3 μmol), CH_2Cl_2 (2.00 ml); 14 h at 50 °C.

Formula: $C_{90}H_{68}F_6IrN_4P_3$ [1604.66].

Yield: 15.0 mg (9.35 μmol , 34 %) of a pale yellow solid.

Melting point: 215 °C.

$^1\text{H NMR}$ (600.1 MHz, d_8 -THF): $\delta = 8.87$ (-, 1H); 8.78 (-, 1H); 8.26 (-, 4H); 8.05 (-, 4H); 7.79 (-, 2H); 7.72 (s, 2H); 7.68 – 7.63 (-, 6H); 7.60 (-, 4H); 7.56 (-, 2H); 7.50 – 7.40 (-, 14 H); 7.34 (-, 4H); 7.12 (-, 2H); 6.95 (-, 4H); 6.74 (-, 2H); 6.53 (-, 2H); 6.31 (-, 2H); 4.42 – 4.28 (-, 4H); 3.41 – 3.09 (-, 8H).

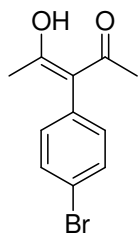
¹³C NMR (150.9 MHz, d₈-THF): δ = 168.5 (quart.); 155.9 (quart.); 155.3 (quart.); 153.9 (tert.); 149.5 (tert.); 149.3 (tert.); 142.9 (quart.); 141.8 (quart.); 139.4 (quart.); 138.3 (tert.); 136.3 (quart.); 134.8 (quart.); 133.7 (tert.); 133.6 (tert.); 132.0 (tert.); 131.8 (quart.); 131.7 (quart.); 130.6 (tert.); 130.0 (tert.); 129.9 (tert.); 129.5 (quart.); 128.84 (tert.); 128.75 (quart.); 128.2 (tert.); 126.4 (tert.); 126.3 (tert.); 125.9 (quart.); 125.8 (quart.); 125.7 (tert.); 124.1 (quart.); 123.5 (tert.); 120.74 (tert.); 120.69 (tert.); 120.4 (tert.); 120.3 (tert.); 110.3 (tert.); 41.1 (sec.); 33.6 (sec.); 33.3 (sec.).

ESI pos. (high resolution): calcd for [M⁺] = C₉₀H₆₈IrN₄P₂⁺: 1457.45196; found: 1457.45197 (Δ = 0.00 ppm).

3.2.3 Synthesis of Neutral Transition Metal Complexes

3.2.3.1 Synthesis of the Acetylacetonate Compounds

3-(4-Bromophenyl)pentane-2,4-dione (22)



$[\text{Cu}(\text{acac})_2]^{196}$ (1.01 g; 3.84 mmol), *p*-phenyldiazoniumtetrafluoroborat¹⁹⁵ (2.08 g; 7.68 mmol) and Copper (488 mg; 7.68 mmol) were mixed with CH_2Cl_2 (15.0 ml) for 3 d under inert gas atmosphere. The reaction mixture was extracted with 1 M HCl (50.0 ml) and water (50.0 ml). The combined organic extracts were dried over MgSO_4 . The crude product was purified by flash column chromatography. (EtOAc : hexane = 1:4).

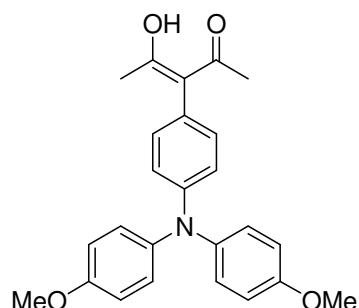
Formula: $\text{C}_{11}\text{H}_{11}\text{BrO}_2$ [253.99].

Yield: 1.20 g (4.68 mmol; 61 %) of a pale yellow solid.

Melting point: 113 °C.

$^1\text{H NMR}$ (400.1 MHz, CDCl_3): δ = 7.90 (d, $^3J_{\text{HH}} = 8.5$ Hz, 2H); 7.54 (d, $^3J_{\text{HH}} = 8.5$ Hz, 1H); 1.88 (s, 6H).²⁰⁹

3-(4,4'-dimethoxydiphenylamino)-pentane-2,4-dione (23)



Following GP2: 3-(4-Bromophenyl)pentane-2,4-dione (**22**) (500 mg, 1.96 mmol), 4,4'-dimethoxydiphenylamine (409 mg, 1.78 mmol), $\text{Pd}_2(\text{dba})_3 \cdot \text{CHCl}_3$ (7.40 mg, 7.13 μmol), sodium *tert*-butoxide (428 mg, 4.45 mmol), P^tBu_3 (35.0 μl , 11.4 μmol), toluene (5 ml), flash chromatography (EA : pentane = 1:4).

Formula: $\text{C}_{25}\text{H}_{25}\text{NO}_4$ [403.18].

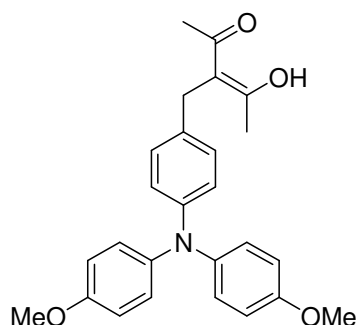
Yield: 136 mg (534 μmol ; 31 %) of a red solid.

Melting point: 197 °C.

$^1\text{H NMR}$ (400.1 MHz, d_6 -acetone): δ = 7.05 (-, 2H); 7.01 (AA', 4H); 6.89 (BB', 4H); 6.82 (-, 2H); 3.78 (s, 6H); 1.87 (s, 6H).

HRMS (70 eV, EI): m/z calcd for $[\text{M}^+]$ = $\text{C}_{25}\text{H}_{25}\text{NO}_4^{+}$ = 403.17861; found: 403.17806 (Δ = 0.62 ppm).

3-((4,4'-dimethoxydiphenylamino)benzyl)-pentane-2,4-dione (**24**)



Following GP2: 3-(4-Bromobenzyl)pentane-2,4-dione¹⁹⁸ (710 mg, 2.64 mmol), 4,4'-dimethoxydiphenylamine (550 mg, 2.40 mmol), $\text{Pd}_2(\text{dba})_3 \cdot \text{CHCl}_3$ (49.8 mg, 48.0 μmol), sodium *tert*-butoxide (288 mg, 3.00 mmol), P^tBu_3 (300 μl , 99.0 μmol), toluene (7 ml), flash chromatography (CH_2Cl_2).

Formula: $\text{C}_{26}\text{H}_{27}\text{NO}_4$ [417.19].

Yield: 390 mg (940 μmol ; 39 %) of a pale brown solid.

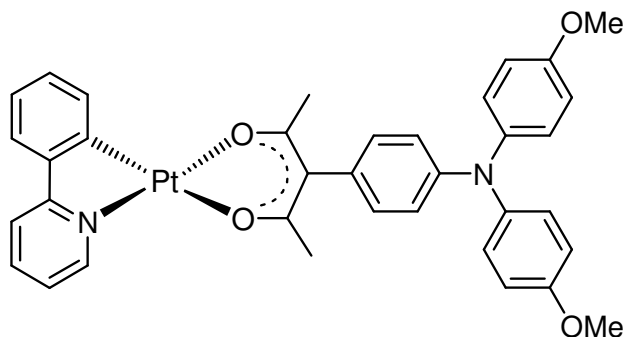
Melting point: 76 °C.

$^1\text{H NMR}$ (400.1 MHz, d_6 -acetone): δ = 7.25 (AA', 2H); 6.97 (AA', 4H); 6.88 (BB', 4H); 6.80 BB', 2H); 2.77 (s, 6H); 2.06 (s, 6H).

3 Experimental Section

¹³C NMR (150.9 MHz, d₆-acetone): δ = 157.1 (quart.); 142.3 (quart.); 133.2 (quart.); 130.5 (tert.); 127.4 (quart.); 127.2 (tert.); 121.8 (quart.); 122.0 (tert.); 115.8 (tert.); 57.1 (quart.); 55.9 (prim.); 38.0 (sec.); 31.2 (prim.).

HRMS (70 eV, EI): *m/z* calcd for [M⁺] = C₂₆H₂₇NO₄^{·+} = 417.19387; found: 417.19332 (Δ = 0.34 ppm).

Complex (20A) [Pt(ppy)(acac₁_{TAA})]

Following GP8: Phenylpyridyl dimer¹⁹³ (38.2 mg, 49.8 μmol), 3-(4,4'-dimethoxydiphenylamino)-pentane-2,4-dione (**23**) (50.0 mg, 124 μmol), TBAOH (281 μl , 225 μmol), CH_2Cl_2 (2.00 ml); 12 h at 50 °C.

Formula: $\text{C}_{36}\text{H}_{32}\text{N}_2\text{O}_4\text{Pt}$ [906.29].

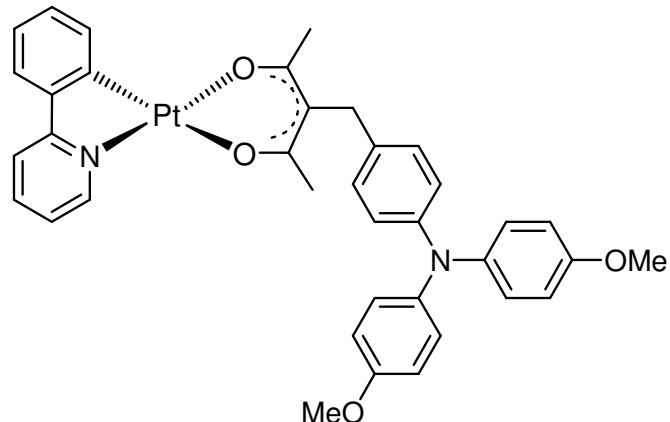
Yield: 68.0 mg (90.3 μmol , 73 %) of an orange solid.

Melting point: 165 °C.

¹H NMR (600.1 MHz, d_6 -acetone): δ = 9.07 (-, 1H); 8.07 (-, 1H); 7.97 (-, 1H); 7.67 (AA', 2H); 7.57 (-, 1H); 7.46 (-, 1H); 7.09 (AA', 4H); 6.97 (-, 1H); 6.92 (BB', 4H); 6.85 (BB', 2H); 6.83 (-, 1H); 6.18 (-, 1H); 3.80 (s, 6H); 2.49 (s, 3H); 2.42 (s, 3H).

¹³C NMR (150.9 MHz, d_6 -acetone): δ = 197.2 (quart.); 175.3 (quart.); 168.3 (quart.); 157.4 (quart.); 150.5 (quart.); 149.7 (quart.); 147.3 (tert.); 146.9 (quart.); 141.8 (quart.); 141.2 (tert.); 138.8 (quart.); 138.0 (quart.); 136.8 (tert.); 129.4 (tert.); 127.6 (tert.); 127.3 (tert.); 124.7 (tert.); 124.2 (tert.); 123.0 (tert.); 120.9 (tert.); 120.1 (tert.); 115.9 (tert.); 55.9 (prim.); 28.7 (prim.); 28.3 (prim.).

Complex (20B) [Pt(ppy)(acac₂_{TAA})]



Following GP7: Phenylpyridyl dimer¹⁹³ (86.0 mg, 112 μ mol), 3-((4,4'-dimethoxydiphenylamino)benzyl)-pentane-2,4-dione (**24**) (140.0 mg, 335 μ mol), Na₂CO₃ 118 mg, 1.12 mmol), 2-ethoxyethanol (2.00 ml); 16 h at 100 °C.

Formula: C₃₇H₃₄N₂O₄Pt [765.75].

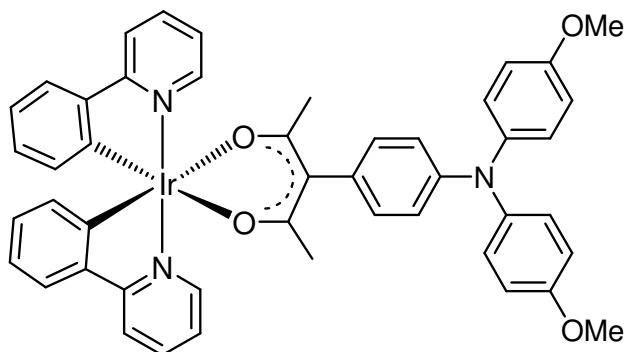
Yield: 139 mg (181 μ mol, 81 %) of a green solid.

Melting point: 192 °C.

¹H NMR (600.1 MHz, d₆-acetone): δ = 9.02 (-, 1H); 8.03 (-, 1H); 7.90 (-, 1H); 7.58 (-, 1H); 7.55 (-, 1H); 7.52 (-, 1H); 7.15 (-, 1H); 7.08 (AA', 2H); 7.05 (-, 1H); 6.99 (AA', 4H); 6.88 (BB', 2H); 6.87 (BB', 4H); 3.79 (s, 2H); 3.77 (s, 6H); 2.08 (s, 3H); 2.06 (s, 3H).

¹³C NMR (150.9 MHz, d₆-acetone): δ = 186.8 (quart.); 184.3 (quart.); 169.4 (quart.); 157.0 (quart.); 148.2 (tert.); 148.1 (quart.); 146.1 (quart.); 142.4 (quart.); 141.5 (quart.); 140.0 (tert.); 134.6 (quart.); 131.8 (tert.); 129.7 (tert.); 129.1 (tert.); 127.1 (tert.); 124.3 (tert.); 124.2 (tert.); 122.9 (tert.); 122.4 (tert.); 119.8 (tert.); 115.7 (tert.); 110.8 (quart.); 55.9 (prim.); 36.0 (sec.); 28.6 (prim.); 27.8 (prim.).

ESI pos. (high resolution): calcd for [M⁺] = C₃₇H₃₄PtN₂O₄⁺: 765.21642; found: 765.21642 (Δ = 0.00 ppm).

Complex (21A) [Ir(ppy)₂(acac¹_{TAA})]

Following GP8: Phenylpyridyl dimer¹⁰³ (124 mg, 115 μmol), 3-(4,4'-dimethoxydiphenylamino)-pentane-2,4-dione (**23**) (116 mg, 288 μmol), TBAOH (650 μl , 520 μmol), CH_2Cl_2 (4.00 ml); 12 h at 50 °C.

Formula: $\text{C}_{45}\text{H}_{39}\text{IrN}_3\text{O}_4$ [878.03].

Yield: 65.0 mg (72.0 μmol , 31 %) of an orange solid.

Melting point: 146 °C.

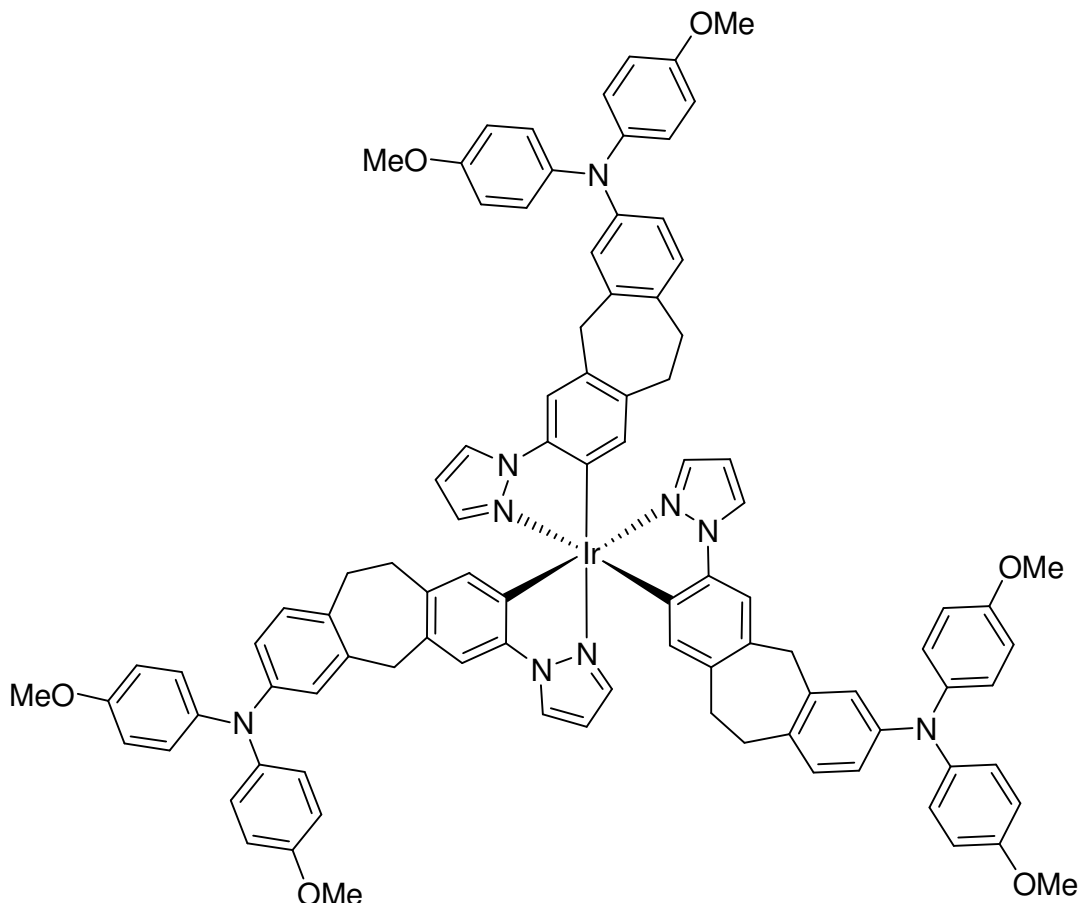
¹H NMR (600.1 MHz, d-chloroform): δ = 8.61 (-, 1H); 8.40 (-, 1H); 7.89 (-, 1H); 7.79 (-, 1H); 7.71 (-, 2H); 7.58 (-, 1H); 7.34 (-, 1H); 7.10 (-, 2H); 6.87 (-, 1H); 6.84 (AA', 4H); 6.76 (BB', 4H); 6.73 (-, 2H); 6.57 (-, 1H); 6.34 (AA', 2H); 6.24 (BB', 2H); 6.18 (-, 1H); 6.15 (-, 1H); 3.78 (s, 6H); 2.37 (s, 3H); 2.25 (s, 3H).

¹³C NMR (150.9 MHz, d-chloroform): δ = 155.2 (quart.); 150.1 (quart.); 149.9 (quart.); 147.6 (quart.); 145.7 (quart.); 144.6 (quart.); 143.5 (quart.); 141.1 (quart.); 137.5 (quart.); 137.4 (tert.); 137.0 (tert.); 133.1 (quart.); 132.5 (tert.); 129.3 (tert.); 129.1 (tert.); 127.5 (tert.); 126.6 (tert.); 125.6 (tert.); 123.8 (tert.); 123.7 (tert.); 122.9 (tert.); 122.1 (tert.); 121.8 (tert.); 121.4 (tert.); 120.3 (tert.); 120.2 (tert.); 119.1 (tert.); 118.3 (tert.); 117.3 (quart.); 114.8 (tert.); 114.3 (tert.); 55.5 (prim.); 29.6 (prim.); 28.4 (prim.).

3 Experimental Section

3.2.3.2 Synthesis of the Homoleptic Ir(ppz_{TAA})₃ Complex

Complex (25) [Ir(ppz_{TAA})₃]



Phenylpyrazole dimer (**16**) (219 mg, 91.1 μmol), 3-Pyrazolyl-7-(4,4'-dimethoxydiphenylamino)-10,11-dihydro-5*H*-dibenzo[*a,d*]-cycloheptene (**10**) (111 mg, 2285 μmol) and Na_2CO_3 (100 mg, 947 μmol) were suspended under inert gas atmosphere in 15.0 ml glycerol and heated in a 3-necked round-bottom flask in a microwave oven (gradient of heating: 10 min RT to 200 °C, holding time: 2 h at 200 °C). After being cooled to RT, the reaction mixture was extracted with water (40.0 ml) and CH_2Cl_2 (40.0 ml). The combined organic extracts were dried over MgSO_4 . The crude product was purified by flash column chromatography. (CH_2Cl_2).

Formula: $\text{C}_{96}\text{H}_{84}\text{IrN}_9\text{O}_6$ [1651.97].

Yield: 15.0 mg (9.08 μmol , 5 %) of a grey solid.

Melting point: 159 °C.

3 Experimental Section

¹H NMR (600.1 MHz, d₆-acetone): δ = 36 (-, 3H); 7.24 (s, 3H); 6.95 (AA', 12H); 6.92 (-, 3H); 6.88 (-, 3H); 6.84 (BB', 12H); 6.72 (-, 3H); 6.66 (s, 3H); 6.60 (-, 3H); 6.42 (-, 3H); 3.97 (-, 6H); 3.77 (s, 18H); 3.04 – 2.68 (-, 12H).

¹³C NMR (150.9 MHz, d₆-acetone): δ = 156.9 (quart.); 147.8 (quart.); 144.1 (quart.); 142.6 (quart.); 1141.4 (quart.); 139.4 (tert.); 138.1 (quart.); 137.7 (tert.); 137.4 (quart.); 133.5 (quart.); 132.1 (quart.); 131.4 (tert.); 127.2 (tert.); 126.5 (tert.); 122.9 (tert.); 120.6 (tert.); 115.8 (tert.); 112.9 (tert.); 107.9 (tert.); 56.0 (prim.); 41.8 (sec.); 33.5 (sec.); 33.4 (sec.).

MS (MALDI): *m/z* (%) calcd for C₉₆H₈₄IrN₉O₆ = 1651.6174 (100); found: 1651.655 (100).

4 Literature

- (1) Balzani, V.; Credi, A.; Venturi, M. *ChemSusChem* **2008**, *1*, 26-58.
- (2) Guldi, D. M. *Chem. Soc. Rev.* **2002**, *31*, 22-36.
- (3) Gust, D.; Moore, T. A.; Moore, A. L. *Acc. Chem. Res.* **2001**, *34*, 40-48.
- (4) Wasielewski, M. R. *Chem. Rev.* **1992**, *92*, 435-461.
- (5) Balzani, V.; Juris, A.; Venturi, M.; Campagna, S.; Serroni, S. *Chem. Rev.* **1996**, *96*, 759-833.
- (6) Fabbrizzi, L.; Poggi, A. *Chem. Soc. Rev.* **1995**, *24*, 197-202.
- (7) Wasielewski, M. R.; O'Neil, M. P.; Gosztola, D.; Niemczyk, M. P.; Svec, W. A. *Pure Appl. Chem.* **1992**, *64*, 1319-1325.
- (8) Verhoeven, J. W.; van Ramesdonk, H. J.; Groeneveld, M. M.; Benniston, A. C.; Harriman, A. *Chem. Phys. Chem.* **2005**, *6*, 2251-2260.
- (9) Marcus, R. A. *J. Chem. Phys.* **1956**, *24*, 966-978.
- (10) Marcus, R. A. *Ann. Rev. Phys. Chem.* **1964**, *15*, 155-&.
- (11) Marcus, R. A. *J. Chem. Phys.* **1965**, *43*, 679-689.
- (12) Marcus, R. A. *Angew. Chem., Int. Ed. Engl.* **1993**, *32*, 1111-1121.
- (13) Marcus, R. A. *Pure Appl. Chem.* **1997**, *69*, 13-29.
- (14) Bolton, J. R.; Archer, M. D. *Adv. Chem. Ser.* **1991**, *7*-23.
- (15) Brunschwig, B. S.; Sutin, N. *Coord. Chem. Rev.* **1999**, *187*, 233-254.
- (16) Miller, J. R.; Calcaterra, L. T.; Closs, G. L. *J. Am. Chem. Soc.* **1984**, *106*, 3047-3049.
- (17) Closs, G. L.; Calcaterra, L. T.; Green, N. J.; Penfield, K. W.; Miller, J. R. *J. Phys. Chem.* **1986**, *90*, 3673-3683.
- (18) Gould, I. R.; Moody, R.; Farid, S. *J. Am. Chem. Soc.* **1988**, *110*, 7242-7244.
- (19) Gould, I. R.; Moser, J. E.; Armitage, B.; Farid, S.; Goodman, J. L.; Herman, M. S. *J. Am. Chem. Soc.* **1989**, *111*, 1917-1919.
- (20) Mataga, N.; Asahi, T.; Kanda, Y.; Okada, T.; Kakitani, T. *Chem. Phys.* **1988**, *127*, 249-261.
- (21) McCleskey, T. M.; Winkler, J. R.; Gray, H. B. *J. Am. Chem. Soc.* **1992**, *114*, 6935-6937.
- (22) Miller, J. R.; Beitz, J. V. *J. Chem. Phys.* **1981**, *74*, 6746-6756.
- (23) Sutin, N.; Brunschwig, B. S.; Creutz, C. *J. Phys. Chem. C* **2003**, *107*, 10687-10690.
- (24) Wasielewski, M. R.; Niemczyk, M. P.; Svec, W. A.; Pewitt, E. B. *J. Am. Chem. Soc.* **1985**, *107*, 1080-1082.
- (25) Marshall, J. L.; Stobart, S. R.; Gray, H. B. *J. Am. Chem. Soc.* **1984**, *106*, 3027-3029.
- (26) Chen, P. Y.; Duesing, R.; Graff, D. K.; Meyer, T. J. *J. Phys. Chem.* **1991**, *95*, 5850-5858.
- (27) Chen, P. Y.; Westmoreland, T. D.; Danielson, E.; Schanze, K. S.; Anthon, D.; Neveux, P. E.; Meyer, T. J. *Inorg. Chem.* **1987**, *26*, 1116-1126.
- (28) Benniston, A. C.; Harriman, A.; Li, P. Y.; Rostron, J. P.; van Ramesdonk, H. J.; Groeneveld, M. M.; Zhang, H.; Verhoeven, J. W. *J. Am. Chem. Soc.* **2005**, *127*, 16054-16064.
- (29) Fukuzumi, S.; Kotani, H.; Ohkubo, K.; Ogo, S.; Tkachenko, N. V.; Lemmetyinen, H. *J. Am. Chem. Soc.* **2004**, *126*, 1600-1601.
- (30) Anglos, D.; Bindra, V.; Kuki, A. *J. Chem. Soc., Chem. Commun.* **1994**, 213-215.

- (31) Borkent, J. H.; Jong, A.; Verhoeven, J. W.; Boer, T. J. D. *Chem. Phys. Lett.* **1978**, *57*, 530-534.
- (32) Flamigni, L.; Ventura, B.; Tasior, M.; Becherer, T.; Langhals, H.; Gryko, D. T. *Chem.-Eur. J.* **2008**, *14*, 169-183.
- (33) Karpiuk, J. *Phys. Chem. Chem. Phys.* **2003**, *5*, 1078-1090.
- (34) Kawauchi, H.; Suzuki, S.; Kozaki, M.; Okada, K.; Islam, D. M. S.; Araki, Y.; Ito, O.; Yamanaka, K. *J. Phys. Chem. A* **2008**, *112*, 5878-5884.
- (35) Smit, K. J.; Warman, J. M. *J. Lumin.* **1988**, *42*, 149-154.
- (36) Suneesh, C. V.; Gopidas, K. R. *J. Phys. Chem. C* **2009**, *113*, 1606-1614.
- (37) Warman, J. M.; Smit, K. J.; Jonker, S. A.; Verhoeven, J. W.; Oevering, H.; Kroon, J.; Paddonrow, M. N.; Oliver, A. M. *Chem. Phys.* **1993**, *170*, 359-380.
- (38) Gust, D.; Moore, T. A.; Moore, A. L.; MacPherson, A. N.; Lopez, A.; Degraziano, J. M.; Gouni, I.; Bittersmann, E.; Seely, G. R.; Gao, F.; Nieman, R. A.; Ma, X. C. C.; Demanche, L. J.; Hung, S. C.; Luttrull, D. K.; Lee, S. J.; Kerrigan, P. K. *J. Am. Chem. Soc.* **1993**, *115*, 11141-11152.
- (39) Imahori, H.; Guldi, D. M.; Tamaki, K.; Yoshida, Y.; Luo, C. P.; Sakata, Y.; Fukuzumi, S. *J. Am. Chem. Soc.* **2001**, *123*, 6617-6628.
- (40) Imahori, H.; Sekiguchi, Y.; Kashiwagi, Y.; Sato, T.; Araki, Y.; Ito, O.; Yamada, H.; Fukuzumi, S. *Chem.-Eur. J.* **2004**, *10*, 3184-3196.
- (41) Flamigni, L.; Baranoff, E.; Collin, J. P.; Sauvage, J. P. *Chem.-Eur. J.* **2006**, *12*, 6592-6606.
- (42) Flamigni, L.; Barbieri, A.; Sabatini, C.; Ventura, B.; Barigelli, F. *Photochem. Photophys. Coord. Comp.* **2007**, *281*, 143-203.
- (43) Flamigni, L.; Collin, J. P.; Sauvage, J. P. *Acc. Chem. Res.* **2008**, *41*, 857-871.
- (44) Flamigni, L.; Dixon, I. M.; Collin, J. P.; Sauvage, J. P. *Chem. Commun.* **2000**, 2479-2480.
- (45) Fortage, J.; Boixel, J.; Blart, E.; Becker, H. C.; Odobel, F. *Inorg. Chem.* **2009**, *48*, 518-526.
- (46) Ghirotti, M.; Chiorboli, C.; You, C. C.; Würthner, F.; Scandola, F. *J. Phys. Chem. A* **2008**, *112*, 3376-3385.
- (47) Ohkubo, K.; Kotani, H.; Shao, J. G.; Ou, Z. P.; Kadish, K. M.; Li, G. L.; Pandey, R. K.; Fujitsuka, M.; Ito, O.; Imahori, H.; Fukuzumi, S. *Angew. Chem., Int. Ed.* **2004**, *43*, 853-856.
- (48) Borgstrom, M.; Shaikh, N.; Johansson, O.; Anderlund, M. F.; Styring, S.; Akerman, B.; Magnusson, A.; Hammarstrom, L. *J. Am. Chem. Soc.* **2005**, *127*, 17504-17515.
- (49) Rawls, M. T.; Kollmannsberger, G.; Elliott, C. M.; Steiner, U. E. *J. Phys. Chem. A* **2007**, *111*, 3485-3496.
- (50) Weber, J. M.; Rawls, M. T.; MacKenzie, V. J.; Limoges, B. R.; Elliott, C. M. *J. Am. Chem. Soc.* **2007**, *129*, 313-320.
- (51) Chiorboli, C.; Fracasso, S.; Scandola, F.; Campagna, S.; Serroni, S.; Konduri, R.; MacDonnell, F. M. *Chem. Commun.* **2003**, 1658-1659.
- (52) Cooley, L. F.; Larson, S. L.; Elliott, C. M.; Kelley, D. F. *J. Phys. Chem.* **1991**, *95*, 10694-10700.
- (53) Danielson, E.; Elliott, C. M.; Merkert, J. W.; Meyer, T. J. *J. Am. Chem. Soc.* **1987**, *109*, 2519-2520.
- (54) Durham, B.; Caspar, J. V.; Nagle, J. K.; Meyer, T. J. *J. Am. Chem. Soc.* **1982**, *104*, 4803-4810.
- (55) Falkenstrom, M.; Johansson, O.; Hammarstrom, L. *Inorg. Chim. Acta* **2007**, *360*, 741-750.

4 Literature

- (56) Flamigni, L.; Armaroli, N.; Barigelli, F.; Balzani, V.; Collin, J. P.; Dalbavie, J. O.; Heitz, V.; Sauvage, J. P. *J. Phys. Chem. B* **1997**, *101*, 5936-5943.
- (57) Flamigni, L.; Barigelli, F.; Armaroli, N.; Collin, J. P.; Sauvage, J. P.; Williams, J. A. G. *Chem.-Eur. J.* **1998**, *4*, 1744-1754.
- (58) Harriman, A.; Odobel, F.; Sauvage, J. P. *J. Am. Chem. Soc.* **1995**, *117*, 9461-9472.
- (59) Huynh, M. H. V.; Dattelbaum, D. M.; Meyer, T. J. *Coord. Chem. Rev.* **2005**, *249*, 457-483.
- (60) Klumpp, T.; Linsenmann, M.; Larson, S. L.; Limoges, B. R.; Burssner, D.; Krissinel, E. B.; Elliott, C. M.; Steiner, U. E. *J. Am. Chem. Soc.* **1999**, *121*, 1076-1087.
- (61) Mecklenburg, S. L.; McCafferty, D. G.; Schoonover, J. R.; Peek, B. M.; Erickson, B. W.; Meyer, T. J. *Inorg. Chem.* **1994**, *33*, 2974-2983.
- (62) Treadway, J. A.; Chen, P. Y.; Rutherford, T. J.; Keene, F. R.; Meyer, T. J. *J. Phys. Chem.* **1997**, *101*, 6824-6826.
- (63) Dixon, I. M.; Collin, J. P.; Sauvage, J. P.; Barigelli, F.; Flamigni, L. *Angew. Chem., Int. Ed.* **2000**, *39*, 1292-1295.
- (64) Tang, C. W.; Vanslyke, S. A. *Appl. Phys. Lett.* **1987**, *51*, 913-915.
- (65) Weiss, J. O.; Krause, R.; Paetzold, R. *Adv. in Solid State Phys.* **2008**, *46*, 321-332.
- (66) Burroughes, J. H.; Bradley, D. D. C.; Brown, A. R.; Marks, R. N.; Mackay, K.; Friend, R. H.; Burns, P. L.; Holmes, A. B. *Nature* **1990**, *347*, 539-541.
- (67) Hertel, D.; Müller, C.; Meerholz, K. *Chem. Unserer Zeit* **2005**, *39*, 336-347.
- (68) Armstrong, N. R.; Wightman, R. M.; Gross, E. M. *Ann. Rev. Phys. Chem.* **2001**, *52*, 391-422.
- (69) Yersin, H. In *Transition Metal and Rare Earth Compounds III*, 2004; Vol. 241.
- (70) D'Andrade, B. W.; Brooks, J.; Adamovich, V.; Thompson, M. E.; Forrest, S. R. *Adv. Mater.* **2002**, *14*, 1032-1036.
- (71) Ikai, M.; Tokito, S.; Sakamoto, Y.; Suzuki, T.; Taga, Y. *Appl. Phys. Lett.* **2001**, *79*, 156-158.
- (72) Braig, T.; Muller, D. C.; Gross, M.; Meerholz, K.; Nuyken, O. *Macromol. Rapid Commun.* **2000**, *21*, 583-589.
- (73) Glebeler, C.; Antoniadis, H.; Bradley, D. D. C.; Shirota, Y. *Appl. Phys. Lett.* **1998**, *72*, 2448-2450.
- (74) Huang, J.; Niu, Y. H.; Yang, W.; Mo, Y. Q.; Yuan, M.; Cao, Y. *Macromolecules* **2002**, *35*, 6080-6082.
- (75) Kido, J.; Hongawa, K.; Okuyama, K.; Nagai, K. *Appl. Phys. Lett.* **1994**, *64*, 815-817.
- (76) Lambert, C.; Schelter, J.; Fiebig, T.; Mank, D.; Trifonov, A. *J. Am. Chem. Soc.* **2005**, *127*, 10600-10610.
- (77) Redecker, M.; Bradley, D. D. C.; Inbasekaran, M.; Wu, W. W.; Woo, E. P. *Adv. Mater.* **1999**, *11*, 241-246.
- (78) Adachi, C.; Baldo, M. A.; Forrest, S. R.; Lamansky, S.; Thompson, M. E.; Kwong, R. C. *Appl. Phys. Lett.* **2001**, *78*, 1622-1624.
- (79) Kawamura, Y.; Yanagida, S.; Forrest, S. R. *J. Appl. Phys.* **2002**, *92*, 87-93.
- (80) Zhou, X.; Qin, D. S.; Pfeiffer, M.; Blochwitz-Nimoth, J.; Werner, A.; Drechsel, J.; Maennig, B.; Leo, K.; Bold, M.; Erk, P.; Hartmann, H. *Appl. Phys. Lett.* **2002**, *81*, 4070-4072.
- (81) Chen, J. S.; Ma, D. G. *J. Lumin.* **2007**, *122*, 636-638.

- (82) Savvate'ev, V.; Friedl, J. H.; Zou, L.; Christensen, K.; Oldham, W.; Rothberg, L. J.; Chen-Esterlit, Z.; Kopelman, R.; Shinar, J. *Synth. Met.* **2001**, *121*, 1713-1714.
- (83) Swanson, S. A.; Wallraff, G. M.; Chen, J. P.; Zhang, W. J.; Bozano, L. D.; Carter, K. R.; Salem, J. R.; Villa, R.; Scott, J. C. *Chem. Mater.* **2003**, *15*, 2305-2312.
- (84) Friend, R. H.; Gymer, R. W.; Holmes, A. B.; Burroughes, J. H.; Marks, R. N.; Taliani, C.; Bradley, D. D. C.; Dos Santos, D. A.; Bredas, J. L.; Logdlund, M.; Salaneck, W. R. *Nature* **1999**, *397*, 121-128.
- (85) Reitzenstein, D.; Lambert, C. *Macromolecules* **2009**, *42*, 773-782.
- (86) Spreitzer, H.; Becker, H.; Kluge, E.; Kreuder, W.; Schenk, H.; Demandt, R.; Schoo, H. *Adv. Mater.* **1998**, *10*, 1340-1342.
- (87) Wang, R.; Wang, W. Z.; Yang, G. Z.; Liu, T. X.; Yu, J. S.; Jiang, Y. D. *J. Pol. Sci. a - Polymer Chem.* **2008**, *46*, 790-802.
- (88) Gong, X. O.; Iyer, P. K.; Moses, D.; Bazan, G. C.; Heeger, A. J.; Xiao, S. S. *Adv. Func. Mater.* **2003**, *13*, 325-330.
- (89) Wang, Y.; Herron, N.; Grushin, V. V.; LeCloux, D.; Petrov, V. *Appl. Phys. Lett.* **2001**, *79*, 449-451.
- (90) Adachi, C.; Baldo, M. A.; Forrest, S. R.; Thompson, M. E. *Appl. Phys. Lett.* **2000**, *77*, 904-906.
- (91) Markham, J. P. J.; Lo, S. C.; Magennis, S. W.; Burn, P. L.; Samuel, I. D. W. *Appl. Phys. Lett.* **2002**, *80*, 2645-2647.
- (92) Ostrowski, J. C.; Robinsen, M. R.; Heeger, A. J.; Bazan, G. C. *Abstr. Papers of the Am. Chem. Soc.* **2002**, *223*, U635-U635.
- (93) Bolink, H. J.; Coronado, E.; Costa, R. D.; Orti, E.; Sessolo, M.; Graber, S.; Doyle, K.; Neuburger, M.; Housecroft, C. E.; Constable, E. C. *Adv. Mater.* **2008**, *20*, 3910-3913.
- (94) Garces, F. O.; King, K. A.; Watts, R. J. *Inorg. Chem.* **1988**, *27*, 3464-3471.
- (95) Giner-Casares, J. J.; Perez-Morales, M.; Bolink, H. J.; Munoz, E.; de Miguel, G.; Martin-Romero, M. T.; Camacho, L. J. *Colloid Interface Sci* **2007**, *315*, 278-286.
- (96) Goldsmith, J. I.; Hudson, W. R.; Lowry, M. S.; Anderson, T. H.; Bernhard, S. J. *Am. Chem. Soc.* **2005**, *127*, 7502-7510.
- (97) Kim, J. I.; Shin, I. S.; Kim, H.; Lee, J. K. *J. Am. Chem. Soc.* **2005**, *127*, 1614-1615.
- (98) King, K. A.; Watts, R. J. *J. Am. Chem. Soc.* **1987**, *109*, 1589-1590.
- (99) Lo, K. K. W.; Zhang, K. Y.; Chung, C. K.; Kwok, K. Y. *Chem.-Eur. J.* **2007**, *13*, 7110-7120.
- (100) Lowry, M. S.; Hudson, W. R.; Pascal, R. A.; Bernhard, S. J. *Am. Chem. Soc.* **2004**, *126*, 14129-14135.
- (101) Nastasi, F.; Punzoriero, F.; Campagna, S.; Schergna, S.; Maggini, M.; Cardinali, F.; Delavaux-Nicot, W.; Nierengarten, J. F. *Chem. Commun.* **2007**, 3556-3558.
- (102) Ohsawa, Y.; Sprouse, S.; King, K. A.; Dearmond, M. K.; Hanck, K. W.; Watts, R. J. *J. Phys. Chem.* **1987**, *91*, 1047-1054.
- (103) Tamayo, A. B.; Garon, S.; Sajoto, T.; Djurovich, P. I.; Tsypa, I. M.; Bau, R.; Thompson, M. E. *Inorg. Chem.* **2005**, *44*, 8723-8732.
- (104) Wöhrle, D.; Tausch, M. W.; Stohrer, W.-D. *Photochemie*; WILEY-VCH Verlag GmbH: Weinheim, 1998.
- (105) Gade, L. H. *Koordinationschemie*; WILEY-VCH Verlag GmbH: Weinheim, 1998.

4 Literature

- (106) Adachi, C.; Baldo, M. A.; Thompson, M. E.; Forrest, S. R. *J. Appl. Phys.* **2001**, *90*, 5048-5051.
- (107) Baldo, M. A.; Lamansky, S.; Burrows, P. E.; Thompson, M. E.; Forrest, S. R. *Appl. Phys. Lett.* **1999**, *75*, 4-6.
- (108) Nazeeruddin, M. K.; Humphry-Baker, R.; Berner, D.; Rivier, S.; Zuppiroli, L.; Grätzel, M. *J. Am. Chem. Soc.* **2003**, *125*, 8790-8797.
- (109) Slinker, J. D.; Gorodetsky, A. A.; Lowry, M. S.; Wang, J. J.; Parker, S.; Rohl, R.; Bernhard, S.; Malliaras, G. G. *J. Am. Chem. Soc.* **2004**, *126*, 2763-2767.
- (110) Tamayo, A. B.; Alleyne, B. D.; Djurovich, P. I.; Lamansky, S.; Tsby, I.; Ho, N. N.; Bau, R.; Thompson, M. E. *J. Am. Chem. Soc.* **2003**, *125*, 7377-7387.
- (111) Lamansky, S.; Djurovich, P.; Murphy, D.; Abdel-Razzaq, F.; Kwong, R.; Tsby, I.; Bortz, M.; Mui, B.; Bau, R.; Thompson, M. E. *Inorg. Chem.* **2001**, *40*, 1704-1711.
- (112) Lamansky, S.; Djurovich, P.; Murphy, D.; Abdel-Razzaq, F.; Lee, H. E.; Adachi, C.; Burrows, P. E.; Forrest, S. R.; Thompson, M. E. *J. Am. Chem. Soc.* **2001**, *123*, 4304-4312.
- (113) Baldo, M. A.; O'Brien, D. F.; You, Y.; Shoustikov, A.; Sibley, S.; Thompson, M. E.; Forrest, S. R. *Nature* **1998**, *395*, 151-154.
- (114) De Angelis, F.; Fantacci, S.; Evans, N.; Klein, C.; Zakeeruddin, S. M.; Moser, E.; Kalyanasundaram, K.; Bolink, H. J.; Gratzel, M.; Nazeeruddin, M. K. *Inorg. Chem.* **2007**, *46*, 5989-6001.
- (115) Lo, K. K. W.; Chan, J. S. W.; Lui, L. H.; Chung, C. K. *Organometallics* **2004**, *23*, 3108-3116.
- (116) Lo, K. K. W.; Chung, C. K.; Lee, T. K. M.; Lui, L. H.; Tsang, K. H. K.; Zhu, N. Y. *Inorg. Chem.* **2003**, *42*, 6886-6897.
- (117) Lowry, M. S.; Bernhard, S. *Chem.-Eur. J.* **2006**, *12*, 7970-7977.
- (118) Plummer, E. A.; van Dijken, A.; Hofstraat, H. W.; De Cola, L.; Brunner, K. *Adv. Funct. Mater.* **2005**, *15*, 281-289.
- (119) Tinker, L. L.; McDaniel, N. D.; Curtin, P. N.; Smith, C. K.; Ireland, M. J.; Bernhard, S. *Chem.-Eur. J.* **2007**, *13*, 8726-8732.
- (120) Edman, L.; Moses, D.; Heeger, A. J. *Synth. Met.* **2003**, *138*, 441-446.
- (121) Edman, L.; Pauchard, M.; Liu, B.; Bazan, G.; Moses, D.; Heeger, A. J. *Appl. Phys. Lett.* **2003**, *82*, 3961-3963.
- (122) Edman, L.; Summers, M. A.; Buratto, S. K.; Heeger, A. J. *Phys. Rev. B* **2004**, *70*.
- (123) Hosseini, A. R.; Koh, C. Y.; Slinker, J. D.; Flores-Torres, S.; Abruna, H. D.; Malliaras, G. G. *Chem. Mater.* **2005**, *17*, 6114-6116.
- (124) Slinker, J.; Bernards, D.; Houston, P. L.; Abruna, H. D.; Bernhard, S.; Malliaras, G. G. *Chem. Commun.* **2003**, 2392-2399.
- (125) Baldo, M. A.; Adachi, C.; Forrest, S. R. *Phys. Rev. B* **2000**, *62*, 10967-10977.
- (126) Baldo, M. A.; Thompson, M. E.; Forrest, S. R. *Nature* **2000**, *403*, 750-753.
- (127) Kondakov, D. Y. *J. Appl. Phys.* **2007**, *102*.
- (128) Reineke, S.; Walzer, K.; Leo, K. *Phys. Rev. B* **2007**, *75*.
- (129) Turro, N. J. *Modern Molecular Photochemistry*; University Science Books: Sausalito, 1991.
- (130) Avilov, I.; Marsal, P.; Bredas, J. L.; Beljonne, D. *Adv. Mater.* **2004**, *16*, 1624-1629.
- (131) Zalesskaya, G. A.; Pavlova, V. T.; Sambor, E. G.; Bely, N. N. *Chem. Phys. Lett.* **2003**, *373*, 448-453.
- (132) Chattopadhyay, N.; Serpa, C.; Purkayastha, P.; Arnaut, L. G.; Formosinho, S. J. *Phys. Chem. Chem. Phys.* **2001**, *3*, 70-73.

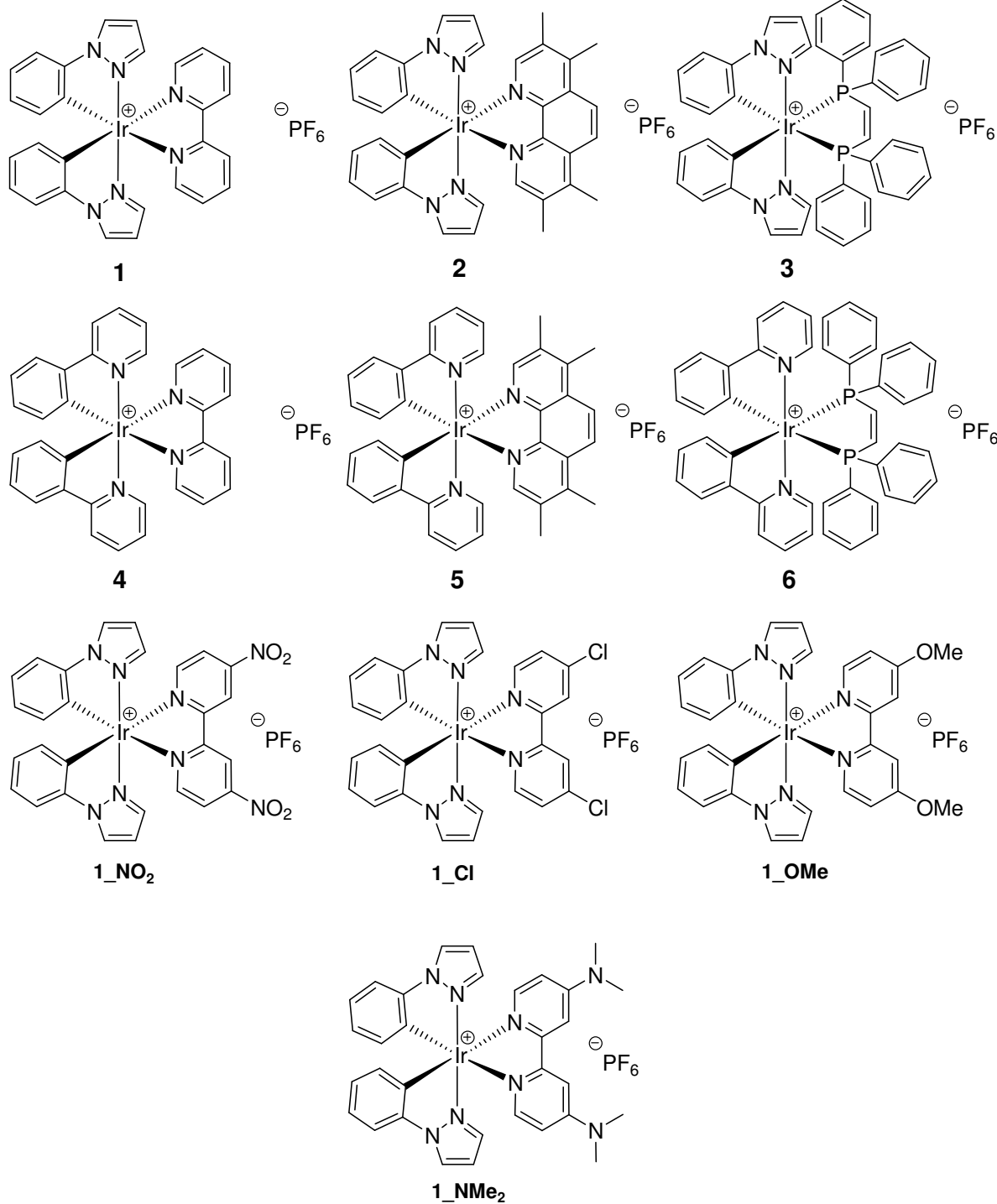
- (133) Gupta, N.; Santhanam, K. S. V. *J. Chem. Soc. - Chem. Comm.* **1994**, 2409-2410.
- (134) Geiss, B.; Lambert, C. *Chem. Commun.* **2009**, 1670-1672.
- (135) Dedeian, K.; Shi, J. M.; Shepherd, N.; Forsythe, E.; Morton, D. C. *Inorg. Chem.* **2005**, 44, 4445-4447.
- (136) Wu, L. L.; Sun, I. W.; Yang, C. H. *Polyhedron* **2007**, 26, 2679-2685.
- (137) Yang, C. H.; Li, S. W.; Chi, Y.; Cheng, Y. M.; Yeh, Y. S.; Chou, P. T.; Lee, G. H.; Wang, C. H.; Shu, C. F. *Inorg. Chem.* **2005**, 44, 7770-7780.
- (138) Colombo, M. G.; Hauser, A.; Gudel, H. U. *Inorg. Chem.* **1993**, 32, 3088-3092.
- (139) Wilde, A. P.; King, K. A.; Watts, R. J. *J. Phys. Chem.* **1991**, 95, 629-634.
- (140) Kalyanasundaram, K. *Photochemistry of Polypyridine and Porphyrine Complexes*; Harcourt Brace Jovanovich: London, 1992.
- (141) Calogero, G.; Giuffrida, G.; Serroni, S.; Ricevuto, V.; Campagna, S. *Inorg. Chem.* **1995**, 34, 541-545.
- (142) Colombo, M. G.; Gudel, H. U. *Inorg. Chem.* **1993**, 32, 3081-3087.
- (143) Didier, P.; Ortmans, I.; Kirschdemesmaeker, A.; Watts, R. J. *Inorg. Chem.* **1993**, 32, 5239-5245.
- (144) Dixon, I. M.; Collin, J. P.; Sauvage, J. P.; Flamigni, L.; Encinas, S.; Barigelli, F. *Chem. Soc. Rev.* **2000**, 29, 385-391.
- (145) Neve, F.; Crispini, A.; Serroni, S.; Loiseau, F.; Campagna, S. *Inorg. Chem.* **2001**, 40, 1093-1101.
- (146) Sprouse, S.; King, K. A.; Spellane, P. J.; Watts, R. J. *J. Am. Chem. Soc.* **1984**, 106, 6647-6653.
- (147) Vandiemen, J. H.; Haasnoot, J. G.; Hage, R.; Muller, E.; Reedijk, J. *Inorg. Chim. Acta* **1991**, 181, 245-251.
- (148) Oberhauser, W.; Bachmann, C.; Stampfl, T.; Haid, R.; Bruggeller, P. *Polyhedron* **1997**, 16, 2827-2835.
- (149) Sussuchi, E. M.; de Lima, A. A.; De Giovani, W. F. *J. Mol. Catal. A: Chem.* **2006**, 259, 302-308.
- (150) Tung, Y. L.; Chen, L. S.; Chi, Y.; Chou, P. T.; Cheng, Y. M.; Li, E. Y.; Lee, G. H.; Shu, C. F.; Wu, T. I.; Carty, A. J. *Adv. Func. Mater.* **2006**, 16, 1615-1626.
- (151) Holzapfel, M.; Lambert, C. *J. Phys. Chem. C* **2008**, 112, 1227-1243.
- (152) Klapars, A.; Antilla, J. C.; Huang, X. H.; Buchwald, S. L. *J. Am. Chem. Soc.* **2001**, 123, 7727-7729.
- (153) Hartwig, J. F. *Synlett* **1997**, 329-340.
- (154) Hartwig, J. F. *Angew. Chem., Int. Ed.* **1998**, 37, 2047-2067.
- (155) Nishiyama, M.; Yamamoto, T.; Koie, Y. *Tetrahedron Lett.* **1998**, 39, 617-620.
- (156) Wolfe, J. P.; Wagaw, S.; Marcoux, J. F.; Buchwald, S. L. *Acc. Chem. Res.* **1998**, 31, 805-818.
- (157) Yamamoto, T.; Nishiyama, M.; Koie, Y. *Tetrahedron Lett.* **1998**, 39, 2367-2370.
- (158) Bouillon, A.; Lancelot, J. C.; Santos, J. S. D.; Collot, V.; Bovy, P. R.; Rault, S. *Tetrahedron* **2003**, 59, 10043-10049.
- (159) Heckmann, A.; Lambert, C. *J. Am. Chem. Soc.* **2007**, 129, 5515-5527.
- (160) Miyaura, N.; Suzuki, A. *Chem. Rev.* **1995**, 95, 2457-2483.
- (161) Nonoyama, M. *Bull. Chem. Soc. Jpn.* **1974**, 47, 767-768.
- (162) De Crisci, A. G.; Lough, A. J.; Multani, K.; Fekl, U. *Organometallics* **2008**, 27, 1765-1779.
- (163) Wehman, P.; Dol, G. C.; Moorman, E. R.; Kamer, P. C. J.; Vanleeuwen, P.; Fraanje, J.; Goubitz, K. *Organometallics* **1994**, 13, 4856-4869.
- (164) Lo, K. K. W.; Chung, C. K.; Zhu, N. Y. *Chem.-Eur. J.* **2003**, 9, 475-483.

- (165) Lo, K. K. W.; Ng, D. C. M.; Chung, C. K. *Organometallics* **2001**, *20*, 4999-5001.
- (166) Neve, F.; Crispini, A.; Campagna, S.; Serroni, S. *Inorg. Chem.* **1999**, *38*, 2250-2258.
- (167) Vandiemen, J. H.; Hage, R.; Haasnoot, J. G.; Lempers, H. E. B.; Reedijk, J.; Vos, J. G.; Decola, L.; Barigelli, F.; Balzani, V. *Inorg. Chem.* **1992**, *31*, 3518-3522.
- (168) Griffiths, P. M.; Loiseau, F.; Puntoriero, F.; Serroni, S.; Campagna, S. *Chem. Commun.* **2000**, 2297-2298.
- (169) Amthor, S.; Noller, B.; Lambert, C. *Chem. Phys.* **2005**, *316*, 141-152.
- (170) Dapperheld, S.; Steckhan, E.; Brinkhaus, K. H. G.; Esch, T. *Chem. Ber.* **1991**, *124*, 2557-2567.
- (171) Schmidt, W.; Steckhan, E. *Chem. Ber.-Recueil* **1980**, *113*, 577-585.
- (172) Stahl, R.; Lambert, C.; Kaiser, C.; Wortmann, R.; Jakober, R. *Chem.-Eur. J.* **2006**, *12*, 2358-2370.
- (173) Belser, P.; Vonzelewsky, A.; Juris, A.; Barigelli, F.; Balzani, V. *Chem. Phys. Lett.* **1984**, *104*, 100-104.
- (174) Cook, M. J.; Lewis, A. P.; McAuliffe, G. S. G.; Skarda, V.; Thomson, A. J.; Glasper, J. L.; Robbins, D. J. *J. Chem. Soc., Perk. Trans. II* **1984**, 1293-1301.
- (175) Dragonetti, C.; Falciola, L.; Mussini, P.; Righetto, S.; Roberto, D.; Ugo, R.; Valore, A.; De Angelis, F.; Fantacci, S.; Sgamellotti, A.; Ramon, M.; Muccini, M. *Inorg. Chem.* **2007**, *46*, 8533-8547.
- (176) Hou, Y. J.; Xie, P. H.; Wu, K. W.; Wang, J. H.; Zhang, B. W.; Cao, Y. *Sol. Energy Mater. Sol. Cells* **2001**, *70*, 131-139.
- (177) Skarda, V.; Cook, M. J.; Lewis, A. P.; McAuliffe, G. S. G.; Thomson, A. J.; Robbins, D. J. *J. Chem. Soc.* **1984**, 1309-1311.
- (178) Tseng, H. W.; Zong, R.; Muckerman, J. T.; Thummel, R. *Inorg. Chem.* **2008**, *47*, 11763-11773.
- (179) Wang, D.; Mendelsohn, R.; Galoppini, E.; Hoertz, P. G.; Carlisle, R. A.; Meyer, G. J. *J. Phys. Chem. B* **2004**, *108*, 16642-16653.
- (180) Mamo, A.; Stefio, I.; Parisi, M. F.; Credi, A.; Venturi, M.; DiPietro, C.; Campagna, S. *Inorg. Chem.* **1997**, *36*, 5947-5950.
- (181) Ortmans, I.; Didier, P.; Kirschdemesmaeker, A. *Inorg. Chem.* **1995**, *34*, 3695-3704.
- (182) Serroni, S.; Juris, A.; Campagna, S.; Venturi, M.; Denti, G.; Balzani, V. *J. Am. Chem. Soc.* **1994**, *116*, 9086-9091.
- (183) Klassen, D. M.; DelPup, R. V. *Inorg. Chem.* **2002**, *41*, 3155-3160.
- (184) Weiner, M. A.; Basu, A. *Inorg. Chem.* **1980**, *19*, 2797-2800.
- (185) *Electronic absorption spectra of radical ions*; Shida, T., Ed.; Elsevier: Amsterdam, 1988.
- (186) Hayashi, H.; Nagakura, S. *Bull. Chem. Soc. Jpn.* **1984**, *57*, 322-328.
- (187) Mori, Y.; Sakaguchi, Y.; Hayashi, H. *J. Phys. Chem. A* **2002**, *106*, 4453-4467.
- (188) Werner, U.; Sakaguchi, Y.; Hayashi, H.; Nohya, G.; Yoneshima, R.; Nakajima, S.; Osuka, A. *J. Phys. Chem.* **1995**, *99*, 13930-13937.
- (189) Kobori, Y.; Sekiguchi, S.; Akiyama, K.; Tero-Kubota, S. *J. Phys. Chem. A* **1999**, *103*, 5416-5424.
- (190) Mauser, H. *Formale Kinetik*; Bertelsmann Univ.-Verl.: Düsseldorf, 1974.
- (191) Verhoeven, J. W. *J. Photochem. Photobiol., C* **2006**, *7*, 40-60.
- (192) Kroon, J.; Oevering, H.; Verhoeven, J. W.; Warman, J. M.; Oliver, A. M.; Paddonrow, M. N. *J. Phys. Chem.* **1993**, *97*, 5065-5069.

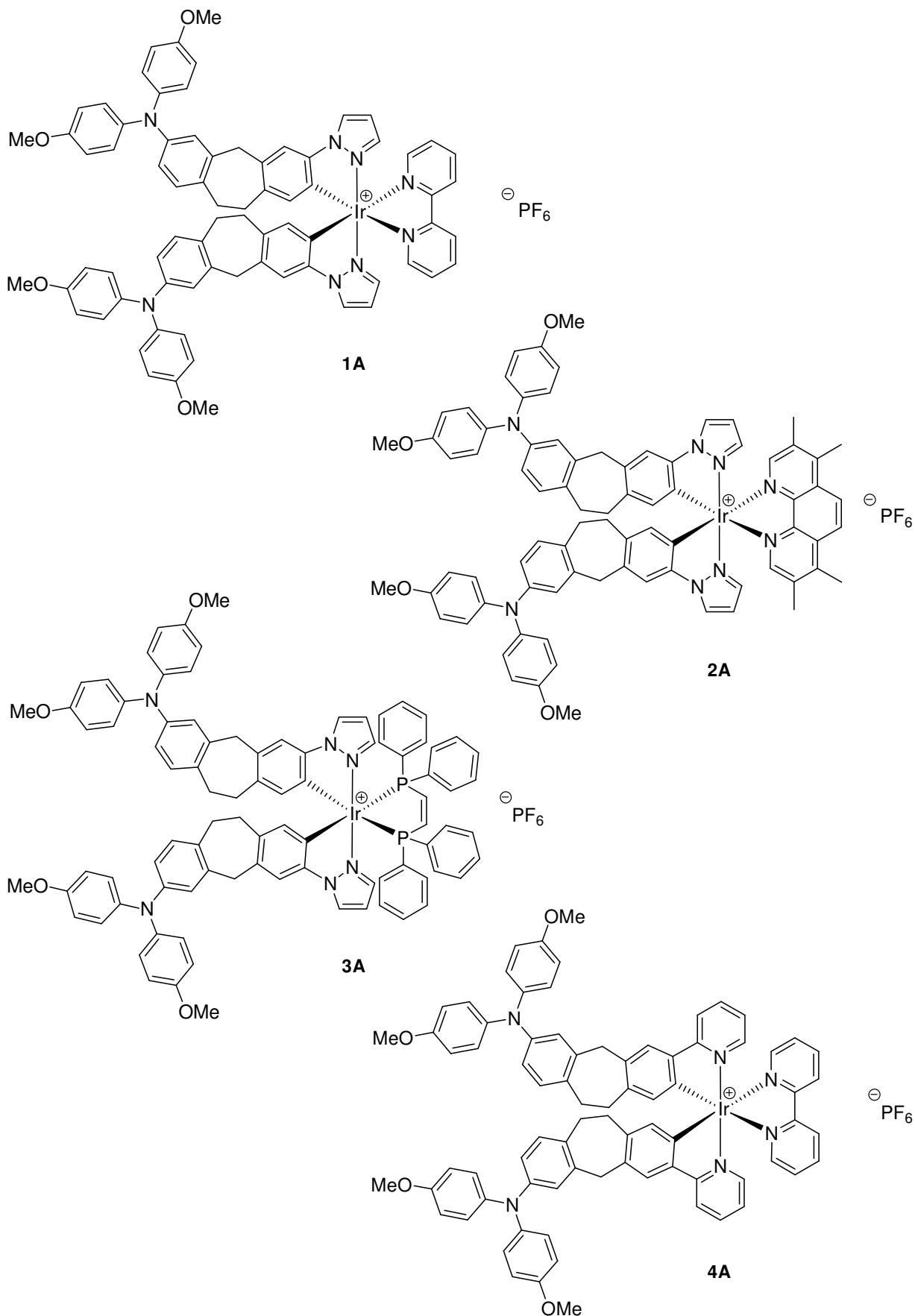
- (193) Brooks, J.; Babayan, Y.; Lamansky, S.; Djurovich, P. I.; Tsyba, I.; Bau, R.; Thompson, M. E. *Inorg. Chem.* **2002**, *41*, 3055-3066.
- (194) Tsuzuki, T.; Tokito, S. *Advanced Materials* **2007**, *19*, 276-280.
- (195) Lloris, M. E.; Abramovitch, R. A.; Marquet, J.; Morenomanas, M. *Tetrahedron* **1992**, *48*, 6909-6916.
- (196) Hanson, P.; Jones, J. R.; Taylor, A. B.; Walton, P. H.; Timms, A. W. *J. Chem. Soc. Perkin Trans. 2* **2002**, 1135-1150.
- (197) Christoffers, J. *Synth. Comm.* **1999**, *29*, 117-122.
- (198) Zhong, Z. Q.; Tang, H. T.; Zhang, P. *Chem. Res. Chin. Univ.* **1998**, *14*, 30-37.
- (199) Ragni, R.; Plummer, E. A.; Brunner, K.; Hofstraat, J. W.; Babudri, F.; Farinola, G. M.; Naso, F.; De Cola, L. *J. Mater. Chem.* **2006**, *16*, 1161-1170.
- (200) Grushin, V. V.; Herron, N.; LeCloux, D. D.; Marshall, W. J.; Petrov, V. A.; Wang, Y. *Chem. Commun.* **2001**, 1494-1495.
- (201) Dedeian, K.; Djurovich, P. I.; Garces, F. O.; Carlson, G.; Watts, R. J. *Inorg. Chem.* **1991**, *30*, 1685-1687.
- (202) Salbeck, J. *Anal. Chem.* **1993**, *65*, 2169-2173.
- (203) Scaiano, J. C.; Charette, G.; Simard, A., 2004.
- (204) Karstens, T.; Kobs, K. *J. Phys. Chem. C* **1980**, *84*, 1871-1872.
- (205) Lakowicz, J. R. *Principles of fluorescence spectroscopy*; 2nd ed.; Kluwer Academic/Plenum Publisher: New York, 1999.
- (206) Whittle, V. L.; Williams, J. A. G. *Inorg. Chem.* **2008**, *47*, 6596-6607.
- (207) Cline, E. D.; Adamson, S. E.; Bernhard, S. *Inorg. Chem.* **2008**, *47*, 10378-10388.
- (208) Ichimura, K.; Kobayashi, T.; King, K. A.; Watts, R. J. *J. Phys. Chem.* **1987**, *91*, 6104-6106.
- (209) Labadie, S. S. *Synth. Comm.* **1994**, *24*, 709-719.

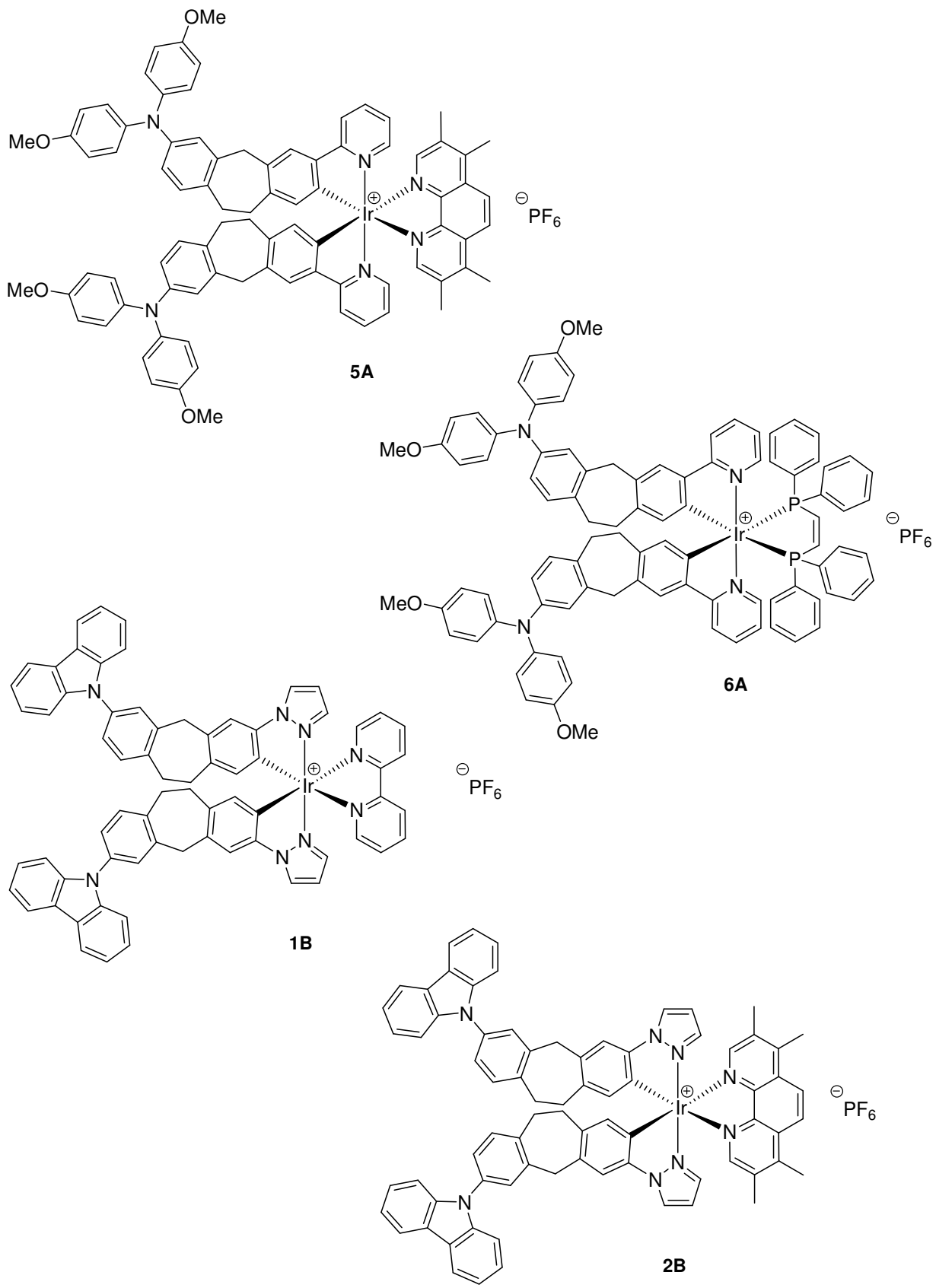
5. Table of Formulas

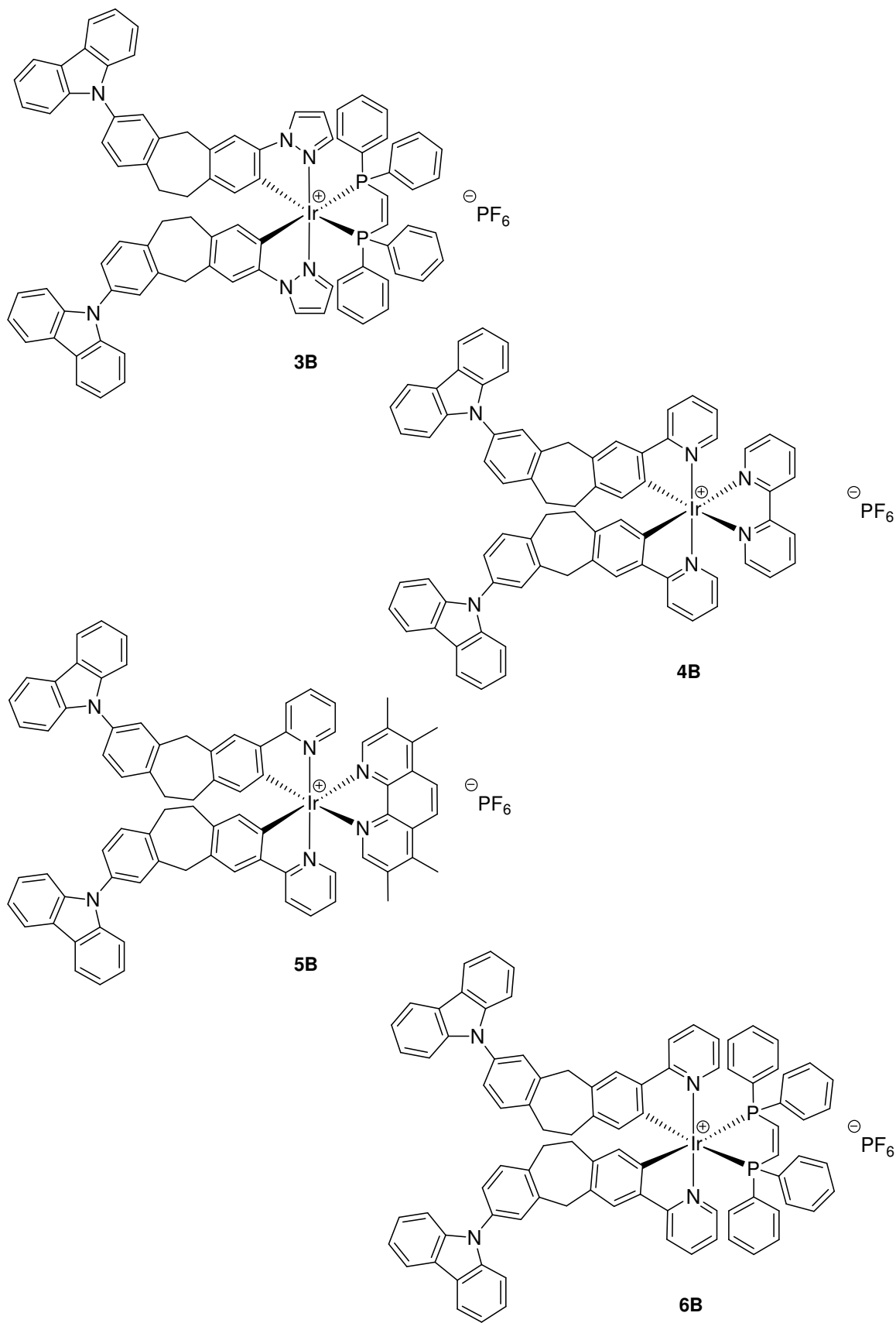
5.1 Reference Compounds

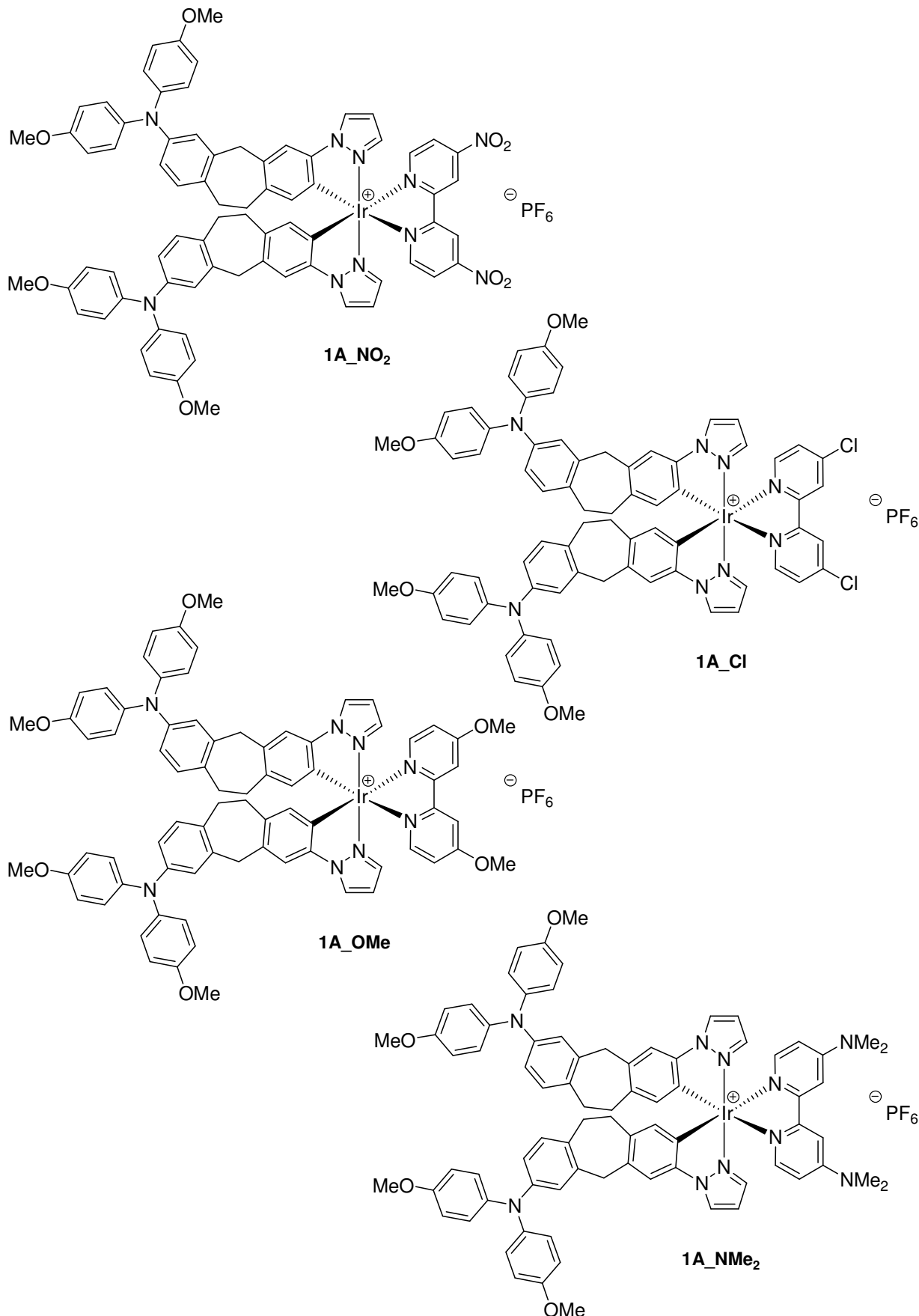


5.2 Cationic Complexes

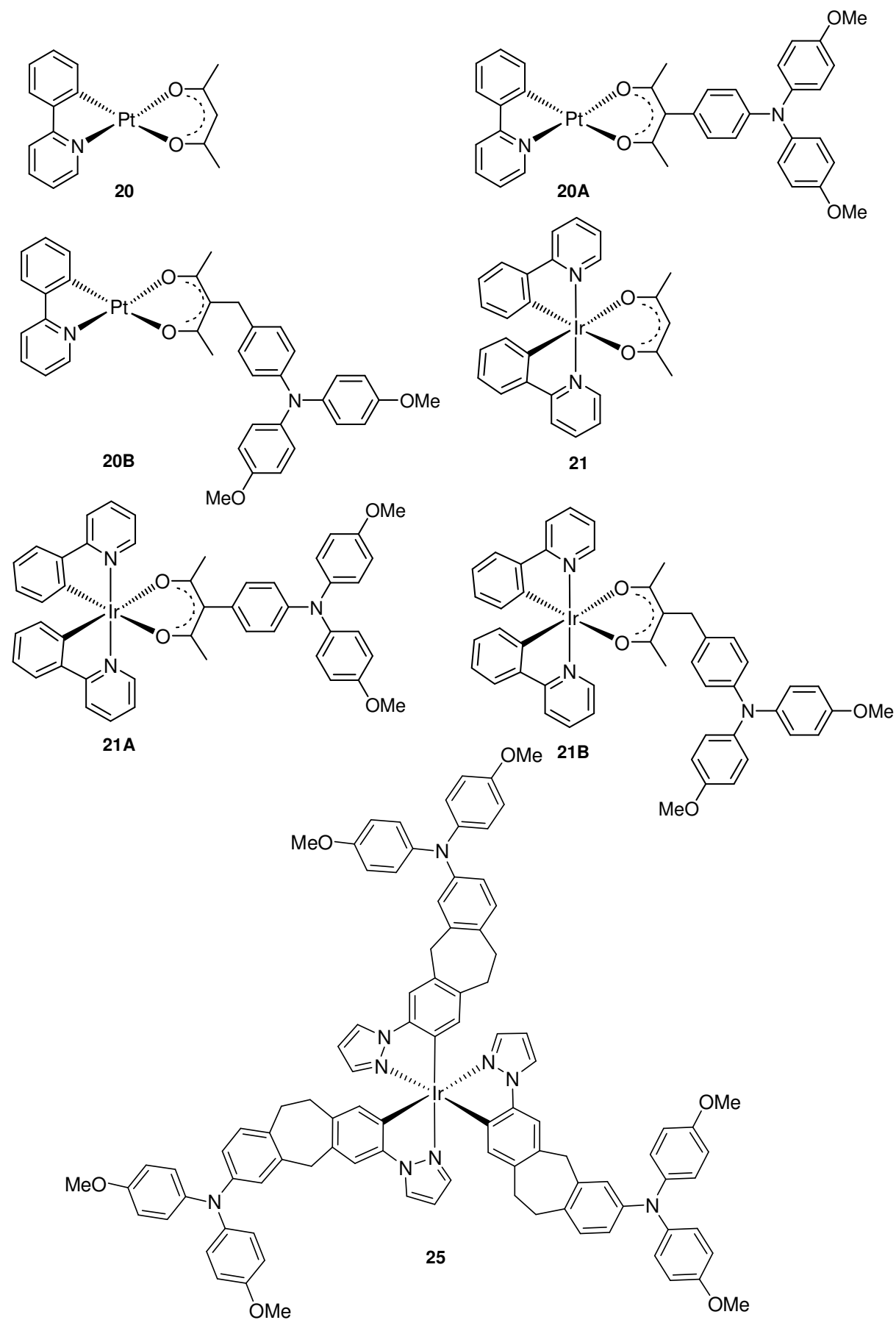




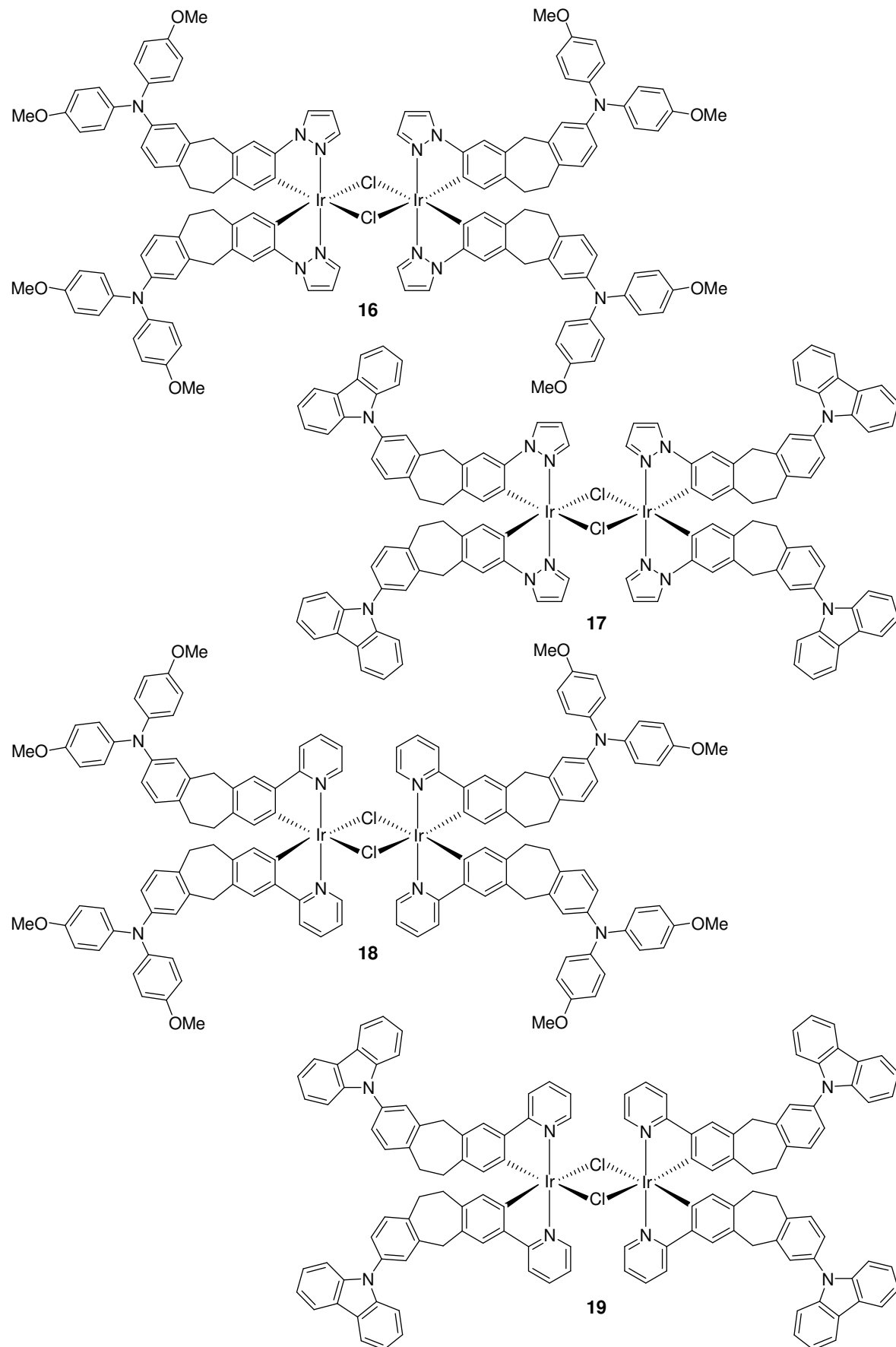




5.3 Neutral Complexes

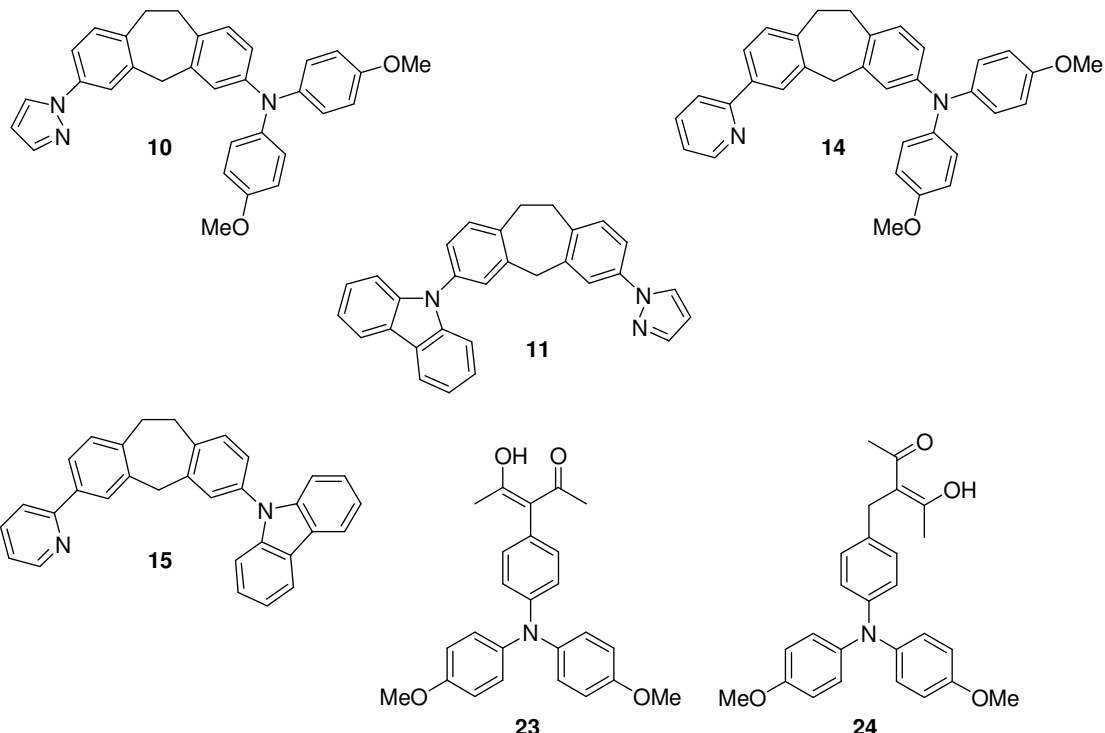


5.4 Dimers

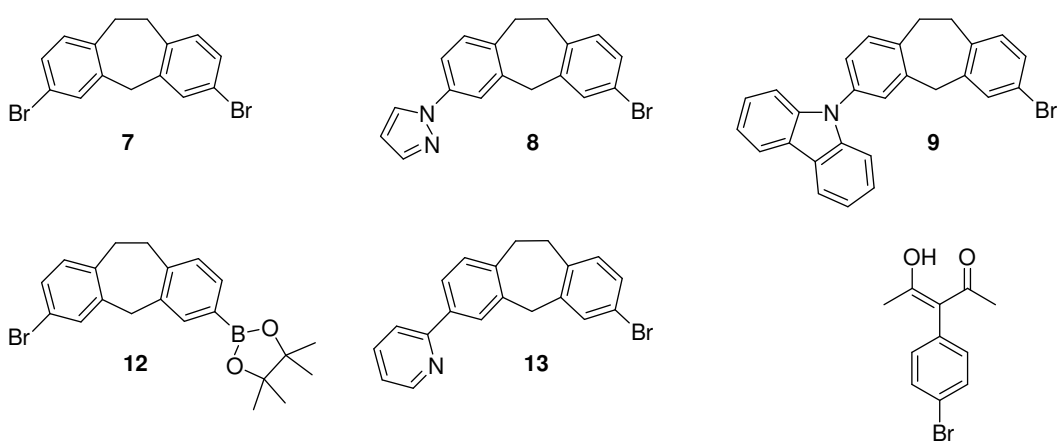


5.5 Ligands and Precursors

Ligands



Precursors



22

Appendix

Zusammenfassung

Im ersten Teil dieser Arbeit wurden die Synthesen und photophysikalischen Eigenschaften mehrerer Donor-Akzeptor-substituierter Übergangsmetallkomplexe des Typs $[(C^N)_2Ir(N^N)][PF_6]$ vorgestellt. Das Ir(III) wurde mit Lochleitern wie Carbazol (CZ) und Triarylamin (TAA), die über eine Methyl- und Ethylbrücke mit dem cyclometallierten C^N-Liganden Phenylpyrazol (ppz) und Phenylpyridin (ppy) verbunden waren, verknüpft. Zweizähnige neutrale N^N- und P^P-Liganden wie 2,2'-Bipyridyl (bpy), 3,4,7,8-Tetramethyl-1,10-phenanthrolin (tmp) und *cis*-1,2-Bis(diphenylphosphino)ethylen (bdppe) wurden als Akzeptoren ausgewählt. Um den Einfluss der Elektronendichte am bpy-Liganden auf die photophysikalischen Eigenschaften zu untersuchen, wurden TAA-Komplexe mit akzeptor- und donorschichtsubstituiertem bpy hergestellt. Dafür wurden folgende N^N-Liganden ausgewählt: 4,4'-Dinitro-2,2'-bipyridyl, 4,4'-Dichloro-2,2'-bipyridyl, 4,4'-Dimethoxy-2,2'-bipyridyl and 4,4'-Dimethylamino-2,2'bipyridyl. Um die Eigenschaften in Vergleich setzen zu können, wurden die entsprechenden Referenzverbindungen ohne Lochleiter hergestellt.

Alle Carbazol-Komplexe, bis auf die bdppe-Verbindungen, zeigen Emission und transiente Absorption ähnlich denen ihrer Referenzverbindungen, was sie für Anwendungen in der OLED-Forschung interessant macht. Untersuchungen an LECs (lichtemittierende elektrochemische Zellen) zeigen eine rotverschobene Lumineszenz.

Die Triarylamin-Komplexe zeigen keine Emission bei RT, allerdings weisen diese eine intensive, blauverschobene und langlebige Lumineszenz bei 77 K in einer festen Matrix auf. Die transienten Absorptionsspektren unterscheiden sich stark von denen der Referenzverbindungen. Sie weisen charakteristische Merkmale von den Spektren der isolierten Radikalanionen und Radikalkationen auf, was durch spektroelektrochemische Messungen bewiesen wurde. Daraus kann geschlossen werden, dass es sich bei dem angeregten Zustand um einen ladungsgesetzten (CS) Zustand handelt, wo die positive Ladung am Triarylamin-Donor und die negative Ladung am N^N-Akzeptor sitzt. Die Abklingzeiten der angeregten Zustände verlaufen

biexponentiell, was ein Hinweis auf das Vorhandensein zweier angeregter Zustände, dem ^1CS und ^3CS Zustand, ist.

Um dieses Verhalten zu untersuchen, wurden verschiedene substituierte bpy-Komplexe synthetisiert und analysiert. Temperaturabhängige Messungen der transienten Absorption zeigten, dass alle Ratenkonstanten temperaturunabhängig sind, mit Ausnahme des OMe-substituierten Komplexes. Die Gleichgewichtskonstante $K = k_1 / k_2$ ist nahezu eins für alle Komplexe. Bei dem OMe-Komplex sinkt sie mit steigender Temperatur. Eine Auftragung der Ratenkonstanten gegen die Energiedifferenzen, die durch cyclovoltammetrische Messungen erhalten wurden, zeigte, dass alle Konstanten mit steigender Donorstärke am bpy-Liganden abfallen. DFT-Rechnungen an der OMe-Verbindung sind noch in Arbeit.

Im zweiten Teil dieser Arbeit wurden neutrale Ir(III) und Pt(II) Komplexe des Typs $[(\text{O}^\text{O})\text{Ir}(\text{N}^\text{N})_2]$ und $[(\text{O}^\text{O})\text{Pt}(\text{N}^\text{N})]$ vorgestellt. Hier wurde TAA mit Acetylacetonat (acac) direkt, oder über eine CH_2 -Brücke verbunden, um den Einfluss der Art der Verbrückung auf die photophysikalischen Eigenschaften zu beobachten. Als zweizähniger N^N-Ligand wurde 2,2'-Bipyridyl (bpy) gewählt. Auch hier wurden alle entsprechenden Referenzverbindungen ohne Triarylamin als Vergleich hergestellt. Zudem wurde der homoleptische *fac* Ir(N^N)₃ Komplex mit Triarylamin, welches über eine Methyl- und Ethylbrücke an Phenylpyrazol angeknüpft wurde, synthetisiert.

Die Synthese des Ir(III)-Komplexes mit TAA substituiertem acac-Liganden verknüpft über eine CH_2 -Brücke konnte nicht hergestellt werden. Alle neutralen TAA-substituierten β -diketonato Pt(II) und Ir(III) Komplexe zeigen keine Lumineszenz, außer dem Pt(II)-Komplex mit CH_2 -Gruppe. Dieser zeigt angeregte Zustände die in guter Übereinstimmung mit den Emissionslebenszeiten bei RT sind. Diese sind ähnlich denen der Referenz, was auf einen $^3\text{Pt}(\text{N}^\text{N})(\text{O}^\text{O})$ -Zustand schließen lässt. Die Komplexe ohne CH_2 -Brücke zeigen zudem keine transiente Absorption was auf ein Charge-Transfer-Quenching aufgrund der direkten Verknüpfung zwischen Donor und Akzeptor zurückzuführen sein könnte.

Der homoleptische *fac* Ir(N^N)₃ Komplex weist weder Emission bei RT, noch transiente Absorption auf. Bei 77 K ist eine stark strukturierte Emission mit einer Abklingzeit von 14 μs zu beobachten. Verglichen mit dem literaturbekannten

Appendix

Vergleichskomplex ist die Emission auf die Bevölkerung eines $^3\text{Ir}(\text{ppz})_3$ -Zustandes zurückzuführen.

Unsere Ergebnisse sind grundlegend für die Synthese weiterer Verbindungen mit stärkeren Akzeptoren, wie z. B. Naphthalenimid, um längerlebige ladungsgtrennte Zustände zu erhalten. Diese könnten Anwendung als Photosynthesizer in Solarzellen und anderen optoelektronischen Bauteilen finden. Zudem sind weiter Untersuchungen an LECs und OLEDs für die Carbazol-Komplexe noch immer von Interesse, um das Ausmaß der Triplett-Triplett-Annihilierung zu quantifizieren.

Danksagung

An dieser Stelle möchte ich mich bei allen Personen bedanken, die zum Gelingen dieser Arbeit beigetragen haben. Mein besonderer Dank gilt dabei:

Herrn Dr. Matthias Grüne und Frau Elfriede Ruckdeschel für die Aufnahme der NMR-Spektren.

Herrn Dr. Michael Büchner, Herrn Fritz Dadrich und Frau Antje Hautzinger, für die Aufnahme der Massenspektren.

Herrn Dipl.-Ing. Bernd Brunner, für seine bereitwillige Hilfe bei Computerproblemen und der geduldigen Einweisung in unseren Potentiostaten („Weiber!!!“)

Herrn Markus Braun, für seine ständige Hilfsbereitschaft in allen handwerklichen Belangen. Vor allem natürlich für seinen Einsatz bei der Konstruktion unserer Eis-Sau für die Kaiserliche Hochzeit.

Herrn Michael Ramold, für das Durchhaltevermögen und die Geduld beim Bau einer Vielzahl von Sonderanfertigungen für die Charakterisierung unserer OLEDs und für die Apparatur zu den temperaturabhängigen Messungen.

Allen weiteren Angestellten des Instituts für Organische Chemie, *Herrn Dr. Christian Stadler, Frau Angela Dreher, Frau Anette Krug, Frau Petra Leckert, Frau Ursula Rüppel, Herrn Matthias Fromm, Herrn Manfred Ludwig und Herrn Frank Förtsch*, für ihre ständige Hilfsbereitschaft.

Den Jungs in der Werkstatt, *Fritz* und *Thomas* die mir so manchen schweren Tag durch ihre Herzlichkeit erleichtert haben. *Fritz*, Dir natürlich einen ganz besonderen Dank für die weihnachtlichen Schokoladen-Lieferungen und die Lotterie-Lose.

Daniel Rauh aus dem Arbeitskreis von *Herrn Prof. Dr. Dyakonov* für die Hilfe bei der Anfertigung unserer OLED-Prototypen.

Herrn Prof. M. Kaupp für die DFT-Rechnungen zu meinen substituierten ppz-Verbindungen.

Besonderer Dank gebührt natürlich allen Mitgliedern des Arbeitskreises Lambert für das lockere Arbeitsklima und dafür, dass ich Euch auch als ein paar wichtige Freunde gewonnen habe.

Die Ehemaligen:

Dr. Volker Kriegisch, für die die Organisation der AK-Ausflüge, unsere gemeinsamen Theater-Abende und unseren kleinen Gemüse- und Kräutergarten.

Dr. Stephan Amthor, unserem „Brain“, der für alles immer die richtige Antwort hatte. Du hast mit Deinem Abgang eine große Lücke hinterlassen!

Dr. Rainer Stahl, unser „Godfather of Electrochemistry“ für die vielen Blutwurze und die ständige Hilfsbereitschaft vor allem bei den elektrochemischen Messungen.

Simone Krakert, die mir in ihrer kurzen Zeit hier und die Jahre danach eine richtige Freundin geworden ist. Wie freue ich mich schon auf unsere Reise als Rentnerinnen auf der Queen Mary 2, Shisha rauchend und „Don Camillo und Peppone“ schauend. Wir sollten auch dringend nochmal das „Sziget Festival“ besuchen, diesmal mit imprägniertem Zelt, und – vielleicht treffen wir dort ja Kai Pflaume und Henry Maske?

Appendix

Ruben Ramon, für Deine Unbeschwertheit und herzerfrischende Komik. Was gäbe ich darum, Dich im Tütü oder mit Deinem Wildleder-Werkzeuggürtel bekleidet für uns tanzen zu sehen!

Und die Aktuellen:

Sascha Heckmann, für unsere gemeinsamen Kaffeepausen, die mir immer einen guten Start in den Tag ermöglicht haben. Von Dir habe ich gelernt, dass es keine Kraftausdrücke gibt. Außerdem weiß ich nun auch, dass Geld die Welt regiert und den Ein oder Anderen sogar glücklich macht. Ich wünsche Dir von ganzen Herzen, dass Du den Sinn Deines Lebens findest. Sascha, keiner kann so gut und ausdauernd Raketen-Buggies lenken wie Du!!!

Christian Müller, für Deine Aufopferungsbereitschaft bei der Vernichtung diverser Kuchen. Außerdem warst Du ein wichtiger Bestandteil unseres Göteborg-Teams. Ohne Achterbahnfahrt, Weezer, Conny-Attaken und Deinen rabenschwarzen Humor wäre das kein so unvergessliches Erlebnis geworden. Ich werde Dich mit Sicherheit mal unter der Bank in der Gerbrunner Bushaltestelle besuchen!

Dörte Nowak, für Deine stetige Hilfsbereitschaft und Ehrlichkeit. Ich glaube, es gibt keinen Menschen von dem Du jemals schlecht geredet – ja, nicht einmal gedacht hast. Mit Dir die LECs zu bauen war eines der Highlights während der Doktorarbeit! Ohne Deine Ausdauer beim Basteln hätten die LECs niemals geleuchtet. Vielen vielen Dank!

Conrad Kaiser, für Deine immer „positiven“ Beiträge in jeder Lebenslage. Auch Du hast Göteborg unvergesslich gemacht und ich habe da viel von Dir gelernt. Ich gehe niemals mit meinem Schlüssel in der Tasche schwimmen und Essen kaufe ich auch immer viel zu viel! Conny, bleib so, wie Du bist, dann kann unserer späteren Hochzeit nichts mehr im Wege stehen!

Nina Dürrbeck, für Deine tatkräftige Unterstützung bei der Reinigung unseres Seminarraumes, die es mir sogar ermöglichte, diesen Job langsam aber sicher auf Dich abzuwälzen. Auch zum Göteborg-Team gehörend hatten wir zwei wunderschöne Dio- und ACDC-Erlebnisse, an die ich mich immer erinnern werde. Ich hoffe, wenn ich Dich auf der Bank in der Gerbrunner Bushaltestelle besuchen komme, dass Du auch dann immer noch ein offenes Ohr für meine Probleme haben wirst!

Markus Steeger, für die Ablöse am Laser - was mir den Abnabelungsprozess erleichterte! Göteborg wäre ohne Deine literarischen Beiträge und den großen Einsatz bei der Stadtführung auch nur halb so schön geworden! Pflege Deinen Garten weiterhin so liebevoll und vielleicht hast Du ja einen Whiskey und eine Zigarre für mich übrig, wenn ich Dich im Irish Pub besuchen komme!

Unsere Jung-Doktoranden *Sebastian („Ramos“) Völker* und *Fabian („unser Zieschang“) Zieschang* für den frischen Wind im AK. Nicht nur fachlich gesehen seid Ihr eine immense Bereicherung für uns - auch mit Hilfe Eures fußballerischen Talents konnten wir endlich mal der restlichen Fakultät zeigen, wer wir sind!!!

Meinen F-Praktikanten *Manuela Groß* und *Julian Mager* für die erfolgreiche Bearbeitung ihrer Praktika.

Besonderer Dank gilt hierbei meinem einzigen Sohn *Johannes Klein*, der brav in die Fußstapfen seiner Mama gestiegen ist und bei dem ich mir sicher bin, dass er meine Arbeit gebührend fortsetzen wird. Ich danke Dir für Deine Fröhlichkeit, die immer für eine gute Stimmung sorgt. Und ich danke dir auch noch dafür, dass Du keine Skrupel davor hast, mit Deiner Mama tanzen zu gehen! USA!!!!!!!

Ganz besonderer Dank gilt meinen Bekannten und der gesamten Familie:

Den Seglern *Klaus, Günter, Roland, Anna, Falco, Caro, Erica, Tobias* und *Jens* für die unvergesslichen Törns während der letzten Jahre. Auch vielen Dank für Euer Verständnis bei meinem spontanen Rückzug bei dem letzten Törn! Nächstes Motto: Flucht in die Karibik 2011 – mehr Rum als Diesel!!!

Den Sportfreunden *Michael, Yvonne, Gerald, Frances, Markus* und *Harald* für die vielen schönen Sport- und Partyabende. Die antrainierte Ausdauer hat sich vor allem bei diversen Disko- und Biergärten-Gängen bewährt gemacht! Besonders unsere Mittwochabende, die mit zwei Stunden Uwe-Spinning eingeläutet wurden und irgendwann früh um fünf im Odeon ihr Ende fanden werde ich nie vergessen! Vielen Dank Euch!

Meinen Freundinnen *Caro* und *Julia* für die langjährige Freundschaft. Ich hoffe, wir werden noch viele schöne Erlebnisse im Nürnberg, München oder Seßlach haben!

Meinem langjährigen Mentor *Ottmar Knote* ohne dessen finanzielle Unterstützung ich niemals diese Karriere hätte anstreben können!

Anita Neckermann, meiner „Ersatzmama“, die mich im letzten Jahr so liebevoll aufgenommen hat. Anita, vielen Dank für die schönen Gespräche mit Dir, das gute Essen und – vor allem für diese unglaubliche Massage!!!

Dirk Rausch, für die schöne Zeit, die wir hatten. Auch im Labor waren wir ein spitzen Team - vor allem beim 'BuLi abzapfen warst Du immer hilfreich mit Flamme Auspusten zur Seite gestanden. Ich wünsche Dir, dass Du weiterhin an Dir arbeiten kannst und die größte Hürde Deines Lebens bewältigen kannst! Auch Deiner Familie möchte ich für die vielen schönen Jahre danken und natürlich für die tatkräftige Unterstützung bei meinem Umzug im letzten Jahr.

Slex und *Peter* für diverse kulturelle und lukullische (Drei???) Ereignisse, die mir so manchen schönen Abend beschert haben. Besondere Highlights, wie der Urban-Priol-Abend und unsere Sweet-Konzerte („we want sweet“) schreien nach Wiederholung!

Sabine, Flatter, Lea und *Lara*. Zu Euch fällt mir immer das Sprichwort ein: Wenn der Prophet nicht zum Berg kommt, dann muss eben der Berg zum Propheten kommen. Ich danke Euch für Eure Flexibilität, mich so oft hier besuchen zu kommen. Was haben wir schöne Tage hier verlebt! Und ich möchte an dieser Stelle auch noch für die unkomplizierte Hilfe bei meinem Spontan-Umzug danken und Dir, Sabine, für Deine engagierten Rathausgänge für mein amtliches Führungszeugnis©!

Manf und *Klaus*, dafür, dass ihr Euch uns Würzburgern oftmals brav angepasst habt und immer geduldig die Fahrt von Wülfingen hierher zu uns aufgenommen habt um den ein oder anderen gemütlichen Abend mit uns zu verleben. Manf, Dir nochmal ein dickes Dankeschön für Deine ausdauernden Kastelruth - Planungen! Vermisse unsere zweite Heimat schon wieder!

Vor allem natürlich *meinen Eltern*, für ihren finanziellen und moralischen Rückhalt und die Geduld, mein Gejammer immer ertragen zu haben. Entschuldigt bitte, dass ich mich die letzten Jahre zu Hause so rar gemacht habe! Auch wenn man es nicht meint, für mich ist es zu Hause immer noch am Schönsten! Draußen, mit der Familie in der Sonne sitzend, dazu ein schönes, frischgezapftes Scharpf-Bräu und leckere Bratwürste vom Grill, im Hintergrund schöne Musik aus Manfs Jukebox („kalinichta, kalinichta, gute Nacht...“).... Ich hoffe, das werden wir noch ganz ganz oft haben! Vielen Dank Euch!!!